

SYSTEMS BIOENGINEERING: MODELING  
ANGIOGENESIS AND MAPPING THE GENE  
THERAPY INDUSTRY

A Dissertation

Presented to the Faculty of the Graduate School

of Cornell University

in Partial Fulfillment of the Requirements for the Degree of

Doctor of Philosophy

by

William Robert Bedell

May 2019

© 2019 William Robert Bedell

ALL RIGHTS RESERVED

SYSTEMS BIOENGINEERING: MODELING ANGIOGENESIS AND  
MAPPING THE GENE THERAPY INDUSTRY

William Robert Bedell, Ph.D.

Cornell University 2019

In this dissertation, I recount my contributions to the emerging discipline of systems bioengineering in two contexts: expanding our ability to simulate the biomolecular circuitry underlying blood vessel growth; and developing a business to reduce the cost of life-saving gene therapies by filling gaps in the network of firms behind drug development and manufacturing.

A rapidly advancing set of experimental and computational tools have enabled vascular biologists to build increasingly complex *in silico* recreations of angiogenesis – the process by which new blood vessels sprout from pre-existing vasculature – hinting at future where specialized biomedical software helps predict tissue vascularization in regenerative medicine and oncology. I combined rigorous mathematical analysis with a broad search for potentially interacting signaling processes within the vascular endothelial cells to show why the orthodox view of “tip cell selection” (a sub-process within angiogenesis) is unlikely to recapitulate the full range of observed angiogenic sprouting behaviors. I propose two qualitatively new hypotheses for the molecular underpinnings of tip cell selection which could predict angiogenic phenomena that previous simulations have failed to capture. Code samples for the mechanisms analyzed are included as supplements.

Gene therapies using recombinant adeno-associated viruses (AAV) to deliver DNA into a patient’s cells have reached market access in Europe, with the US expected to soon follow. AAV gene therapies might permanently cure hereditary

diseases such as hemophilia and amyotrophic lateral sclerosis, but many emerging treatments are plagued by extraordinarily high manufacturing costs (some in excess of \$1 million per patient). I pursued the goal of introducing a cost-saving technology – improved insect cell lines for use as a production substrate – into commercial use for AAV manufacturing. After performing in-depth industry analysis and business model design, I found that the raw price-performance was a minor component of the value that biotechnology firms placed on new manufacturing technologies. Rather, engineers attempting to solve real-world problems in biotechnology must account for a range of commercial, medical, legal, and social constraints to be successful – raising important implications for the future of systems bioengineering as it attempts to distinguish itself from its roots in basic research.

## **BIOGRAPHICAL SKETCH**

Bill Bedell was raised in Portland, Oregon. He completed his high school coursework at Portland Community College in 2009. He attended Oregon State University in Corvallis, Oregon as an undergraduate, completing a Bachelor's of Science with a major in chemical engineering in 2012. In 2012, Bill joined the School of Chemical and Biomolecular Engineering at Cornell University in Ithaca, New York as a doctoral student in chemical engineering.

I dedicate this dissertation to my parents, Dan and Jane, whose unceasing love and encouragement made so much in my life possible.

## ACKNOWLEDGEMENTS

I would first like to thank my advisor, Dr. Abraham D. Stroock, for embracing and nurturing the independent spirit we both share, for challenging me to accomplish more than I thought I could, and above all, for somehow maintaining unwavering patience and belief in an unconventional student like me.

I would like to thank my committee members – Drs. Julius Lucks and Jeff Varner – for daring me to bridge my work to other frontiers in science.

I would like to thank the organizers and participants in the 2016 Cornell Technology Commercialization Fellowship for believing in my potential as an innovator above and beyond whatever inventions I could call my own.

I would like to thank my lab mates in the Stroock Group – particularly Mengrou Shan and John Morgan – for maintaining an enthusiasm for the mysteries of endothelial biology and ensuring there was never a shortage of fascinating questions for us to pursue.

I would like to thank the people who shared with me their friendship during my time in Ithaca; you made the years here not only bearable, but delightful, and I know we will remain in each other's lives.

I would like to thank my family for filling the few times we could see each other each year with warmth and laughter.

A portion of the work described was supported by the Center on the Physics of Cancer Metabolism through Award Number 1U54CA210184-01 from the National Cancer Institute. The content is solely the responsibility of the authors and does not necessarily represent the official view of the National Cancer Institute or the National Institutes of Health.

A portion of the work described was supported by the Cornell Technology Commercialization Fellowship organized by the Cornell College of Engineering and

the Young family.

## TABLE OF CONTENTS

Biographical Sketch . . . . .	iii
Dedication . . . . .	iv
Acknowledgements . . . . .	v
Table of Contents . . . . .	vii
List of Tables . . . . .	ix
List of Figures . . . . .	x
<b>1 Introduction</b>	<b>1</b>
1.1 Modeling tip cell selection in angiogenesis . . . . .	3
1.2 Analyzing business opportunities in commercial gene therapy manufacturing . . . . .	8
<b>2 Modeling biological pattern formation</b>	<b>13</b>
2.1 What is biological pattern formation? . . . . .	13
2.2 Mathematical history of biological pattern formation . . . . .	15
2.3 Future(s) of modeling pattern formation . . . . .	23
<b>3 Analyzing existing hypotheses for tip cell selection</b>	<b>27</b>
3.1 Introduction . . . . .	27
3.2 Methods . . . . .	30
3.2.1 Governing equations . . . . .	32
3.2.2 Identification of steady-states . . . . .	37
3.2.3 Linear stability analysis . . . . .	39
3.2.4 Numerical simulation . . . . .	44
3.3 Results . . . . .	46
3.3.1 Lateral inhibition . . . . .	46
3.3.2 Lateral induction . . . . .	51
3.3.3 Long-range lateral inhibition . . . . .	55
3.4 Discussion . . . . .	57
3.5 Conclusion . . . . .	66
<b>4 New hypotheses for tip cell selection</b>	<b>67</b>
4.1 Introduction . . . . .	67
4.1.1 Expanding on juxtacrine signaling . . . . .	68
4.1.2 Other biophysical and biomolecular phenomena . . . . .	73
4.2 Methods . . . . .	78
4.2.1 Two-dimensional approximation of diffusion . . . . .	79
4.2.2 Governing equations . . . . .	83
4.2.3 Identification of steady-states . . . . .	90
4.2.4 Linear stability analysis . . . . .	92
4.2.5 Numerical simulation . . . . .	99
4.3 Results . . . . .	102
4.3.1 Double-juxtacrine . . . . .	102

4.3.2	Diffusion and endocytosis . . . . .	105
4.4	Discussion . . . . .	111
4.5	Conclusion . . . . .	123
<b>5</b>	<b>Designing a Business for Insect Cell-based Manufacturing of Gene Therapies</b>	<b>124</b>
5.1	Introduction . . . . .	124
5.2	Methods . . . . .	127
5.2.1	Literature review . . . . .	127
5.2.2	Business model design methodologies . . . . .	134
5.2.3	Generating and investigating business concepts . . . . .	138
5.2.4	Integrating business concepts . . . . .	141
5.2.5	Plan-to-market . . . . .	143
5.3	Results . . . . .	144
5.3.1	A set of business concepts for insect cells in AAV production	145
5.3.2	Search pattern . . . . .	149
5.3.3	Interview process around each concept . . . . .	151
5.3.4	Business concept integration . . . . .	172
5.3.5	Business concept validation & implementation . . . . .	182
5.4	Discussion . . . . .	186
<b>6</b>	<b>Conclusion</b>	<b>195</b>
<b>A</b>	<b>Code samples</b>	<b>199</b>
A.1	Parameter setup . . . . .	199
A.2	Kinetics . . . . .	203
A.2.1	Lateral inhibition . . . . .	203
A.2.2	Lateral induction . . . . .	205
A.2.3	Double-juxtacrine . . . . .	207
A.2.4	Diffusion & endocytosis . . . . .	209
A.3	Initial conditions . . . . .	212
A.3.1	Lateral inhibition . . . . .	212
A.3.2	Lateral induction . . . . .	230
A.3.3	Double-juxtacrine . . . . .	248
A.3.4	Diffusion & endocytosis . . . . .	255
A.4	Dynamics . . . . .	265
A.4.1	Lateral inhibition . . . . .	265
A.4.2	Lateral induction . . . . .	267
A.4.3	Double-juxtacrine . . . . .	269
A.4.4	Diffusion & endocytosis . . . . .	271

## LIST OF TABLES

3.1	Parameters for numerical simulation of existing hypotheses . . . . .	45
4.1	Parameters for numerical simulation . . . . .	100
5.1	Comparison of AAV expression systems . . . . .	131
5.2	Scoring matrix for business concepts . . . . .	150
5.3	Interview Process for Concept 2a . . . . .	153
5.4	Interview Process for Concept 2b . . . . .	156
5.5	Interview Process for Concept 1 . . . . .	160
5.6	Interview Process for Concept 4 . . . . .	163
5.7	Interview Process for Concept 3 . . . . .	167
5.8	Interview Process for Concept 5 . . . . .	170
5.9	Business concept pairing matrix . . . . .	173
5.10	Evaluation of business concept pairings . . . . .	174

## LIST OF FIGURES

1.1	Overview of tip cell pattern formation . . . . .	4
1.2	Bioscientific and biotechnological value chain . . . . .	12
2.1	The cell lattice and the connectivity matrix . . . . .	17
2.2	The spectrum of the connectivity matrix . . . . .	18
3.1	Existing hypotheses of tip cell pattern formation . . . . .	28
3.2	Lattice and pattern formation of the endothelium . . . . .	31
3.3	Lattice and connectivity matrix for long-range mechanism . . . . .	36
3.4	Two-cell models for calculating steady-states . . . . .	38
3.5	Lateral inhibition . . . . .	48
3.6	Lateral induction . . . . .	53
3.7	Long-range lateral inhibition . . . . .	57
4.1	New hypotheses of tip cell pattern formation . . . . .	73
4.2	Lateral cross-section of the diffusion problem . . . . .	80
4.3	Double juxtacrine mechanism . . . . .	103
4.4	Diffusion and endocytosis . . . . .	107
5.1	Overview of AAV manufacturing . . . . .	126
5.2	AAV production with adherent vs. suspension cultures . . . . .	129
5.3	AAV production with BEVICS . . . . .	132
5.4	Set of business concepts . . . . .	145
5.5	Concept 2a, Before . . . . .	152
5.6	Concept 2a, After . . . . .	154
5.7	Concept 2b, Before . . . . .	155
5.8	Concept 2b, After . . . . .	157
5.9	Concept 1, Before . . . . .	159
5.10	Concept 1, After . . . . .	161
5.11	Concept 4, Before . . . . .	162
5.12	Concept 4, After . . . . .	164
5.13	Concept 3, Before . . . . .	166
5.14	Concept 3, After . . . . .	168
5.15	Concept 5, Before . . . . .	169
5.16	Concept 5, After . . . . .	171
5.17	Permutations of integrated businesses . . . . .	181
6.1	Analogs to multiscale modeling in design of architecture . . . . .	197

# CHAPTER 1

## INTRODUCTION

Biomolecular engineering encompasses broad attempts, born out of chemical engineering, to exert mechanistic control over living systems. The emphasis on understanding how emergent properties of macroscopic organisms, industrial bioprocesses, and ecosystems arise from nanoscale behaviors of biomolecules and complex fluids is largely a response to society's desires. Biomolecular engineers have been tapped to eradicate disease with rationally-designed biopharmaceuticals, breed microorganisms with the singular purpose of providing us usable energy, and author computer programs that simulate life to shortcut the need for experiments.

Biomolecular engineers are equipped with a growing set of tools for measuring and modifying the nanoscale basis of biology: the birth of “-omics” and computational informatics which can classify a wealth of new intensive data about cells; new gene-editing technologies including CRISPR<sup>1</sup> and gene delivery vectors;<sup>2;3</sup> a growing repertoire of logical elements and design motifs in synthetic biology;<sup>4</sup> and experimental platforms that expand the scale of questions that can be address *in vitro* from cells to tissues.<sup>5</sup> While the discipline of systems biology has provided the computational tools necessary process experimental data into holistic views of macroscopic biological systems for over a decade, the applied counterpart of systems biology – recently referred to as systems bioengineering – has only recently started to take shape.<sup>6</sup> In this dissertation, I will present two projects in which I contributed to the latter activity in biomolecular engineering: analyzing and designing biological systems that solve humanity's problems.

First, I will discuss my role in advancing our ability to simulate the growth of blood vessels. Blood vessels have a special importance in a chemical engineer's con-

ceptualization of the human body: the vascular system is the piping that connects our organs and the microfluidic circuitry that exchanges gases and nutrients the entire volume of our tissues. The vascular system is assembled by a developmental program whose complexity mirrors that which gives rise to our nervous system; vascular network formation will likely not be fully comprehensible to humans without the aid of computers. The creation of computational models that can recapitulate blood vessel formation is an ongoing challenge which involves both science (in the interplay between experiment and simulation) and engineering design (in formalizing biological hypotheses into mathematical constructs and defining the logical structures of the programs for maximum utility). In the section below, I will describe a sub-process within a sub-process of vascular network formation (“tip cell selection” within “angiogenesis”), I will summarize the progress and obstacles in modeling it and how I planned to contribute to the simulation – and larger theory – of this small component of the developmental program for the vascular system. My research in this area is contained in Chapters 2 – 4.

Next, I will describe a system which is biomolecular in a more abstract sense: the network of academic and industrial firms that are making human gene therapy a reality through innovations in biological manufacturing. Gene therapy, which involves biomolecules which can permanently alter a person’s gene expression, is rapidly advancing towards commercial use in the United States; in the US, over 1500 clinical trials have been opened, and hundreds have been completed. Gene therapies may hold the key to treating debilitating hereditary diseases such as hemophilia, ALS, and spinal muscular atrophy, provided that scientists and bioprocess engineers can work together to design vectors that effectively transport the genes into a patients cells and large-scale, cost-effective manufacturing process for those vectors. While the design of gene therapy vectors has improved drastically

over the last two decades, there are still hurdles facing their commercial production. As I will discuss in the section below and in Chapter 5, the cost of producing clinical-grade gene therapy vectors can range from the tens of thousands of dollars into the millions – there are few diseases for which such enormous costs can reasonably be borne by health care payers or pharmaceutical companies. I performed an analysis of the industry surrounding the manufacturing of a particular gene therapy vector – recombinant adeno-associated virus (AAV) – to understand what the barriers were to introducing new, cost-saving biological technologies into practical use, and I will present concepts for new businesses which could overcome those barriers to earn a sustainable profit while lowering costs for developers and patients of gene therapy. Understanding the values and behaviors governing human systems, whether networks of businesses or public spheres, represents a critical aspect of delivering on the promises of biomolecular engineering to address society’s needs and desires.

## 1.1 Modeling tip cell selection in angiogenesis

Sprouting angiogenesis builds new blood vessels in early development, wound healing, and tumor growth<sup>7</sup>. The process requires a population of endothelial cells to perform repeated cycles of collective differentiation and motion.<sup>8</sup> Continuing advancement of angiogenesis-related therapies<sup>9</sup>, methods for fabricating artificial tissues<sup>5;10;11</sup>, and our fundamental understanding of vascular development<sup>8</sup> depend on the ability to explain and predict the multicellular processes governing angiogenesis. Multiscale modeling has emerged as a primary tool that vascular biologists used to synthesize observations from experiment and results of simulating molecular and cellular sub-processes within angiogenesis.<sup>12;13</sup>

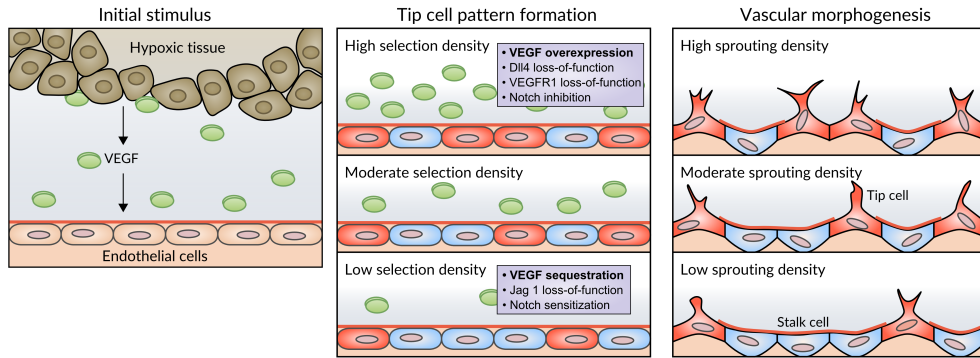


**Figure 1.1: Overview of tip cell pattern formation.** Overview of tip cell selection. Quiescent (gray) endothelial cells (ECs) are stimulated by VEGF (V) and other angiogenic factors, causing the ECs to differentiate into tip (red) and stalk (blue) endothelial cells. The density of tip cells in the resultant pattern is influenced by a number of molecular factors and determines the density of angiogenic sprouts that form<sup>13;17</sup>. Tip cell selection might occur in a two-dimensional endothelium (see Figure 3.2), or in a roughly one-dimensional array of cells (like on the leading edge of a growing vascular plexus)<sup>16</sup> as depicted here.

Many early attempts to control blood vessel growth looked for an on-off switch – molecular or biophysical stimuli that could halt or induce the formation of angiogenic sprouts.<sup>14</sup> However, some of our most potent angiogenesis inhibitors (such as the anti-VEGF therapeutic bevacizumab) have been most successful at reducing the density of vascular sprouting, as opposed to eliminating it altogether.<sup>15</sup> To explain how the density of sprouts is governed *in vivo*, many researchers have pointed to changes in the density of tip cell selection (Figure 1.1) prior to sprouting<sup>16;17</sup>.

Upon stimulation by vascular endothelial growth factor (VEGF) from nearby tissues, quiescent endothelial cells spontaneously differentiate into a heterogeneous pattern of cells with the competency to become either migratory tip cells or proliferative stalk cells. Given additional time, these tip- or stalk-competent cells will undergo morphological change to become the tips or stalks of new angiogenic sprouts.<sup>18</sup> The balance of tip cell selection – the number of tip cells selected and their levels of activity – is hypothesized to have significant impact on the structure

of the vasculature produced by angiogenesis, in particular, the number of vessel branching points and the length of each branch.<sup>17;19–21</sup> Critical to this balance, researchers have hypothesized, is a “central pattern generator” that determines how the endothelium enforces variability between neighboring endothelial cells to control the local density of tip cell formation.<sup>22</sup>

Tip cell *selection* is therefore a narrower concept than tip cell *formation*: the selection hypothesis states that endothelial cells do not differentiate into tip cells by virtue of being at the tip of a nascent sprout; rather, a spatial pattern of gene expression, causing tip cell differentiation in a fraction of endothelial cells, spontaneously emerges within the endothelium prior to the formation of sprouts. Prior to the widespread consideration of tip cell selection, multi-scale models of angiogenesis usually relied on biophysical phenomena similar to dendrite growth, where the frequency of branching was coupled to interplay between diffusion limitations (i.e., of VEGF) and the movement of a surface (i.e., due to cell migration in response to VEGF), to explain the formation of tip cells and new vascular sprouts.<sup>23</sup> As tip cell selection gained popularity, multi-scale models of angiogenesis increasingly attempted to couple tip cell (and sprout) formation to a mechanism of deliberate selection.<sup>12;24</sup>

As I will discuss in Chapter 3, researchers in the field of tip cell selection have nearly-unanimously agreed about the nature of that mechanism: simply put, tip cells use ligands for the Notch receptor to inhibit the formation of other tip cells in their immediate vicinity.<sup>16;19;25</sup> While this explanation aligns with experimental observation that Notch is important to tip cell formation and angiogenesis,<sup>17;25</sup> as previous computational studies<sup>26</sup> and my work (see Figure 3.5 show, the essential mechanism of this hypothesis – known as “lateral inhibition” – is extremely limited

in how it can select tip cells. In angiogenesis, the reliance on lateral inhibition as a means for selecting tip cells implies that (in theory) 50% of cells in the endothelium will attempt to lead a new sprout in response to angiogenic stimulus – not only does this fixed fraction conflict with observations that sprouting frequency changes in a variety of contexts, but 50% would appear to be a pathologically high number of tip cells according to past depictions in the literature.<sup>17;21;27</sup>

I foresee problems in the community forming such a strong consensus about the nature of a hypothetical process like tip cell selection – which must involve the dynamic regulation of multiple signaling pathways of which we have limited knowledge – so early in our attempts to understand angiogenesis. In Chapter 2, I will describe what I see as an ideal methodology for deciphering complex developmental processes like angiogenesis through multi-scale modeling: an approach that combines theory, optimization algorithms, and formal classification of multicellular structures to arrive at hypotheses of local, biomolecular mechanisms that best match global, tissue-scale experimental observations – this vision for the future is shared by many computational biologists.<sup>6;28</sup> However, I shall argue that even modeling approaches built around computational algorithms should search among sets of multiple biophysical hypotheses that capture the logic of how cells might interact. If a particular sub-process (e.g., tip cell selection) within a larger developmental program (e.g. angiogenesis) has only one hypothesis that might explain it (e.g., lateral inhibition), the entire multi-scale modeling effort might be constrained in how it can adapt to experimental observations. Indeed, computational biologists Palm, et al., who recently simulated angiogenesis, found that reliance on lateral inhibition as a means to dictate tip cell behaviors would have restricted them from exploring many questions about vascular growth; this group was able to simulate a wider range of realistic vascular morphologies by simply assuming

a predetermined tip cell fraction (ranging from 0% to 100%) than they could by modeling spontaneous tip cell selection via lateral inhibition.<sup>29</sup>

The possible trend, established by Palm, et al.,<sup>29</sup> of bypassing tip cell selection via reintroducing phenomenological rules for tip formation (such as a predetermined fraction) would, in my view, constitute a setback for the ultimate goal of understanding the mechanistic basis of angiogenesis; to avert this possibility, it was my goal to provide alternative hypotheses for the biophysical mechanisms underlying tip cell selection that might overcome the limited utility of lateral inhibition in future multi-scale modeling efforts. Having established this goal, the question arose how I would explicitly show that two mechanisms constituted two different hypotheses; in the proposed computational context, two models with superficial differences – the names of species or the values of parameters changed – would not necessarily be two separate hypotheses. One class of theories, I found, provided the ideal mathematical means to define and analyze the logical structure of hypothetical mechanisms for endothelial tip cell selection: biological pattern formation as described with principles of nonlinear dynamics.<sup>30</sup>

In Chapter 2, I will summarize key advances in the mathematics of biological pattern formation beginning with a seminal work by Alan Turing;<sup>31</sup> I will elaborate on my vision for future multi-scale modeling of developmental processes like angiogenesis using nonlinear dynamics as the theoretical foundation, but with a scope extended by algorithms that optimize the dynamical sub-models and classify experimental data. In Chapter 3, I provide additional details about the state of literature’s understanding about dynamical mechanisms that govern tip cells selection and might form a set of competing hypotheses in present multi-scale modeling efforts; I will use stability analysis and numerical simulation to argue why this set

of hypotheses, which is based on the conventional understanding of the couplings between endothelial Notch signaling and tip cell selection, is too limited to enable the computational approach I envision. In Chapter 4, I will take an unconventional look at the molecular mechanisms governing tip cell differentiation to identify possible sources of qualitatively new hypotheses for biological pattern formation; I will present two new hypothetical mechanisms for tip cell selection that can be used to guide experiments and compete with lateral inhibition in future multi-scale modeling efforts of angiogenesis.

## **1.2 Analyzing business opportunities in commercial gene therapy manufacturing**

Gene therapies are a new class of biopharmaceuticals that treat diseases by introducing genes, in the form of RNA or DNA, into a patients' cells to achieve desired biological activity. Many gene therapies deliver DNA that encodes for proteins that are otherwise absent or impaired in a patient as a result of hereditary disease. For example, some gene therapies under development can introduce genes for the Factor VIII blood clotting protein, restoring normal clotting function to patients with hemophilia A, who are deficient in the protein. In all gene therapies, the RNA or DNA must be introduced into the patient's cells by means of a vector: some clinical trials injected naked DNA into intramuscular tissue, perhaps aided by electroporation or "gene guns", but the majority of gene therapies – comprising nearly 70% of clinical trials to date – use recombinant viruses to infect cells with the target genes.

Gene therapies have the potential to permanently cure many disease that are

debilitating, lifelong, and extremely costly to treat with existing therapeutic options. Hemophilia A inflicts over 90,000 people worldwide, with an estimated 17,000 sufferers living within the United States. The cost of treating a patient with hemophilia A, which currently involves regular administration of recombinant Factor VIII and blood transfusions, averages \$162,000 per annum (or \$292,000 per annum for patients with a severe case);<sup>32</sup> in total, the United States spends roughly \$2.7 billion each year treating this disease. Gene therapy may be able to shrink the regular costs of hemophilia A: in July of 2016, clinical trials for a gene therapy called BMN-270 showed that a recombinant adeno-associated virus (AAV) containing the Factor VIII gene was able to restore activity of the clotting factor in patients with hemophilia A to as much as 60% of normal levels – this effect is expected to be lifelong, and to drastically reduce or eliminate the need for patients to continue protein replacement regimens.<sup>33</sup>

In spite of this clinical promise, a major problem faces the commercial viability of gene therapies: the manufacturing cost for recombinant viruses can be extraordinarily high. BMN-270 saw the strongest and most consistent results when it injected patients with doses of  $6 \times 10^{13}$  vg/kg (AAV particles, or “vector genomes”, per kilogram of patient bodyweight).<sup>33;34</sup> BMN-270 was produced in the baculovirus expression system (discussed in Chapter 5): one price listing for manufacturing of research-grade AAV using this system advertises that  $5 \times 10^{14}$  vg can be produced (without purification) at a cost of \$59,950.<sup>35</sup> Given a body mass for adult American of roughly 80 kg ( $\approx 175$  lbs), the cost of producing non-purified, research-grade AAV for a single patient using this manufacturing facility would be \$575,520; the true cost of manufacturing clinical materials may be much higher than this figure because clinical-grade manufacturing incurs much higher costs than research-grade manufacturing, the price quote does not include the cost

of purification, and purification can have yields of 10% (i.e., 90% of the AAV is lost between harvest and administration). My estimate, that clinical-grade production costs for AAV gene therapies can range into the millions of dollars per patient, is supported by the first gene therapy to ever win market approval in Europe: Glybera (discussed in Chapter 5) had a launch price of over \$1 million per treatment, and some experts speculate that this price merely broke even with the manufacturing cost of the AAV therapy.<sup>36</sup>

Several avenues exist for lowering the manufacturing cost of AAV gene therapies. Arguably the most ideal solution is to design gene therapy vectors that require lower doses to be effective; one recent trial by Spark Therapeutics raised activities of clotting Factor IX (deficient in patients with hemophilia B) using doses of only  $5 \times 10^{11}$  vg/kg.<sup>34</sup> All else being equal, one would estimate that manufacturing AAV for this treatment would cost in the tens of thousands of dollars per patient as opposed to millions. However, this low of a dose is unusual for AAV treatments that use intravenous or intramuscular injections – doses ranging from  $1 \times 10^{12}$  to  $1 \times 10^{14}$  vg/kg are more common; it remains to be seen if Spark can adapt its hemophilia B vector to a treatment targeting the much more prevalent hemophilia A.<sup>34</sup>

The other option, which might be universal to all AAV therapies and does not face the same limits as decreasing dosage through AAV vector design, is to reduce the manufacturing costs per viral particle. Manufacturing costs can be associated with purification and formulation of AAV drugs, or, as will be discussed in great detail in Chapter 5, these costs can arise from the raw demands of producing AAV particles in living cells. Chapter 5 will focus around how businesses that accelerate the adoption and improvement of new expression systems (in particu-

lar, the baculovirus expression system mentioned previously) for AAV production can reduce the costs of manufacturing for all gene therapies. The key challenge that I will address is not so much in demonstrating the technical performance of any expression system, but in analyzing and navigating the network of research institutions, startup companies, contractors, and investors that define the industry around AAV manufacturing so that I might define a path to introducing new technologies to these firms. Perhaps more-so than any other industry, the complexity of the biotechnology sector – as one researcher attempted to capture in Figure 1.2 – demanded a systematic approach to mapping out how these firms interact and perceive the value of new technologies.

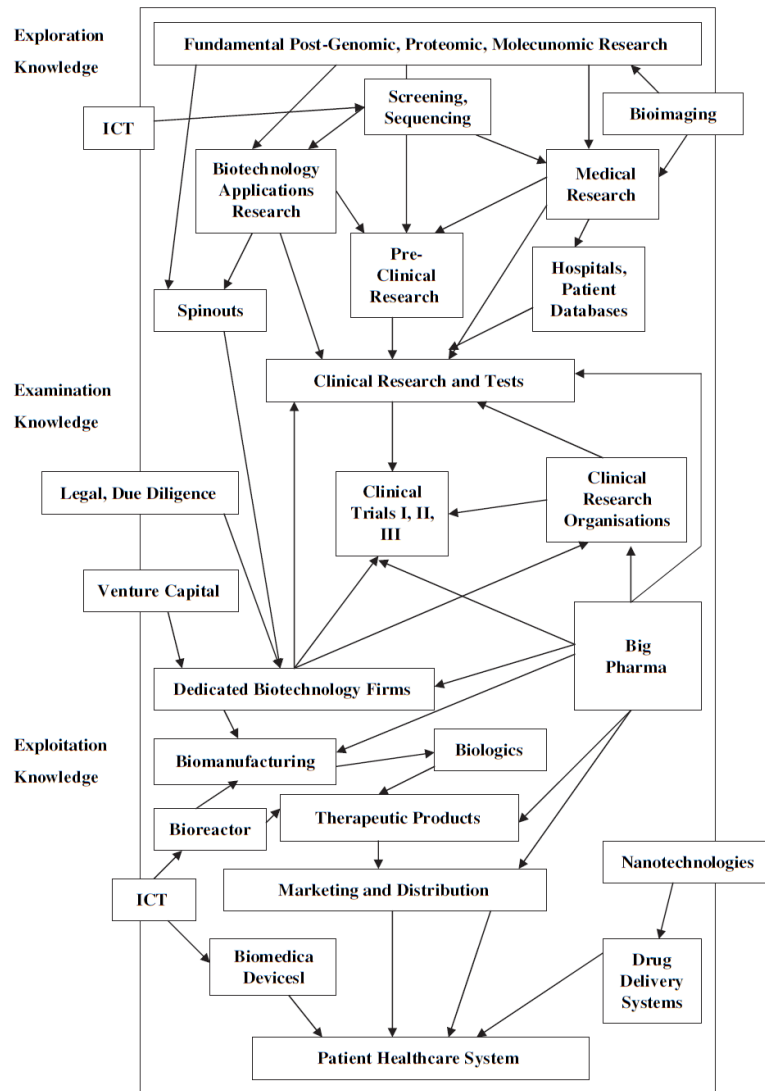


Figure 1.2: Bioscientific and biotechnological value chain. Reproduced with permission from Cooke, 2005.<sup>37</sup>

CHAPTER 2  
MODELING BIOLOGICAL PATTERN FORMATION

## 2.1 What is biological pattern formation?

The evolution of plants and animals was synonymous the evolution of biological development programs which could transform single-celled zygotes into organisms of immeasurable structural and functional complexity. During human embryogenesis, the fundamental nature of those developmental programs are not on display for the first four doublings of the zygote: at 3 to 4 days post-fertilization, the embryo is a roughly spherical clump of 16 undifferentiated cells, known as a morula, held together by adhesive forces. However, as time passes, the outer cells of the morula form tight gap junctions with each other and begin pumping sodium ions into the center of the 16-cell mass, creating an osmotic gradient that fills the center of the sphere with water. In creating the water-filled blastocyst, the outer cells of the morula achieve one of the principle feats of biological development: pattern formation, in which cells are able to infer and heterogeneously respond to their position within a tissue by sensing biophysical fields, such as chemical gradients or contact forces.

Pattern formation is relied on frequently and broadly during plant and animal development:

- Pattern formation frequently precedes *cellular differentiation*: the embryonic formation of somites blocks (multicellular precursors of connective tissues) is governed by an oscillating “molecular clock” of gene expression within each pre-somitic mesodermal cell; signaling by the Notch receptor synchronizes

those clocks to create a traveling wavefront of somite differentiation which allows neighboring cells to coordinate the “pinching off” or segmentation of each somite block.<sup>38</sup>

- Pattern formation can also allow the rate and orientation of *cell growth* to be predetermined: the formation of the *Arabidopsis* root vascular cylinder, which contains two phloem poles separated by a flat xylem, results from a pattern of gene expression which emerges in just four undifferentiated cells in the plant embryo; two cells become enriched in auxin and elongate as they divide to form the flat xylem, two cells become enriched in cytokinin and divide quickly and without polarizing to form the phloem poles.<sup>39</sup>
- Finally, patterning can have an impact on *morphogenesis*, the emergence of multicellular structures through directed cell migration and deformation: most refinement and reorganization of the circuitry of the mature central nervous system is performed by neuronal activity, but the formation of the earliest neuronal networks is governed by diffusible molecular species that direct the migration of neuronal growth cone; how the embryo establishes the patterns repulsive and attractive molecular cues which guide the growth cone to its proper destination remains a fundamental mystery in developmental biology.<sup>40–42</sup>

However, it is those three processes which couple to biological pattern formation – cell growth, cell differentiation, and morphogenesis – which make up the classical pillars of developmental biology. Rather than being a literal developmental process, pattern formation is a theory of multicellular behavior which is at times more generalized and abstract than the biomolecular and genetic machinery that executes it, but which must remain grounded in empirical biological fact. Put more bluntly, the field of pattern formation might be most accurately described

as a continuation of the work of Alan Turing towards understanding how spatial instabilities can lead to new structures in living systems.

## 2.2 Mathematical history of biological pattern formation

### Turing's unfinished machine

In 1952, Turing published a paper entitled “The chemical basis of morphogenesis”,<sup>31</sup> in which he hypothesized that common biological patterns – the spots on a leopard’s fur being the classic example – were the product of the diffusion and nonlinear reaction of biomolecules he dubbed “morphogens”. To demonstrate this phenomena, Turing created systems of partial differential equations that predicted the reaction and diffusion of two (or more) chemical species across a spatial domain. He proved the existence of pattern formation using linear stability analysis of these differential equations. First, Turing defined a steady-state in which the concentrations of each species was uniform across the spatial domain, and then linearized the governing equations about that uniform steady-state. By performing a spatial Fourier transform of the linearized equations, Turing showed that a uniform distribution of species across the domain could become conditionally unstable on certain spatial wavelengths, implying that any minor perturbation would create a trajectory of heterogeneous pattern formation – concentrations of each species would shrink or grow, depending on their position within the domain and the initial perturbation.

However, knowing that a linear stability analysis was only valid around the linearized point (in this case, the uniform steady-state), Turing completed his

analysis using a tool that few before him had access to: he used a computer to perform a numerical integration of the full, nonlinear governing equations and produced the first simulation of biological pattern formation. Although Turing was modest about claiming his model was biologically accurate, going so far as to claim “The theory does not make any new hypotheses”, he planned to follow up his 1952 study with a computational study of phyllotaxis – the process plants use to make spiral structures of leaves. Turing’s work in this area was unfinished before his tragic death in 1954.

## **Pattern formation on discrete cell lattices**

Some 20 years later, chemical engineers Othmer & Scriven revisited theoretical pattern formation in an attempt to simplify the arduous math that Turing used to predict spatial instabilities and provide additional biological realism by enabling analysis within spatial domains that more closely matched the cellular structure of tissues.<sup>43</sup> In particular, Othmer & Scriven devised a way of easily performing linear stability analysis in discretized lattices consisting of tiled, regular polygons. Their primary contributions to pattern formation were introducing the “connectivity matrix”, which formalizes the structure (or topology) of the cellular lattice, and deriving the “symmetry-adjusted Jacobian”, which allows the dynamics of the uniform steady-state –in reality a spectrum of trajectories– to be collapsed into a single matrix.

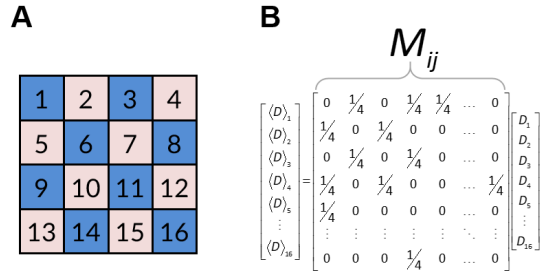


**Figure 2.1: The cell lattice and the connectivity matrix.** (A) A population of sixteen cells can be arranged into a  $4 \times 4$  grid with a periodic boundary condition. In a square grid (shown here), each cell contacts four neighbors. (B) The contacts formed by all sixteen cells can be formally defined with the connectivity matrix (also known as the “adjacency matrix” in graph theory<sup>44</sup>).

**The connectivity matrix**

The connectivity matrix formalizes how the concentration of a species in each cell impacts the concentration of species in neighboring cells. In Othmer & Scriven’s examples, the connectivity matrix acts as a discrete analog to the Laplacian; multiplying this connectivity matrix by a vector of concentrations for each cell produces a vector containing the difference in concentration for that species each has versus its neighbors (this is useful in calculating molar fluxes due to diffusive mass transport). However, as will be discussed in a later section, the connectivity matrix does not have to model diffusion; it can also produce the “average concentration” of a species contained within the neighbors of each cell. An example of a connectivity matrix which takes an average of concentrations in neighboring cells is given in Figure 2.1.

The connectivity matrix, being symmetrical, has real eigenvalues (called “structural eigenvalues”) and eigenvectors (called “structural eigenvectors”):

$$\mathbf{M}\mathbf{u}_k = q_k\mathbf{u}_k \tag{2.1}$$

where  $\mathbf{M}$  is the connectivity matrix,  $\mathbf{u}_k$  is an eigenvector of  $\mathbf{M}$ , and  $q_k$  is an eigen-

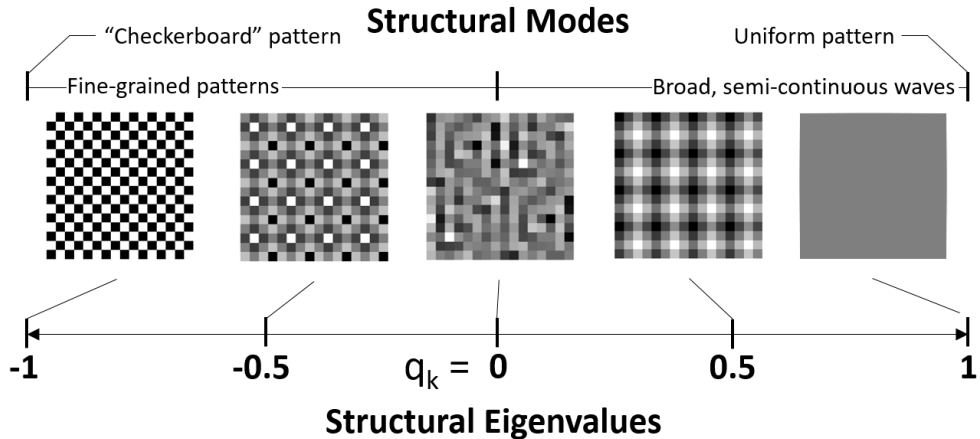


**Figure 2.2: The spectrum of the connectivity matrix.** The spectrum of the connectivity matrix for a  $16 \times 16$  square lattice, similar to that shown in Figure 2.1. The structural modes, or eigenvectors of the connectivity matrix, are shown as  $16 \times 16$  patterns. Any patterns which emerge during a pattern formation event on the square lattice will linear combinations of these eigenvectors. The structural eigenvalues (denoted  $q_k$ ) which correspond to those structural modes (eigenvectors) range from -1 to 1 for a square lattice.

value of  $\mathbf{M}$ . The structural modes ( $\mathbf{u}_k$ ) form a spectrum of spatial patterns (shown in Figure 2.2) with the smallest eigenvalues corresponding to short-wavelength patterns, and the largest eigenvalues corresponding to the longest-wavelength patterns.

### The symmetry-adjusted Jacobian

In a standard ODE-based formulation, linear stability analysis on discrete cell lattices would be a monumental challenge. The dynamics of the chemical species in all the cells are linked, meaning that a traditional Jacobian for the system would have to have  $n \times N$  entries, where  $n$  is the number of chemical species in the system and  $N$  is the number of cells – this matrix would be extremely difficult to analyze. To overcome this issue, Othmer & Scriven provided a derivation of a symmetry-adjusted Jacobian in cellular lattices, essentially generalizing the spatial “Fourier

series” that Turing used to give an exact prediction for pattern formation around a one-dimensional ring.

As in all Fourier transforms, the operator that gives rise to the wavelength (the Laplacian in a typical diffusion equation, or the connectivity matrix in our discrete problem) is replaced by its eigenvalue ( $k^2$  for the Laplacian, or  $q_k$  for the connectivity matrix) in the transformed Jacobian. The benefits of the symmetry-adjusted Jacobian are two-fold: the dynamics of the species on each structural mode are independent of the dynamics of the species on other structural modes, meaning that a  $n \times n$  Jacobian independently captures the dynamics of each structural mode; and the  $n \times n$  Jacobian of each structural mode differs only the value of corresponding structural eigenvalue. For symmetric connectivity matrices, which have real eigenvalues, a single determinant of an  $n \times n$  matrix provides a full, exact description of the stability of a uniform steady-state.

Othmer & Scriven further separated the symmetry-adjusted Jacobian into its intracellular, and signaling-dependent components, as demonstrated in the following equation for a system with two chemical species (A and B):

$$\mathbf{J}_k = \mathbf{K} + q_k \mathbf{D} = \begin{bmatrix} \frac{\partial A'}{\partial A} & \frac{\partial A'}{\partial B} \\ \frac{\partial B'}{\partial A} & \frac{\partial B'}{\partial B} \end{bmatrix} + q_k \begin{bmatrix} \frac{\partial A'}{\partial \langle A \rangle} & \frac{\partial A'}{\partial \langle B \rangle} \\ \frac{\partial B'}{\partial \langle A \rangle} & \frac{\partial B'}{\partial \langle B \rangle} \end{bmatrix} \quad (2.2)$$

where  $A'$  refers to the partial derivative  $\frac{\partial A}{\partial t}$  and  $\langle A \rangle$  refers to the average concentrations of species A in neighboring cells. Equation 2.2 is specific to systems where the connectivity which averages neighboring concentrations. It should be noted that at a uniform steady-state, neighboring concentration of all cells are equal, so  $\langle A \rangle = A$  when the partial derivatives are evaluated.

## Calculating initial trajectories

The symmetry-adjusted Jacobian in Equation 2.2 can be used to predict the early response of an almost-uniform initial condition to a initial perturbation (where the linearization still holds valid). Othmer & Scriven provide a formula for calculating this trajectory:

$$\mathbf{x}(t) = \sum_{k=1}^N \mathbf{u}_k \otimes e^{(\mathbf{K}+q_k\mathbf{D})t} \mathbf{y}_k^o \quad (2.3)$$

where  $\mathbf{x}(t)$  is the vector of concentration excursions (i.e.  $c_i(t) - c^o$ ) for all  $n$  species in  $N$  cells, the operator  $\otimes$  is an *ad hoc* product that organizes all species and all cells into a single vector (defined in Othmer & Scriven<sup>43</sup>), and  $\mathbf{y}_k^o$  is component of the initial perturbation on each structural mode.

## Stability criteria

Many mathematical biologists (incl. Turing, Othmer & Scriven) complete the linear stability analysis by calculating exact forms of the eigenvalues and eigenvectors of the connectivity matrix. The mathematicians substituted in the exact eigenvalues into the symmetry-adjusted Jacobians (Equation 2.2) to predict the dynamics of each structural mode as an exponential equation. The mathematicians substituted the exact eigenvectors, the exponential equations, and the initial perturbation into the trajectory equation (Equation 2.3) to see how each cell's concentration changes as a linear combination of the responses on each structural mode.

However, the stability of the uniform steady-state, and therefore the possibility of pattern formation, can be predicted directly from the determinant of the

symmetry-adjusted Jacobian:

$$|\mathbf{J}_k - \lambda_k \mathbf{I}| = 0 \tag{2.4}$$

where  $\lambda_k$  is the vector of  $n$  dynamic eigenvalues for each structural mode  $k$ ,  $\mathbf{I}$  is an  $n \times n$  identity matrix.

Solving for  $\lambda_k$  in Equation 2.4 can determine whether the uniform is stable (if all dynamic eigenvalues have negative real components), or unstable (if any dynamic eigenvalues have a positive real component). Because the symmetry-adjusted Jacobians for each structural mode are identical except for the value of the structural eigenvalue, exact criteria for stability on any structural mode can be derived from the following constraint:

$$\lambda_k > 0 \tag{2.5}$$

where  $\lambda_k$  is an algebraic function of  $q_k$ .

Broad trends, such as whether a pattern formation mechanisms generally favors short-wavelength or long-wavelength patterning trajectories, can be gathered directly from the criterion in Equation 2.5; this fact will be used extensively in Chapters 3 & 4 to predict the existence of a pattern-forming instability. While the full trajectory calculated from Equation 2.3 provides a more complete description of the dynamic response to a perturbation, nothing beyond the symmetry-adjusted Jacobian (Equation 2.2) and its determinant (Equation 2.4) is unique to the biomolecular system under examination. The structural eigenvectors and the general form of trajectory equation (except for the exponential term) are all derived from connectivity matrix, which is a formalization of the multicellular structure of the tissue – the connectivity matrix doesn't change all that much between problems. If it's necessary to actually predict the early stages of patterning, this can be done numerically.

## Juxtacrine pattern formation: Notch/Delta

<sup>26;45</sup> The work of both Turing and Othmer & Scriven largely assumed that information about chemical species would be transmitted across the domain using diffusion or other forms of mass transport.<sup>43</sup> However, the discretized cell lattices matured by Othmer & Scriven permitted another mode of relating chemical species between cells: juxtacrine signaling, in which the expression of a ligand in one cell could impact the reaction of a receptor in a neighboring cells, thereby allowing the transmission of information across the spatial domain to be independent of chemical gradients.

For a juxtacrine signaling process, the connectivity matrix cannot be an analog of the Laplacian operator, as in Othmer & Scriven, because ligands are not freely diffusing: cells use a receptor to sample the ligand concentration in neighboring cells, so a connectivity matrix which averages neighboring concentrations (provided in Figure 2.1) should be used. An example of pattern formation using this mechanism was given a theoretical treatment more than 20 years following Othmer & Scriven's work, in 1996, by Collier, et al.<sup>26</sup> Collier was inspired by the discovery of the Notch receptor, a protein which was expressed on the surface of cells in a huge variety of organisms and tissues, and was activated by Delta ligands expressed on neighboring cells (but not the same cell). Using the linear stability analysis which had become traditional in theoretical studies of biological pattern formation, Collier showed that if the activation of Notch in a cell would inhibit the expression of Delta in that same cell, an instability could be formed that resulted in a "checkerboard" pattern of cell enriched in Delta surrounded by cells depleted of Delta.

This mechanism is known as "lateral inhibition", as expression of Delta in one

cell has negative feedback on the expression of Delta, but only laterally – that is, the in neighboring cells. Lateral inhibition gained popularity as an explanation for “fine-grained patterns”, or instances where single cells within a tissue visibly differentiated from surrounded cells during development, in contexts that ranged from the “organization of bristles on the *Drosophila notum*”<sup>46</sup> to the sprouting of new blood vessels from existing vasculature during tumor growth<sup>17</sup>.

### **2.3 Future(s) of modeling pattern formation**

In the above sections, I reviewed many of the major developments in analyzing biological pattern formation in the Turing tradition up until about the year 2000. In the years following, a number of parallel paths have emerge which each apply the mathematical principles of pattern formation differently in attempts to understand developmental processes. Below, I will propose three archetypal approaches to modeling developmental processes which, together, are creating progress towards validation of Turing’s theory.

#### **Murray: Purist Turing model**

Some researchers, like James Murray, have dived head-first into translating biological systems into mathematical models that closely follow Turing’s original formalization.<sup>47</sup> Murray has modeled pattern formation in an vast number of subjects, ranging from population dynamics to neovascularization. His models are usually simple and are based on partial differential equations – much of the analysis can be done by hand; but he is fearless when it comes to incorporating new

biophysical phenomena – his hypothesized bases for pattern formation range from classic reaction-diffusion to mechanotransduction and neural networking. Murray rarely validates his model predictions directly against experiments, but rigorously explores the parameter space of his models to understand the different patterning regimes they might have. He also provides lengthy discussion about the biological context and acknowledges where his prediction agree or conflict with observations.

### **Sharpe: Algorithmic Turing model**

Others have adopted explored Turing pattern formation using a highly computerized approach. Raspopovic, et al., matched a simulated Turing system closely to experimental results by creating an optimization algorithm that could screen through a large set of different hypothetical reaction-diffusion networks and their parameter spaces.<sup>48</sup> The results were powerful: this group was able to simulate dynamic patterning on a growing (and constantly deforming) lattice to match time-series experiments of digit formation on a mouse foot. Their approach provides a rational way to infer biological mechanism from global outcomes when high-quality experimental data is available.

### **Krasnow: Hierarchical system of Turing models**

The third approach is to forgo mathematical analysis and simulation of individual instabilities and focus on a global understanding of how different pattern formation mechanisms combine with cell growth, differentiation, and morphogenesis in the development of whole organs. Mark Krasnow, published in Metzger, et al. (2008), approached branching morphogenesis more like a taxonomist than a math-

ematician: he identified key phenomenological “sub-processes” which are reused during fractal-like growth of the lung, such as domain branching (new orthogonal sprouting along an existing branch) and planar bifurcation (splitting of an existing branch at the tip), and collected large amounts of experimental data about the genes which controlled them.<sup>49</sup> The Krasnow group’s use of computers was limited to constructing diagrams, using image analysis and sorting algorithms, that trace the “lineage” of a mature branch in terms of the succession of branching sub-processes that assembled it. This type of analysis is helpful as a first step towards establishing formal descriptions of the global results that Turing instability-driven self-assembly events, or hierarchies of them, must achieve in conjunction with cell growth, differentiation, and morphogenesis – what might constitute an “objective function” for an algorithmic approach like that used by Raspopovic, et al.<sup>48</sup> Krasnow’s work might enable a rational, computerized approach to screening through biomolecular hypotheses of pattern formation within branching morphogenesis of the lung – a developmental process far more complex than the digit patterning studied in Raspopovic, et al.<sup>48</sup>

## **Next steps**

Each of these archetypal approaches to continuing the work of applying and validating the theory of biological pattern formation are powerful in their own respects. I can imagine a future where all three are employed to build multiscale models of organ development: the “pure” theorists providing sets of qualitatively new hypotheses for biophysical phenomena that might drive spatial instabilities, the “algorithmic” engineers planning the rational search among competing hypotheses that might best match experimental results, and the architects of the “hierarchical”

system providing the global objective function for the whole effort to match. However, the foundations for each of these approaches, especially those based around sophisticated algorithms, are still being built; a monolithic modeling effort which masters all three approaches has, to my knowledge, yet to be undertaken for any developmental process. I suspect that the near future for most questions about pattern formation in development holds piecemeal improvement along one of these lines at a time.

In the previous chapter, I provided a brief description of the field of angiogenesis – the outgrowth of new blood vessels from pre-existing vasculature – which involves a rich assortment of developmental processes, including cell growth, cell differentiation, and morphogenesis. Angiogenesis – along with sub-processes within it, such as tip cell selection – is frequently described using the language of biological pattern formation. In the following chapters, I will make the case that one of the archetypal lines for modeling development processes presented above, what I call the "purist" approach focused on mathematical analysis of new biophysical hypotheses for pattern formation, is the most underdeveloped dimension in analyzing tip cell selection. In Chapter 3, I will perform a Turing-like analysis of three hypotheses which most closely match the consensus understanding of tip cell selection, with the goal of explaining why the set of hypotheses is incomplete (e.g., for potential future "algorithmic" approaches to experimental validation). In Chapter 4, I will present two new hypotheses for the molecular mechanisms underlying tip cell pattern formation which demonstrate patterning behaviors that the previous hypotheses cannot – expanding the range of experimental observations that future "algorithmic" modeling efforts will be able to match.

CHAPTER 3  
ANALYZING EXISTING HYPOTHESES FOR TIP CELL  
SELECTION

### 3.1 Introduction

In the previous chapters, I introduced the concept of tip cell selection (Figure 1.1), summarized some of the present challenges in simulating tip cell selection within multi-scale models of angiogenesis, and proposed steps that can be taken to improve our efforts in this area. My proposal rests on two central theses: (1) that tip cell selection suffers from a lack of hypotheses regarding its essential mechanisms which have enough flexibility to adapt to experimental observations, and (2) that new hypotheses can be inductively reasoned from the literature which might be more useful in future multi-scale modeling efforts of angiogenesis. In this chapter, I will address the first thesis by formalizing hypotheses for the mechanisms of tip cell selection which mirror the consensus understanding that ‘Notch signaling is necessary and sufficient to explain how endothelial cells coordinate tip versus stalk fates in advance of angiogenic sprouting.’

Figure 3.1A illustrates the prevailing hypothesis for tip cell pattern formation, in which extracellular VEGF activates VEGF Receptor 2 (VEGFR2) and this activated receptor in turn up-regulates the expression of Delta-like ligand 4 (henceforth “Delta”). Delta activates the Notch receptor in adjacent endothelial cells, and active Notch down-regulates VEGFR2 expression. This network of signaling and gene regulation – cumulatively referred to as lateral inhibition – could allow nascent tip cells (as defined by their high activation level of VEGFR2 and expression of Delta) to prevent other tip cells from forming in their immediate

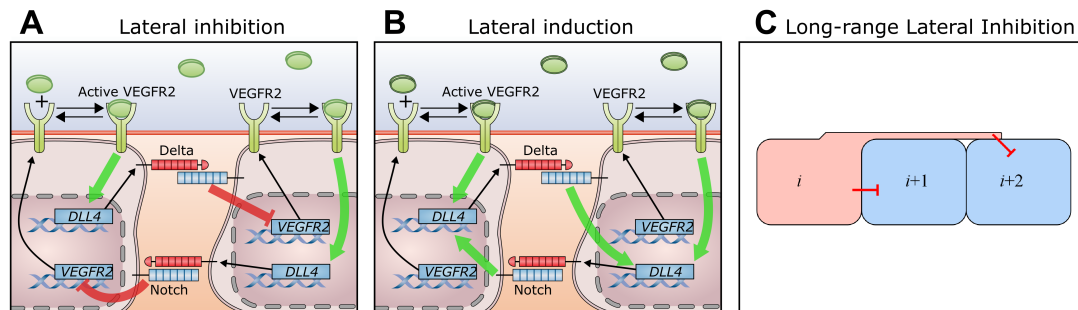


**Figure 3.1: Existing hypotheses of tip cell pattern formation.** (A) Diagram of tip cell lateral inhibition by Notch. The most common hypothesis for the mechanism behind tip cell pattern formation states that VEGFR2 activation by VEGF induces the expression of Delta, a ligand for neighboring Notch receptors. Notch activation reduces the expression of VEGFR2, such that cells with high VEGFR2 activation become tip cells and laterally inhibit their neighbors from doing the same<sup>16</sup>. (B) Diagram of tip cell lateral induction by Notch. An alternative hypothesis states that Notch activation promotes the expression of Delta, effectively causing cells with high VEGFR2 activation and Delta expression to induce high Delta expression in their neighbors<sup>50</sup>. (C) Diagram of long-range lateral inhibition. The network of signaling and gene regulation in this hypothesis are identical to lateral inhibition (A), but each cell ( $i$ ) is able to laterally inhibit second-nearest neighbors ( $i + 2$ ) via Delta-containing filopodia.

vicinity<sup>16</sup>. However, there is a body of evidence suggesting that endothelial cells engage in lateral induction (favoring the convergence of phenotypes) through Notch (Figure 3.1B) rather than lateral inhibition<sup>19;21;50</sup>. In addition, researchers in other contexts have suggested that filopodia (narrow extensions of the cell membrane), which tip cells produce, are essential to refining patterns during lateral inhibition (Figure 3.1C)<sup>46</sup>. The three hypotheses above – lateral inhibition, lateral induction, and long-range lateral inhibition – are all dependent on Notch signaling as the main driver of multicellular differentiation, and are therefore consistent with the existing body of literature on tip cell pattern formation.

The hypothesis of Notch-mediated lateral inhibition as the driver of tip cell formation dominates the existing literature on tip cell selection<sup>17;19;25</sup> and provided

the basis for previous solutions to modules of tip cell selection in prominent multi-scale simulations of angiogenesis<sup>12;51–53</sup>. Mathematicians have repeatedly demonstrated lateral inhibition is a robust mechanism for pattern formation, but it suffers from an inability to create anything other than the most dense patterns<sup>26;54;55</sup>. Indeed, previous simulations of tip cell formation have largely been unable to select variable densities of tip cells; most predict that only a “salt-and-pepper” pattern of 50% tip cells can be selected<sup>51</sup>, while others can only predict fewer than 50% tip cells being *globally* selected from an endothelium by limiting the area in which the “salt-and-pepper” patterns can *locally* form<sup>56</sup>. A major goal in understanding vascular morphogenesis is to predict how changes in the distribution of VEGF, for instance during anti-angiogenic treatment<sup>15</sup>, can increase or decrease vascular density following angiogenesis. In regards to this goal, the limited ability for lateral inhibition to locally form patterns other than 50% tip cells is problematic: the explanation that changes in the numbers of tip cells selected are responsible for the connection between VEGF distribution and angiogenic sprouting density<sup>19–21</sup> is dependent on the “central pattern generator” of tip cell selection<sup>22</sup> having multiple possible outcomes.

In this chapter, I translate three hypotheses for Notch-based tip cell selection drawn from the existing literature – lateral inhibition (Figure 3.1A), lateral induction (Figure 3.1B), and long-range lateral inhibition (Figure 3.1C) – into mathematical constructs to help understand whether these hypotheses can constitute “central pattern generating” mechanisms that can select tip cells at various densities, and why (or why not). I used these constructs, which consisted of systems of nonlinear ordinary differential equations (ODEs) to extract analytical, linear stability criteria for the onset of spontaneous differentiation and to simulate the full dynamics of tip cell pattern formation on uniform networks of endothe-

lial cells. In agreement with previous computational studies<sup>26;51;57</sup>, I found that lateral inhibition (Figure 3.1A) and lateral induction (Figure 3.1B) were fundamentally restrictive patterning mechanisms. For both of these mechanisms, parameter choices (such as VEGF concentration) could not finely control the local density of tip cell selection. Long-range lateral inhibition was able to select variable densities of tip cells depending on the strength of the long-range Notch signaling relative to close-range Notch signaling; however, the density of pattern formation did not respond to changes in VEGF concentration. This work elucidates the limitations of relying solely on Notch signaling to model multicellular cooperation during endothelial tip cell selection and provides clues for how to construct new hypotheses for the connections between molecular factors and vascular structures arising from angiogenesis. Chapter 4 discusses alternative hypotheses for the mechanisms underlying tip cell pattern formation, which don't rely solely on juxtacrine signaling through Notch to coordinate multicellular behaviors, and analyzes two newly proposed mechanisms that exhibit variable patterning density.

## 3.2 Methods

Tip cell selection (Figure 1.1A) is hypothesized to be a process by which a population of neighboring endothelial cells elect a subset of individuals to differentiate into filopodia-expressing tip cells. Tip cell selection can occur within a wall of a mature blood vessel (Figure 3.2A, left) or in a growing vascular plexus (Figure 3.2A, right); in both cases, the endothelium forms a 2D structure, with each endothelial cell having about four neighboring cells which make membrane contact. Experiments have shown that tip cells are selected among endothelial cells at regular intervals<sup>18;58</sup>, suggesting that selection is a process of biological pattern

formation (Figure 3.2B which triggers in response to external stimulation<sup>51;56</sup>.

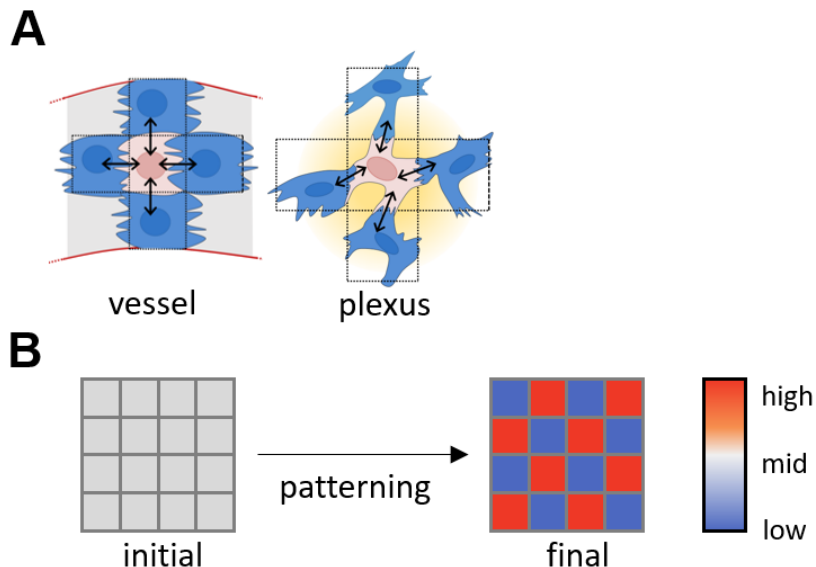


**Figure 3.2: Lattice and pattern formation of the endothelium.** (A) Cells in both the endothelium of a mature vessel (left) and the immature vascular plexus (right) are in contact with roughly four neighboring endothelial cells, so modeling endothelial cell networks as rectangular grids is appropriate from a connectivity perspective. (B) The endothelium is modeled as a two-dimensional lattice of cells which can exchange signals. I assume that each cell begins at the same concentration of each dynamic species, but that cells may differentiate into a spatial pattern of gene expression that corresponds to tip competency.

To analyze the formation of tip cell patterns, I model the endothelium as a set of  $N$  compartments, each of which represents an endothelial cell and the interstitial fluid space directly above it. Within each compartment,  $n$  relevant species participate in signaling processes of — and are dynamically regulated by — the local endothelial cell. The identities and governing dynamics of the relevant species varies with the tip cell differentiation mechanism under consideration. I tested each tip cell differentiation mechanism using two approaches, introduced in Chapter 2: (1) a theoretical framework based on linear stability analysis and (2) numerical simulation of the governing equations. In the following subsection, I will derive the nonlinear ordinary differential equations I hypothesize to govern the dynamics

of species in each of mechanism in Figure 3.1.

### 3.2.1 Governing equations

First, I will derive the governing equations for the lateral inhibition mechanism (Figure 3.1A) using the available knowledge about the responsible molecular mechanisms. I will use simplifying assumptions to reduce the number of equations to two, which clarifies subsequent analyses. I will generate the governing equations for the subsequent mechanisms, lateral induction and long-range lateral inhibition, by reconfiguring the equations for lateral inhibition – not by repeating a full derivation.

#### Derivation of governing equations for lateral inhibition

The reaction network underling lateral inhibition (Figure 3.1A) consists of four species: VEGFR2 (R), the Delta ligand (D), VEGF (V), and the Notch receptor (N)<sup>52</sup>. Here, we will give a general description of how these four species interact, but we can not offer a complete, stoichiometric reaction network which contains all protein and nucleic acid intermediates, because they are not currently known in full detail<sup>13</sup>.

Lateral inhibition requires VEGF to be present<sup>52</sup>. In this hypothesis, VEGF (V) interacts with VEGFR2 to form activated VEGFR2 complexes ( $R_A$ ) in a reversible reaction, represented by the following ODE for the concentration of  $R_A$  in cell  $i$ :

$$\frac{dR_{Ai}}{t} = k_{on}V_iR_i^* - k_{off}R_{Ai} \quad (3.1)$$

where  $k_{\text{on}}$  is the forward rate constant and  $k_{\text{off}}$  is the reverse rate constant.  $R_i^*$  denotes the concentration of unbound VEGFR2 in cell  $i$ , which together with activated VEGFR2, comprises the total VEGFR2 in each cell ( $R_i$ ),

$$R_i = R_i^* + R_{Ai} \quad (3.2)$$

Activated VEGFR2 complexes, through some downstream action, promote the expression of Delta ligand,

$$\frac{dD_i}{dt} = \beta_D \frac{(R_{Ai})^{n_D}}{(K_D)^{n_D} + (R_{Ai})^{n_D}} - \gamma_D D_i \quad (3.3)$$

where  $\beta_D$  is the maximum production rate of Delta,  $K_D$  is the dissociation constant of the regulatory interaction (i.e., the concentration of  $R_A$  at 1/2 maximum Delta production), and  $\gamma_D$  is the first-order decay rate of Delta ligand.

The parameter  $n_D$  is referred to as the cooperativity<sup>45</sup>, and it models the steepness of the regulatory interaction. Delta converts Notch (N) to activated Notch ( $N_A$ ) on neighboring endothelial cells,

$$\frac{dN_{Ai}}{t} = k_n N_i \langle D \rangle_i - \gamma_N N_{Ai} \quad (3.4)$$

where  $\langle D \rangle_i$  is the average concentration of Delta in cells neighboring cell  $i$ ,  $k_N$  is the reaction rate constant, and  $\gamma_N$  is the decay rate of activated Notch.

Activated Notch down-regulates the expression of VEGFR2,

$$\frac{dR_i}{dt} = \beta_R \frac{(K_R)^{n_R}}{(K_R)^{n_R} + (N_{Ai})^{n_R}} - \gamma_R R_i \quad (3.5)$$

where the parameters follow the conventions established in Equation 3.3.

Equations 3.1 & 3.4 represent signaling processes, while Equations 3.3 & 3.5 represent changes in gene expression as the cell responds to signaling cues. As such,

we can assume that Equations 3.1 & 3.4 occur on a much faster time scale than Equations 3.3 and 3.5, allowing us to make a quasi-steady-state approximation for species  $R_A$  and  $N_A$ ,

$$\frac{dN_{Ai}}{t} = 0 \rightarrow N_{Ai} = k_N \langle D \rangle_i \quad (3.6)$$

where  $k_N = \frac{k_n N_i}{\gamma_N}$ .

The quasi-state-state of activated VEGFR2 can be found similarly,

$$\frac{dR_{Ai}}{t} = k_{on} V_i (R_i - R_{Ai}) - k_{off} R_{Ai} = 0 \rightarrow R_{Ai} = \frac{V_i}{K_V + V_i} R_i \quad (3.7)$$

where  $K_V = \frac{k_{off}}{k_{on}}$ .

These quasi-steady-state concentrations can be substituted into Equations 3.3 & 3.5 to arrive at our final governing equations for R and D, as given in the next section.

### Lateral inhibition

I model the dynamics of VEGFR2 and Delta in the lateral inhibition mechanism (see Figure 3.1A) using the following equations:

$$\frac{dR_i}{dt} = \beta_R \frac{(K_R)^{n_R}}{(K_R)^{n_R} + (k_N \langle D \rangle_i)^{n_R}} - \gamma_R R_i \quad (3.8)$$

$$\frac{dD_i}{dt} = \beta_D \frac{\left(\frac{V_i}{K_V + V_i} R_i\right)^{n_D}}{(K_D)^{n_D} + \left(\frac{V_i}{K_V + V_i} R_i\right)^{n_D}} - \gamma_D D_i \quad (3.9)$$

Equations 3.8 & 3.9 model a mode of endothelial gene regulation in which Notch activation represses the expression of Delta via downregulation of VEGFR2 (see Figure 3.1A). Here,  $R_i$ ,  $D_i$ , and  $V_i$  refer to the concentrations of VEGFR2,

Delta, and VEGF in cell  $i$ .  $\langle D_i \rangle$  refers to the average concentration of Delta in the cells neighboring cell  $i$ . The kinetic parameters used in Equations 3.8 & 3.9 can be interpreted as follows:

- $\beta_R, \beta_D$ : maximum production rates of VEGFR2 and Delta.
- $K_R, K_D, K_V$ : dissociation constants of VEGFR2 gene regulation, Delta gene regulation, and VEGF-VEGFR2 signaling, respectively.
- $n_R, n_D$ : Hill coefficients for VEGFR2 and Delta gene regulation.
- $\gamma_R, \gamma_D$ : first-order degradation rates of VEGFR2 and Delta.

### Lateral induction

I assumed lateral induction (see Figure 3.1B) to differ from lateral inhibition only in the gene regulatory action of Notch: Notch signaling should up-regulate Delta rather than down-regulating VEGFR2.

I adapted Equations 3.8 & 3.9 to lateral induction by removing a Hill function from the governing equation for VEGFR2 and adding one to the governing equation for Delta. I model the dynamics of VEGFR2 and Delta in the lateral induction mechanism using the following equations:

$$\frac{dR_i}{dt} = \alpha_R - \gamma_R R_i \quad (3.10)$$

$$\frac{dD_i}{dt} = \alpha_D \frac{\left(\frac{V_i}{K_V + V_i} R_i\right)^{n_R}}{(K_R)^{n_R} + \left(\frac{V_i}{K_V + V_i} R_i\right)^{n_R}} + \beta_D \frac{(k_N \langle D \rangle_i)^{n_D}}{(K_N)^{n_D} + (k_N \langle D \rangle_i)^{n_D}} - \gamma_D D_i \quad (3.11)$$

Equations 3.10 & 3.11 model a mode of endothelial signaling where Notch activation directly increases the expression of Delta. Here,  $\alpha_R$  refers to the constant

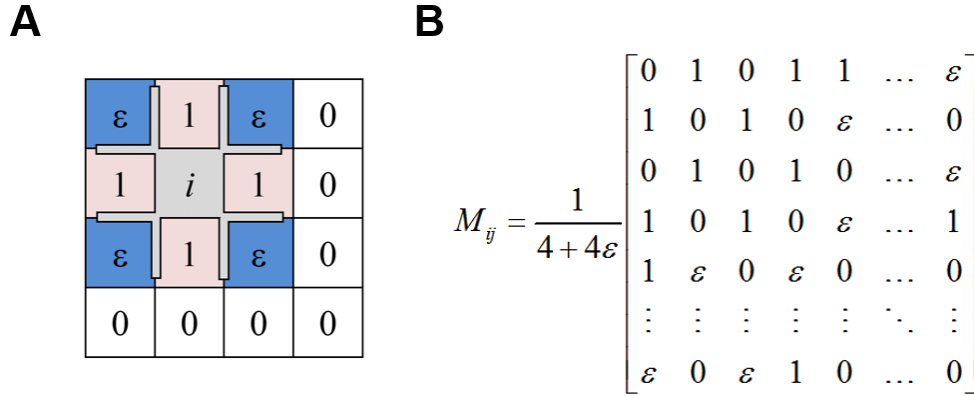


**Figure 3.3: Lattice and connectivity matrix for long-range mechanism.** (A) Long-range cell lattice. Long-range cellular structures, such as EC filopodia, may extend the reach of the cell membrane to non-nearest neighbors in a geometric lattice<sup>46</sup>. I modeled this by allowing second-nearest neighbors to have a degree of membrane contact scaled to the parameter  $\varepsilon$  (versus nearest-neighbors signaling with strength 1). (B) Long-range connectivity matrix. The connectivity matrix is modified to include long-range interactions by adding  $\varepsilon$  into each row four times. The matrix must be normalized to assure each row sums to unity.

production rate of VEGFR2, and  $\alpha_D$  and  $\beta_D$  refer to the production rates of Delta that are attenuated by VEGFR2 and Notch signaling, respectively.

### Long-range lateral inhibition

In long-range lateral inhibition (see Figure 3.1C), each endothelial cell can exchange Delta ligand with second-nearest neighbors using filopodia, as depicted in Figure 3.3A. While this is a slightly inaccurate representation of filopodia, because they are not hypothesized to exist until *after* tip cells have formed, I hypothesized this formalization would be suitable to understand the basics of how long-range signaling impacts pattern formation. A study by Cohen, et al.<sup>46</sup> might simulate pattern formation more accurately, only allowing filopodia to facilitate juxtacrine signaling after an initial patterning phase.

The governing equations of this mechanism are identical to those of lateral inhibition (Equations 3.8 & 3.9), but with a change to how neighboring Delta concentrations ( $\langle D_i \rangle$ ) are calculated. Neighboring Delta concentrations are calculated in this mechanism by the following equation:

$$\langle D \rangle_i = \frac{\sum_{1^\circ} D_j + \varepsilon \sum_{2^\circ} D_j}{n_{1^\circ} + \varepsilon n_{2^\circ}} \quad (3.12)$$

where  $1^\circ$  refers to nearest-neighbor cells of cell  $i$ ,  $2^\circ$  refers to second-nearest-neighbor cells of cell  $i$ ,  $n$  refers to the total number of cells which are neighbors of each type,  $\varepsilon$  is a factor which controls the relative strength of second-nearest-neighbor versus nearest-neighbor signaling. This alternate definition for calculating neighboring Delta concentration is captured in the connectivity matrix that is unique to this mechanisms, shown in Figure 3.3B. When  $\varepsilon = 0$ , Equation 3.12 becomes a simple average of nearest-neighbor cells, and the long-range lateral inhibition mechanism is identical to the standard lateral inhibition mechanism.

### 3.2.2 Identification of steady-states

Before I could perform a linear stability analysis or simulation of each mechanism, I needed to calculate the steady-states which would provide an initial condition from which to investigate spontaneous pattern formation. This uniform initial condition would represent an endothelium of a blood vessel which has recently been exposed to angiogenic stimulus, which is typically hypothesized to exist prior to tip cell selection<sup>19</sup>. Calculating these steady-states was not trivial because of the concentration of each species in each cell were coupled. Rather than calculating these concentrations using the whole lattice, I used a two-cell model to identify uniform steady-states, as depicted in Figure 3.4.

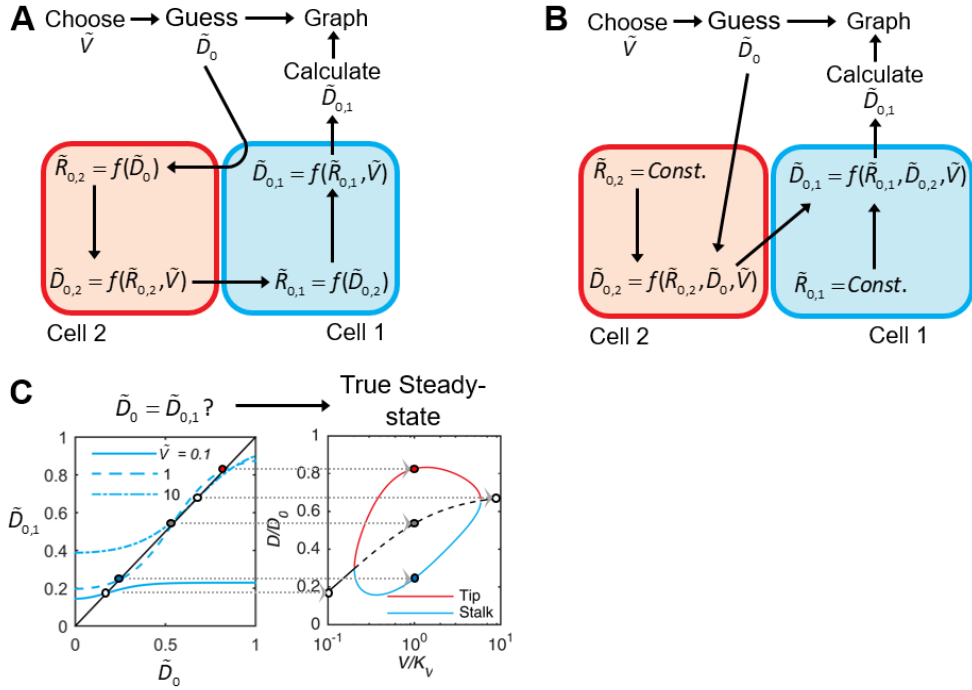


**Figure 3.4: Two-cell models for calculating steady-states.** (A) Generating partial steady-states for lateral inhibition. I found the partial steady-states for the lateral inhibition hypothesis by “opening the loop” at the concentration of Delta in “Cell 1”. For each imposed concentration of VEGF ( $\tilde{V}$ ), I calculated a vector of concentrations for Delta in Cell 1 ( $\tilde{D}_{0,1}$ ) using a vector of guessed concentrations for Delta in Cell 1 ( $\tilde{D}_0$ ). The non-dimensional governing equations of lateral inhibition, Equations 3.16 & 3.15, were used for calculations. (B) Generating partial steady-states for lateral induction. A similar process was used to that shown in (A), except that I calculated the concentration of VEGFR2 directly from model parameters. The non-dimensional governing equations of lateral induction, Equations 3.24 & 3.25, were used for calculations. (C) Graphing steady-states for lateral inhibition. True steady-states occur when the  $\tilde{D}_{0,1} = \tilde{D}_0$  in a partial steady-state. For each partial steady-state curve (left) corresponding to an imposed concentration of VEGF ( $\tilde{V}$ ), I graphed the vector of  $\tilde{D}_{0,1}$  against the vector of  $\tilde{D}_0$ . True steady-states exist where each curve intersects the black line. I could predict if a particular imposed VEGF concentration would a tip-stalk pattern depending on whether its curve of partial steady-states intersect the black line one (no patterning predicted) or three (patterning predicted) times. I plotted the uniform steady-states, tip cell states, and stalk cell states for each imposed concentration of VEGF to create the figure on the right. Parameter values are given in Table 3.1.

I used the non-dimensional forms of the governing equations for lateral inhibition and lateral induction (defined in Equations 3.16 & 3.15 and Equations 3.24 & 3.25 below).

Figure 3.4A provides the path I used to calculate *partial* steady-states of lateral inhibition, which I define as steady-states that exist when all the ODEs in the governing equations have been set to zero, but there is an “open loop”. In other words, a certain concentration (in this case the concentration of Delta in “Cell 1”) is allowed to have two values. Figure 3.4B provides a similar path used to calculate partial steady-states for lateral induction.

Figure 3.4C demonstrates how these partial steady-states can be used to calculate the true steady-states of the system, as provided in Figure 3.5B: a partial steady-state is a true steady-state when the concentrations at the point of the “open loop” (again, Delta in “Cell 1”) are equal. The loop can “close” if there is a uniform steady-state (which could form an initial condition for patterning) or if there is a heterogeneous pattern (which could be a final steady-state following pattern formation). Figure 3.4C is specific to lateral inhibition, but a comparable technique was used to calculate the true steady-states shown in Figure 3.6B for lateral induction. The initial conditions for the long-range lateral inhibition mechanism were found using the same technique I used for standard lateral inhibition, albeit with different parameters

### 3.2.3 Linear stability analysis

I predicted the early stages of tip cell differentiation from the quiescent endothelium (Figure 1.1A) using the method of linear stability analysis in discrete cell lattices,

as described in Chapter 2. This method is best performed by substituting any “neighboring concentrations” (e.g.,  $\langle D \rangle_i$ ) found in Equations 3.8-4.31 with

$$\langle C \rangle_i = M_{ij}C_j, \quad (3.13)$$

where matrix  $\mathbf{M}$  is referred to as the connectivity matrix.

I describe the eigenvalues of  $\mathbf{M}$ , denoted  $q_k$  (where  $k = 1, 2, 3, \dots, N$ ), as the structural eigenvalues; the values of the elements in  $q_k$  range from -1 to 1 for a square lattice (see Figure 2.2). Each structural eigenvalue corresponds to a *structural mode* (an eigenvector of  $\mathbf{M}$ ), which defines a spatial pattern of gene expression that can grow or shrink in the endothelium. Smaller values of  $q_k$  (i.e.,  $q_k \rightarrow -1$ ) correspond to short-wavelength patterns (e.g., an alternating “salt-and-pepper” when  $q_k = -1$ ), while larger values of  $q_k$  (i.e.,  $q_k \rightarrow 1$ ) correspond to long-wavelength patterns (e.g., completely uniform when  $q_k = 1$ ).

Following the substitution given by Equation 3.13, the first-order dynamics governing the expression of all species in all cells collapse into a set of  $N$  independent symmetry-adjusted Jacobian matrices ( $\mathbf{J}_k$ ) which can be used to calculate the dynamic eigenvalues ( $\lambda_k$ ) of a uniform steady-state using the Jacobian determinant:

$$|\mathbf{J}_k(q_k) - \lambda_k \mathbf{I}| = 0 \quad (3.14)$$

where  $\lambda_k$  is the vector of dynamic eigenvalues the  $N$  structural modes, and  $\mathbf{I}$  is an  $n \times n$  identity matrix. The system is unstable if any  $\lambda_k$  is positive. Each Jacobian matrix  $\mathbf{J}_k$  is a function of one scalar element of  $q_k$ , such that the stability of each steady-state varies with the structural mode. Given any minor perturbation (e.g., minor differences in protein concentration between neighboring cells), spatial patterns of gene expression will begin to emerge within the endothelium for those structural modes which are unstable.

I derive exact *stability criteria* (e.g., Equation 3.33) for each mechanism from Equation 3.14 that hold true for all possible values of the kinetic parameters appearing in the governing equations.

### Stability analysis for lateral inhibition

The governing equations for lateral inhibition (Equations 3.8 & 3.9) were nondimensionalized into the following two ODEs:

$$\frac{d\tilde{D}_i}{d\tilde{t}} = \tau \frac{\left(\frac{\tilde{R}_i \tilde{V}_i}{1+\tilde{V}_i}\right)^{n_D}}{(\kappa_D)^{n_D} + \left(\frac{\tilde{R}_i \tilde{V}_i}{1+\tilde{V}_i}\right)^{n_D}} - \tau \tilde{D}_i = \tilde{D}' \quad (3.15)$$

$$\frac{d\tilde{R}_i}{d\tilde{t}} = \frac{1}{1 + \left(\kappa_R M_{ij} \tilde{D}_j\right)^{n_R}} - \tilde{R}_i = \tilde{R}' \quad (3.16)$$

where  $\tilde{R}_i = \frac{R_i \gamma_R}{\beta_R}$ ,  $\tilde{D}_i = \frac{D_i \gamma_D}{\beta_D}$ ,  $\tilde{V}_i = \frac{V_i}{K_V}$ ,  $\tilde{t} = t \gamma_R$ ,  $\kappa_R = \frac{k_N \beta_D}{K_R \gamma_D}$ ,  $\kappa_D = \frac{K_D \gamma_R}{k_V \beta_R}$ , and  $\tau = \frac{\gamma_D}{\gamma_R}$ . All the parameters and dependent in these equations are without units.

The symmetry-adjusted Jacobian<sup>43</sup> for lateral inhibition, using the dimensionless form of the governing equations (Equations 3.15 & 3.16), is

$$\mathbf{J}_k = \begin{bmatrix} \frac{\partial \tilde{R}'}{\partial \tilde{R}} & \frac{\partial \tilde{R}'}{\partial \langle \tilde{D} \rangle} q_k \\ \frac{\partial \tilde{D}'}{\partial \tilde{R}} & \frac{\partial \tilde{D}'}{\partial \tilde{D}} \end{bmatrix} = \begin{bmatrix} -1 & -\frac{1}{\tilde{D}_0} g_R q_k \\ \frac{1}{\tilde{R}_0} \tau g_D & -\tau \end{bmatrix} \quad (3.17)$$

where

$$g_R = \frac{n_R (\kappa_R)^{n_R} \left(\tilde{D}_0\right)^{n_R}}{\left[(\kappa_R)^{n_R} + \left(\tilde{D}_0\right)^{n_R}\right]^2} \quad (3.18)$$

$$g_D = \frac{n_D (\kappa_D)^{n_D} \left(\tilde{R}_{A0}\right)^{n_D}}{\left[(\kappa_D)^{n_D} + \left(\tilde{R}_{A0}\right)^{n_D}\right]^2} \quad (3.19)$$

$$\tilde{R}_{A0} = \frac{\tilde{R}_0 \tilde{V}}{1 + \tilde{V}} \quad (3.20)$$

$$\tilde{D}_0 = \frac{\left(\tilde{R}_{A0}\right)^{n_D}}{\left(\kappa_D\right)^{n_D} + \left(\tilde{R}_{A0}\right)^{n_D}} \quad (3.21)$$

$$\tilde{R}_0 = \frac{\left(\kappa_R\right)^{n_R}}{\left(\kappa_R\right)^{n_R} + \left(\tilde{D}_0\right)^{n_R}} \quad (3.22)$$

The values  $\tilde{R}_0$  and  $\tilde{D}_0$  refer to the uniform, dimensionless, initial concentration of VEGFR2 and Delta. The Jacobian for each structural eigenvalue of  $q_k$  is independent, meaning the dynamic eigenvalues ( $\lambda_k$ ) for each structural mode can be found independently. Obtaining a polynomial for the dynamic eigenvalues of the Jacobian using the equation  $|\mathbf{J}_k - \lambda_k \mathbf{I}| = 0$  and applying the Routh-Hurwitz stability theorem<sup>59</sup> for said polynomial yields the following inequality:

$$q_k n_R n_D \frac{\left(\kappa_D\right)^{n_D}}{\left[\left(\kappa_D\right)^{n_D} + \left(\tilde{R}_{A0}\right)^{n_D}\right]} \frac{\left(\tilde{D}_0\right)^{n_R}}{\left[\left(\kappa_R\right)^{n_R} + \left(\tilde{D}_0\right)^{n_R}\right]} + 1 > 0 \quad (3.23)$$

When the inequality is true, the system is stable. When it is not true, the system is unstable. Because all terms of the left-hand side are positive with the exception of the structural eigenvalues  $q_k$ , the inequality can only be violated for negative values of  $q_k$ . Because the left-hand side of the inequality is monotonic with respect to  $q_k$ , the system will be unstable if-and-only-if the smallest structural eigenvalue (corresponding to the “salt-and-pepper” structural mode) is unstable.

## Stability analysis for lateral induction

The governing equations for lateral induction (Equations 3.10 & 3.11) were nondimensionalized into the following two ODEs:

$$\frac{d\tilde{R}_i}{d\tilde{t}} = \tau (1 - \tilde{R}_i) = \tilde{R}' \quad (3.24)$$

$$\frac{d\tilde{D}_i}{d\tilde{t}} = a \frac{\left(\frac{\tilde{R}_i \tilde{V}_i}{1 + \tilde{V}_i}\right)^{n_R}}{(\kappa_R)^{n_R} + \left(\frac{\tilde{R}_i \tilde{V}_i}{1 + \tilde{V}_i}\right)^{n_R}} + \frac{\left(M_{ij} \tilde{D}_j\right)^{n_N}}{(\kappa_N)^{n_N} + \left(M_{ij} \tilde{D}_j\right)^{n_N}} - \tilde{D}_i = \tilde{D}' \quad (3.25)$$

where  $\tilde{R}_i = \frac{R_i \gamma_R}{\alpha_R}$ ,  $\tilde{D}_i = \frac{D_i \gamma_D}{\beta_D}$ ,  $\tilde{V}_i = \frac{V_i}{K_V}$ ,  $\tilde{t} = t \gamma_D$ ,  $a = \frac{\alpha_D}{\beta_D}$ ,  $\kappa_R = \frac{K_R \gamma_R}{k_V \alpha_R}$ ,  $\kappa_N = \frac{K_N \gamma_D}{k_N \beta_D}$ , and  $\tau = \frac{\gamma_R}{\gamma_D}$ .

The symmetry-adjusted Jacobian<sup>43</sup> for lateral induction, using the dimensionless form of the governing equations, is

$$\mathbf{J}_k = \begin{bmatrix} \frac{\partial \tilde{R}'}{\partial \tilde{R}} & 0 \\ \frac{\partial \tilde{D}'}{\partial \tilde{R}} & \frac{\partial \tilde{D}'}{\partial \tilde{D}} + \frac{\partial \tilde{D}'}{\partial \langle \tilde{D} \rangle} q_k \end{bmatrix} = \begin{bmatrix} -\tau & 0 \\ \frac{a}{\tilde{R}_0} g_R & -1 + \frac{1}{\tilde{D}_0} g_N q_k \end{bmatrix} \quad (3.26)$$

where

$$g_R = \frac{n_R (\kappa_R)^{n_R} \left(\tilde{R}_{A0}\right)^{n_R}}{\left[(\kappa_R)^{n_R} + \left(\tilde{R}_{A0}\right)^{n_R}\right]^2} \quad (3.27)$$

$$g_N = \frac{n_N (\kappa_N)^{n_N} \left(\tilde{D}_0\right)^{n_N}}{\left[(\kappa_N)^{n_N} + \left(\tilde{D}_0\right)^{n_N}\right]^2} \quad (3.28)$$

$$\tilde{R}_{A0} = \frac{\tilde{R}_0 \tilde{V}}{1 + \tilde{V}} \quad (3.29)$$

$$\tilde{D}_0 = a \frac{\left(\tilde{R}_{A0}\right)^{n_D}}{(\kappa_D)^{n_D} + \left(\tilde{R}_{A0}\right)^{n_D}} + \frac{\left(\tilde{D}_0\right)^{n_N}}{(\kappa_N)^{n_N} + \left(\tilde{D}_0\right)^{n_N}} \quad (3.30)$$

$$\tilde{R}_0 = 1 \tag{3.31}$$

Obtaining a polynomial for the eigenvalues of the Jacobian using the equation  $|\mathbf{J}_k - \lambda_k \mathbf{I}| = 0$  and applying the Routh-Hurwitz stability theorem<sup>59</sup> yields the following inequality:

$$-q_k \frac{n_N (\kappa_N)^{n_N} (\tilde{D}_0)^{n_N-1}}{\left[ (\kappa_N)^{n_N} + (\tilde{D}_0)^{n_N} \right]^2} + 1 > 0 \tag{3.32}$$

Because all terms of the left-hand side of Equation 3.32 are positive with the exception of the structural eigenvalues ( $q_k$ ), the inequality can only be violated for positive values of  $q_k$ . Because the left-hand side of the inequality is monotonic with respect to  $q_k$ , the system will be unstable if-and-only-if the largest structural eigenvalue (corresponding to uniform differentiation across the lattice) is unstable.

### Stability analysis for long-range lateral inhibition

The governing equations for long-range lateral inhibition are identical to those of standard lateral inhibition (Equations 3.8 & 3.9), so a separate linear stability analysis was not necessary. Rather, the difference in stability between the two mechanisms is captured in the connectivity matrix, as shown in Figure 3.3B. A parameter  $\varepsilon$  is introduced to control the strength of second-nearest neighbor signaling (while nearest-neighbor signaling has a strength fixed at 1).

#### 3.2.4 Numerical simulation

I simulated each mechanism in dimensionless form (e.g., Equations 3.16 & 3.15) in MATLAB using the ode45 numerical integrator. Unless otherwise noted, I assumed

endothelial cells to form a square lattice (Figure 3.2A)<sup>45;56</sup>.

I provide values for kinetic parameters in Table 3.1. These parameters were not extracted from previous experimental or computational literature, as there is little known about the quantitative changes in gene expression for each species in response to a continuously varying inputs; experiments typically perform knock-outs of these genes or inhibit signaling processes with a single concentration of inhibitor.<sup>16;60</sup> Rather, the parameters in Table 3.1 were chosen based on their ability to exhibit pattern formation, as predicted by an instability of the uniform steady-state. Ideally, the stability of the uniform steady-state would change depending on the imposed VEGF concentration.

**Table 3.1: Parameters for numerical simulation of existing hypotheses.**

Hypothesis	Governing equations	Parameters
Lateral inhibition	Equations 3.16 & 3.15	$\kappa_R = 2.5, \kappa_D = 0.166, \tau = 1,$ $n_R = 2, n_D = 2$
Lateral induction	Equations 3.24 & 3.25	$a = 0.2, \kappa_R = 0.512, \kappa_N = 0.166,$ $\tau = 1, n_R = 2, n_N = 2$
Long-range lateral inhibition	Equations 3.16 & 3.15	$\kappa_R = 6, \kappa_D = 0.25, \tau = 1,$ $n_R = 3, n_D = 3, \tilde{V} = 1$

I identified uniform steady-states to use as initial conditions for each simulation, as shown in Figs 3.5B and 3.6B, using the methods depicted in Figure 3.4. I determined stability for a given initial condition by calculating its dynamic eigenvalues ( $\lambda_k$  in Eq 3.14), as shown in Figures 3.5C & 3.6C.

I initiated each simulation at a uniform steady-state with a small, random perturbation of less than 5% of the tip cell marker species (see below) in each cell. Integration proceeded until I did not observe changes to concentrations within the endothelium for multiple time steps. Following simulation, I identified tip cells

as any cells having a final concentration of the Delta ligand significantly ( $> 1\%$ ) higher than the homogeneous initial condition.

I chose Delta concentration ( $D_i$ ) to define tip cells because it was common to all mechanisms, was expected to be preferentially expressed in tip cells by previous researchers<sup>16</sup>, and had a wider range of behaviors than VEGFR2 activation in the case of lateral induction.

I interpreted simulations with stable initial conditions as having zero tip cells.

### 3.3 Results

#### 3.3.1 Lateral inhibition

##### Biological basis

Figure 3.1A gives a graphical illustration of the dominant hypothesis in the literature for tip cell selection<sup>17;25</sup>: lateral inhibition by Notch-Delta-VEGF. Experiments in the mouse retina<sup>18</sup> and in vitro engineered tissues<sup>61</sup> have shown that VEGF-VEGFR2 signaling can induce tip cell characteristics in endothelial cells and promote expression of the Notch ligand Delta-like 4 (Delta)<sup>60;62</sup>. Delta is sometimes enriched at the tips of angiogenic sprouts, suggesting that high rates of VEGF signaling and Delta expression may be indicators of tip cell competency<sup>52;58</sup>. Further experiments indicate that stimulation of Notch by Delta in adjacent cells inhibits the tip cell characteristics in endothelial cells (conversely, blockage of Notch promotes tip cell characteristics)<sup>16;63</sup>, and represses the transcription of VEGFR2<sup>64;65</sup>. These observations suggest a mechanism in which Notch

signaling effectively downregulates the expression of its ligand Delta through the modulation of VEGF-VEGFR2 signaling<sup>52</sup>.

## Analysis

Figure 3.5A gives an overview of our formalization for tip cell selection by lateral inhibition. We assume that the upregulation of Delta expression in response to VEGF-VEGFR2 signaling can be approximated by an activating Hill function using VEGF-VEGFR2 complexes (RA in Figure 3.5A) as an input, as given in Eq 3.9. Similarly, we model the downregulation of VEGFR2 in response to Notch signaling as a repressive Hill function using neighboring Delta ligand ( $\langle D \rangle_i$ ) as an input, as given in Eq 3.8.

Simulating the selection of tip cells from a uniform endothelium (Figure 1.1A) undergoing lateral inhibition required that we first determine the steady-states (SS) in which all endothelial cells were uniform in phenotype. The jagged strike-through in the bar-headed line connecting Delta (D) and VEGFR2 (R) in Figure 3.5A signifies that the juxtacrine signaling interaction crosses cell boundaries and thus requires consideration of multicellular nature of the endothelium. This feature of the gene regulatory network posed a challenge for calculating steady-state concentrations. While we generally assumed the endothelium to resemble a square lattice (see Figure 3.2), a two-cell model (see Figure 3.4) was sufficient to determine the steady-states that existed during lateral inhibition.

Figure 3.5B presents the steady-states of R and D concentration for lateral inhibition for the parameters values given in Table 3.1. We see that for high or low concentrations of VEGF, only a single, uniform SS of Delta expression should exist (solid segment of black curve). For intermediate concentrations of

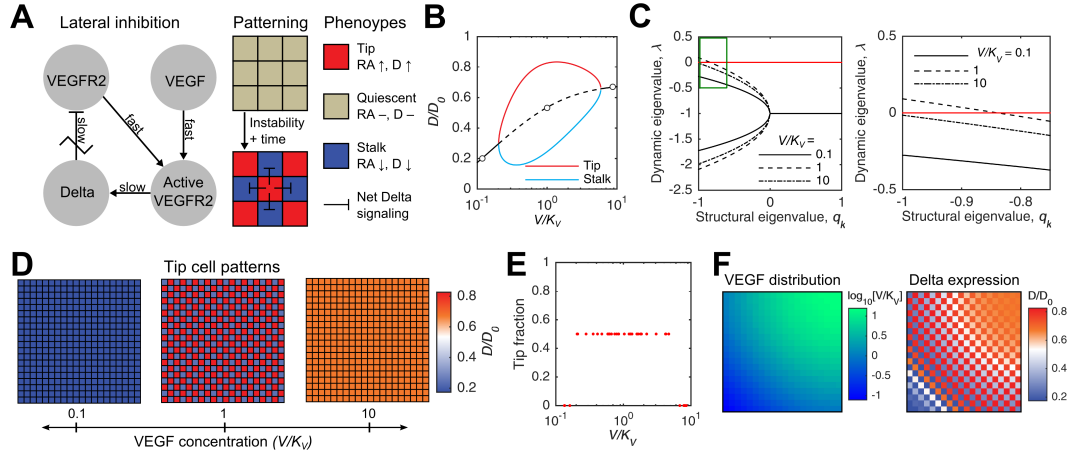


**Figure 3.5: Lateral inhibition.** (A) Overview of lateral inhibition. VEGFR2 (R) and VEGF (V) combine to form activated VEGFR2 (RA), which upregulates Delta (D). Delta inhibits the expression of VEGFR2 in neighboring cells. The jagged strike-through denotes an intercellular process. The homogeneous initial condition (gray) can become unstable and pattern into tip (red) and stalk (blue) cells. (B) Steady-states of lateral inhibition. A two-cell model (see Figure 3.4) was used to find both uniform and heterogeneous steady-states in lateral inhibition. Here, solid segments represent stable steady-states in terms of the normalized levels of VEGF ( $V/K_V$ ) and Delta ( $D/D_0$ ), and the dashed segment represents unstable states. The red and blue lines represent heterogeneous steady-states (only exist in tandem), and do not exist in a uniform lattice. (C) Stability profile of lateral inhibition. Dynamic eigenvalues of the symmetry-adjusted Jacobian matrices (from Eq 3.14) with respect to the structural eigenvalues of the connectivity matrix for uniform steady-states at various levels of VEGF. Steady states with positive, real dynamic eigenvalues are unstable. The inset expands the profile as  $q_k \rightarrow -1$ , where lateral inhibition is most unstable and the corresponding structural mode is a dense “salt-and-pepper” (see Figure 2.2). The steady states at each VEGF level are given by white circles in (B). (D) Patterning of lateral inhibition. As VEGF concentration is increased, the final steady-state goes from one of uniformly low Delta expression, to a “salt-and-pepper” pattern of 50% tip cells, to uniformly high Delta expression. Unless otherwise noted, all simulations were initialized with a random perturbation in each cell with a 5% maximum excursion. (E) Fraction of tip cells with respect to VEGF concentration. When the uniform endothelium is unstable (see Figure 3.2B), exactly 50% of cells become tips in a square lattice. Changing parameter values (e.g., uniform VEGF concentration) within this range ( $V/K_V \approx 1$ ) has no effect on the final tip cell population. (F) Spatially dependent VEGF and lateral inhibition. Imposing a spatially varying distribution of VEGF over a lattice (top) can cause localized tip-stalk selection to occur within a cell population (bottom), but the pattern of selection locally remains a 50% tip – 50% stalk “salt-and-pepper” in the actively patterning regions. Parameter values are given in Table 3.1.

VEGF, we observe that three steady-states are available to the endothelial cells: a uniform SS (dashed segment of black curve) bounded by two complementary states representing tip (red curve) and stalk (blue curve) phenotypes. These tip and stalk states do not exist as uniform steady-states, rather, these two phenotypes can only occur in tandem. The two-cell model predicts that tip and stalk cells can exist together under some sets of parameters, but linear stability analysis is necessary to confirm if tip and stalk cells will spontaneously be selected from an undifferentiated initial condition (dashed segment of black curve).

Using Equation 3.14, we derived a criterion for the stability of the uniform steady-states (dashed, black segment in Figure 3.5B):

$$q_k C_1 + 1 > 0, \tag{3.33}$$

where  $C_1$  is a positive function of the system’s kinetic parameters and the concentrations of the steady-state (no dependence on  $q_k$ ). The uniform steady state is unstable on any structural modes for which the expression is true; in other words, a pattern of tip cell selection will emerge on those modes where the left-hand side (LHS) is negative.

Equation 3.33 shows that the uniform SS will be most unstable for the largest negative structural eigenvalues ( $q_k$ ). This trend is evident in Figure 3.5C, which calculates values of the dynamic eigenvalues ( $\lambda_k$ ) for each structural eigenvalue ( $q_k$ ) at the circled steady-states in Figure 3.5B. The structural modes corresponding to  $q_k \rightarrow -1$  correspond to the most fine-grained patterns available in a square lattice (see far left of Figure 2.2) – which resemble a “salt-and-pepper” of 50% tip cells. Equation 3.33 and Figure 3.5C therefor demonstrate that patterns of 50% tip cells will always emerge the fastest from an unstable, square-shaped endothelium undergoing lateral inhibition.

Figure 3.5C demonstrates that the system was only unstable for intermediate VEGF concentrations ( $V/K_V \approx 1$ ) – corresponding to the dashed curve segment in Figure 3.5B. Uniform steady-states with low ( $V/K_V \approx 0.1$ ) or high ( $V/K_V \approx 10$ ) concentrations of VEGF, corresponding to the solid black curve segments in Figure 3.5B, were stable.

## Simulation

We investigated the dynamic evolution and final steady-states of lateral inhibition-based tip cell selection by numerically integrating the dimensionless forms of the governing equations, Equations 3.16 & 3.15 within a simulated endothelium. Figure 3.5D shows the final concentrations of Delta ligand in the endothelium when a uniform initial condition (lying on the black line in Figure 3.5B) was perturbed by a minor, random disturbance (<5%) in Delta expression and numerically integrated forward in time until it reached a new steady-state. We only observed tip cells (red) – with elevated Delta concentrations relative to their immediate neighbors – in the final endothelium when simulating intermediate concentrations of VEGF ( $V/K_V \approx 1$ ). We observed cells uniformly under- (blue) or over-expressing (orange) Delta for significantly lower or higher concentrations of VEGF.

When tip cells did emerge, they always appeared in a “salt-and-pepper” pattern matching the fastest-growing trajectory in Figure 3.5C (see  $q_k \rightarrow -1$  in Figure 2.2). Figure 3.5E depicts the number of tip cells counted in the final states of systems with varying concentrations of VEGF: every unstable initial condition led to a pattern with 50% tip cells.

Figure 3.5F depicts the spatial expression of Delta ligand when VEGF concentration varied continuously from high (upper right) to low (lower left): fewer than

50% of the total endothelial cells became tip-competent because tip cell selection was limited to areas where VEGF concentration was intermediate ( $V/K_V \approx 1$ ). The total number of tip cells that emerges from an entire endothelium could hypothetically be modulated by the changing the size of the region where VEGF expression is intermediate. However, the density of tip cells in regions of intermediate VEGF conforms to the same “salt-and-pepper” pattern as in the uniform-VEGF simulations (i.e., 50% tip cells for small sampling areas).

### 3.3.2 Lateral induction

#### Biological basis

Figure 3.1B illustrates lateral induction, a competing explanation for how Notch signaling is propagates between endothelial cells. Experiments have shown that endothelial Delta expression is uniformly absent or strongly reduced following blockage of Notch signaling in the zebrafish embryo<sup>66</sup>, in human microvascular endothelial cells<sup>50</sup>, and in the mouse retinal vasculature<sup>21</sup>. In human ECs, Delta transcription is only observed in cells with activated Notch, and Delta expression is increased by simulation of VEGF or membrane contact with a cell highly expressing Delta<sup>50</sup>.

These observations suggest that endothelial Delta-Notch signaling likely results in lateral induction of Delta rather than lateral inhibition<sup>19</sup>. Intuitively, one expects lateral induction to cause cells to converge in phenotype rather than diverge into a pattern, conflicting with the notion of Notch being the driver of tip-stalk differentiation during sprouting – as is observed for lateral inhibition (Figure 3.5). Some authors have hypothesized that endothelial cells may engage in both lateral

inhibition and lateral induction occurring on different time scales<sup>25</sup>, or depending on the broader signaling state of the cell<sup>56</sup>, but here we analyze pure lateral induction to understand its intrinsic characteristics. As such, we present a mechanism in which the down-regulation of VEGFR2 by Notch signaling is not considered (Figure 3.1B).

## Analysis

Figure 3.6A provides an overview for the reaction network and patterning behavior observed using our mathematical description of lateral induction. Like in lateral inhibition, we assumed that VEGF-VEGFR2 signaling up-regulated Delta expression. However, we hypothesized that Notch activation would directly up-regulate Delta expression instead of indirectly down-regulating it through regulation of VEGFR2.

The curve in Figure 3.6B represents the steady states of the lateral induction mechanism as a function of VEGF concentration; these were found a two-cell model similar to that used for lateral inhibition (see Figure 3.4). At low concentrations of VEGF, only a single, uniform steady-state with low Delta expression exists (solid, black section of curve). For intermediate concentrations of VEGF ( $V/K_V \approx 1$ ), three uniform steady-states exist: one with low (blue segment of curve), one with intermediate (dashed segment of curve), and one with high (red segment of curve) concentrations of Delta. At high concentrations of VEGF, only a single steady-state exists – exhibiting high Delta expression.

Using Equation 3.14, we again derived a criterion for the stability of the uniform

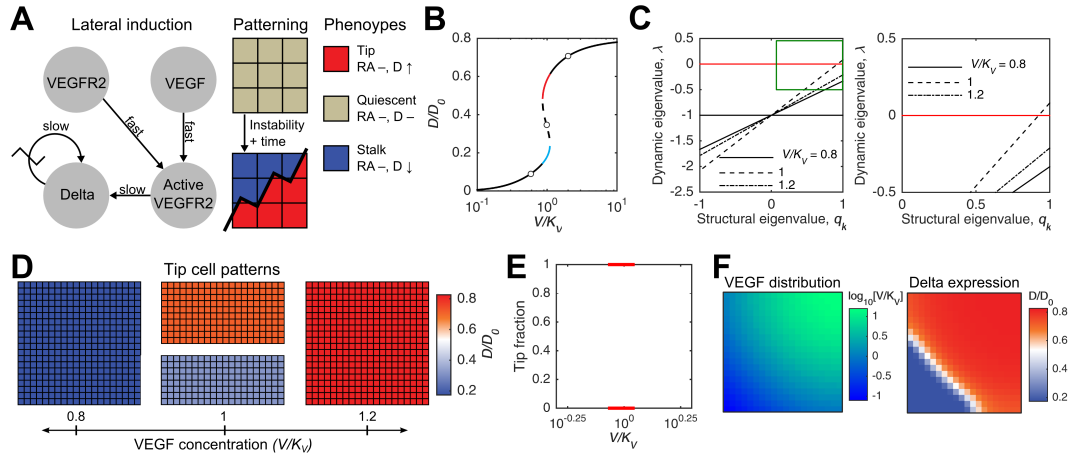


**Figure 3.6: Lateral induction.** (A) Overview of lateral induction. In lateral induction, Notch signaling has the overall effect of increasing Delta gene expression rather than inhibiting it. Cells encourage their neighbors to reach an equal level of Delta expression, so unstable steady-states tend to lead to stable uniform steady-states. VEGFR2 expression is no longer a function of Notch signaling, so the level of VEGFR2 signaling is unchanged following differentiation. (B) Steady-states of lateral induction. The steady-states of lateral induction were calculated using the method shown in Figure 3.4. All states shown here are uniform. Simulations initialized to the steady states on the dashed line are unstable and the cells in the lattice will differentiate towards a uniform state lying on either the red or blue segments of the curve. (C) Stability profile of lateral induction. Dynamic eigenvalues of the symmetry-adjusted Jacobian matrix (from Eq 3.14) for lateral induction at various levels of VEGF. The inset expands the profile as  $q_k \rightarrow 1$ , where lateral induction is most unstable. The structural mode corresponding to  $q_k = 1$  is uniform (Figure 2.2). The steady states at each VEGF level are given by white circles in (B). (D) Patterning of lateral induction. As VEGF concentration is increased, the final steady-state goes from one of uniformly low Delta expression, to one of either moderately low (blue) or high (orange) Delta expression, to one of high Delta expression. (E) Fraction of tip cells with respect to VEGF concentration. The final patterns of lateral induction are always uniform. When an instability does occur, the final state has either 0% or 100% tip cells. As previously mentioned, initial conditions which are stable as a uniform endothelium are assumed to select zero tip cells. (F) Spatially dependent VEGF and lateral induction. A spatially varying VEGF concentration (top) causes cells undergoing lateral induction to form a sharp boundary (bottom). The phenotype changes little on either side of the boundary, but rises sharply at the boundary due to the instability at  $V/K_V \approx 1$  in (B). Parameter values given in Table 3.1.

steady-states depicted in Figure 3.6B:

$$-q_k C_1 + 1 > 0, \quad (3.34)$$

where  $C_1$  is another positive function. In a reversal of the previous mechanism, Equation 3.34 shows that the uniform SS will be most unstable for the largest positive structural eigenvalues ( $q_k$ ); the coefficient in front of  $q_k$  has changed from positive to negative, but otherwise the criterion in Equation 3.34 is identical in form to Equation 3.33.

A similarly reversed trend can be seen in Figure 3.6C, which relates the dynamic and structural eigenvalues for the steady-states circled in Figure 3.6B. As with the previous example, uniform steady-state with low ( $V/K_V \approx 0.8$ ) or high ( $V/K_V \approx 1.2$ ) concentrations of VEGF were stable, and the uniform steady state with an intermediate VEGF concentration ( $V/K_V \approx 1$ ) was unstable. However, the intermediate steady-state has positive dynamic eigenvalues ( $\lambda$ ) that increase as the structural eigenvalue ( $q_k$ ) grows larger. This trend predicts that for lateral induction, the fastest growing “pattern” of Delta expression following a perturbation of an unstable steady state is in fact uniform across all cells (see  $q_k \rightarrow 1$  in Figure 2.2).

## Simulation

Figure 3.6D depicts all the patterns of Delta expression predicted in the final states of lateral induction by simulation; each endothelium was spatially uniform. Following perturbation of uniform initial conditions lying on the dashed segment in Figure 3.6B (identified as unstable in Figure 3.6C), Delta concentrations within the endothelium moved to a state lying on either the red segment or blue segment

in Figure 3.6B. However, Delta concentrations did not remain perfectly uniform throughout the transient process; rather, they increased or decreased heterogeneously with long spatial wavelengths (see DF VIDEO)[I need to see if/how I can attach a video to my dissertation]. The random initial perturbation determined whether an unstable endothelium differentiated into a lower (blue) or higher (orange) level of Delta expression.

Figure 3.6E shows the number of tip cells counted following simulation of the endothelium at various concentrations of VEGF. Tip cells only emerged from an unstable initial condition at either 0% or 100%; under no uniform VEGF conditions did an intermediate fraction of cells spontaneously increase in Delta expression from an unstable endothelium. Figure 3.6F shows that a spatial pattern of Delta expression could be observed following lateral induction under a non-uniform VEGF profile. Intrinsically, lateral induction appears to be capable of forming a sharp boundary between endothelial cells with low and high expression of Delta, even when the underlying stimulus of Delta expression (VEGF concentration) varies smoothly.

### **3.3.3 Long-range lateral inhibition**

#### **Biological basis**

Tip cells have filopodia, which long, narrow extensions of the cell membrane<sup>18</sup>. Filopodia have been observed to carry Delta/Notch<sup>46;67</sup> to enable juxtacrine signaling at a distance, and some filopodia are even referred as “cytonemes” to reflect how effectively they carry signaling molecules<sup>68</sup>. Previous studies have shown that extension of juxtacrine signaling to more distance neighbors via filopodia allows

lateral inhibition to pattern at reduced densities<sup>46;67</sup>, but I analyzed the hypothesis of long-range lateral inhibition in my own framework to see how it compares to the other hypotheses.

## Analysis

Because the inclusion of long-range signaling does not alter the governing equations of lateral inhibition (Equations 3.8 & 3.9), much of the linear stability analysis was identical, including the form of the stability criterion (Equation 3.33). However, as shown in Figure 3.3, the connectivity matrix for this hypothesis is different. The eigenvectors of the connectivity matrix are unchanged; the “shortest wavelength” eigenvectors are still “salt-and-pepper” patterns (see Figure 2.2), and the linear stability criterion (Equation 3.33) predicts a “salt-and-pepper” pattern will emerge during an instability. However, the eigenvalues of the connectivity matrix ( $q_k$ ) are truncated; the smallest eigenvalue increases from -1 as the strength of second-nearest neighbor signaling increases. For example, a connectivity matrix with  $\varepsilon = 0.4$  for a  $16 \times 16$  cell lattice (see Figure 3.7B) has a minimum eigenvalue of approximately  $-0.43$ . Based on the stability criteria for lateral inhibition (Equation 3.33), long-range signaling confers additional stability to the uniform steady-state.

## Simulation

When the governing equations of lateral inhibition were integrated on the long-range lattice, the early moments of patterning showed a “salt-and-pepper” pattern of tip cell selection emerging, as predicted by the linear stability analysis. However, as the simulation proceeded, the tip cell selection patterns matured into something

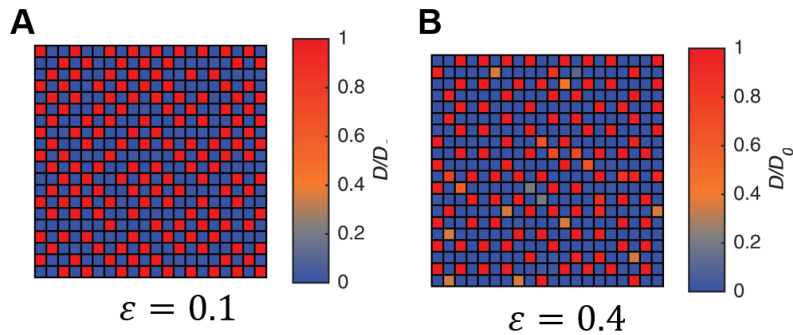


**Figure 3.7: Long-range lateral inhibition.** The patterning density of the long-range lateral inhibition mechanism depended on the strength of second-nearest neighbor signaling. ( $\varepsilon$  in Eq 3.12). (A) Tip cell selection pattern for weaker second-nearest-neighbor signaling ( $\varepsilon = 0.1$ ). (B) Tip cell selection pattern for stronger second-nearest-neighbor signaling ( $\varepsilon = 0.4$ ).

with a lower density than 50%, as typical in a “salt-and-pepper” pattern. As shown in Figure 3.7, the density of tip cell selection varied in the final pattern according to the strength of second-nearest neighbor signaling ( $\varepsilon$  in Eq 3.12): for low values of  $\varepsilon$ , the density was only slightly lower than lateral inhibition (Figure 3.7A); for higher values of  $\varepsilon$ , the fraction of tip cells selected approached 20% (Figure 3.7B). When second-nearest-neighbor signaling was eliminated  $\varepsilon = 0$ , patterning resembled that of standard lateral inhibition (not shown; see Figure 3.5D). These results are interesting for two reasons: (1) they shows that the inclusion of filopodia (modeled by static second-nearest-neighbor connections) can allow lateral inhibition to pattern at lower densities, and (2) they provide an example of the full simulation of patterning having behavior that the linear stability analysis did not predict.

### 3.4 Discussion

Researchers of angiogenesis have, for many years, hypothesized (explicitly or implicitly) the existence of a “central pattern generator” that limits the density at

which endothelial cells are selected to form tips of new angiogenic sprouts. Observations that experimental controls, such as knockdown of Notch signaling, interference with soluble VEGF traps, and inhibition of receptor internalization machinery, could modify the density of sprouting during angiogenesis were explained in terms of their hypothesized impact on the pattern formation mechanisms underlying tip cell selection. If sprouting (or its resulting new vasculature) was too dense, it was because the output of “central pattern generator” of tip cell selection was increasing in density; if sprouting was too sparse, it was because the patterns were decreasing in density.

However, in recent years, some researchers in angiogenesis have begun to reframe their interpretations of the mechanisms connecting molecular controls to multicellular coordination; the hypothesized importance of spontaneous pattern formation has been reduced, and hypotheses have shifted towards broader angiogenic phenomena, for example, coupling tip cell selection to endothelial migration, proliferation, or changes in cellular morphology. I expect that this shift in scope is at least partially a response to two factors (discussed below): (1) the inability of previous modeling efforts to define hypotheses for the “central pattern generator” underlying tip selection that exhibited the range of local patterning outputs that were originally ascribed to it, and (2) experimental evidence that conflicted with certain critical mechanisms of existing hypotheses. In this study, I analyzed three hypotheses for how coupled signaling and gene regulation of the Notch and VEGFR2 receptors and their ligands, the set of biomolecules most commonly proposed to underly tip cell selection, to elucidate why they are incomplete explanations for how endothelial cells might use spontaneous pattern formation to limit the local density of tip cell selection.

## Lateral inhibition as the key to tip cell selection

This computational study, and many others before it<sup>12;51;56</sup>, have used the lateral inhibition hypothesis of Notch signaling (Figs 3.1A and 3.5) as a starting point in modeling endothelial tip cell selection. The understanding that Notch is a key regulator of endothelial phenotype during sprouting angiogenesis follows from numerous experiments that show vascular phenotype and sprouting morphology are severely disrupted following interruption of Notch signaling<sup>17;25</sup>. Lateral inhibition as an explanation for the multicellular “logic” of Notch finds support from several compelling experiments<sup>16;52</sup>, existing mathematical treatments<sup>26;54</sup>, and well-established examples of Notch-based lateral inhibition occurring in other developmental contexts<sup>69;70</sup>.

However, certain experimental observations conflict with the molecular basis of Notch-based lateral inhibition. There is direct evidence that endothelial Notch engages in lateral induction<sup>19;50</sup>, rather than lateral inhibition. Also, some experiments have shown that endothelial VEGFR2 and Notch activity were not coupled<sup>71;72</sup>. Finally, some of the most regarded experts in tip cell selection have noted in published protocols that it is not possible to distinguish tip cells from other endothelial cells based on their expression of species central to the lateral inhibition hypothesis – VEGFR2 and Delta<sup>58</sup>.

In addition to these experimental inconsistencies, the computational predictions presented here (Fig 3.5) and in previous works<sup>26;51</sup> indicate lateral inhibition is incapable of producing patterns of tip cell selection at variable densities. In conclusion, the sum of evidence refutes the hypothesis that mechanisms of spontaneous patterning (via lateral inhibition) prior to the formation of tip cells can explain how molecular controls impact the structure of new vasculature resulting from

angiogenesis, or even the density of sprouting<sup>17;19–21</sup>. The previously mentioned shift in recent literature away from placing importance on spontaneous pattern formation is one possible way for the community to proceed; another is to define new hypotheses that overcome the limitations of Notch-based lateral inhibition.

## Can Notch still play a role?

Avenues for predicting variable tip cell density while remaining dependent on Notch signaling exist, but they face some challenges. In one previous example, Boareto et al.<sup>56</sup> proposed and simulated a Notch-based mechanism of endothelial differentiation that was capable of diverse tip cell patterns; their model relied on expanded regulatory mechanisms of Notch ligands, such as the upregulation of Notch ligand Jagged-1 by Notch signaling. Regulation of Jagged-1 by Notch has been observed in vascular smooth muscle cells<sup>73</sup>, but not in endothelial cells<sup>21</sup>. Likewise, a second regulatory step invoked by Boareto, et al.<sup>56</sup> involving the downregulation of Delta by NICD, conflicts with direct evidence that Notch signaling promotes the expression of Delta in ECs<sup>21;50</sup>.

I also note that the patterned steady states predicted in Boareto et al. were composed of “patches” of approximately 50% patterned tip cells (as in Fig 3.5, here) and uniform states (as in Fig 3.6, here); the global numbers of tip cells varied according to the relative sizes of each patch. Pathological angiogenesis being a result of “patchy” (but locally fixed at 50%) tip cell formation was proposed in a previous computational study that also relied on Notch-based lateral inhibition<sup>51</sup>. Recent experiments<sup>74</sup> have lent some support to aspects of this hypothesis by showing that chronically high VEGF can result in patches of high Delta expression, as predicted by both lateral inhibition (Figure 3.5F) and lateral

induction (Figure 3.6F). However, experimental support for the existence of “salt-and-pepper” patterns (Figure 3.5D) that locally select 50% of endothelial cells to become tips remains lacking.

The long-range extension of lateral inhibition explored in Figure 3.7 and elsewhere<sup>46</sup> could model the extension of Notch signaling distance by Delta-carrying endothelial filopodia<sup>58</sup>. The long-distance lateral inhibition mechanism is capable of multiple tip cell patterns, but requires filopodia to form strong connections between distant endothelial cells; this explanation is challenged by observations that tip cell filopodia grow towards hypoxic tissues<sup>18</sup> (not towards neighboring endothelial cells) and are dispensable for tip cell selection in zebrafish<sup>75</sup>.

In Chapter 4, I will discuss additional avenues for defining mechanisms for spontaneous pattern formation which rely on Notch (or other juxtacrine signaling pathways), which are consistent with previous experiments on endothelial cells, and which can exhibit a range of tip cell selection patterns. I will perform an analysis of a new hypothetical patterning mechanism which was informed by the analyses in this chapter.

## **Limitations of modeling tip cell pattern formation**

As previously mentioned, it is possible that spontaneous pattern formation is not sufficient to explain how molecular controls impact the density of angiogenic sprouting; in such a case, reducing the importance placed on the mechanisms and output of the “central pattern generator” of tip cell selection would be warranted<sup>22</sup>. This study highlighted the limitations of modeling spontaneous pattern formation – in particular, using the approaches outlined in Chapter 2 – to explain complex

phenomena like angiogenesis.

The mathematical tools provided by Othmer & Scriven<sup>43</sup>, while powerful, cannot account endothelial migration, which dynamically alters the signaling topology of the endothelium – the structure of the network formed by cell membranes in contact with one another, here captured in the static connectivity matrix (Figure 2.1). Some researchers hypothesize that dynamic changes in structure of the endothelium are critical to understanding tip cell selection and formation<sup>22;28</sup> and require simulations which are capable of capturing endothelial migration to validate their hypotheses with live experiments (in which endothelial cells are in constant motion)<sup>53</sup>. Some authors have even gone so far as to formalize the endothelium as a continuum (eliminating the modeling of discrete endothelial cells) to explain how molecular phenomena couple to the motion and branching of angiogenic sprouts<sup>23</sup>. However, the literature is clear that tip cells are a distinct phenotype<sup>18;58;76</sup>, as defined by gene expression. Even in multiscale simulations which account for endothelial migration, sprout elongation, and anastomosis, researchers have highlighted the importance of establishing “proper criteria” for tip cell selection which are based on accurate models for the underlying *molecular* mechanisms of tip cell differentiation<sup>12</sup>.

More generally, mathematical analysis of hypotheses for tip cell selection which include dynamic phenomena more complex than basic reaction kinetics and mass transport – the realm of pattern formation in the tradition of Turing<sup>31</sup> – remains challenging. There is an emerging hypotheses for tip cell selection based around the idea of Notch serving to synchronize or (or asynchronize) oscillatory “molecular clocks” in each endothelial cell<sup>20;77</sup>. This hypothesis may permit local selection of tip cells at variable densities if only a small fraction of cells are in the “phase”

of the molecular clock in which endothelial cells are receptive to tip cell-inducing signals<sup>20</sup>. While this hypothesis is fully defined in terms of reaction kinetics and mass transport, it involves what might be described as “dynamic initial conditions” which are unsteady before, during, and after “patterning” takes places; I would struggle to define these initial conditions using the symmetry arguments presented in Chapter 2. Preliminary results for numerical simulation of a Notch-based synchronization mechanism have been published in an unrelated biological context (segmentation during somitogenesis)<sup>78</sup>, and may help explore the hypothesis in the context of angiogenesis; however, theoretical understanding of such systems is not as developed as those used here, in the linear stability analysis of each mechanism. Exact analysis of mechanisms which synchronize (or desynchronize) oscillators may require application of chaos theory<sup>79</sup>.

Finally, I emphasized understanding the *structure* of existing hypothesis for the mechanisms underlying tip cell selection and elucidating how their abilities to form variable-density patterns were constrained; by structure, I refer to the networks of logical interactions between different species (as captured in Figures 3.5A and 3.6A) and cells (as captured by the connectivity matrices shown in Figures 2.1 and 3.3) pertaining to each hypothesis. I chose parameters (given in Table 3.1) based on their ability to explore both stable (non-pattern-forming) and unstable (pattern-forming) regimes as I increased VEGF concentration. As such, the quantitative simulations employed here should not be taken as accurate predictions of how concentrations of the corresponding biomolecular species will evolve during real experiments of tip cell selection. It is possible that attempting to validate the predictions made here against quantitative experiment could have helped falsify some or all of these hypotheses; however, computational researchers have noted that the universal “sloppiness” of parameter sensitivities in models of biomolecular

systems limits the ability of measurements of quantitative global phenomena (i.e., protein concentrations) to accurately constrain model parameters (e.g., estimate kinetic rate constants)<sup>80</sup>, or even to clarify internal system structure (i.e., the qualitative interactions between molecular species)<sup>81</sup>.

## Application to experiments

Although I do not intend for the simulations presented in this chapter to be (quantitatively) validated with experiments, my hope is that they will inform future experiments around tip cell selection. I believe that there is a need to “reset” the discussion on tip cells, such that researchers will consider a wider range of hypotheses for the “central pattern generator” of tip cell selection when designing and interpreting experimental results – not defaulting to Notch-based lateral inhibition, and not avoiding the concept of spontaneous pattern formation altogether. However, the evolution of the literature over the last decade suggests this may be a formidable challenge.

The direct experimental evidence that Notch engages lateral induction in endothelial cells<sup>50</sup> has not seemed to falsify the hypothesis of tip cell selection by lateral inhibition for many researchers in the field (but not all of them<sup>19</sup>). Studies performed since I began this project continued to argue that lateral inhibition is the “central pattern generator” of tip cell selection, pointing to evidence that “salt-and-pepper” patterns of Delta expression dynamically exist in mouse “embryoid bodies”<sup>22;74</sup>; embryoid bodies are actually stem cells which have been induced to differentiate towards an endothelial phenotype *in vitro*, but they are considered by some researchers to be accurate experimental models of sprouting angiogenesis from blood vessels<sup>52;82</sup>. However, the evidence of lateral inhibition provided by

existence of patterns of Delta expression in these endothelial-like stem cells is less direct than the evidence of lateral induction in primary endothelial cells provided by the experiments performed by Caolo, et al (2010)<sup>50</sup>.

As such, the first experiment I would like to see is a replication of the study performed by Caolo (2010)<sup>50</sup>, to reaffirm that primary endothelial cells (preferably of various origins) engage in lateral induction. The next experiment I would like to see is a study which uses the same methods (those used to establish that primary endothelial cells engage in lateral induction via Notch) to elucidate if mouse endothelial-like stem cells (i.e. those used to construct *in vitro* embryoid bodies<sup>52;53;74;82</sup>) engage in lateral induction via Notch. If mouse embryoid bodies and primary endothelial cells differ in how they propagate Notch signaling, this difference could impact our interpretation of almost a decade of experiments<sup>52;53;74;82</sup> which were critical in defining the consensus on endothelial tip cell selection. If such differences exist between different types of primary endothelial cell (e.g., between HUVECs and HMVECs), we may need to consider whether there are fundamentally different forms of tip cell selection in at work in different physiological or pathological contexts of angiogenesis. It is well-known that predefined “tracks of VEGF” which can guide tip cells, once hypothesized to be a general feature of tip cell formation<sup>18;83</sup>, are actually limited to the central nervous system (including the retina), where astrocytes are present<sup>84</sup>; later experiments elucidated other molecular mechanisms that uniquely impact angiogenesis of the central nervous system<sup>85</sup>. These differences could hypothetically extend down to the basic mechanisms of tip cell selection.

### 3.5 Conclusion

A longstanding goal in the study of angiogenesis is the ability to accurately predict how molecular intervention (i.e., from a drug which sequesters VEGF) shapes the formation of new vasculature. Multiscale modeling is likely key to our ability to connect phenomena at the molecular and tissue scale; the definition and investigation of specific processes within angiogenesis – such as tip cell selection – is an essential part of rationally designing and validating these multiscale models. This study develops a mathematical method for analyzing hypotheses for the spontaneous formation of tip cell selection patterns, and applies it to three mechanisms which are dependent on Notch signaling as the main facilitator of multicellular cooperation prior to angiogenic sprouting. The results of this study provide lessons on how to define hypotheses which might overcome the challenges that previous modeling efforts have had in connecting molecular controls to changes in angiogenic sprouting density; these lessons will be used extensively in Chapter 4, in which I will discuss of potential sources of new hypotheses drawn from the existing literature of sprouting angiogenesis, propose two new hypothesis for the mechanisms underling tip cell selection, and analyze the ability of those mechanisms to generate patterns of variable density in response to changes in the magnitude of key signals.

CHAPTER 4  
NEW HYPOTHESES FOR TIP CELL SELECTION

## 4.1 Introduction

In Chapter 3, I introduced and analyzed three hypotheses (see Figure 3.1) for the molecular mechanisms underpinning the formation of tip cell patterns, all based around juxtacrine Notch signaling as the basis by which endothelial cells locally limit tip cell formation. Myself and others<sup>19;74</sup> were motivated to study spontaneous pattern formation during tip cell selection because it offered a path towards explaining how changes in the magnitude of certain signaling process can determine the density of angiogenic sprouting and impact global outcomes in the growth of new vasculature. Each of the three hypotheses had flaws: the lateral inhibition hypothesis was contradicted by experimental evidence that endothelial cells propagate Notch signaling via lateral induction, and the patterns formed by lateral inhibition did not alter their densities in response to changes in the magnitude of signaling; the lateral induction hypothesis was unable to select individual tip cells from a uniform endothelium; and the long-range lateral inhibition hypothesis relied on a non-physiological role of filopodia in forming membrane contacts between distant endothelial cells.

In this chapter, I will take a broader look at the signaling and gene regulatory processes of endothelial cells to elucidate whether new hypotheses, which may or may not involve Notch signaling, can explain the spontaneous formation of tip cell selection patterns at multiple densities while remaining consistent with the experimental literature. I will employ the methods derived in Chapter 2, and used in Chapter 3 to understand the patterning constraints of the previous

hypotheses, to analyze the basic logic of two new hypotheses that will emerge from this literature search. I will use numerical simulation to demonstrate how each mechanism can have different patterning outcomes depending on the magnitude of certain signaling processes. Finally, I will discuss how these new hypotheses, and the broader insights that my derivation and analysis of them provided, can be used to improve the design and interpretation of future experiments and modeling efforts around tip cell selection.

### **4.1.1 Expanding on juxtacrine signaling**

In spite of the doubts raised by my studies in Chapter 3, juxtacrine signaling remains an attractive explanation for how patterns of tip cell selection can spontaneously form. Numerous experiments show that disruption of Notch signaling can have profound impacts on sprouting angiogenesis, whether increasing sprouting density by broadly inhibiting Notch<sup>16</sup> or decreasing sprouting density by changing the balance of Notch ligands.<sup>21</sup> As such, I considered whether Notch could “learn new tricks” which qualitatively expanded upon the simple circuits of lateral inhibition or induction commonly attributed to it. In this section, I will describe some emerging research directions in the literature which may indicate new functions for Notch (or other juxtacrine signaling pathways) which could play a role in tip cell selection.

#### **Additional ligands for Notch**

One of the first complications to the lateral inhibition hypothesis came from the discovery that Jagged, another ligand for Notch, may play a role in tip cell for-

mation.<sup>21</sup> Benedito, et al., observed that while endothelial tip cells expressed high levels of Delta ligand, neighboring stalk cells were enriched in Jagged.<sup>21</sup> In general, both Delta and Jagged activate Notch, and in both cases, that activation leads to the same downstream signaling through the Notch intracellular domain (NICD).<sup>86</sup> However, the Fringe family of proteins, which is expressed in the endothelium, is able to prevent Notch from releasing NICD in response to Jagged (but not Delta); in the presence of Fringe, Jagged may act as an antagonist of Notch signaling in tip cells.<sup>21</sup>

The question arises, “Could Jagged play a role in controlling the density tip cell selection?” Indeed, Benedito, et al., observed that while knockdown of Delta expression increased the number of cells showing tip cell characteristics, knockdown of Jagged had the opposite effect.<sup>21</sup> A group of computational researchers later attempted to explain how changes in the balance of Jagged and Delta expression in endothelial cells could impact tip cell formation.<sup>56</sup> As discussed in the previous chapter, Boareto, et al. simulated tip cell selection using a mechanism which proposed that Notch activation upregulated Jagged and downregulated Delta.<sup>56</sup> This mechanism was therefore capable of both lateral inhibition and lateral induction depending on the initial conditions of the simulation, but it was unable to predict a *local* density of tip cells to emerge at anything other than 50% or 100%, as with the hypotheses of Chapter 3. In other words, Boareto, et al. may have been able to explain high tip cell densities induced by lack of Delta,<sup>16</sup> but not low tip cell densities induced by lack of Jagged.<sup>21</sup>

In conclusion, it is evident that Jagged plays a role in regulating tip cell formation, but the existing roles of Notch as facilitator of lateral induction or lateral inhibition alone will probably not suffice to explain that role.

## **Complex, dynamic signal processing**

In the previous chapter, I briefly discussed an emerging hypothesis that certain species downstream of Notch signaling oscillate as a “molecular clock”.<sup>20;77</sup> This hypothesis opens the possibility of certain downstream Notch targets being receptive only in certain “phases” of the clock, making the precise timing of the Notch signal (that is, the presentation of a ligand on a neighboring cell) as important as its magnitude. One can speculate that dynamic signal processing would enable something like cellular “Morse code”, where cells can encode arbitrarily complex information in a binary format. While tantalizing, this idea needs a great deal of additional experiment to clarify whether these molecular clocks actually exist in endothelial cells and how the timing of Notch activation is regulated upstream (i.e., in the ligand-presenting cell) and interpreted downstream before any meaningful modeling can be done.

## **Notch coordinating with other signaling pathways**

Numerous studies have explored how Notch signaling interfaces with signaling pathways involving soluble morphogens that are known to impact angiogenesis – the hypotheses in Chapter 3 fall under this umbrella, as they are concerned with how VEGF (a soluble morphogen), through VEGFR2, can induce tip cell formation with help from lateral inhibition. Previous studies have connected Notch signaling to other soluble signaling pathways such as Angiopoietins<sup>87</sup>, BMP<sup>77</sup>, VEGFR3<sup>71</sup>, etc. However, in most cases, these pathways seem to broadly effect the activity of Notch (i.e., generally raising or lowering the Notch activation across whole tissues).<sup>25</sup> The soluble ligand itself does not necessarily form a new layer of multicellular coordination that could overcome the basic logic of lateral induction

or lateral inhibition; I will discuss hypothesis in which a soluble signaling does play a role in the pattern-forming mechanism in the following section, “Other biophysical and biomolecular phenomena.”

However, the possibility of Notch coordinating with *other juxtacrine* signaling pathways is less studied. Recent experiments have shown that endothelial cells respond to a wide variety of juxtacrine signals, which can be highly localized to region of the vascular plexus where tip cell selection occurs. Below, I will highlight three juxtacrine signaling pathways that are of growing interest to the field.

EphrinB2 is a ligand for the EphB receptor, but it also engages in some interesting signaling in the absence of its receptor: endothelial cells must express EphrinB2 to internalize VEGFR2 and adopt the tip phenotype.<sup>88</sup> EphrinB2 is up-regulated by Notch,<sup>89</sup> and can form complexes with a EphB in *trans* (i.e., ligand and receptor are expressed on neighboring cells),<sup>90</sup> which could hypothetically alter the ability for ephrin-B2 to aid in VEGFR2 internalization in *cis* (i.e., cell-autonomously); this juxtacrine interaction might open up the possibility that cells compete to express more ephrin-B2 than their neighbors, an additional layer of juxtacrine signaling.

In addition, Notch activation downregulates the expression of Neuropilin-1 (NRP1).<sup>91</sup> NRP1 was recently found to be essential to tip cell formation, perhaps even more so than Notch: NRP1 suppresses genes which induce the stalk cell phenotype.<sup>91</sup> NRP1 also forms both *cis* and *trans* complexes with VEGFR2: in *cis*, NRP1 helps VEGFR2 undergo endocytosis, which enhances the rate and intensity of VEGF-VEGFR2 signaling;<sup>92</sup> in *trans*, NRP1 anchors VEGFR2 at the cell surface, prolonging its signaling but preventing key downstream pathways from activating.<sup>93</sup> However, it is not clear how the interplay of VEGF, NRP1, and Notch

impacts tip cell selection.

A third possible juxtacrine partner for Notch is VE-Cadherin, which is an essential component of the gap junctions that define the border between two endothelial cells.<sup>94</sup> VE-Cadherin is known to be important to angiogenesis because its stability at the cell surface impacts VEGF-induced vascular permeability,<sup>95</sup> and recent studies have suggested that tip and stalk cells differ in how they use VE-Cadherin to control their adhesion and motility.<sup>53</sup> VE-Cadherin also impacts VEGFR2 signaling: VEGFR2 can be trapped in complexes with VE-Cadherin which prevent full downstream signaling following VEGF stimulation.<sup>96</sup> With enough VEGF stimulation, VEGFR2 can break free from VE-Cadherin, weaken the gap junctions, and ultimately cause VE-Cadherin to be internalized.<sup>95</sup> The potential role of Notch signaling in regulating the activity of VE-Cadherin is still unknown, but may involve interplay from NRP1<sup>97</sup> or VEGFR2.

Experimentalists are still exploring the basics of how other juxtacrine pathways may interface with Notch, but I sought to provide an example of how interplay between these pathways might allow the endothelium to select tip cell patterns at multiple densities. In particular, I wanted to explore what would happen if in addition to tip cells being repressed by lateral inhibition through Delta/Notch, stalk cells expressed another ligand in response to Notch signaling which repressed Delta expression in neighboring cells independently of Notch. I hypothesized that this second juxtacrine pathway might allow fewer tip cells to be selected: too much Notch signaling in a stalk cells, perhaps caused by the stalk cell neighboring four different Delta-expressing tip cells, would increase the concentration of the second ligand to the point where the neighboring tip cells would be repressed.

In Figure 4.1A, I provide a hypothetical mechanism which could embody this



## Mechanical deformation

Turing's original theories for how spatial instabilities can lead to biological pattern formation were based around coupled reaction and diffusion,<sup>31</sup> but subsequent researchers found that modeling the dynamics of mechanical stress and strain as a response to biological cues was equally capable of predicting the creation of new structures. James Murray, mentioned as the "Purist" in the Turing tradition in Chapter 2, even developed a theory for how endothelial cells used mechanics to establish vascular networks during embryonic development.<sup>47</sup> Murray cited experimental observations that endothelial cells, having been deposited within a thin layer of sufficiently soft extracellular matrix (ECM), would begin to form percolated networks of endothelium which resembles microvascular networks. He used mathematical modeling to argue that these networks were a result of endothelial cells pulling on each other and on their surrounding ECM: as cells were pulled closer to each other into clusters of higher cell density, those areas with higher cell density would exert greater traction, forming an instability that continued to cluster cells. Microvascular networks were formed, rather than isolated clumps of endothelial cells, because fibers of the ECM would align between clusters as they pulled, providing enhanced mobility to endothelial cells which would bridge each cluster.

It is easy to speculate that mechanical forces may be an overlooked dimension in tip cell selection based on these results, but some challenges exist in attempting to develop a hypothesis around this concept. Most immediately, the formation of percolated vascular networks from endothelial cells distributed uniformly in an ECM is a description of vasculogenesis, rather than angiogenesis; tip cell selection does not exist in vasculogenesis, as there are no sprouts for endothelial cells to

occupy the tip. More generally, the endothelium certainly does interact with the ECM during angiogenic sprouting: tip cells excrete matrix metalloproteases to weaken the ECM prior to invasion and the stiffness of the ECM can determine how easily tip cells migrate. However, for mechanical forces to play a role in tip cell selection via interaction with the ECM, endothelial cells would have to both alter and sense changes the ECM prior to adopting the tip phenotype. Several months prior to the time of writing, one study reported that the Notch receptor and Delta ligand must be under tension for tip cell lateral inhibition to be productive<sup>101</sup>; while I did not have time to consider this revelation in significant detail, I do not see an immediate reason why Notch or Delta being under tension would impact the predictions of lateral inhibition.

### **Mass transfer**

In Chapter 1, I mentioned that early simulations of angiogenesis did not include tip cell selection as a mechanism for determining the location of new sprouts. Rather, sprouts were hypothesized to grow analogously to branches in a dendritic crystal:<sup>102</sup> VEGF would stimulate endothelial cells to divide and migrate towards its source, and endothelial cells would consume VEGF.<sup>23</sup> The spacing between sprouts was determined by spatial instabilities, as with tip cell selection, but those instabilities would result from the interplay between the motion of a boundary (due to cell migration) and the consumption of a diffusible species at the boundary (due to internalization of VEGF receptors) – the phenotype of the cells at the boundary, aside from their motility or velocity, was largely irrelevant.<sup>23</sup> While this fully migration-based view of angiogenesis fell out of favor with the advent of the tip cell selection hypothesis, it captured something lost in many models of tip cell selection: the potential role of VEGF diffusion.

The simplest models for tip cell selection (e.g., lateral inhibition) have assumed that VEGF is present at a constant concentration to activate all endothelial cells in the sprouting plexus equally;<sup>51;56</sup> this assumption aligns with the view of VEGF as an “angiogenic switch”<sup>14</sup>, as opposed to an active component of a biomolecular patterning mechanism. Some previous simulations of tip cell selection attempted to increase their realism by including a proximal (i.e., near mature vessel)-distal (i.e., near avascular tissue) gradient;<sup>53</sup> this gradient acknowledges that VEGF diffuses to the endothelium from avascular tissues (diffusion requires a chemical gradient), and allows the simulation to predict filopodia extension along a VEGF gradient (hypothesized to help guide sprout elongation). Other simulations have included local (i.e., cell-to-cell), but fixed, patterns of VEGF concentration to match experimental observations that astrocytes in the mouse retina leave “tracks” of VEGF bound to the extracellular matrix which may guide tip cell selection and migration in the central nervous system.<sup>103</sup>

However, few previous simulations have incorporated the recent evidence that microscale gradients of freely-diffusing VEGF near the sprouting front are maintained by local, dynamic cellular processes. The dynamic control of local VEGF gradients was recently observed in interactions between neurons and endothelial cells in the mouse retina.<sup>27</sup> Neurons expressed high levels of VEGFR2 that efficiently bound VEGF, but the VEGF-VEGFR2 complexes did not appear to be actively signaling. Deletion of VEGFR2 in the neurons had little effect on the neurons themselves, but caused nearby vessels to aberrantly sprout towards the neurons. It appeared that neurons were using VEGFR2 to deplete their local concentrations of free VEGF, creating a diffusive flux of VEGF away from nearby endothelium, limiting those endothelial cells’ ability to become tip cells.<sup>27</sup>

Neurons controlling the diffusion of VEGF to actively guide angiogenesis was itself a remarkable discovery, but a follow-up article posed a striking question: can endothelial cells use VEGFR2 to limit the formation of tip cells, just as neurons do? In other words, can nascent tip cells “steal VEGF from thy neighbor” as a means of controlling sprouting density?<sup>104</sup>

Known mechanisms of VEGF and VEGFR2 in endothelial cells can shed light on this hypothesis. The endocytosis of VEGF by VEGFR2 – the basis by which neurons control VEGF diffusion – is essential to the formation of endothelial tip cells.<sup>88;105</sup> Full activation of the VEGFR2 signaling cascade also requires the endocytosis and trafficking of VEGF-VEGFR2 complexes.<sup>88;92;105</sup> Unlike most receptor tyrosine kinases (the class of receptors to which VEGFR2 belongs), the endocytosis of a VEGFR2 complex is not dependent on its binding to a ligand.<sup>99</sup> Rather, VEGFR2 is constitutively (i.e., independent of ligand binding) internalized by endocytosis and recycled back to the cell surface<sup>99;105</sup>; the rate at which VEGFR2 is internalized and trafficked depends on the larger signaling state of the cell, with species such as atypical protein kinase C<sup>105</sup>, ephrin-B2<sup>105</sup>, Rab5<sup>100</sup>, and VE-Cadherin<sup>96</sup>, and dynamin<sup>88;106</sup> playing important roles. (VEGFR2 endocytosis and trafficking is reviewed in Simons, 2016<sup>92</sup>.)

VEGFR2 signaling has broad effects on the signaling state of the cell, and it is possible that signaling from internalized VEGF-VEGFR2 complexes could accelerate the internalization of other VEGF-VEGFR2 complexes on the cell surface, creating a cycle of positive feedback. For example, movement of VEGF-VEGFR2 complexes into dynamin-dependent vesicles is required for VEGF-stimulated activation of Akt (a.k.a. protein kinase B).<sup>88;106</sup> Active Akt has been shown to rapidly increase the production nitric oxide (NO) in endothelial cells by activating en-

endothelial nitric oxide synthase (eNOS).<sup>107</sup> Nitric oxide enhances the the ability of dynamin to form vesicles<sup>108</sup> and is enriched in, and important for the formation of, endothelial tip cells.<sup>109</sup>

Figure 4.1B depicts a hypothetical mechanism in which endothelial cells in the sprouting front compete to form dynamin-dependent vesicles containing VEGF-VEGFR2 complex, which provide signals to increase the activity of dynamin through Akt and NO; successful tip cells form the most vesicles, have the strongest signaling from internalized VEGF-VEGFR2 complexes, and produce the most NO. Fates of neighboring endothelial cells diverge because the capture of VEGF within dynamin-dependent vesicles (followed by trafficking and the degradation of VEGF) depletes the local concentration of free VEGF; the strong depletion of free VEGF at nascent tip cells creates a diffusive flux away from neighboring cells, preventing them from becoming tips – completing the analogy to neuronal sequestration of free VEGF. In this chapter, I will analyze the ability of the hypothesis in Figure 4.1B to form tip cell patterns.

## 4.2 Methods

The methods used to analyze the new hypotheses (shown in Figure 4.1) for tip cell selection mirror those used in Chapter 3 for the existing hypotheses. In this section, I will provide a derivation of the governing equations used to model each of the new mechanisms, details on the linear stability analysis of each mechanism, and any unique considerations for the numerical simulation of each mechanism. For a more extensive explanation of the methods used to analyze these two hypotheses, please refer to Section 3.2.

### 4.2.1 Two-dimensional approximation of diffusion

Here, we examine our 2D approximation of the fluid space above the endothelium by analyzing a similar reduction in dimensionality from a 2D system (where concentrations vary in  $x$  and  $z$ ) to a 1D system (where concentrations vary only in  $x$ ). Consider steady-state diffusion problem in a lateral cross-section (Figure 4.2), in which a solute is introduced to the fluid space from adjacent tissue at a constant flux  $J_0$  at height 0 and removed via a sinusoidal flux at height  $-h_0$ .

We divide the problem into two components:  $C_I(x, z)$ , which accounts for the sinusoidal flux, and  $C_{II}(x, z)$ , which accounts for the constant flux. To understand the importance of accounting for two-dimensionality, we only need to consider the solution  $C_I$ . The other component of the solution,  $C_{II}$ , is a simple linear profile in  $z$  and would match the homogeneous initial condition prior to pattern formation; the present study is concerned with concentration deviations that arise as a result of instability at the homogeneous initial condition, and the deviations here would be equal to  $C_I$ .

We represent the system for  $C_I$  via a virtual domain with two mirrored boundary conditions, as shown in Figure 4.2B. Our governing equation in for the concentration in the fluid volume,

$$\frac{d^2 C_I}{dx^2} + \frac{d^2 C_I}{dz^2} = 0 \quad (4.1)$$

has a general solution of

$$C_I(x, z) = [c_1 \cos(2\pi x) + c_2 \sin(kx)] [c_3 \cosh(kz) + c_4 \sinh(kz)] \quad (4.2)$$

where  $k$  [ $\text{cm}^{-1}$ ] is the wavenumber of the spatial pattern, and  $c_n$  are coefficients determined by the boundary conditions.

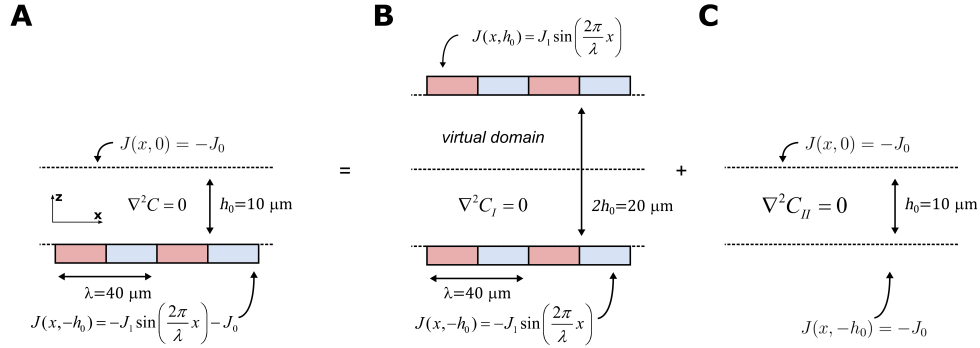


**Figure 4.2: Lateral cross-section of the diffusion problem.** (A) Lateral cross section and boundary conditions. In the final steady-state, VEGF is continuously introduced into the fluid volume from adjacent proangiogenic tissues at rate  $J_0$ . We approximate consumption of VEGF by endothelial cells from the fluid volume by a flux of  $J_1$  multiplied by a sinusoid with wavelength  $\lambda$ . The fluid volume has a height  $h_0 = 10 \mu\text{m}$ , and each cell has a length  $l = 20 \mu\text{m}$ , for an overall minimum wavelength in the cellular pattern of  $\lambda = 40 \mu\text{m}$ . (B) Component of the solution to scenario in (A) with a patterned boundary condition. This is the solution of interest for examining the appropriateness of the 2D approximation. (C) Component of the solution to scenario in (A) with a homogeneous boundary condition.

The boundary conditions for  $C_I$  are:

$$\left. \frac{dC_I}{dz} \right|_{z=h_0} = \frac{J_1}{D} \sin\left(\frac{2\pi}{\lambda}x\right) \quad (4.3)$$

$$\left. \frac{dC_I}{dz} \right|_{z=0} = 0 \quad (4.4)$$

where  $\lambda$  [ $\mu\text{m}$ ] is the wavelength of the spatial pattern in VEGF consumption at the final steady-state.

The first boundary condition stipulates that the flux at  $z = h_0$  is proportional to  $\sin(kx)$  and not  $\cos(kx)$ , hence  $c_1 = 0$  and  $\frac{2\pi}{\lambda} = k$ . With this, our problem reduces to only two unknown coefficients:

$$C_I(x, z) = [c_5 \cosh(kz) + c_6 \sinh(kz)] \sin(kx) \quad (4.5)$$

Applying the second boundary condition,

$$\left. \frac{dC_I}{dz} \right|_{z=0} = kc_5 \sin(kx) = 0 \rightarrow c_5 = 0 \quad (4.6)$$

Reapplying the first boundary condition,

$$\left. \frac{dC_I}{dz} \right|_{z=h_0} = \frac{J_1}{D} \sin(kx) = kc_6 \sinh(kh_0) \sin(kx) \quad (4.7)$$

$$c_6 = \frac{\lambda J_1}{2\pi D \sinh(kh_0)} \quad (4.8)$$

Substituting this coefficient, our governing equation (as a function of  $k$ ) is:

$$C_I(x, z) = \frac{J_1}{kD \sinh(kh_0)} \cosh(kz) \sin(kx) \quad (4.9)$$

We are interested in the behavior of this solution at the surfaces of the real cells at  $z = -h_0$  in Figure 4.2B, where the concentration of VEGF interacts with the VEGF receptors. Furthermore, we want to compare this result to the fully 1-D limit (with variations only in  $x$ ):

$$C_I(x, -h_0) = C^{2D}(x) = \frac{J_1}{kD} \coth(kh_0) \sin(kx) \quad (4.10)$$

In the 1-D approximation of the same system, our governing equation now appears to have a sinusoidally-varying reaction rate in the bulk of the fluid volume, rather than fluxes at the vertical boundaries:

$$D \frac{d^2 C}{dx^2} + \frac{J_1}{h_0} \sin(kx) \quad (4.11)$$

Here, the impact of  $J_0$  is not observed, as it is equally balanced in the top and bottom of the domain in Figure 4.2A and thus negated when the system does not vary in  $z$ .

The general solution for this governing equation is,

$$C(x) = c_1 + c_2x + \frac{J_1}{k^2 Dh_0} \sin(kx) \quad (4.12)$$

can be simplified by first observing that the concentration will be periodic and not growing infinitely with  $x$ , hence  $c_2 = 0$ . Furthermore, the limit where  $J_1 \rightarrow 0$  is synonymous with a homogeneous steady-state; as before, we are only interested in the concentration deviations resulting from pattern formation, hence, for the purposes of comparison to the 2D case,  $c_1 = 0$ .

$$C^{1D}(x) = \frac{J_1}{k^2 Dh_0} \sin(kx) \quad (4.13)$$

To estimate the appropriateness of the approximation, we take the ratios of Equations 4.10 & 4.13,

$$\frac{C^{1D}(x)}{C^{2D}(x)} = \frac{\tanh(kh_0)}{kh_0} \quad (4.14)$$

Equation 4.14 indicates that the 1-D and 2-D treatments of the diffusion problems have different dependencies on the pattern of sources and sinks, as captured by the dependence on  $kh_0$ . These distinct dependencies could influence pattern selection in the model developed in this study. To determine whether the effect is significant for the patterns explored in this study, we consider different types of patterns that may emerge.

In the case of a pattern with a long wavelength:

$$\lim_{kh_0 \rightarrow 0} \frac{C^{1D}}{C^{2D}} = \lim_{kh_0 \rightarrow 0} \frac{4}{(e^{kh_0} + e^{-kh_0})^2} = 1 \quad (4.15)$$

In the case of a pattern with a short wavelength:

$$\lim_{kh_0 \rightarrow \infty} \frac{C^{1D}}{C^{2D}} = \lim_{kh_0 \rightarrow 0} \frac{1}{kh_0} = 0 \quad (4.16)$$

In the case of a pattern with an intermediate wavelength:

$$\lim_{kh_0 \rightarrow 1} \frac{C^{1D}}{C^{2D}} = \tanh(1) \approx 0.76 \quad (4.17)$$

In this study, the shortest wavelength pattern is the “checker board” (see Figure 2.2) with  $\lambda = 2d_{cell} = 40 \mu\text{m}$  and  $h_0 = 10 \mu\text{m}$ , so  $kh_0 = \frac{2\pi \cdot 10}{40} \approx 1.5$ . To a reasonable approximation,  $C_{1D} = C_{2D}$  for this study. If the depth of the fluid volume were to be any larger (i.e.,  $h_0 \gg \lambda$ ), the distinction between 1-D and 2-D treatments of the diffusion problem could have significant impact on the pattern selection process. In general, Equation 4.14 suggests that a model including concentration gradients in the direction normal to the endothelium (z axis) will predict greater concentration gradients across the x axis, potentially driving stronger overall pattern formation, than one that does not.

## 4.2.2 Governing equations

### Double-juxtacrine

I explored a hypothetical mechanism of tip cell pattern formation (Figure 4.1A) which relies on a second juxtacrine signaling pathway that represses tip cell characteristics alongside, but independently of, Notch-based lateral inhibition. However, in the absence of a well-supported suggestion for what the other juxtacrine signaling pathway may represent in endothelial biology, I used a reduced representation

of the essential mechanism of the “double-juxtacrine” hypotheses, shown in Figure 4.3A, which uses to generic names “A” and “B” to represent the species at work. In the reduced representation, species A is analogous to Delta in the model for lateral inhibition (see Figure 3.5A) and species B is analogous to Notch activation; the new juxtacrine pathway, by analogy, involves a ligand which is upregulated by Notch signaling and activates a receptor in neighboring cells which, when active, represses Delta expression and other tip cell characteristics.

As in the derivation of the governing equations for lateral induction (Equations 3.10 & 3.11), I created the governing equations for the double-juxtacrine mechanism by reconfiguring the governing equations of lateral inhibition (Equations 3.8 & 3.9).

Species A is down-regulated by species B both cell autonomously and through juxtacrine signaling. As such, I modeled species A using a sum of two repressive Hill functions, similar to what used to model the regulation of Delta by VEGFR2 and Notch signaling in the lateral induction hypothesis (see Equation 3.11):

$$\frac{dA_i}{dt} = \beta_P \frac{1}{1 + (K_P B_i)^{n_P}} + \beta_A \frac{1}{1 + (K_A M_{ij} B_j)^{n_A}} - \gamma_A A_i \quad (4.18)$$

where the parameters follow the conventions established in Section 3.2. (I also could have made Equation 4.18 a product of two repressive Hill functions; as I will explain in the discussion section, this might allow for more robust patterning, and I hope to explore this alternative formalization soon.)

The connectivity matrix has already been substituted into the second Hill function in Equation 4.18 to signify that the function takes as input the *average of B concentrations in neighboring cells*. The form of Equation 4.18 implies that the mechanisms which down-regulate species A in the the presence of species B in the same cell (first Hill function) or in neighboring cells (second Hill function) are inde-

pendent. This independence is an important feature, because it rules out paracrine signaling (or other diffusive mechanisms) as the biophysical means by which species B propagates its signals to the local and neighboring cells – in paracrine signaling, a cell would not be able to determine whether molecules of species B arose locally or from neighboring cells.

Species B is upregulated by species A in neighboring cells:

$$\frac{dB_i}{dt} = \beta_B \frac{(K_B M_{ij} A_j)^{n_B}}{1 + (K_B M_{ij} A_j)^{n_B}} - \gamma_B B_i \quad (4.19)$$

### Derivation of governing equations for diffusion and endocytosis

Figure 4.1B depicts a patterning mechanism based solely on the diffusion (green, wavy arrow) and internalization (solid, black arrow) of VEGF. The equations for this mechanism depart from those of the previous two networks in that only the transport and intracellular trafficking of VEGF are explicitly considered; juxtacrine signaling (e.g., via Notch) does not appear. Furthermore, this mechanism consider VEGF to be a freely diffusible species, whereas the previous mechanisms assumed that the local VEGF concentration was fixed over time. In the following section, I will derive the governing equations I used to explore this mechanism.

The derivation of the model for tip cell pattern formation based on the reaction and diffusion of VEGF begins with a mass balance equation for extracellular VEGF in a fluid compartment above each endothelial cell:

$$\frac{d(\text{mol } V)}{dt} = (\text{rate produced}) - (\text{rate consumed}) + [(\text{flux in}) - (\text{flux out})] \quad (4.20)$$

where I assume VEGF to be produced at a constant rate by nearby tissues, consumed by the endocytosis of VEGF-VEGFR2 complexes on the endothelial cell surface, and transported between compartments via a diffusion.

I can express this mass balance in terms of VEGF concentrations using the following equation:

$$v_{comp} \frac{dV_i}{dt} = a_{cell}(\dot{V} - \dot{r}_{V,i}) + [(\text{flux in}) - (\text{flux out})] \quad (4.21)$$

where  $v_{comp}$  gives the volume of the fluid compartment,  $a_{cell}$  is area of the cell surface,  $V_i$  gives the molar concentration of VEGF in the fluid compartment,  $\dot{V}$  gives the constant VEGF production rate (with units of [mol area<sup>-1</sup> time<sup>-1</sup>]), and  $\dot{r}_{V,i}$  gives the VEGF consumption rate at the endothelial cell surface (with units of [mol area<sup>-1</sup> time<sup>-1</sup>]). I chose to use per-area consumption and production rates for VEGF reaction because they most closely mirror the available experimental and computational data<sup>110</sup>.

The diffusive flux of VEGF into (or out of) the compartment can be modeled using Fick's second law:

$$\frac{\partial V(x, y)}{\partial t} = D_V \nabla^2 V(x, y) \quad (4.22)$$

where  $D_V$  is the diffusivity of VEGF and  $\nabla^2$  is the Laplace operator.

The spatial domain is discretized into fluid compartments corresponding to each endothelial cell, so I use a discrete approximation of the Laplace operator (known as the five-point stencil) to determine the flux between compartments, given by the following equation:

$$\nabla^2 V_i \approx 4 \frac{\langle V \rangle_i - V_i}{l^2} \quad (4.23)$$

where  $\langle V \rangle_i$  is the average concentration of VEGF across each of the four neighbors of cell  $i$ , and  $l$  is the grid size (i.e., the length of a cell). I can use the connectivity matrix to calculate  $\langle V \rangle_i$ :

$$\langle V \rangle_i = M_{ij} V_j \quad (4.24)$$

Making substitutions into Equation 4.21, our mass balance becomes the following:

$$v_{comp} \frac{dV_i}{dt} = a_{cell}(\dot{V} - \dot{r}_{V,i}) + v_{comp} \frac{4D_V}{l^2} (M_{ij}V_j - V_i) \quad (4.25)$$

Dividing both sides of Equation 4.25 by the volume of the fluid compartment ( $v_{comp}$ ) yields the following equation:

$$\frac{dV_i}{dt} = \frac{1}{h_0}(\dot{V} - \dot{r}_{V,i}) + \frac{4D_V}{l^2} (M_{ij}V_j - V_i) \quad (4.26)$$

where  $1/h_0$  is an effective capacitance (with units of  $[\text{length}^{-1}]$ ) arising from the fraction  $a_{cell}/v_{comp}$ . The parameter  $h_0$  equals the height of the fluid compartment, which has a depth of  $l$  and width of  $l$ , and controls how sensitive the extracellular VEGF concentration is to reaction versus diffusion.

The consumption of VEGF by each endothelial cell is given by the following flux:

$$\begin{aligned} \dot{r}_{V,i} = & (R \text{ internalization rate } [t^{-1}]) \times (R \text{ conc. } [\text{mol area}^{-2}]) \\ & \times (VR \text{ occupancy } [\%]) \end{aligned} \quad (4.27)$$

where  $R$  refers to VEGFR2, the first term gives the internalization rate of VEGFR2 at the cell surface, the second term gives the concentration of VEGFR2 at the cell surface available for endocytosis, and the third term refers to the fraction of VEGFR2 bound to VEGF. In Equation 4.27, I have made the assumption that VEGFR2 is the only receptor internalizing VEGF. Our decision not to include VEGF internalization or degradation by other means was motivated by the high rate of VEGF uptake by VEGFR2 compared to other processes<sup>110</sup>, our lack of knowledge about uptake and trafficking of other VEGF receptors (i.e., VEGFR1)<sup>111</sup>, and our desire to keep the model simple.

I combined the first two terms in Equation 4.27 into a single variable,  $\kappa_i$  (with units [mol area<sup>-2</sup> time<sup>-1</sup>]), which collectively models the “maximum internalization rate” at which VEGF will be up-taken by the cell when it is present at a high extracellular concentration. Biologically, I assume that VEGF-VEGFR2 begins the internalization process by moving into a dynamin-dependent vesicle, followed by endocytosis, activation of the full VEGFR2 signaling cascade, and finally, breakdown of VEGF.<sup>88;92;106</sup> This hypothesis assumes that movement of VEGFR2 into dynamin-dependent vesicles is the rate-limiting step, such that the maximum rate of endocytosis is governed by the activity of dynamin (discussed below).

The occupancy of VEGFR2 by VEGF can be approximated by simple Michaelis-Menton kinetics as in our treatment of lateral inhibition (see Equation 3.7), giving us the following equation for the VEGF internalization rate:

$$\dot{r}_{V,i} = \kappa_i \frac{V_i}{K_V + V_i} \quad (4.28)$$

Substituting Equation 4.28 into our mass balance yields our governing equation for extracellular VEGF:

$$\frac{dV_i}{dt} = \frac{\dot{V} - \kappa_i \frac{V_i}{K_V + V_i}}{h_0} + \frac{4D_V}{l^2} (M_{ij}V_j - V_i) \quad (4.29)$$

VEGF, once internalized, is present as an intracellular VEGF-VEGFR2 complex in a dynamin-dependent vesicle or endosome.<sup>92</sup> Experiments have shown that these intracellular complexes – and not simply VEGF-bound VEGFR2 at the cell surface – are critical to activating the full VEGF-VEGFR2 signaling cascade<sup>92</sup> and the tip cell phenotype<sup>105</sup>. I assume the intracellular complexes ( $I$ ) are formed at the same rate VEGF is shuttled into dynamin-dependent vesicles and degraded via a first-order process:

$$\frac{dI_i}{dt} = \kappa_i \frac{V_i}{K_V + V_i} - k_{\text{deg}} I_i \quad (4.30)$$

where  $I_i$  is the concentration of intracellular VEGF complexes (with units [mol area<sup>-2</sup>]), and  $k_{deg}$  is the first-order decay rate (with units [time<sup>-1</sup>]). I chose to quantify the concentration of intracellular VEGF complexes as an area density, rather than a volumetric density, to simplify calculations; this was done for convenience and has no bearing on the assumed intracellular localization of VEGF, nor the predictions of the model.

The final component of the diffusive mechanism relates the maximum internalization rate ( $\kappa$ ) to the concentration of intracellular VEGF-VEGFR2 complexes ( $I$ ). As discussed previously, full activation of certain pathways downstream of VEGFR2 (such as Akt) require the receptor to be contained in a dynamin-dependent vesicles or endosomes,<sup>88;106</sup> and dynamin activity is under the control of Akt (through eNOS).<sup>107-109</sup> I hypothesized that the movement of VEGFR2 into dynamin-dependent vesicles was the rate-limiting step, as mentioned above, and that the activity of dynamin, and therefore the rate of dynamin-dependent vesicle formation, was governed by intracellular (i.e., in a vesicle or endosome) VEGF-VEGFR2 signaling I formalized this hypothetical link by making the maximum rate of internalization an activating Hill function of intracellular VEGF-VEGFR2 concentration:

$$\kappa_i = a + b \frac{(I_i)^n}{(K_I)^n + (I_i)^n} \quad (4.31)$$

where  $a$  is the basal internalization rate in the absence of feedback from intracellular VEGF-VEGFR2 signaling,  $b$  is the gain in the internalization rate that can occur in the presence of strong intracellular VEGF-VEGFR2 signaling, and  $K_I$  is the concentration of intracellular VEGF-VEGFR2 complexes when the gain is at 1/2 maximum. As in previous examples, I use a Hill function to model the necessary nonlinearity of the mechanism; this nonlinearity might arise in the activation of Akt, eNOS, dynamin, or some combination of those.

In Equation 4.31, I assume that the regulation of endocytosis by VEGF-VEGFR2 signaling is fast compared to the degradation rate of intracellular VEGF ( $k_{deg}$ ); this assumption is most valid if the underlying mechanism is allosteric in nature (as opposed to transcriptional or translation control), which is consistent with the hypothetical mechanisms I provided in Figure 4.1B.

### 4.2.3 Identification of steady-states

I calculated uniform steady-states for each of the mechanisms in Figure 4.1. In this section, I will provide the the methods I used to calculate the steady states for the diffusion and endocytosis hypothesis (Figure 4.1B). However, I assumed, rather than calculated, the steady-states for the double-juxtacrine hypothesis (Figure 4.1A); I had specific goals for the linear stability analysis of this mechanism which required an alternative approach for identifying steady-states. My approach for calculating the steady-state for the double-juxtacrine hypotheses are therefore described in the section labeled “Stability analysis for double-juxtacrine mechanism” below.

The governing equations for diffusion and endocytosis (Equations 4.29-4.31) were nondimensionalized into the following two ODEs:

$$\frac{d\tilde{V}_i}{d\tilde{t}} = \gamma \left( \dot{\tilde{V}} - \left[ \tilde{a} + \tilde{b} \frac{(\tilde{I}_i)^n}{1 + (\tilde{I}_i)^n} \right] \frac{\tilde{V}_i}{1 + \tilde{V}_i} \right) + \tilde{D} (M_{ij}\tilde{V}_j - \tilde{V}_i) = \tilde{V}' \quad (4.32)$$

$$\frac{d\tilde{I}_i}{d\tilde{t}} = \left[ \tilde{a} + \tilde{b} \frac{(\tilde{I}_i)^n}{1 + (\tilde{I}_i)^n} \right] \frac{\tilde{V}_i}{1 + \tilde{V}_i} - \tilde{I}_i = \tilde{I}' \quad (4.33)$$

where  $\tilde{V}_i = \frac{V_i}{K_V}$ ,  $\tilde{I}_i = \frac{I_i}{K_I}$ ,  $\tilde{t} = k_{deg}t$ ,  $\tilde{a} = \frac{a}{k_{deg}K_I}$ ,  $\tilde{b} = \frac{b}{k_{deg}K_I}$ ,  $\gamma = \frac{K_I}{K_V h_0}$ ,  $\dot{\tilde{V}} = \frac{\dot{V}}{k_{deg}K_I}$ ,

and

$$\tilde{D} = \frac{4D_V}{l^2 k_{\text{deg}}}$$

These equations can be simplified by reintroducing  $\kappa$  as a non-dimensional variable:

$$\tilde{\kappa} = \tilde{a} + \tilde{b} \frac{(\tilde{I}_i)^n}{1 + (\tilde{I}_i)^n} \quad (4.34)$$

Using  $\tilde{\kappa}$ , the governing equations can be rewritten as:

$$\frac{d\tilde{V}_i}{d\tilde{t}} = \gamma \left( \dot{\tilde{V}} - \tilde{\kappa}_i \frac{\tilde{V}_i}{1 + \tilde{V}_i} \right) + \tilde{D} (M_{ij} \tilde{V}_j - \tilde{V}_i) = \tilde{V}' \quad (4.35)$$

$$\frac{d\tilde{I}_i}{d\tilde{t}} = \tilde{\kappa}_i \frac{\tilde{V}_i}{1 + \tilde{V}_i} - \tilde{I}_i = \tilde{I}' \quad (4.36)$$

At a uniform steady-state, there is no difference in extracellular VEGF concentration between cells, so Equation 4.35 simplifies to:

$$\dot{\tilde{V}} - \tilde{\kappa}_0 \frac{\tilde{V}_0}{1 + \tilde{V}_0} = 0 \quad (4.37)$$

where the subscript 0 refers to the steady-state value of that species.

Also at the steady-state, Equation 4.36 simplifies to:

$$\tilde{\kappa}_0 \frac{\tilde{V}_0}{1 + \tilde{V}_0} - \tilde{I}_0 = 0 \quad (4.38)$$

From Equations 4.37 & 4.38, it is clear that the steady-state concentration of intracellular VEGF-VEGFR2 complexes ( $\tilde{I}_0$ ) is equal to the non-dimensional parameter  $\dot{\tilde{V}}$ :

$$\tilde{I}_0 = \tilde{\kappa}_0 \frac{\tilde{V}_0}{1 + \tilde{V}_0} = \dot{\tilde{V}} \quad (4.39)$$

The steady-state concentration for extracellular VEGF can be obtained by rearranging Equation 4.37:

$$\tilde{V}_0 = \frac{\dot{V}}{(\tilde{\kappa}_0 - \dot{V})} \quad (4.40)$$

Finally, we can use the equivalence between  $\tilde{I}_0$  and  $\dot{V}$  to calculate  $\tilde{\kappa}_0$ :

$$\tilde{\kappa}_0 = \tilde{a} + \tilde{b} \frac{(\tilde{I}_0)^n}{1 + (\tilde{I}_0)^n} = \tilde{a} + \tilde{b} \frac{(\dot{V})^n}{1 + (\dot{V})^n} \quad (4.41)$$

In conclusion, the steady-state extracellular concentration of VEGF can be calculated directly from the production rate of VEGF (captured in  $\dot{V}$ ), which is an imposed parameter:

$$\tilde{V}_0 = \frac{\dot{V}}{\left( \tilde{a} + \tilde{b} \frac{(\dot{V})^n}{1 + (\dot{V})^n} - \dot{V} \right)} \quad (4.42)$$

I used Equation 4.42 to calculate the steady-state curve in Figure 4.4B directly; the more complex methods used to calculate the steady-states in Figure 3.4 were unnecessary.

#### 4.2.4 Linear stability analysis

As in the previous chapter, I performed a linear stability analysis of the uniform steady-states for each hypothesis to predict whether spatial patterns would begin to form in response to minor, random perturbations. See Chapter 2 for background on the mathematics of pattern formation and Section 3.2 for an introduction to my techniques. Here, I will derive the symmetry-adjusted Jacobian matrices and linear stability criteria for the mechanisms in Figure 4.1.

## Stability analysis for double-juxtacrine

The governing equations for the double juxtacrine mechanism (Equations 4.18 & 4.19) were nondimensionalized into the following two ODEs:

$$\frac{d\tilde{A}_i}{d\tilde{t}} = \frac{1}{1 + \left(\frac{\tilde{B}_i}{\kappa_P}\right)^{n_P}} + \tilde{\beta} \frac{1}{1 + \left(M_{ij} \frac{\tilde{B}_j}{\kappa_A}\right)^{n_A}} - \tilde{A}_i = \tilde{A}' \quad (4.43)$$

$$\frac{d\tilde{B}_i}{d\tilde{t}} = \frac{\left(M_{ij} \frac{\tilde{A}_j}{\kappa_B}\right)^{n_B}}{1 + \left(M_{ij} \frac{\tilde{A}_j}{\kappa_B}\right)^{n_B}} - \tau \tilde{B}_i = \tilde{B}' \quad (4.44)$$

where  $\tilde{A}_i = \frac{A_i \gamma_A}{\beta_P}$ ,  $\tilde{B}_i = \frac{B_i \gamma_A}{\beta_B}$ ,  $\tilde{t} = t \gamma_A$ ,  $\tau = \frac{\gamma_B}{\gamma_A}$ ,  $\kappa_P = \frac{K_P \gamma_A}{\beta_B}$ ,  $\kappa_A = \frac{K_A \gamma_A}{\beta_B}$ , and  $\kappa_B = \frac{K_B \gamma_A}{\beta_P}$ .

The symmetry-adjusted Jacobian<sup>43</sup> for the double juxtacrine, using the dimensionless form of the governing equations (Equations 4.43 & 4.44), is

$$\mathbf{J}_k = \begin{bmatrix} \frac{\partial \tilde{A}'}{\partial \tilde{A}} & \frac{\partial \tilde{A}'}{\partial \tilde{B}} + \frac{\partial \tilde{A}'}{\partial \langle \tilde{B} \rangle} q_k \\ \frac{\partial \tilde{B}'}{\partial \langle \tilde{A} \rangle} q_k & \frac{\partial \tilde{B}'}{\partial \tilde{B}} \end{bmatrix} = \begin{bmatrix} -1 & -\frac{n_P g_P}{\kappa_P} - \frac{\tilde{\beta} n_A g_A}{\kappa_A} q_k \\ \frac{n_B g_B}{\kappa_B} q_k & -\tau \end{bmatrix} \quad (4.45)$$

where

$$g_P = \frac{\kappa_P \left(\frac{\tilde{B}_0}{\kappa_P}\right)^{n_P}}{\tilde{B}_0 \left(1 + \left(\frac{\tilde{B}_0}{\kappa_P}\right)^{n_P}\right)^2} \quad (4.46)$$

$$g_A = \frac{\kappa_A \left(\frac{\tilde{B}_0}{\kappa_A}\right)^{n_A}}{\tilde{B}_0 \left(1 + \left(\frac{\tilde{B}_0}{\kappa_A}\right)^{n_A}\right)^2} \quad (4.47)$$

$$g_B = \frac{\kappa_B \left(\frac{\tilde{A}_0}{\kappa_B}\right)^{n_B}}{\tilde{A}_0 \left(1 + \left(\frac{\tilde{A}_0}{\kappa_B}\right)^{n_B}\right)^2} \quad (4.48)$$

Obtaining a polynomial for the eigenvalues of the eigenvalues of the Jacobian using the equation  $|\mathbf{J}_k - \lambda_k \mathbf{I}| = 0$  and applying the Routh-Hurwitz stability theorem<sup>59</sup> yields the following inequality:

$$\tau \kappa_A \kappa_B \kappa_P + n_B n_P g_B g_P \kappa_A q_k + \tilde{\beta} n_A n_B g_A g_B \kappa_P (q_k)^2 > 0 \quad (4.49)$$

Importantly, the criterion in Equation 4.49 is parabolic with respect to the structural eigenvalue ( $q_k$ ). I used this property to restrict instability to a limited number of structural eigenvalues — a concept known as mode selection<sup>47</sup>. I can determine which structural mode is most unstable by taking the derivative of the above inequality with respect to  $q_k$  and setting it equal to zero,

$$q_{\max} = -\frac{n_P g_P \kappa_A}{2\tilde{\beta} n_A g_A \kappa_P} \quad (4.50)$$

The maximum dynamic eigenvalue ( $\lambda_{\max}$ ) at this maximally unstable structural mode is

$$\lambda_{\max} = \sqrt{\frac{1}{4}(\tau - 1)^2 - \frac{g_B g_P n_B n_P q_{\max}}{\kappa_B \kappa_P} - \frac{\beta g_A g_B n_A n_B (q_{\max})^2}{\kappa_A \kappa_B}} - \frac{1}{2}(\tau + 1) \quad (4.51)$$

Equations 4.50 & 4.51 can be used to calculate sets of parameters which produce an initial condition that is most unstable at a specified  $q_{\max}$ . My approach to selecting such a mode was to assume that all the Hill functions were at exactly one half of their maximum value for the initial condition, which occurs when

$$\kappa_A = \kappa_P = \tilde{B}_0 \quad (4.52)$$

$$\kappa_B = \tilde{A}_0 \quad (4.53)$$

Under this assumption, Equations 4.50 & 4.51 converge to

$$g_A = g_B = g_P = \frac{1}{4} \quad (4.54)$$

With the additional assumption that  $\tilde{\beta} = 1$ , the equation for  $q_{\max}$  simplifies to

$$q_{\max} = -\frac{n_P}{2n_A} \quad (4.55)$$

The equation for  $\lambda_{\max}$  simplifies to

$$\lambda_{\max} = \frac{1}{8} \sqrt{\frac{2n_B n_P^2}{n_A}} - 1 \quad (4.56)$$

At this point, the only parameters remaining to satisfy the goal of having a maximally unstable mode with structural eigenvalue  $q_{\max}$  and dynamic eigenvalue  $\lambda_{\max}$  are  $n_A$ ,  $n_B$ , and  $n_P$ . With three unknowns and two equations, the system of equations is underconstrained. In simulating the double juxtacrine system, I assumed a value for  $n_P$ , and then used Equations 4.55 & 4.56 to determine appropriate values for  $n_A$  and  $n_B$ . Below, I give an example of how the final parameters are generated for a typical scenario.

$$q_{\max} = -0.45 \quad (4.57)$$

$$\lambda_{\max} = 0.2 \quad (4.58)$$

$$n_P = 6 \quad (4.59)$$

$$n_A = -\frac{n_P}{2q_{\max}} = 6.667 \quad (4.60)$$

$$n_B = 32 \frac{(\lambda_{\max} + 1)^2 n_A}{n_P^2} = 8.533 \quad (4.61)$$

### Stability analysis for diffusion and endocytosis

The symmetry-adjusted Jacobian<sup>43</sup> for the diffusive instability, using the dimensionless form of the governing equations (Equations 4.32 & 4.33), is

$$\begin{aligned} \mathbf{J}_k &= \begin{bmatrix} \frac{\partial \tilde{V}'}{\partial \tilde{V}} + \frac{\partial \tilde{V}'}{\partial \langle \tilde{V} \rangle} q_k & \frac{\partial \tilde{V}'}{\partial \tilde{I}} \\ \frac{\partial \tilde{I}'}{\partial \tilde{V}} & \frac{\partial \tilde{I}'}{\partial \tilde{I}} \end{bmatrix} \\ &= \begin{bmatrix} -\frac{\gamma \tilde{\kappa}_0}{(1+\tilde{V}_0)^2} + \tilde{D} (q_k - 1) & -\frac{\gamma \tilde{V}_0}{(1+\tilde{V}_0)} \left( \frac{\partial \tilde{\kappa}}{\partial \tilde{I}} \right) \Big|_{SS} \\ \frac{\tilde{\kappa}_0}{(1+\tilde{V}_0)^2} & \frac{\tilde{V}_0}{(1+\tilde{V}_0)} \left( \frac{\partial \tilde{\kappa}}{\partial \tilde{I}} \right) \Big|_{SS} - 1 \end{bmatrix} \end{aligned} \quad (4.62)$$

where

$$\left(\frac{\partial \tilde{\kappa}}{\partial \tilde{I}}\right)\Big|_{SS} = \frac{\tilde{b}n(\tilde{I}_0)^{n-1}}{\left[1 + (\tilde{I}_0)^n\right]^2} \quad (4.63)$$

I can simplify the Jacobian and improve its utility in intuitively understanding the mechanism of pattern formation by introducing the partial derivative of uniform, steady-state concentration of extracellular VEGF ( $\tilde{V}_0$ ) with respect to the production rate of VEGF ( $\dot{V}$ ):

$$\left(\frac{\partial \tilde{V}_0}{\partial \dot{V}}\right) = \frac{\partial \left(\frac{\dot{V}}{(\tilde{\kappa}_0 - \dot{V})}\right)}{\partial \dot{V}} = \frac{1}{(\tilde{\kappa}_0 - \dot{V})} - \frac{\dot{V}}{(\tilde{\kappa}_0 - \dot{V})^2} \left[ \left(\frac{\partial \tilde{\kappa}}{\partial \tilde{I}}\right)\Big|_{SS} - 1 \right] \quad (4.64)$$

The partial derivative on the left-hand side of Equation 4.64 is the slope of the curve in Figure 4.4B for any value of  $\dot{V}$  (the dimensionless form of  $V$ ). The slope in Figure 4.4B and the partial derivative in Equation 4.64 are negative for the dashed portion of the curve.

I can rearrange the expression and perform substitutions to isolate the other partial derivative in Equation 4.64:

$$\left(\frac{\partial \tilde{\kappa}}{\partial \tilde{I}}\right)\Big|_{SS} = \frac{(1 + \tilde{V}_0)^2 - \tilde{\kappa}_0 \left(\frac{\partial \tilde{V}_0}{\partial \dot{V}}\right)}{\tilde{V}_0 (1 + \tilde{V}_0)} \quad (4.65)$$

Substituting Equation 4.65 back in the Jacobian of Equation 4.62 and simplifying yields an alternative symmetry-adjusted Jacobian:

$$\mathbf{J}_k = \begin{bmatrix} -\frac{\gamma \tilde{\kappa}_0}{(1 + \tilde{V}_0)^2} + \tilde{D}(q_k - 1) & -\gamma + \gamma \frac{\tilde{\kappa}_0}{(1 + \tilde{V}_0)^2} \left(\frac{\partial \tilde{V}_0}{\partial \dot{V}}\right) \\ \frac{\tilde{\kappa}_0}{(1 + \tilde{V}_0)^2} & -\frac{\tilde{\kappa}_0}{(1 + \tilde{V}_0)^2} \left(\frac{\partial \tilde{V}_0}{\partial \dot{V}}\right) \end{bmatrix} \quad (4.66)$$

Obtaining a polynomial for the dynamic eigenvalues of the Jacobian using the equation  $|\mathbf{J}_k - \lambda_k \mathbf{I}| = 0$  and applying the Routh-Hurwitz stability theorem yields

the following two inequalities:

$$1 - \tilde{D} (q_k - 1) \frac{1}{\gamma} \left( \frac{\partial \tilde{V}_0}{\partial \dot{V}} \right) > 0 \quad (4.67)$$

$$\gamma \tilde{\kappa}_0 + \left( \frac{\partial \tilde{V}_0}{\partial \dot{V}} \right) \tilde{\kappa}_0 - \tilde{D} (q_k - 1) \left( 1 + \tilde{V}_0 \right)^2 > 0 \quad (4.68)$$

The first criterion (Equation 4.67) can only be unstable if the partial derivative on the left-hand side of Equation 4.64 is negative, and the instability will be strongest as  $q_k \rightarrow -1$ . To better understand the second term in Equation 4.67, I made the following rearrangement:

$$1 - \frac{\tilde{D} (q_k - 1)}{\gamma \left( \frac{\partial \dot{V}}{\partial \tilde{V}_0} \right)} > 0 \quad (4.69)$$

The numerator of the second term of Equation 4.69 is a dimensionless representation of the sensitivity of the *diffusive* VEGF flux between cells on a structural mode to the VEGF concentration excursion of that structural mode – it is a measure of how much VEGF will diffuse between cells when there is a spatial pattern of VEGF. A cellular lattice with a VEGF concentration pattern resembling a fine-grained structural mode ( $(q_k \rightarrow -1)$ ) will diffuse VEGF much more efficiently than a concentration pattern resembling a broad structural mode ( $(q_k \rightarrow 1)$ ) because of the differences in the local VEGF gradients; and a system with a high diffusivity ( $\tilde{D}$ ) will diffuse VEGF more efficiently than a system with a low diffusivity.

The denominator of the second term of Equation 4.69 is a dimensionless representation of the sensitivity between the *endocytic* VEGF flux and a cell's local VEGF concentration excursion – it is a measure of how much more(or les) VEGF a cell will internalize when the extracellular VEGF concentration changes. The more nonlinear the machinery governing VEGF endocytosis – and the steeper the

negative slope in Figure 4.4B – the more sensitive the steady-state concentration of VEGF is to the rate of VEGF internalization; inversely, the endocytic VEGF flux grows less sensitive to the steady-state VEGF concentration excursion as the denominator grows larger – cells will consume VEGF at a nearly constant rate regardless of extracellular VEGF concentration if the denominator is large.

This instability can be said to occur when the ratio of each sensitivity is greater than one:

$$\frac{\Delta \vec{V}_{\text{Diffusive}}(q_k)}{\Delta \vec{V}_{\text{Endocytic}}} > 1 \quad (4.70)$$

such that minor increases in a cell's rate of internalization ( $\Delta \vec{V}_{\text{Endocytic}}$ ) effect greater changes in the cell's diffusive flux ( $\Delta \vec{V}_{\text{Diffusive}}(q_k)$ ) through the creation of a local VEGF concentration gradient. The increased flux of VEGF from neighboring cells sustains the elevated rate of VEGF internalization.

The second criterion (Equation 4.68) can likewise only become unstable when the partial derivative in Equation 4.64 is negative, but the instability is not one of spatial pattern formation: this criterion can only be satisfied when the diffusivity of VEGF is low. The instability is strongest when the diffusivity is zero, meaning the instability is not dependent on spatial exchange of VEGF. I did not observe this instability in the numerical simulation, but I expect it may correspond to a switch-like bifurcation between uniformly high or low steady-states of VEGF internalization/concentration, similar to the instability observed during lateral induction (see Figure 3.6).

### 4.2.5 Numerical simulation

I simulated pattern formation for each hypothesis in Figure 4.1 using the same methods provided in Section 3.2.

As in Chapter 3, I chose the parameters used to simulate each hypothesis (provided in Table 4.1) primarily based on their ability to become unstable as predicted by the linear stability analysis. In the section entitled “Stability analysis for double-juxtacrine” above, I explained my rationale for selecting parameters for the double-juxtacrine hypothesis so I could explore the parabolic stability profile of the mechanism. However, in the case of the *diffusion and endocytosis* hypothesis, I did incorporate some previous experimental and computational literature when estimating some parameters, as captured in Table 4.1.

To assign the parameters for the Diffusion & Endocytosis mechanism, we made the following assumptions based on the literature: each endothelial cell had a length  $l = 20 \mu\text{m}$ , or a surface area of 400 square microns<sup>5</sup>. We assumed that the diffusivity of VEGF in interstitial space was  $104 \mu\text{m}^2/\text{s}$ <sup>110</sup>. We assumed that VEGF, once internalized, degraded at a first-order rate  $k_{deg} = 0.05 \text{ s}^{-1}$ <sup>112</sup>. Based on the above three parameters, we calculated the non-dimensional parameter  $\tilde{D} = 5.2$ .

The remaining non-dimensional parameters related mostly to the flux of VEGF into the endothelial cell. Physically, this rate depends on the surface concentration of VEGF receptors, their occupancy, and the internalization rate of the receptors. A previous computational study estimated that VEGF was bound to adult muscular capillaries at a density of  $0.45\text{--}2 \times 10^{-4} \text{ pmol}/\text{cm}^2$ <sup>110</sup>, which translates into a steady-state flux of VEGF into cells of  $0.225\text{--}1 \times 10^{-17} \text{ mol}/\text{cm}^2/\text{s}$  when  $k_{deg} = 0.05 \text{ s}^{-1}$ . We explored a range of steady-state fluxes higher than that,

**Table 4.1: Parameters for numerical simulation.**

Parameter	Description	Value	References
<b>Non-dimensional Parameters (DJ)<sup>a</sup></b>			
$\tilde{\beta}$	Relative portion of A expression sensitive to trans-inhibition	1	
$\kappa_A$	Dissoc. const. of trans-inhibition of A	0.5	
$\kappa_B$	Dissoc. const. of trans-activation of B	1	
$\kappa_P$	Dissoc. const. of cis-inhibition of A	0.5	
$n_p$	Effective Hill coefficient for cis-inhibition of A by B	6	
$\tau$	Relative time scales of A and B	1	
<b>Dimensional Parameters (DE)</b>			
$h_0$	Height of fluid volume	10 $\mu\text{m}$	
$l$	Length of cell edge	20 $\mu\text{m}$	5
$D_V$	Diffusivity of VEGF	104 $\mu\text{m}^2/\text{s}$	110
$k_{deg}$	Degradation rate of internalized VEGF	0.05 $\text{s}^{-1}$	112
$\dot{V}$	VEGF production rate	4.81– $6.73 \times 10^{-17}$ $\text{mol}/\text{cm}^2/\text{s}$	27;105;110
$K_V$	Dissociation constant of VEGFR2	150 $\mu\text{M}$	114
$K_I$	Dissociation constant of Hill function	$1.18^{-17}$ $\text{mol}/\text{cm}^2$	
$a$	Basal capacity for VEGF internalization	$3.47 \times 10^{-17}$ $\text{mol}/\text{cm}^2/\text{s}$	
$b$	Maximum increase in VEGF internalization	$6.96 \times 10^{-17}$ $\text{mol}/\text{cm}^2/\text{s}$	
<b>Non-dimensional Parameters (DE)</b>			
$\tilde{a}$	Basal capacity for VEGF internalization	0.588	
$\tilde{b}$	Max increase in VEGF internalization	1.18	
$\gamma$	Degradation rate of internalized VEGF	7.87	
$\dot{\tilde{V}}$	VEGF production rate	0.816–1.14	
$\tilde{D}$	Diffusivity	5.2	
$n$	Hill coefficient for up-regulation of internalization	4	

(a) Values for  $n_A$  and  $n_B$  are calculated at runtime. See section “Stability analysis for double-juxtacrine” for calculation details.

$\dot{V} = 4.81\text{--}6.73 \times 10^{-17}$  mol/cm<sup>2</sup>/s, because at the proximal end of the plexus during sprouting angiogenesis can have drastically higher VEGF binding than other parts of the capillary vasculature<sup>27;105</sup>.

The only other parameter we could extract from the literature was a dissociation constant of VEGFR2  $K_V = 150$  pM<sup>114</sup>. The remaining physical parameters ( $h_0, K_I, a, b$ ), and non-dimensional parameters based on them, we assigned as needed induce pattern formation.

Following each simulation, we counted the number of tip cells which emerged in the final steady-state. We defined tip cells as those having a concentration of intracellular VEGF-VEGFR2 complexes higher than the concentration of initial condition; experiments have shown that tip cells require signaling from these intracellular complexes to form (as opposed to VEGF bound to the cell surface)<sup>88;105</sup>.

The only other parameters I could extract from the literature was a dissociation constant of VEGFR2 ( $K_V$ ) of 150 pM.<sup>114</sup> The remaining physical parameters, and non-dimensional parameters based on them, I had to guess or assign arbitrarily.

Following simulation of each hypothesis, I counted the number of tip cells which emerged from pattern formation. For the double-juxtacrine hypothesis, I arbitrarily defined tip cells as those having a relatively high concentration of species A. For the diffusion and endocytosis hypothesis, I defined tip cells as those having a relatively high concentration of intracellular VEGF-VEGFR2 complexes ( $I$  in Equation 4.30), as previous experiments have shown that tip cells require signaling from these intracellular complexes to form (as opposed to VEGF bound to the cell surface).<sup>88;105</sup>

## 4.3 Results

### 4.3.1 Double-juxtacrine

#### Biological basis

Figure 4.3A provides an overview of a hypothetical network in which two juxtacrine signaling pathways operate independently to influence each other's expression levels. In this hypothetical network, a species A trans-activates the expression of a species B, which, in turn, reduces the expression of A in its local cell and in neighboring cells. As discussed previously, this network of signaling and gene regulation contains a circuit of lateral inhibition – species A laterally inhibits itself by down-regulating B. As such, the lateral inhibition circuit within the generic model presented here may be analogous to the lateral inhibition of Delta (analogous to species A) through its activation of Notch (analogous to species B). I cannot, as of yet, propose a juxtacrine signaling pathway that would complete the analogy for the whole network; I would need to find a ligand which is up-regulated by Notch activation and activates a receptor in neighboring cells that down-regulates Delta expression when active.

#### Analysis

I analyzed the linear stability of this mechanism, but did not investigate how the stability changes with the concentration of VEGF, as in previous examples (see Figures 3.5B and 3.6B). In the absence of molecular species to map the reaction network in Figure 4.3A onto, there was no obvious parameter to vary. Rather, I

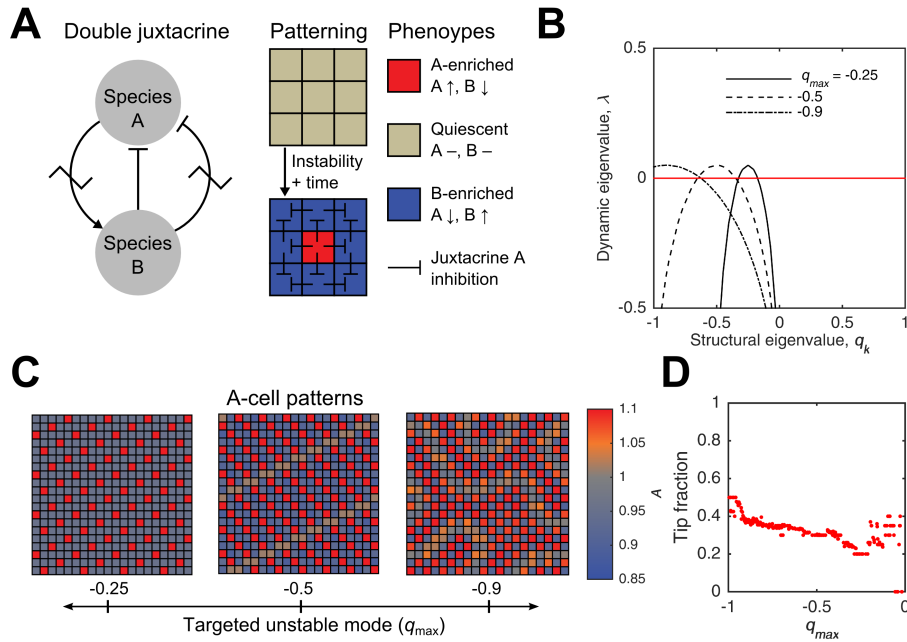


**Figure 4.3: Double juxtacrine mechanism.** (A) Overview of double juxtacrine. Species A promotes the expression of species B through a juxtacrine signaling pathway. Species B represses the expression of species A in the local cell and in neighboring cells through another, hypothetical juxtacrine signaling pathway. (B) Stability profile of double juxtacrine. Dynamic eigenvalues of the symmetry-adjusted Jacobian matrix (from Equation 3.14) are given versus the structural eigenvalue for several selections of the maximally unstable structural mode ( $q_{max}$ ). Our method for generating parameters based on target values of  $q_{max}$  is given in Table 4.1. (C) Patterning of double juxtacrine. The density of tip cell patterning changes with value of  $q_{max}$ . (D) Fraction of tip cells with increasing  $q_{max}$ . The fraction of tip cells in the final pattern decreases from 50% as  $q_{max}$  is increased from -1. Tip cell fraction reaches a minimum of 20% for  $q_{max} \approx -0.25$ .

employed a heuristic for finding valid steady-states with goal of exploring possible “mode selection”<sup>47</sup>, which is the ability to restrict patterning instabilities to certain structural modes, as enabled by the unique stability criterion for this mechanism:

$$C_1(q_k)^2 + C_2q_k + C_3 > 0 \quad (4.71)$$

where  $C_1$ ,  $C_2$ , and  $C_3$  are positive functions that do not depend on  $q_k$ .

Equation 4.71 demonstrates a parabolic dependence of the stability of the system on the structural eigenvalue. Unlike the previous criteria (Equation 3.33 & 3.34), this criterion may remain stable at the high ( $q_k \rightarrow 1$ ) and low ( $q_k \rightarrow -1$ ) extremes of the structural spectrum while being unstable for intermediate values of  $q_k$ .

I selected parameters for this system which to produced uniform steady states with instabilities that peaked at targeted values of  $q_k$ (i.e., mode selection). Figure 4.3B shows dynamic eigenvalues calculated for three sets of parameters intended to produce maximally unstable structural eigenvalues of  $q_{\max} = -0.25, -0.5,$  and  $-0.9$ . The magnitude of largest dynamic eigenvalues in each curve is parabolic with respect to  $q_k$  and matches its specification for  $q_{\max}$ .

## Simulation

Figure 4.3C shows the final steady states of three simulations tailored to have maximal instabilities at the indicated structural eigenvalues. Initial conditions with maximally unstable structural eigenvalues that approached the negative extreme of the structural spectrum ( $q_k \rightarrow -1$ ) produced patterns resembling those of lateral inhibition: checkerboards with phenotypes split between 50% elevated and 50% reduced concentrations of A. However, as I shifted the peak towards the middle

of the spectrum ( $q_k \rightarrow 0$ ), patterns emerged with significantly lower densities of A-enriched cells.

Figure 4.3D gives the tip cell fractions observed for each value of  $q_{\max}$  using either random initial condition. Tip cell fraction reaches a minimum of 20% for  $q_{\max} \approx -0.25$ , and I observed inconsistent patterning for values of  $q_{\max}$  above -0.25. The inconsistent patterning may be a result of our parameter generation heuristic, as the calculated Hill coefficients become very large to achieve values of  $q_{\max}$  that approach zero. Nonetheless, these results provide a proof-of-concept for compound juxtacrine signaling networks – utilizing more than just the Notch receptor – having the ability to select tip cell patterns with intermediate densities.

### 4.3.2 Diffusion and endocytosis

#### Biological basis

Figure 4.1B illustrates an example of a mechanism in which the diffusion of a species (in this case VEGF), rather than juxtacrine signaling, plays the leading role in facilitating multicellular cooperation during tip cell selection. Our proposed mechanism follows from observations that internalization of VEGF is required for full VEGF-VEGFR2 activation and tip cell formation<sup>88;105</sup>; internalization and subsequent degradation might be self-reinforcing because components of the VEGFR2 endocytosis pathway – namely, Akt, eNOS, and dynamin – are downstream of signaling from internalized VEGF-VEGFR2 complexes.<sup>106–109</sup> Such positive feedback permits a model in which successful tip cells require relatively high rates of VEGF internalization, signaling, and degradation to deplete the VEGF available to other endothelial cells. In essence, emerging tip cells might “steal

VEGF”<sup>104</sup> to reduce the total number of tip cells, permitting tunable density of tip cell selection in contrast to the hypothesis of Notch-based lateral inhibition (Figure 3.5).

## Analysis

Our analysis of this diffusive mechanism differs from the previous examples in that I did not include Notch signaling (to be discussed), and I considered extracellular VEGF to be a dynamic species rather than a controlled parameter or imposed function of position. Figure 4.4A summarizes the core of the hypothesis: extracellular VEGF ( $V$ ) can diffuse (wavy arrow) or be internalized to form intracellular VEGF complexes ( $I$ ) through a saturable endocytosis pathway where the rate-limiting step is the movement of VEGF-VEGFR2 complexes into dynamin-dependent vesicles.<sup>106</sup> Signaling from endosomal VEGF complexes can increase the maximum rate of internalization ( $\kappa$ ) through a non-linear process (dashed arrow). A final pattern can be reached in which a sub-population of cells are selected as tip cells (red), with elevated rates of VEGF endocytosis despite having low VEGF concentrations; while the remaining cells become stalk cells (blue), with slow VEGF endocytosis and higher local VEGF concentrations. The pattern of VEGF concentration is maintained by a diffusive flux of VEGF (green, wavy arrows) from stalk to tip cells.

Figure 4.4B shows the uniform steady-states of VEGF concentration ( $V/V_0$ ) which can occur for given rates of extracellular VEGF production ( $\dot{V}/\dot{V}_C$ ). Here, VEGF production rates are given relative to the location of the local maximum in VEGF concentration, where I assume  $\dot{V}/\dot{V}_C = 1$ . Briefly, the production rate of VEGF ( $\dot{V}$  in Equation 4.29) adjacent to the tissue serves as the control parameter

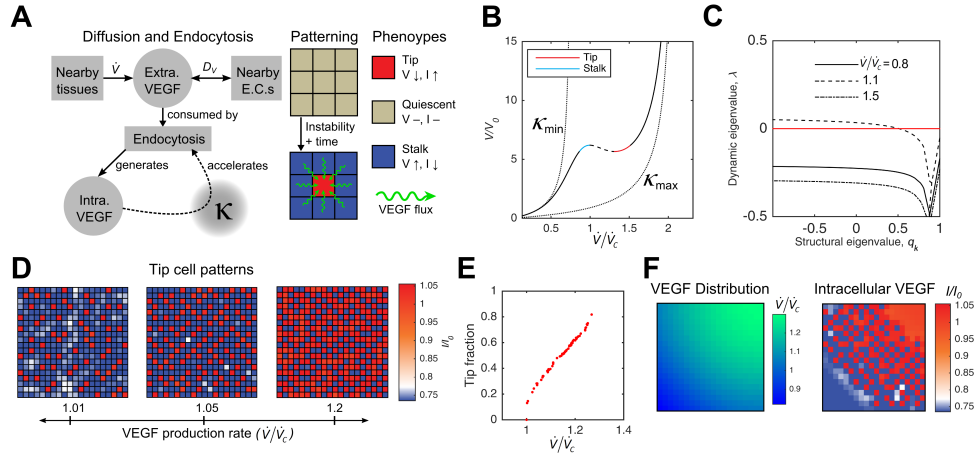


**Figure 4.4: Diffusion and endocytosis.** (A) Overview of diffusion and endocytosis. Extracellular VEGF ( $V$ ) can be internalized to form intracellular VEGF complexes ( $I$ ). The concentration of  $I$  sharply increases the maximum VEGF internalization rate ( $\kappa$ ) when above a certain threshold. This mechanism can create a spatial pattern in which tip cells (red) have a high rate of internalization and a low VEGF concentration; tip cells receive a diffusive flux of VEGF (green, wavy arrows) from stalk cells (blue), which have a low rate of internalization and a high VEGF concentration. (B) Steady-states of diffusion and endocytosis. The uniform steady-states of the system with respect to the normalized VEGF concentration ( $V/V_0$ ) and VEGF production rate ( $\dot{V}/\dot{V}_C$ ) can be found using a single-cell model (see DIFFUSIVE STEADY STATE). At low or high production rates of VEGF, the maximum internalization rate ( $\kappa$ ) is approximately constant and the steady state curve approaches the dotted curves at  $\kappa_{min}$  and  $\kappa_{max}$ . As a result of the sharp increase of  $\kappa$  in response to endosomal VEGF signaling, the steady-state curve transitions between the two regimes (solid segments of curve), resulting in the curve having a segment with negative slope (dashed segment). (C) Stability profile of diffusion and endocytosis. Dynamic eigenvalues of the symmetry-adjusted Jacobian (from Equation 3.14) for the diffusive instability at various production rates of VEGF. Steady-states with moderate production rates of VEGF fall on the dashed segment in (B) and are the most unstable. (D) Patterning of diffusion and endocytosis. Increasing the VEGF production above the critical rate ( $\dot{V}_C$  in B) causes tip cells (red) to form sporadically in the endothelium, as defined by their high concentration of intracellular VEGF complexes ( $I/I_0$ ). Increasing the VEGF production rate causes additional tip cells to form until the endothelium is uniformly high in intracellular VEGF complexes. (E) Fraction of tip cells with increasing levels of VEGF production. Increasing the production rate of VEGF smoothly increases the fraction of the tip cells in the final pattern from 10% to 84%. (F) Spatially dependent VEGF and diffusive patterning. A spatially varying production rate of VEGF (top) causes the local pattern of tip cell selection to vary from low to high densities (bottom). Parameter values given in Table 4.1.

for the system; at the uniform steady-state,  $\dot{V}$  is proportional to the concentration of intracellular VEGF complexes ( $I_i$  in Equation 4.30). I identified the uniform steady-states of the system by calculating the VEGF concentrations ( $V/V_0$ , y-axis in Figure 4.4B) for each supplied value of the VEGF production rate ( $\dot{V}/\dot{V}_C$ , x-axis in Figure 4.4B).

Instabilities were predicted for the segment (dashed line) of the curve in Figure 4.4B where the slope of steady-state VEGF concentration to VEGF production rate was negative ( $1 < \dot{V}/\dot{V}_C < 1.26$ ). This region can be understood as a transition between two regimes where the VEGF endocytosis pathway is becoming saturated with extracellular VEGF. To help illustrate this transition, I provide two alternative curves (dotted lines) that relate the steady-state VEGF concentration to the rate VEGF production (or internalization) when the maximum rate of internalization ( $\kappa$ ) is fixed at its lowest ( $\kappa_{min}$ ) or highest ( $\kappa_{max}$ ) possible value. In each case, the steady-state VEGF concentration asymptotically increases towards infinity as the endothelium is unable to internalize VEGF at the rate it is being produced. When nonlinear feedback mechanisms allow the maximum rate of internalization ( $\kappa$ ) to increase sharply above a threshold level of endosomal VEGF signaling (e.g.,  $\kappa$  increases from  $\kappa_{min}$  to  $\kappa_{max}$ ), the system must transition between the regimes. Where the transition is observed, the sharply increasing trend is briefly reversed and I predict a negative slope between the VEGF production rate and the steady-state VEGF concentration. A consequence of this negative slope is that endothelial cells with higher rates of VEGF internalization are able to persist at lower concentrations of VEGF; this state is consistent with our definition of a tip cell in this context (Figure 4.4A).

To verify the existence of an instability for the dashed segment of the curve in

Figure 4.4B, I derived the following stability criterion:

$$1 - \tilde{D} (q_k - 1) \frac{1}{\gamma} \left( \frac{\partial \tilde{V}_0}{\partial \dot{V}} \right) > 0 \quad (4.72)$$

which uses parameters from the non-dimensional forms of the governing equations for this mechanism (Equations 4.32 & 4.33). The dimensionless parameter  $\dot{V}$  corresponds to the production rate of VEGF ( $\dot{V}$ ), while  $\tilde{V}$  denotes the steady-state concentration of VEGF, so the partial derivative in Equation 4.72 directly captures the slope of the curve in Figure 4.4B. It is clear from Equation 4.72 that the partial derivative (and hence slope in Figure 4.4B) must be negative for the system to become unstable: the dimensional parameters  $\gamma$  and  $\tilde{D}$  are always positive, and the structural eigenvalue ( $q_k$ ) is always less than 1.

To further analyze the instability, I numerically calculated the dynamic eigenvalues for each structural mode at several representative production rates of VEGF, as shown in Figure 4.4C. Steady-states which occur below the critical production rate of VEGF ( $\dot{V}/\dot{V}_C < 1$ ) correspond to a region of Figure 4.4B with a positive slope in Figure 4.4B; they were always stable. Steady-states which occurred slightly above the critical production rate of VEGF ( $\dot{V}/\dot{V}_C > 1$ ) correspond to the region of Figure 4.4B with a negative slope; they can become unstable for lower values of  $q_k$ . Steady-states with very high VEGF production ( $\dot{V}/\dot{V}_C > 1.26$ ) again correspond to a region with a positive slope; the initial conditions here are also stable. In each case, the dynamic values gradually increase as the structural eigenvalues decrease. This trend is qualitatively similar to the stability profile of lateral inhibition (Figure 3.5C), indicating that “checkerboard” patterns of tip cells initially grow most rapidly from unstable initial conditions.

## Simulation

I simulated pattern formation under this mechanism for various points along the curve in Figure 4.4B. Figure 4.4D shows the final results of simulating pattern formation for several VEGF production rates which slightly exceed the local maximum in Figure 4.4B ( $\dot{V}/\dot{V}_C > 1$ ). Although Figure 4.4C predicts the initial patterning trajectory favors a checkerboard tip pattern, a wide variety of tip cell patterns formed as a result of simulating this mechanism.

For lower rates of VEGF production (Figure 4.4D, left), the pattern consisted of a small number of tip cells (red) distributed irregularly around the endothelium, with the remaining cells becoming stalk (blue) cells. As the production rate of VEGF increased (Figure 4.4D, right), more tip cells were present in the final endothelium, and for very high production rates, tip cells outnumbered stalk cells. The location of tip cells within the lattice varied between each simulation, although the number of tip cells selected remained consistent for a given production rate of VEGF. This sensitivity to the initial perturbation distinguishes this mechanism from the others (Figures 3.5-4.3) for which the final patterns were periodic and insensitive to the spatial details of the perturbation.

Figure 4.4E shows the number of tip cells counted in the final endothelium as a function of the VEGF production rate. Consistent with the linear stability analysis, tip cells only emerged from initial conditions that fell on the downward-sloping portion of the curve in Figure 4.4B ( $1 < \dot{V}/\dot{V}_C < 1.26$ ). The fraction of tip cells selected jumped discontinuously from 0% to 10% upon increasing beyond  $\dot{V}/\dot{V}_C = 1$ , and dropped from 84% to 0% as VEGF production was increased beyond  $\dot{V}/\dot{V}_C = 1.26$ . However, between these limits, the fraction of tip cells emerging from the endothelium varied continuously and monotonically with respect

to the VEGF production rate.

Figure 4.4F depicts tip cell patterning for an endothelium with spatially varying production rates of VEGF. As in previous cases, tip cell characteristics are uniformly upregulated (orange) in areas of high VEGF, and downregulated in areas of low VEGF (blue). However, this diffusive mechanism is unique among those considered here in that local density of tip cells varies continuously from low to high according to the local production rate of VEGF.

## 4.4 Discussion

In this chapter, I proposed and analyzed two new hypotheses, depicted in Figure 4.1, for the molecular underpinnings of spontaneous tip cell pattern formation. My primary goal was to understand if hypotheses with logical structures and biological interpretations which differed from the standard hypotheses of Notch-based lateral inhibition or induction (explored in Chapter 3) could exhibit a wider range of tip cell selection densities, in line with the consensus view that tip cell selection density is a determinant of angiogenic sprouting density and microvascular structure.<sup>13;17</sup> I found that hypotheses which incorporate new juxtacrine pathways alongside Notch (Figure 4.3) or consider VEGF as tightly-regulated component of a reaction-diffusion mechanism (Figure 4.4) can exhibit a wide range of tip cell selection densities. Below, I will discuss the implications of these results, with an emphasis on interpreting past studies and designing future experiments on endothelial tip cell formation.

## Main findings

### **Inclusion of a second juxtacrine signaling pathway alongside Notch can lower tip cell selection density**

As noted in Chapter 3, lateral inhibition via Notch might provide endothelial cells a robust means to create dense patterns of 50% tip and 50% stalk cells. However, as shown in Figure 3.5, lateral inhibition has no ability to deviate from these percentages in response to changes in the magnitude of signaling processes or gene regulation – this rigidity would prevent tip cells from finely “balancing”<sup>17</sup> the number of stalk cells they recruit, or stalk cells from ensuring they are not neighboring (and therefore beholden to) more than one tip cell. Previous authors have correctly noted that in lateral inhibition, no more than two stalk cells can occur side-by-side in a linear arrangement of cells, because adding a third stalk cell would encourage the middle cell to become a tip cell.<sup>51;103</sup> However, these authors have no explanation for how lateral inhibition could consistently ensure that two (and not one) stalk cell would separate adjacent tip cells (as commonly depicted in “cartoons” of tip cell selection<sup>17</sup>) when lateral inhibition inherently favors a 50% tip cell pattern (i.e., one stalk cell separating two tip cells).

In Figure 4.1A, I hypothesize the existence of a juxtacrine signaling pathway, separate from Delta-Notch signaling, which allows a stalk cell to effectively “report” to its neighbors the number of tip cells bordering it; this juxtacrine signal, when strong, can down-regulate tip cell characteristics. I hypothesized that this mechanism would, in a sense, allow the “cartoon” outcome of exactly two stalk cells separating tip cells to be enforced.

My analysis of the logical structure of this new multicellular signaling network

(depicted in a reduced form in Figure 4.3A) yielded several important insights. First, unlike any other mechanism in Chapters 3 and 4, the stability criterion (4.71) and stability profile (4.3B) of this mechanism are parabolic with respect to the structural eigenvalue; this allows initial tip cell patterning (i.e., near the uniform steady-state) to be restricted to certain wavelengths, in a process known in the mathematical community as “mode selection”.<sup>47</sup> To my knowledge, no previous study has demonstrated mode selection in a biological system based purely on juxtacrine signaling, although some studies have allowed lateral inhibition to achieve more sparse patterns by coupling it to a diffusive mechanism.<sup>115</sup>

Next, I wanted to explore whether this hypothetical mechanism could achieve tip cell patterns sparser than 50% in simulation. The large number of parameters in this model compared to previous hypothesis would have made it difficult to find regimes with sparse patterns by trial-and-error; I hypothesized that mode selection using the parabolic stability profile would allow me to define different regimes of patterning. Indeed, as shown in Figure 4.3C, the final patterns of tip cell selection did change depending on the mode selected by the initial instability. The coupling between tip cell density and patterning mode was generally preserved throughout the “fine-grained” spectrum of the connectivity matrix (i.e.,  $q_k < 0$ , see Figure 2.2) as shown in Figure 4.3D – however the numerical simulation became highly erratic for mode selection above  $q_k = -0.25$ , perhaps due to the method I used to provide parameters in this mechanism or my decisions of how to structure the governing equations.

Together, these results might solve one issue facing the Notch-based hypotheses tip cell selection – the inability for lateral inhibition to incrementally balance tip-stalk ratios – but it does not address another shortcoming explained in Chapter 3

– the experimental evidence that Notch engages in lateral induction in endothelial cells.<sup>50</sup> The reduced network depicted in Figure 4.3A does not contain direct lateral induction by any species: species A (analogous to Delta) laterally activates species B (analogous to Notch), which down-regulates species A in the same cell in a circuit of lateral inhibition. Species B up-regulates species A in neighboring cells, but has no direct impact on species B in neighboring cells. Altering the cell-autonomous influence of species B on species A from inhibitory to activating would switch the circuit from lateral inhibition to lateral induction, creating an analogy to Notch-based lateral induction; however, this alteration would cause a sign change in the stability criterion (Equation 4.71) which would prevent mode selection at negative structural eigenvalues (which are necessary to select individual tip cells). As such, this hypothesis is most likely to be relevant if future experiments resolve that Notch *does* engage in lateral inhibition in sprouting endothelial cells, rather than lateral induction.

### **Tip cell selection as a VEGF reaction-diffusion mechanism**

As an alternative to juxtacrine signaling-based patterning mechanisms, I proposed a mechanism that used competition for diffusing VEGF (Figure 4.1B) as the basis for tip cell selection. Historically, reaction-diffusion mechanisms have been the most obvious explanation for branching morphogenesis (drawing analogies to dendrite formation<sup>102</sup>) and formed the basis for many simulations of angiogenic sprouting.<sup>23;116;117</sup> These simulations rely on endothelial cells (or neighboring sprouts) jostling for position as the means by which cells (or sprouts) compete to access the diffusing morphogen (typically VEGF) and “win” the race to vascularize new tissues. In contrast, tip cell selection is hypothesized to occur between cells which are equidistant from the hypoxic source of VEGF,<sup>19</sup> and is known to be orchestrated

prior to any morphological change by intricate networks of multicellular signaling.<sup>25</sup> The reaction-diffusion hypothesis I propose and analyze here is, in some respects, a way to reconcile the initially hypothesized role of VEGF in regulating angiogenic branching and the hypothesized ability for endothelium to select tip cells independently of local tissue geometry.

Previous experiments showed that retinal neurons used VEGF internalization via VEGFR2 to limit tip cell formation in their vicinity<sup>27</sup>, and subsequent authors hypothesized that emerging tip cells may similarly use VEGF consumption to limit formation of new tip cells in their vicinity.<sup>104</sup> I proposed a network of signaling and gene regulation that could fulfill this hypothetical role for VEGF endocytosis (Figure 4.1B) and provided the first simulations of tip cell selection via competition for VEGF (Figure 4.4).

A notable feature of this mechanism is the dramatic response of tip cell selection density to changes in VEGF production rate (Figure 4.4E). Research from the early 2000s, oriented towards clinical application of VEGF inhibitors, found that availability of VEGF quantitatively impacted the density (or branching frequency) of the vasculature following angiogenesis<sup>15;83;118;119</sup> – including the foundational study on endothelial tip cells.<sup>18</sup> However, in the years following, the tip cell selection community focused most experiments on exploring how *Notch* signaling affected tip cell density<sup>16;21;50;52;53</sup>. Only recently has the focus returned to VEGF: a series of experiments showed that tight regulation of VEGF receptor endocytosis was essential for proper tip cell formation and sprouting.<sup>88;105;120</sup> In response, there has been some renewed interest in understanding how tip cell selection patterns are impacted by chronically low or high VEGF,<sup>74</sup> but as I will discuss in more detail below, more experimental work is needed to understand how tip cell selection is

impacted by small changes in VEGF production.

## **Limitations of this study**

In addition to the fundamental limitations of my ODE-based formalism discussed in the previous chapter, the hypotheses explored here have some unique concerns.

### **The double juxtacrine hypothesis is lacking biological details**

In Figure 4.1A, the identity of the second juxtacrine signaling pathway is unspecified. At the start of this chapter, I provided a list of three juxtacrine signaling pathways that are of growing importance to the tip cell selection community – Ephrin-B2, Neuropilin-1, and VE-Cadherin – but I was unable to provide an explanation for any of these species would allow Notch activation in one cell to down-regulate Delta expression in neighboring cells without using the Notch receptor.

My uncertainty about the molecular species in the double-juxtacrine hypothesis limited the analysis I could perform in a number of ways. I was unable to predict how VEGF might impact tip cell pattern in this hypotheses, because I did not know where VEGF should enter the governing equations; modifying the production rate of Delta (analogous to species A in Figure 4.3A) is one option, and I plan to explore this in the near future.

I also had to guess how the governing equation for species A (Equation 4.18) should be structured: I chose to sum the two repressive Hill functions, which is analogous to a situation where Notch and the unnamed species can each only

partially repress the expression of Delta (i.e., total repression is a logical AND). I plan to test combining the two repressive Hill functions in Equation 4.18 as a product, as this change might produce more robust patterning at the expense of mathematical complexity – this network would be analogous to a situation where strong activation of either juxtacrine pathway can fully repress Delta (i.e., total repression is a logical OR).

### **The endothelium as a perfect lattice**

As in Chapter 3, I assumed here that the endothelium was a perfect 2D lattice of square-shaped endothelial cells. This assumption was relatively safe when I was focused on juxtacrine signaling: only the *topology* of the endothelium matters for juxtacrine signaling, not the *geometry*, endothelial cells have roughly four neighbors *in vivo*<sup>51</sup> and in *in vitro* monolayers.<sup>5</sup>

However the simplified lattice may conflict with the realities of testing hypotheses of VEGF reaction-diffusion: while I have argued that this hypothetical mechanism *can* select tip cells in the absence of positional advantage (i.e., a potential tip cell being closer to the source of VEGF) real vessels have three-dimensional geometries, and in some cases, certain cells will be closer to a tip position than others.<sup>16;58</sup> My hope is that if and when the VEGF reaction-diffusion hypothesis explored here passes some degree of experimental validation, the proposed mechanism could be used in larger multiscale models of angiogenesis which can simulate more complex vessel geometries.<sup>12;103</sup>

## Application to experiments

### Experiments around double-juxtacrine hypothesis

It the broadest terms, the hypothesis I've presented as "double-juxtacrine" (Figure 4.1A) here states that endothelial cells – and in particular stalk cells – express a ligand that represses tip characteristics in neighboring cells. This ligand should be upregulated by Notch, but should not be a ligand for Notch. (Another biological hypothesis which has the same reduced representation as the network shown in Figure 4.3A states that Notch activation *down-regulates* a ligand which needs to be present in *trans* for a tip cell to form.) Validation of this hypothesis should begin with continued search for juxtacrine signaling pathways which are upstream of Delta expression, and downstream of Notch, in endothelial cells; once candidate pathways are identified, experiments should be designed to test whether ligands for those pathways down-regulate (or up-regulate) Delta expression and are up-regulated (or down-regulated) by Notch activation.

Earlier in this chapter, I discussed three juxtacrine signaling pathways which each fit some, but unfortunately not all, parts of this mold. EphrinB2 is upregulated by Notch<sup>89</sup>, is an important regulator of tip cell function (possibly including Delta expression),<sup>88</sup> and has some interesting juxtacrine interactions with the EphB4 receptor;<sup>121</sup> but ephrinB2 does not appear to be enriched in stalk cells<sup>105;120</sup>. Neuropilin-1 is down-regulated by Notch<sup>91</sup>, might antagonize VEGF-VEGFR2 signaling (and subsequent Delta activation) when presented to a cell in *trans*<sup>93</sup> and is thought to be necessary in *cis* for tip cell formation<sup>91</sup>; however, this network would only fit the reduced representation given in Figure 4.3A if Neuropilin-1 promoted tip cell formation when presented in *trans*. VE-cadherin inhibits VEGFR2 signal-

ing in *cis*,<sup>92</sup> and might stabilize gap junctions in *trans* (helping to inhibit VEGFR2 in those cells);<sup>122</sup> but it is not clear that this mechanism can be accurately modeled using the governing equations provided here,<sup>122</sup> nor whether VE-cadherin is downstream of Notch. As experimental observations of how these and other juxtacrine pathways interact with Notch signaling in endothelial cells continue to emerge, my hope is that researchers will consider whether the reduced representation given in Figure 4.3A might apply.

The above pathways might clarify the molecular basis for this hypothesis, but the multicellular basis for it – reflected in the common illustration of tip cells being separated by two or more (not one) stalk cells<sup>17;20</sup> – also needs to be firmly established. Some experiments, especially those in the mouse retina, may support the notion of tip cells being selected at 50% from cells at the leading edge of the growing plexus<sup>16;52</sup>; others, even in the mouse retina, suggest that tip cells are selected at a lower ratio, especially under pathological conditions.<sup>17;21;27</sup> Granted, any illustrations or simulations that enforce a perfect geometry and easily-counted tip cell pattern on an endothelium are simplifications; the real endothelium is more disorderly and dynamic than the lattices used here,<sup>21;53</sup> and tip versus stalk phenotypes are dynamic, reversible, and perhaps only partially realized in some cells in the normal course of angiogenesis.<sup>52</sup> I still presume that the recurrent depiction of tip cells being separated by more than one stalk cell is a reflection of researchers’ cumulative observation of the multicellular structure of the vascular plexus (i.e., perhaps drawing only one stalk cell wouldn’t “look right” based on those researchers’ experiences in microscopy).

Mature techniques to systematize how tip cells and stalk cells are counted are few: the gold standards for identifying tip cells continue to revolve around

classifying the morphology (mostly based on filopodia), not gene expression or signaling states, of endothelial cells in the sprouting front.<sup>58</sup> My hope is that continued work will go towards enabling a rational and quantitative system for capturing the multicellular structure of the sprouting endothelium, and identifying (biomolecular) patterns of tip cell selection within it, so we can start validating models for tip cell pattern formation more directly – Gerhardt and colleagues’ recent efforts to create live reporters of Delta expression are a promising step in this direction.<sup>74</sup>

### **Experiments around diffusion and endocytosis**

The “diffusion and endocytosis” hypothesis proposed here essentially states that tip cells create a local sink in the concentration of freely-diffusing VEGF in the interstitial fluid which allows them to “steal VEGF”<sup>104</sup> from neighboring endothelial cells, limiting the formation of competing tip cells in their vicinity. Experimental validation of this hypothesis can occur on two fronts: the hypothetical positive feedback mechanism that allows tip cells to form a local sink in VEGF (proposed here to involve Akt, eNOS, dynamin, and endosomal trafficking) can be dissected, and the global predictions of the model – such as the continuous response of tip cell selection density to VEGF production rate (Figure 4.4E) – can be tested.

Perhaps the quickest way to falsify the hypothesis I have proposed is to show that a species which I’ve implicated as a component of the underlying mechanism – namely Akt, eNOS, and dynamin – does not function as I have purported. For example, there are conflicting accounts about whether Akt activation following stimulation of endothelial cells with VEGF is dependent on VEGFR2 internalization: some studies have shown that Akt continues to be activated if full endocytosis

of VEGFR2 is prevented,<sup>105</sup> but other studies suggest that movement of VEGFR2 from the cell surface into a dynamin-dependent vesicle (not full endocytosis) is the required step before Akt is activated by VEGF-VEGFR2 signaling.<sup>88;106</sup> If, hypothetically, it could be shown that inclusion of VEGF-VEGFR2 complexes into dynamin-dependent *vesicles* (and subsequent activation of Akt) is not tightly coupled to VEGF endocytosis and degradation, my proposed mechanism would be incomplete – I would need to identify a signaling pathway which is downstream of VEGF-VEGFR2 signaling from *endosomes* (such as ERK1<sup>92</sup>) and positively regulates VEGFR2 endocytosis and trafficking to lysosomes.<sup>106</sup>

However, I will argue that the core of my hypothesis is not the molecular players that are ostensibly responsible for the underlying mechanism. Rather, the non-monotonic relationship between steady-state extracellular VEGF concentration and intracellular VEGF concentration – captured quantitatively in Figure 4.4B – is the most critical aspect of the hypothesis. Endothelial cells must be able to accelerate their rate of VEGF internalization in response to rising levels of intracellular VEGF signaling, such that a tip cell can sustain an increased rate VEGF internalization even as the local concentration of extracellular VEGF decreases, for VEGF reaction-diffusion to be the medium on which the endothelium limits the density of tip cell selection (in the absence of positional competition).

I expect that *in vitro* experiments on primary endothelial cells would be the most appropriate method for establishing an empirical relationship resembling the curve in Figure 4.4B. Measuring VEGF concentrations *in vivo* is notoriously difficult<sup>123</sup>, and attempts to eliminate baseline VEGF expression in whole organism (so a controlled amount of VEGF can be released) are hindered by the embryonic lethality of eliminating even a single allele of VEGF.<sup>124</sup> In contrast, previous *in*

*in vitro* experiments using endothelial cell monolayers have been successful in measuring how titrating an imposed concentration of VEGF impacts cellular responses including gene expression,<sup>125</sup> migration,<sup>126;127</sup> and VEGFR2 signaling state.<sup>128</sup> The primary challenge in creating an empirical curve to match that shown in Figure 4.4B is that VEGF flux into the cells ( $\dot{V}$ ) is the imposed parameter, rather than local VEGF concentration; each steady-state VEGF flux has only one possible VEGF concentration, but an endothelial cell can have one of several VEGF fluxes if VEGF concentration is fixed. Numerous studies have proposed biomaterials that can slowly release VEGF *in vitro*,<sup>129</sup> perhaps providing a means to impose a steady-state flux of VEGF on a monolayer, but I am unsure how local VEGF concentration at the cell surface might be measured *in vitro*.

I expect that the other important component of this reaction-diffusion model – diffusion of VEGF – is better suited to validation through simulation. The transport of a soluble protein like VEGF can be modeled from first principles, and numerous computational studies have predicted how gradients of VEGF can form and be maintained in a variety of contexts, including tip cell formation.<sup>23;110;130</sup> A three-dimensional simulation of this hypothesis, with accurate models for VEGF diffusion, might be possible once the regulation and kinetics of VEGF endocytosis (i.e., with steady-states like this depicted in Figure 4.4B) is elucidated.

The global model prediction of tip cell density being a function of a the flux (or production rate) of VEGF might require *in vivo* experiments or tissue engineered *in vitro* constructs which can recapitulate sprouting angiogenesis.<sup>5;61</sup> As mentioned previously, there are limited tools available to measure tip cell selection patterns directly, so using more traditional methods of counting fully-formed tip cells<sup>58</sup> might be a first step towards validating these predictions. One recent study began

to test whether the density of tip cell formation responded to changes in VEGF availability and found that spiking the mouse retinal vasculature with concentrated VEGF solutions (1  $\mu\text{g}/\text{ml}$ ) appeared to eliminate tip cell formation altogether.<sup>74</sup> This result does not meaningfully support or falsify any of the VEGF-centered hypothesis explored in Chapters 3 and 4 – lateral inhibition (Figure 3.5), lateral induction (Figure 3.6), and VEGF reaction-diffusion (Figure 4.4) – because all predict uniform activation of tip cell-related species under chronically high VEGF, but do not count tip cells if the uniform initial condition is stable. I hypothesize that adding or subtracting *large* amounts of VEGF disturbs the endothelium to an extent that tip cell pattern formation is no longer functional. In the future, I hope that experiments will be designed around adding or subtracting *small* amounts of VEGF to the endothelium to elucidate whether marginal VEGF availability has a marginal impact on tip cell density.

## 4.5 Conclusion

In conclusion, I have injected some much-needed fresh ideas into the discussion about how the organization of angiogenic sprouts is initiated by the multicellular selection of endothelial tip cells. I created qualitatively new hypotheses for the logic which endothelial cells might execute to form varied patterns of tip-competent cells, and I identified the biomolecular species which might convey that logic. In the short term, these hypotheses can be used to design experiments that might falsify them. In the long term, these hypotheses might inspire the discovery of the “true” solution to tip cell selection, either because one of these hypotheses resembles the real biomolecular logic the endothelium uses or because the techniques I used to create these hypotheses are helpful in finding it.

CHAPTER 5  
DESIGNING A BUSINESS FOR INSECT CELL-BASED  
MANUFACTURING OF GENE THERAPIES

## 5.1 Introduction

In July of 2012, the European Medicines Agency approved the drug Glybera for sale, marking the beginning of commercial gene therapy in the Western world.<sup>131</sup> The treatment injected a live virus – a recombinant adeno-associated virus (AAV) – into a patient’s muscle tissue where it infected cells with DNA encoding the gene for an enzyme called lipoprotein lipase; in effect, Glybera cured a hereditary disease known as lipoprotein lipase deficiency – which causes debilitating abdominal pain and frequent hospitalizations – within hours of administration. However, in April of 2017, the makers of Glybera announced they would not be seeking market reauthorization, meaning the drug would cease to be available in October of that year.<sup>132</sup> The first gene therapy in Europe was a commercial failure (having reportedly been sold to a single patient<sup>133</sup>) because of its cost: at \$1 million per dose,<sup>36</sup> it was not only the most expensive drug off all time – the active ingredients of Glybera may have been among the most expensive *materials* of all time, requiring on the order of \$1 billion per gram of recombinant AAV to manufacture. Experts in the AAV community hold a consensus that manufacturers must achieve drastic cost reductions if viral gene therapies are ever to reach commercial viability and cure hereditary diseases from whole patient populations.<sup>36;134</sup>

At first glance, the manufacturing process (summarized in Figure 5.1) for recombinant AAV resembles that of other biopharmaceuticals, such as monoclonal antibodies: a plasmid containing the genes of the recombinant protein are inserted

into a living cell substrate, which is grown in a bioreactor while it translates and assembles the final protein product. The essential reaction and culturing schemes of the recombinant product and the cells which produce it – collectively known as the expression system – are designed early in the process of developing the biotherapy, likely when production runs are carried out by scientists using bench-scale equipment such as T-flasks or roller bottles. Once the basic expression system is fixed, the execution and improvement of the manufacturing process become the purview of specialized bioprocess engineers who perform scale-up; process development, as it is known, enables cell culture to take place in large bioreactors, and eventually, for the drug to be mass-produced at medical-grade pharmaceutical plants. By the time a typical biological drug advances through its three clinical trials, receives market authorization, and is ready to be produced for commercial use, manufacturing costs account for a negligible portion of the sales price: as of 2009, bioprocess development experts estimated that the production costs for monoclonal antibodies – which can cost healthcare payers tens of thousands of dollars per year at the time of launch – had approached \$100 per gram, and were trending towards \$20 per gram.<sup>135</sup>

However, recombinant AAV is not like most biological products. Each AAV particle is an icosahedral *capsid* – the protein-based outer shell of the virus which contains numerous receptor-binding sites necessary to infect host cells – harboring a short (roughly 5,000 base-pair), double-stranded DNA payload. The capsid consists of 60 protein sub-units, each an alternative splicing of a single gene: proteins of the three splicings must be expressed by the host cell at a precisely-defined stoichiometric ratio for the virus to be infectious. AAV “Rep” proteins must also be expressed by the host cell which help replicate the payload DNA and shuttle it into the capsid, but these proteins alone are often not sufficient for these crit-

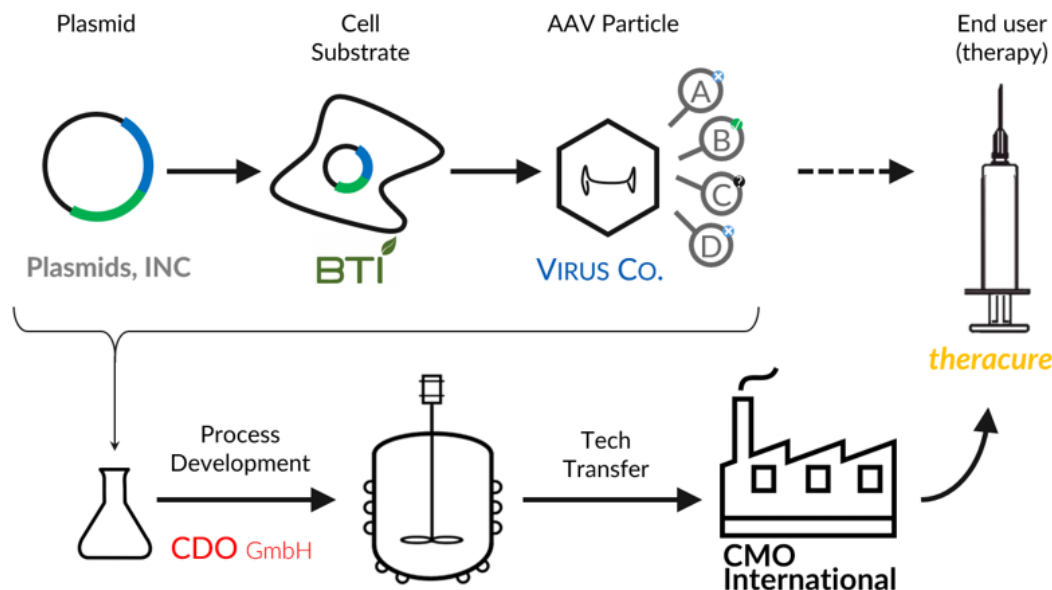


**Figure 5.1: Overview of AAV manufacturing.**

ical steps: in many cases, the host cell must be infected with a wholly separate “helper” virus to enable proper DNA replication and packaging (adeno-associated virus gets its name from the helper *adenovirus*, which a host organism must first be infected with before wild-type AAV can replicate). Furthermore, AAV purification processes are challenging: AAV does not bind as strongly to affinity columns as antibodies, and novel techniques must be employed to separate empty capsids from fully-functional AAV particles.

The manufacturing costs of AAV are a direct result of the complexity of expressing, purifying, and charactering the live virus particles – and the lack of experience that most bioprocess developers and manufacturing organizations have with gene therapy. In this project, I explored how the burdens of AAV manufacturing might be reduced by new businesses that improve different aspects of the bioprocess development pathway shown in Figure 5.1; in particular, I hypothesized how firms

might profit from accelerating the adoption of insect cells as a production substrate for AAV – which could potentially unlock vast cost savings over traditional mammalian cell-based manufacturing techniques. I will begin by performing review of the literature around AAV manufacturing and insect cell-based protein expression. Then, I will provide a list of several business concepts around insect cells for AAV manufacturing, which span from “plasmids” to “contract manufacturing” in Figure 5.1. I will summarize the interview process I used to test each of the business concepts, and then provide my final recommendations for the potential new firms which warrant continued efforts to implement with the goals of making AAV gene therapies more affordable to develop, manufacture, and ultimately, administer to patients.

## 5.2 Methods

### 5.2.1 Literature review

#### Recombinant adeno-associated virus (AAV)

Adeno-associated virus (AAV) is a viral gene therapy vector; AAV therapies use recombinant viruses to deliver DNA payloads (as opposed to the AAV genome) into to a patient’s cells which replace lost protein function or introduce new RNA functions (e.g., gene silencing).<sup>131</sup>[Better citation]? Each AAV virion has a complex, multimeric protein coat – known as the viral capsid – which is specialized to infect a particular tissue (or set of tissues) in a host organism; natural and recombinant AAVs are classified into a number of distinct *serotypes* which describe their capsid compositions and the tissues they are specific to.<sup>136</sup> Important quality attributes

of therapeutic AAV include how closely a sample matches to its targeted serotype (as measured by how efficiently it infects patient cells) and the *empty-to-full ratio* (or the percentage of AAV particles in the final product which are missing a DNA payload).<sup>134</sup>

Assembly of, and integration of payload DNA into, the AAV capsid requires certain host cell processes, so therapeutic AAV must be produced in genetically engineered eukaryotic cells.<sup>134</sup> Recombinant AAV has traditionally been produced in immortalized human cell lines (such as Human Embryonic Kidney, or HEK, cells) in adherent cultures (e.g., T-flasks) using transient transfection (i.e., introducing the recombinant AAV genome and payload DNA directly into cells as DNA);<sup>134</sup> these components – the cell substrate, the culture format, and the gene delivery method – collectively make up the *expression system* that AAV is manufactured in.

While expression systems based on transient transfection of HEK cells serve scientists well during early-stage AAV research, it is unlikely to be suitable for commercial manufacturing of gene therapies due to the extremely high projected costs.<sup>134</sup> For example, Glybera had a launch price of over \$1 million per patient, largely due to its manufacturing costs.<sup>36</sup> Glybera was manufactured using an insect-cell based expression system (discussed in more detail below) – not with transfection – which allowed it to be produced in a suspension format, as opposed to the adherent cultures used in traditional AAV production. As demonstrated in Figure 5.2, suspension-based cultures scale significantly more cost-effectively than adherent cultures. In conclusion, attempting to commercialize a gene therapy using transfection-based, adherent-culture manufacturing would likely incur costs to the patient much greater than Glybera’s €1.1 million; there are few (if any) diseases

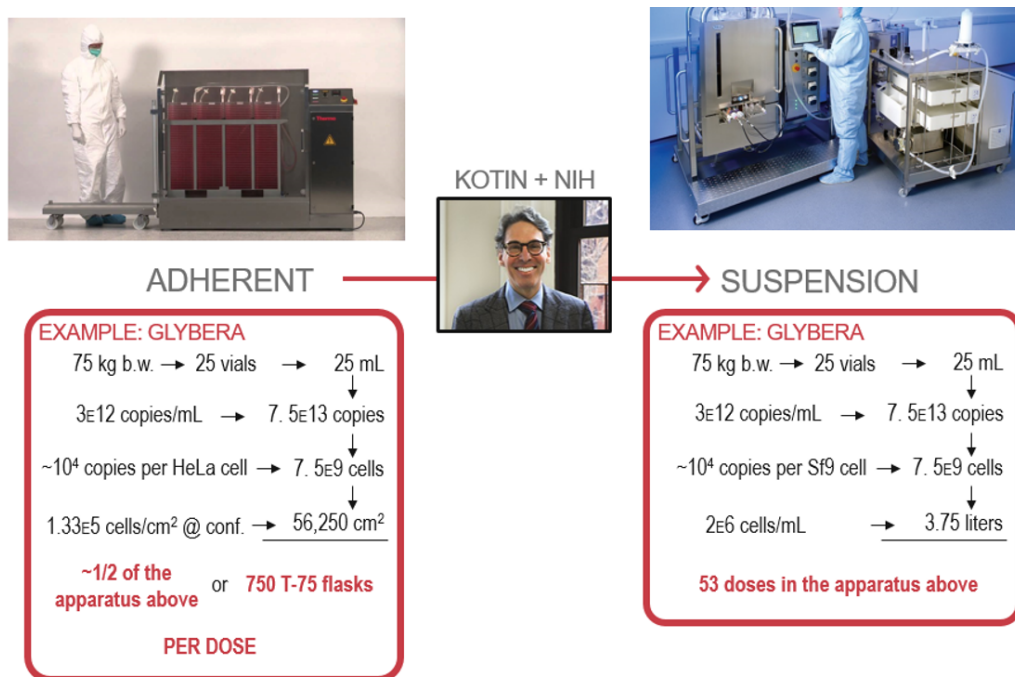


**Figure 5.2: AAV production with adherent vs. suspension cultures.**

where such costs, even if they offset a lifetime of treatment, would be justifiable to insurers or other healthcare payers.<sup>36</sup>

Luckily, several new AAV expression systems are under development which allow for more cost-effective AAV production, as summarized in Table 5.1. Some have simply attempted to adapt their HEK/transfection systems to a suspension format; while this begins to address the issue of reactor scaling, it can still be very costly to produce the purified plasmid DNA needed for each cell in each batch, and there are some outstanding issues with process variability and safety (e.g., risk of producing replication-competent AAV).<sup>134</sup> One approach seeks to eliminate transfection's recurrent need for input DNA, and permit cells to be fully adapted to a suspension format, by creating stable cell lines which continually express a specific recombinant AAV.<sup>137</sup> However, in this approach, new cell lines would need to be established any time a change is made to the AAV capsid or payload (which

takes months), and a potentially dangerous virus (wild-type adenovirus) would need to be introduced to replace certain “helper” functions lost when switching from away transfection.<sup>137</sup> Another option uses a recombinant Herpes Simple Virus (HSV) as a *viral expression vector* to introduce the AAV genome and payload DNA into mammalian cells in suspension; this both reduces the need for recurrent plasmid (although HSV must be produced beforehand) and enables more suspension-friendly Baby Hamster Kidney cells to be used in place of HEK cells.<sup>137</sup> The HSV expression system produces a high yield of AAV with a good empty-to-full ratio, but introduces a human virus (HSV) which, though replication-deficient, poses some additional purification requirements to guarantee product safety.<sup>134</sup> Finally, AAV can be produced in insect cells; as I will discuss in more detail below, this expression system uses a *replicating* and *non-human* baculovirus to introduce the AAV and payload DNA, which reduces both the prerequisite titer and safety concerns of the viral expression vector compared to HSV, and scales up with ease.<sup>137</sup> However, maintaining AAV quality in the baculovirus expression vector/insect cell system (BEVICS) can be more challenging than in mammalian systems.<sup>134</sup>

### **Baculovirus expression vector/insect cell system (BEVICS)**

In contrast to the mammalian cells typically used in the production of recombinant antibodies,[CITE] insect cells have a record of commercial successes in the production of recombinant virus-like particles (VLPs) for use as human and veterinary vaccines.<sup>138</sup> Two prominent examples are *Cervarix*, a vaccine against human papillomavirus which is popular in the United Kingdom, and *Flublok*, which is an annual trivalent flu vaccine which is mainly targeted at patients with allergies to chicken eggs.<sup>138</sup> In the early 2000s, scientists at the National Institutes of Health invented a method for producing live, recombinant AAV in insect cells by improving

	Suspension	Replication	Safety	COGM
Transfection + mammalian	X			
Stable HeLa producer lines with Adeno helper virus	✓			
Herpes Simplex Virus Expression Vector/Human Embryonic Kidney Cells	✓			
Baculovirus Expression Vector/Insect Cell System (BEVICS)	✓			

**Table 5.1: Comparison of AAV expression systems.**

upon previous techniques for producing inactive VLPs in insect cells – albeit these early tests produced AAV with imbalances in the capsid protein composition.<sup>139</sup> A decade later, these and other scientists had engineered baculovirus expression vectors to produce high-quality AAV of multiple serotypes<sup>140</sup> and performed pilot studies using the largest bioreactors ever published for AAV production (200 L).<sup>141</sup>

Early in this development effort, researchers recognized that the BEV system would be capable of scaling up AAV production more easily than any expression system at the time.<sup>139</sup> Much of this scaling ability owes to the kinetics of baculovirus infection: instead of using a high multiplicity-of-infection (MOI; the number of copies of a plasmid or expression vector per cell) which is then diluted as the cells divide, as with transient transfection or HSV infection, insect cells can be infected with a baculovirus at low MOI – the virus will propagate on its own, increasing the strength of gene expression as the cells divide.<sup>142</sup> Furthermore, insect

cells are easily adapted to a suspension format and can easily be grown without costly and relatively unsafe serum-containing growth media.<sup>138</sup>

The baculovirus expression vector/insect cell system consists of a number of baculoviruses and the insect cells which they are grown in, as shown in Figure 5.3. Throughout this chapter, I will reference baculovirus plasmids which enable the production of different serotypes of AAV in insect cells. These plasmids refer to those used to make the baculoviruses which introduce Rep and Cap genes into the insect cells during production. As mentioned previously, initial attempts to create AAV in insect cells produced virus which was not as infectious as that made in mammalian cells, largely arising from insufficient expression of the *VP1* capsid (Cap) protein.<sup>139</sup> Several groups spent years engineering baculovirus plasmids that produced optimal levels of the Rep and Cap proteins,<sup>140;143</sup> and designs for these insect-cell compatible plasmids are covered under numerous patents.

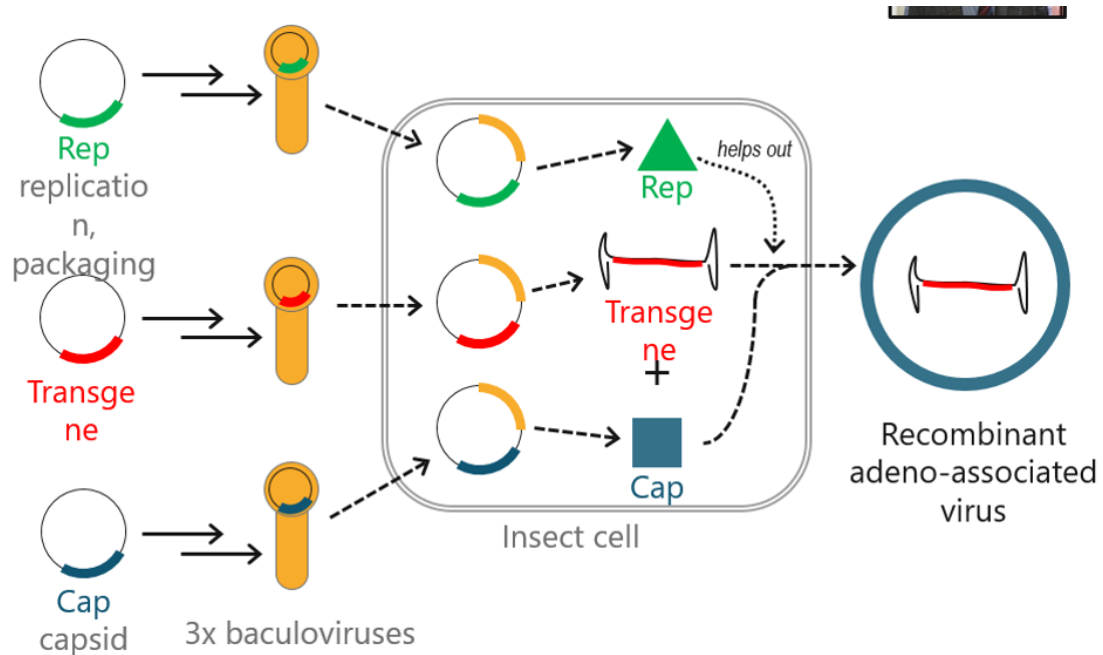


**Figure 5.3: AAV production with BEVICS.**

## Insect cell lines

Historically, AAV has been produced in insect cells from a cell line called *Sf9*, from *Spodoptera frugiperdia*, a moth of the order Lepidoptera.<sup>139;141</sup> Sf9 is the most popular cell line for recombinant protein production using BEVICS, and it is celebrated for its fast growth rate, its ability to rapidly propagate a baculovirus infection, and its ability to survive in suspension and in serum-free media.<sup>138</sup> However, the second-most popular cell line for recombinant protein production using BEVICS, *Hi5*<sup>144</sup>, from *Trichoplusia ni*, another Lepidopteran, also has the potential to be used for the production of AAV. Compared to Sf9, Hi5 is slightly less hardy (requiring more care to adapt to a suspension format), but has the potential to reach higher yields of recombinant protein and produces less baculovirus (which can be difficult to separate from the recombinant protein product).<sup>145</sup>

Both Sf9<sup>146</sup> and Hi5<sup>147</sup> were recently discovered to suffer from adventitious (i.e., unwanted) viral infections. The FDA requires any cell line used in the manufacture of drug materials to be screened for adventitious viruses; companies with processes found to be infected with adventitious viruses should ideally eliminate the infection, use separations process to remove the virus from the final product, or minimally, demonstrate that the virus poses no risk to humans.<sup>148</sup> Because the adventitious viruses in insect cells were only recently discovered, it is expected that the market-approved drugs which were manufactured with insect cells contain some virus; neither the *Rhabdovirus* found in Sf9, nor the *Alphanodavirus* found in Hi5, are known to infect humans<sup>146;147</sup>, so these products remain on shelves. Regardless, known adventitious agents present regulatory complications and some experts in the bioprocessing industry anticipate that therapy companies will take steps to eliminate them, perhaps adopting insect cell lines which are similar to Sf9 or Hi5,

but cured of the undesirable infections.<sup>148–150</sup>

## **5.2.2 Business model design methodologies**

In the following section, I will provide background on the methodologies for business model design I used to guide this project. For a more detailed explanation of my activities, proceed to the next section, “Generating and investigating business concepts.”

### **Business concept generation**

Practitioners of technology commercialization highlight the need to establish and test concepts for a new business early and often.<sup>151</sup> The process of business design, like the process of science, is generally one of falsifying hypotheses; it is likely that the first concept an entrepreneur has for a new business will either be fundamentally flawed, or in need to significant changes before it can be implemented. To account for the likely possibility that some concepts will fail, and to increase the chances that a valid business concept is identified, it is good practice to begin the design process with a set of distinct concepts which can be tested in series or in parallel.

For the purposes of technology commercialization, the broad topic of this project, those concepts might all share a common theme, such as ideas for different products which incorporate a new invention (e.g., imaging several types of electronic devices which could incorporate a new integrated circuit) or different companies that might benefit from a new invention (e.g., considering different manufacturing processes that could be built around a new unit operation). Better

yet, the entrepreneur can help ensure he is performing a wide search of business concepts by proposing ideas that span the range of license (i.e., selling the invention to a third party outright) to company (i.e., forming a startup around the invention).

### **The business model canvas**

To advance from hypothesis to validated idea, a concept must be tested; for a concept to be tested, it needs to have some degree of formality. However, the details of future cash flows and company organization – what many tend to think of as the “business model” that formalizes an idea for a new enterprise – are time-consuming to construct and may not contain accurate and useful predictions when created early in the commercialization process. To address this issue, Osterwalder<sup>152</sup> developed an ontology which can be used to construct architectures (or minimal business models) for new business concepts using a common set of terms; these architectures directly capture the “logic” of the business and can be used to create testable hypotheses.

Osterwalder’s business ontology eventually grew into the user-friendly business model canvas (BMC)<sup>153</sup>, which contains a table of nine categories of features that must be described to design a successful business:

- the *customer segments* being targeted;
- the *value propositions*, which describe the offerings that solve an unmet need of the target customers;
- the expected *revenue* streams;
- the *relationships* with customers that will be maintained;

- the *channels* the company will use to reach and distribute to customers;
- any *key partnerships* that need to be established with other organizations;
- the *key activities* that the company will engage in to sustain its operations;
- the *key resources* the company will need to build or acquire;
- and the expected startup and operating *cost structure*.

According to Osterwalder, a business model should contain hypotheses for each of the categories to maximize its chance of succeeding; the process of business design is in testing hypotheses that arise from this business model canvas.

### **Value proposition design**

The BMC, while appropriate for describing a whole business concept, contains some components which are more critical to the validity of a business concept than others; for example, a company must identify and understand its *customer segments* to have any hope of viability, but concerns such as *partnerships* and *cost structures* are generally not relevant until the relatively late in the design process. As such, Osterwalder developed a methodology of “value proposition design”<sup>154</sup>, which allowed practitioners to iterate more quickly on the three most critical aspects of a business model: the *customers*, the *value proposition* offered to them with the new venture, and the potential sources of *revenue*. These three components hypothesize how a company will earn money by solving an unmet need of potential customers; Osterwalder’s value proposition design methodology revolves around generating testable hypotheses for iterating through early-stage business designs based on deeper analysis of the *value map* and *customer profile* targeted by a particular business concept.

## Environment maps

In addition to detailing an important subset of the business model canvas in value proposition design (“zooming in”), Osterwalder provided a sketch for how to investigate the environment that a business model exists within (“zooming out”).<sup>153</sup> Osterwalder described this environment using what he called an “environment map”, which consists of four broad categories of factors external to a business concept – key trends, industry forces, market forces, and macroeconomic forces – and subdivisions within those categories. As Osterwalder puts it, the content of these categories describes the “design space” in which a business model must operate; without knowledge of this design space, it is not possible to generate the hypotheses and tests *about the business model* that will lead to a successful business design. However, Osterwalder did not describe a methodology for creating hypotheses and tests *about the environment* – which may be just as necessary testing and improving of the business model itself – perhaps finding that the process of learning the environments surrounding a business may be too complex and diverse to generalize.

## Summary

Osterwalder’s design methods, whether limited to the three categories in value proposition design or inclusive of the whole business model canvas, describe an iterative process of forming hypotheses based on the essential “logic” of the business, determining what tests can falsify those hypotheses, executing those tests, and then updating or rejecting the concepts as necessary. As a business concept matures, the tests advance from simple conversations with potential customers and other stakeholders to attempts at creating physical prototypes or pilot implementations

of the business.

### **5.2.3 Generating and investigating business concepts**

I developed a set of business concepts around the theme of using insect cells to manufacture AAV for human gene therapy, spanning the range of licensing opportunities (of an insect cell line to be used as a production substrate) to companies based around the operation of a physical plant. I used aspects of Osterwalder’s value proposition design methodology to generate hypotheses relating to the basic logic of how each concept created value for its customers. However, I developed my own methodology for generating hypotheses of the environment in which each concept would operate based around what I call “industry maps” (defined below). I tested my hypotheses regarding the environment of the AAV industry, and the value propositions which could benefit customers within it, by interviewing experts in the AAV industry.

#### **Industry maps**

Osterwalder suggested that entrepreneurs develop “environment maps” to capture the context that customers of a new business concept would exist within; the importance of these maps was especially stressed in sectors which are “networked”, contend with “greater uncertainty” due technological innovation, and experience “severe market disruptions” due to shifting economic conditions, versus sectors which are relative mature, stable, and well-understood (e.g., most types of consumer goods)<sup>153</sup>. As discussed in Chapter I (see Figure 1.2), the biotechnology industry involves a complex network of non-profit and commercial entities, and

is in a state of constant change due to new scientific discoveries, technological advancements, and changes in regulatory policy<sup>37</sup>. I grappled with this complexity by creating “industry maps”, or diagrams of the network of firms surrounding AAV manufacturing, to test and improve my understanding of the context that my business concepts would operate within.

These maps described relationships of how I hypothesized different firms in the industry interacted with one another; for example, “Small therapy firm *X* grows into large therapy firm *Y*”, or “Process technology developer *X* sells technology *A* to therapy firm *Y*”. Each relationship depicted in a map represented a testable hypothesis which I could falsify by interviewing people at a firm described by one or both of the entities in a relationship; for example, I could ask a manager at firm *Y* whether there were technologies like *A* available on the market

For each business concept, I will provide two industry maps: one created before the interview process, and one after. Both maps will contain the three components of value proposition design for each concept: the customers, the value proposition, and the predicted sources of revenue. The maps provided “after” the interview process will contain any changes in my understanding of the AAV manufacturing industry around each concept, notes of any observations that challenged the hypotheses of each concept (in red), and notes of any observations that the original hypotheses did not cover (in yellow).

### **Search pattern**

After generating the set of business concepts, I planned the search pattern of how I would investigate them using a matrix which ranked each concept according to how I hypothesized it perform in seven factors that influence company profitability:

- Market Size: the total addressable size (in dollars) of the market that a product or service will compete in
- Capital Requirements: the upfront costs of starting each business
- Value Propositions: the strength of the value propositions underlying each idea
- High Margin: the expected markup on each sale of a product or service
- Unfair Edge: the long-term advantages that the company would have over its competitors
- Big Problem: the urgency that customers feel towards seeing the unmet need being met
- Good Fit: how well the proposed team is positioned to implement the business concept

I assigned a score for each factor of each concept according to its rank, ranging from 1 (ranked worst) to 5 (ranked best); concepts which I hypothesized to tie were each given a rank plus half-point (e.g., two concepts which tie for second-best each get a 3.5). These rankings were based on rough estimates from my review of the literature around AAV manufacturing using insect cells; for the sake of brevity, I will not provide detailed explanations for each ranking, though in results section, I will discuss a few trends I hypothesized to exist. I summed the scores to produce a total for each concept, and I planned to investigate each concept by order of descending total score.

## 5.2.4 Integrating business concepts

At the conclusion of the interview process, I had four business concepts which I felt showed enough promise to continue developing (Concepts 2, 3, 4, and 5 in Figure 5.4). If the initial phases of business model design produce a number of business concepts which show promise, the entrepreneur must either chose one (or more) of the business concepts to pursue independently, or demonstrate that several of the business concepts can be successfully integrated into a single firm<sup>153</sup>. In the following sections, I will provide some background on the topic of business intengration, and then describe how I investigated whether each of my concepts was suitable for integration with the others.

### Background on business integration

The process of merging two business concepts (also known as “strategic business units” when applied to existing enterprises) into one firm is known as vertical integration if the two units form a supplier-customer relationship; if not, the merger is known diversification (or horizontal integration). Diversification can be further broken down into related and unrelated diversification. In unrelated diversification, the two businesses do not have meaningful relationships, or they may operate in entirely different markets – this type of diversification is helpful for mitigating risk within an investment portfolio, but is considered by most business scholars to be poor practice in the strategic management of a single company.<sup>155</sup> However, if the merger of the two business would unlock *long-term competitive advantage* (defined below) which would otherwise not exist if the firms remained separate, the process is called related diversification.

Competitive advantage is broadly defined as the the ability to succeed versus one's rivals; the clearest sign of competitive advantage is the ability to extract "economic rent," which is compensation for goods or service that exceeds the opportunity cost to the owner. In other words, competitive advantage allows a company to make an "unreasonable" amount of money for the actual work they perform, by virtue of owning something important; Markides & Williamson (1994)<sup>155</sup> refer to that "owned important thing" as a "strategic asset," and it can be tangible (land, facilities, equipment, etc.) or intangible (expertise, intellectual property, contractual rights, etc.). Coca-Cola's brand name is a classic example of a strategic asset, because it is what allows the company to sell a simple product (cola), which is virtually identical to generic products in the market, at a higher price than competitors.<sup>156</sup>

Markides & Williamson further explain that successful business integration enables the *continuous* creation of strategic assets<sup>155</sup>; for example, one company buying another solely to access its existing patents (themselves strategic assets) will not create a sustainable (i.e., long-term) competitive advantage because the patents will eventually expire. Rather, Markides & Williamson proposed that "core competences," which are the (mostly intangible) assets that allow a company to continuously improve the value of its offerings<sup>157</sup>, are the strategic assets which businesses transfer in a successful merger. A successful merger is also a necessary one; if a strategic asset is easily transferred via trade or contract, a merger of two businesses – a complex affair – is unnecessarily wasteful. For example, land can provide sustainable advantages and economic rent, but it is easily transferable between parties and should not be the reason two businesses are integrated.

Based on these arguments, Markides & Williamson<sup>155</sup> propose two criteria that

a process of integration must satisfy to be successful:

- As a result of the merger, a competence must be shared between the business units which catalyzes the creation of strategic assets which are nontradeable, nonsubstitutable, and slow or costly to accumulate;
- and it must be more efficient to transfer the competence internally (within a single firm) than to transfer the competence by trade or contract.

If either or both of these criteria are not met, the merger should not take place

A third consideration is the potential for conflicts that might arise from business integration<sup>153</sup> These conflicts might include a clash between the company cultures in the merging firms, or it may arise from a loss of performance in one or both of the firms – the combined entities may become less efficient if they cannot benefit from the competition of the open market in areas where they form a customer-supplier relationship.<sup>158</sup>

### **5.2.5 Plan-to-market**

The business concepts that emerged from the interview-oriented testing phase, and their attractive permutations, require additional testing before they should be considered “validated”; in the design of business models, the only way to truly validate an idea is to implement it. In the design of physical products, creating a prototype is an important milestone on the path to implementing an idea which follows interviews, but precedes product launch; the analogy for ideas around manufacturing processes or other services might be a pilot study. I screened through the individual concepts which survived the interview-oriented testing phase of this

project and estimated how difficult it would be for me to produce a prototype or pilot study of each concept, and estimated how much impact the success of each individual concept would have on the integrated concepts. I attempted to arrange for a pilot study to occur for one of the concepts – the attempt itself forming an important test of the concept – and will briefly describe the outcome of those efforts.

### 5.3 Results

Insect cells lines have long established their utility in the production of various recombinant proteins<sup>138;144</sup>, but the discovery of adventitious viruses in the two major cell lines (Sf9 and Hi-5) have created some concern among industry experts<sup>146-148</sup>. The Boyce Thompson Institute (BTI; Ithaca, NY) isolated three immortalized cell lines descended from the cabbage looper (*Trichoplusia ni*, or *T. ni*) which were absent of the adventitious viral infections (of the genus Alphanodavirus) which infect comparable cell lines available on the market today<sup>149;150</sup>; this absence of adventitious viruses was confirmed using RT-PCR<sup>149;150</sup> and high-throughput small RNA screening (*unpublished data*).

I undertook a project to investigate how these new insect cell lines might form the core technology of a new business involved in the manufacturing of human biotherapeutics. I decided to focus my efforts on adeno-associated virus (AAV) as the recombinant product because it was the area in which BTI had performed the least amount of commercialization efforts prior to my arrival, and because the AAV industry was growing and in need of improved manufacturing technologies<sup>134</sup>. I generated five concepts for businesses around using the baculovirus expression

vector-insect cell system (BEVICS) to produce AAV for human gene therapy (Figure 5.4).

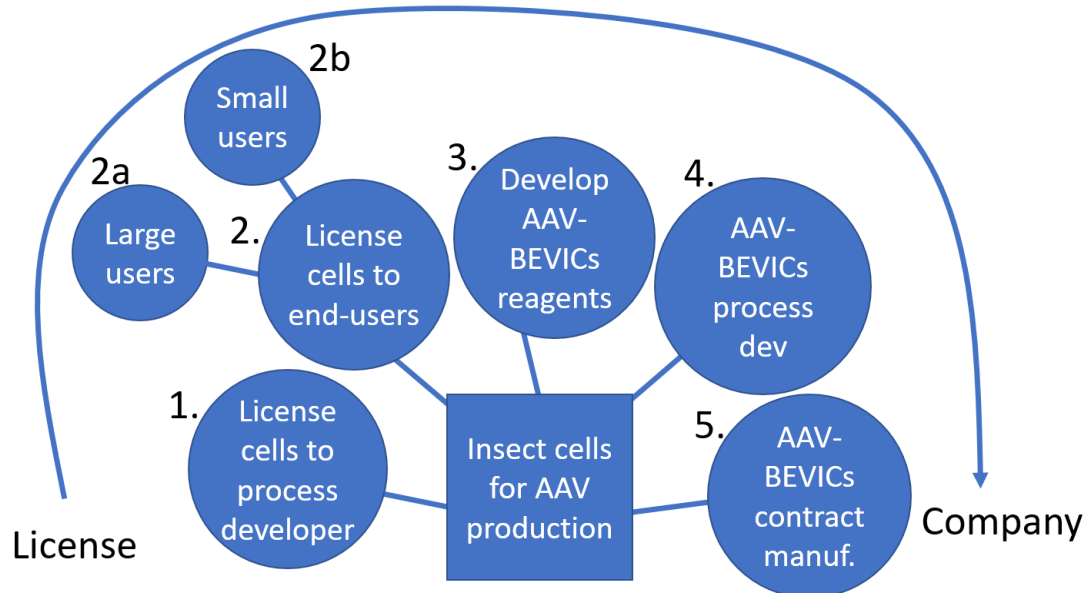


Figure 5.4: Set of business concepts.

### 5.3.1 A set of business concepts for insect cells in AAV production

#### Concept 1: Licensing of cell lines to process technology developers

Certain firms in the pharmaceutical industry develop technologies that can form the basis of multiple different manufacturing processes, such as physical equipment or chemical reagents for use in clinical-grade manufacturing of several independent drugs; or, they may invent entirely new methods spanning multiple aspects of manufacture, such as whole gene expression systems that require special processing, but can deliver significant improvements in recombinant protein production. These

process technology developers (PTDs) out-license those technologies to firms which produce drug materials, either for in-house therapies or as contract manufacturing services.

This concept defines the business as the original rights-holder to a new insect cell line, who grants an outside company – a process technology developer – the rights to invent and sell new manufacturing techniques around the cell lines. The process technology developer would earn revenue from consulting to third parties, from selling reagents for use with their process, and from licensing their technologies to end users (i.e., manufacturers); the original rights-holder (the actual firm defined in this concept) would earn revenue from royalties on some or all of these services. I assumed the benefits of this concept to be that end users could access Alphanodavirus-free insect cell lines using their existing process technology providers (and, perhaps, in conjunction with their existing expression systems) – simplifying the process of licensing the cells and incorporating them into existing manufacturing programs.

## **Concept 2: Direct licensing of cell lines to end-users**

This concept bypasses the step of collaborating with an outside process technology developer by interfacing directly with end-users of the cell lines. Here, I assumed the end-users would be gene therapy companies or contract manufacturers who specialize in the use of insect cells as a production substrate, so they would require less outside assistance than typical customers of the process technology developer in the previous concept. Unlike the previous concept, implementing this idea would likely require the formation of a new company to raise funds; rigorous characterization and viral safety testing, which is mandated by the FDA and is more extensive

than the tests performed by BTI, on the cell lines would need to be performed before they are released to end-users, and these testing services would be too costly for BTI to shoulder as an academic institution. In these respects, the business identified in this concept resembles the outside process technology developer in the previous example, albeit limited to the most basic additional development of the cell lines. I assumed the benefits of this concept to be that end-users could access the cells quickly following the previously mentioned testing, and receive the cells from a dedicated supplier who can be available for basic assistance when working with the cells.

### **Concept 3: Design and out-licensing of custom AAV/Baculovirus plasmids compatible with insect cells**

This concept further achieves the role of the process technology developer by inventing new reagents for use with the insect cell lines (see Figure 5.3). A major hurdle in the production of AAV using the BEVICS method is that the original plasmids used to create the AAV in mammalian cells are not immediately compatible with insect cells. Custom baculovirus plasmids would need to be engineered for each serotype of AAV, with targeted edits in the genetic code which alter the relative expression levels of different protein components of AAV. This work of designing new plasmids, while complicated and time-consuming, would result in extremely valuable intellectual property that could be licensed to gene therapy companies who need to improve their manufacturing performance or switch to a different serotype. For example, work performed by Rob Kotin at the National Institutes of Health in the 2000s allowed three serotypes of AAV to be produced in Sf9 insect cells; patents based on these designs continue to be licensed by gene therapy companies. I assumed the benefits of this concept would be that end-

users could obtain plasmids for baculovirus-based AAV expression which would be guaranteed to have high quality and performance in the new insect cell lines, and ideally, be able to avoid infringing on existing designs.

#### **Concept 4: Contract process development for AAV manufacturing using IC lines**

This concept further builds on the idea of accumulating expertise in the industrial use of insect cells to encompass hiring experts in process development and making their services available to end-users. Process developers, often chemical engineers or related biotechnologists with years of experience in creating and improving laboratory- and clinical-grade bioprocesses, are in high demand across the biopharmaceutical world; process developers with experience working with insect cells are even more uncommon; those who have produced recombinant AAV using insect cells are rarely available for hire. This rarity suggests that a firm with extensive knowledge in adapting bench-scale methods for AAV production into economical IC-based processes, and the ability to provide licensable process designs, might be able to extract large consulting and royalty fees from end-users who are unable or unwilling to build such process development expertise in-house. I assumed the benefits of this concept to be that the expertise of each process developer in the firm could be applied to the largest number of end-users – maximizing the value that he or she could create and capture – and that more gene therapy developers would be able to explore IC-based production with confidence that assistance would be available when needed.

### **Concept 5: Contract manufacturing of AAV using IC lines**

This last concept strays the farthest from the passive approach of the first concept to a firm which derives its revenue from the manufacture and sale of physical goods. Across the pharmaceutical industry, companies which own the rights to a therapy and manage its development may outsource some or all of the burden of producing drug material to contract manufacturing organizations (CMOs). Much like the firm in the previous concept would pool process development expertise and make it available to any paying client, a CMO would pool manufacturing capabilities and capacity and make it available to therapy companies at various stages of development. I assumed the benefits of this concept to be that a small-scale CMO with the ability to produce high-quality AAV in insect cells would meet clients' needs at a lower cost than comparable CMOs using mammalian cells and would enable companies to test IC-derived versions of their AAV therapies early in the drug development process.

#### **5.3.2 Search pattern**

I planned the rough order in which I would investigate these five concepts by ranking how I hypothesized each concept would fare in seven factors that influence the profitability of a new business, as shown in Table 5.2. In general, I hypothesized that businesses which could generate royalties on sales of future gene therapies would address larger markets than those which did not (e.g., C2, “Direct licensing of cells to end users” ranked higher than C5, “Contract manufacturing organization”). I also hypothesized that licensing opportunities would require less capital requirements than ideas based around operating manufacturing facilities. I hypoth-

Idea	Market Size	Capital Req.	Value Prop.	High Margin	Unfair Edge	Big Problem	Good Fit	Total	Order
C1	<b>3.5</b>	<b>5</b>	<b>4</b>	<b>5</b>	<b>4</b>	<b>4</b>	<b>5</b>	<b>30.5</b>	<b>2</b>
C2	<b>5</b>	<b>4</b>	<b>5</b>	<b>4</b>	<b>5</b>	<b>5</b>	<b>4</b>	<b>32</b>	<b>1</b>
C3	<b>2</b>	<b>3</b>	<b>2</b>	<b>2</b>	<b>2</b>	<b>3</b>	<b>2</b>	<b>16</b>	<b>4</b>
C4	<b>3.5</b>	<b>2</b>	<b>3</b>	<b>3</b>	<b>3</b>	<b>2</b>	<b>3</b>	<b>19.5</b>	<b>3</b>
C5	<b>1</b>	<b>1</b>	<b>1</b>	<b>1</b>	<b>1</b>	<b>1</b>	<b>1</b>	<b>7</b>	<b>5</b>

**Table 5.2: Scoring matrix for business concepts.**

esized that the ownership of adventitious virus-free cell lines generally provided better value propositions (i.e., reduced risk and better yield), higher margins (i.e., from royalties), more sustainable advantages (i.e., from patents on the cells), and an easier fit (i.e., my relationship with the cells' existing owner, BTI) than ideas which would require me to create new IP, build new process development skills, or assemble manufacturing capabilities. As a result, my rankings heavily skewed towards Concepts 1 and 2, both of which revolving around the out-licensing of insect cells to companies in the AAV industry. From the total scores assigned to each business concept, I planned to investigate the direct licensing of insect cell lines to gene therapy companies (Concept 2) first and the creation of an AAV contract manufacturing organization (Concept 5) last.

### 5.3.3 Interview process around each concept

#### Concept 2a: License insect cells to large gene therapy company

I hypothesized that the largest potential source of revenue for a proprietary cell line comes from royalties on sales of drugs manufactured with the cell line; for technologies used in pharmaceutical manufacture, royalties can be in the range of 0.5% to 5% of sales, meaning a single “blockbuster” drug can generate revenues in excess of \$10 million per year to the owner of a licensed technology. As such, I hypothesized that marketing the cell lines to large gene therapy companies and their contract manufacturers, the two entities closest to manufacturing AAV for commercial sale, had the potential to make the most money from the cell lines, the soonest.

I recorded my hypotheses in a map of the industry (Figure 5.5), which roughly depicts the origin of large gene therapy companies, their relationship to contract manufacturers, and how this business concept might address their needs. In Figure 5.5, I provide the two value propositions of this concept, which are both relevant to commercial manufacture of AAV: the new insect cell lines may provide an approximately 2-fold increase in AAV yield compared to existing insect cell lines, and they do not have any adventitious viral infections that might complicate regulatory compliance of the manufacturing process. The most significant revenue stream of this concept, royalties on sales of drugs, is highlighted in green in Figure 5.5.

I conducted a series of interviews to test whether the industry map and value propositions recorded in Figure 5.5 were accurate. This concept being the first I tested in this project, these interviews included a very broad sampling across the biopharmaceutical industry to correct any major misconceptions I might have

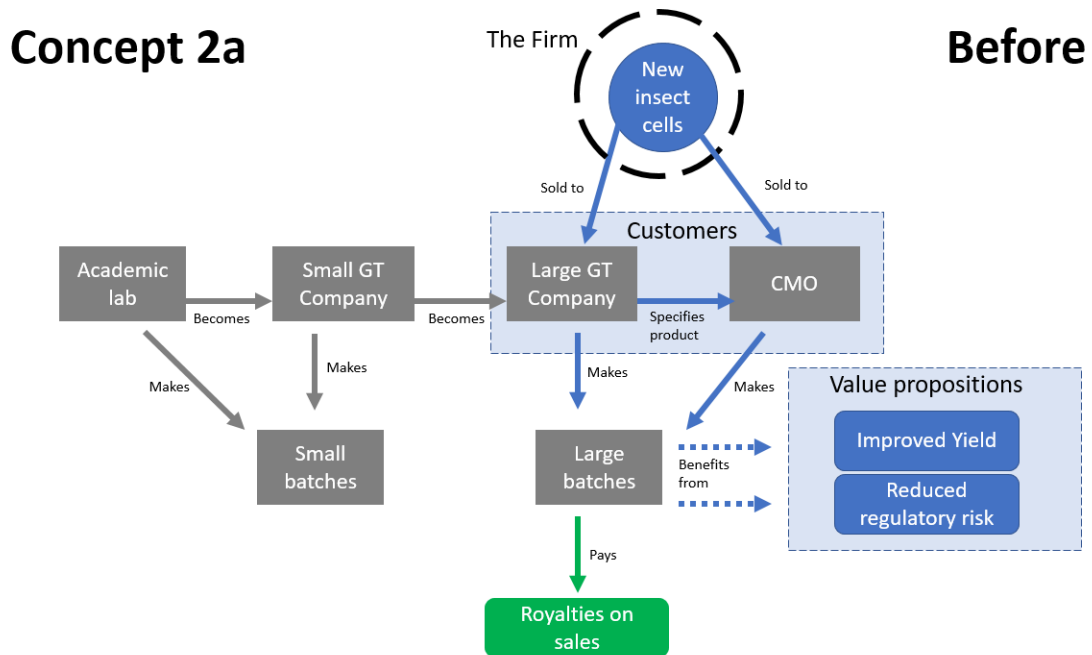


**Figure 5.5: Concept 2a, Before.**

had about drug development. Table 5.3 summarizes the interviews which had the largest impact on this business concept; the table includes an anonymized list of the people I spoke with, a brief rationale for why their perspective was relevant to this concept, and the insights I gathered from the interview. In general, I spoke with executives at therapy companies and CMOs who broadly understood the business of drug manufacturing, scientists and engineers who understood the practical considerations of using a new cell lines, and gene therapy companies who might be potential customers.

From the very first interview of this project, in which I asked a CEO of a large biopharmaceutical company about the basics of drug development, I found that many of my original hypotheses were incorrect. Figure 5.6 depicts an industry map for Concept 2a which includes the the results of the interview process in the form of notes (explaining misconceptions in my original hypotheses or new observations)

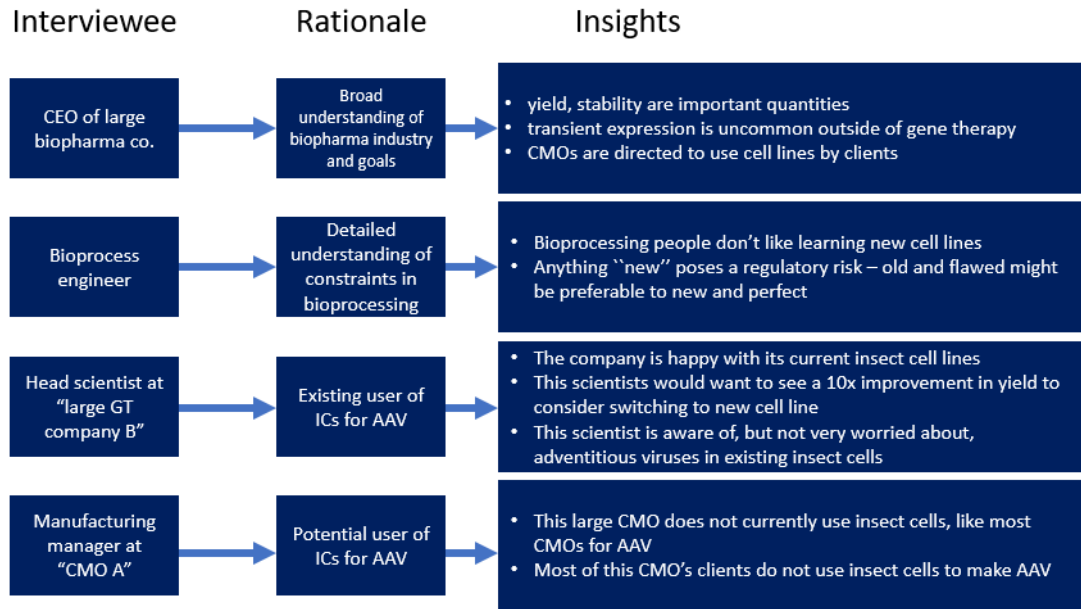


**Table 5.3: Interview Process for Concept 2a.**

and changes to the map itself. Notes highlighted in red explain falsified hypotheses, and notes highlighted in yellow explain new observations not addressed by previous hypotheses.

The business concept which I originally thought had the highest potential – licensing new insect cell cell lines to gene therapy companies with drugs closest to market launch – was flawed. By the time a drug reaches the final stages of development, the manufacturing process is essentially fixed: CMOs do not have input about what materials will be used, switching cell lines would likely constitute a bigger regulatory risk than adventitious viral infections (specifically, those present in existing insect cells), and anything less than a roughly 10x improvement in yield from a new cell line is unlikely to get the attention of most companies at this stage.

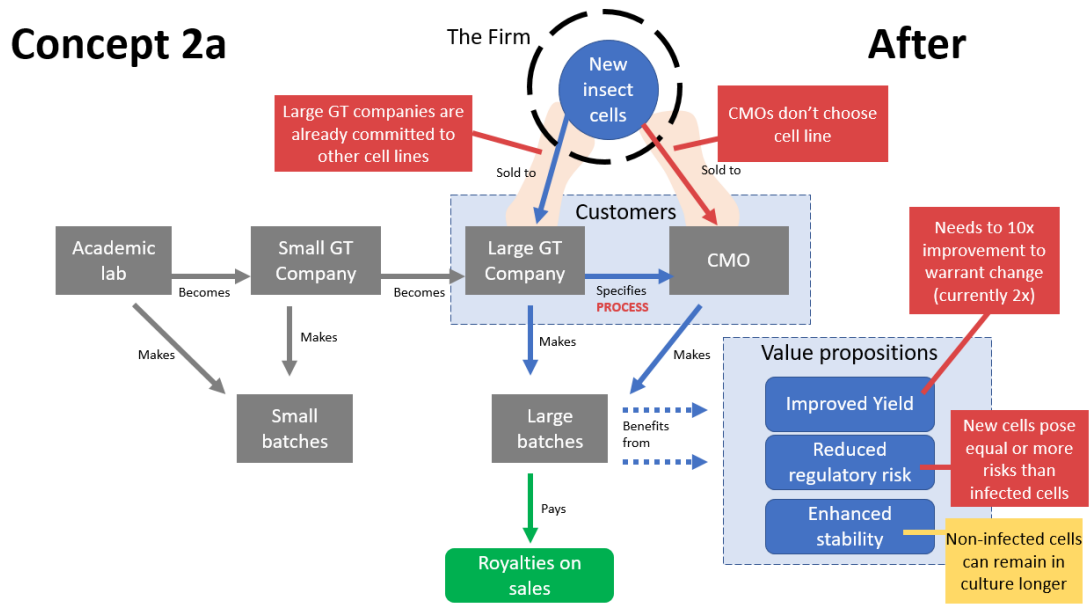
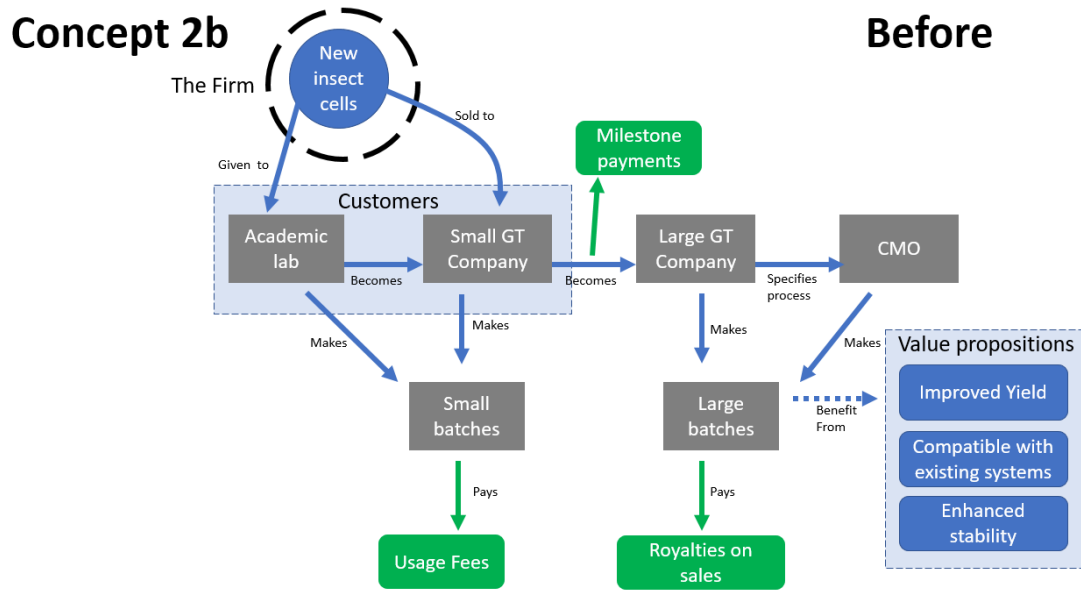


Figure 5.6: Concept 2a, After.

### Concept 2b: License insect cells to small AAV producers

My original industry map for the potential licensees of insect cell lines (Figure 5.5) was based on a flawed hypothesis – that companies with AAV therapies at an advanced stage of development would be interested in new cell lines. Before I moved on to an entirely different concept, I instead considered whether gene therapy companies, or even academic researchers, in the early stages of developing an AAV therapy might agree to use the insect cell lines for R& D, and then work ]towards using them for a commercial process. My original map of this hypothesis, provided in Figure 5.7, describes some of the potential sources of short-term revenue for a company who would license cells in this manner, including flat fees for the permission of small therapy companies to use the cell lines for R& D (on the order of \$1,000 per year per company) and larger payments made by a company when they pass certain regulatory milestones using the cell lines (\$10 to \$100 thousand per milestone).



**Figure 5.7: Concept 2b, Before.**

Table 5.4 summarizes the interviews that I used to investigate this variation on the concept of licensing to end users. I spoke with a CEO of an early-stage company, who explained the needs of a company that has no revenues and large research expenses – the future performance of a commercial manufacturing process based on his product is a low priority compared to progressing quickly through pre-clinical studies. I also spoke with managers of companies and academic facilities that provide services to early-stage gene therapy companies – they understood common problems that early-stage companies encountered, and assisted early stage companies in choosing process technologies (incl. cell lines), which suggested they would be the first to “convince” of the value of the cell lines when implementing this concept. I had lengthy conversations with a scientist who managed the manufacturing department as a mid-size gene therapy and he provided a highly valuable perspective from a company transitioning from early R& D to later-stage development; this company was stable enough that they could start to worry about

long-term manufacturability, but were still open adopting new process technologies for some drugs in their pipeline.

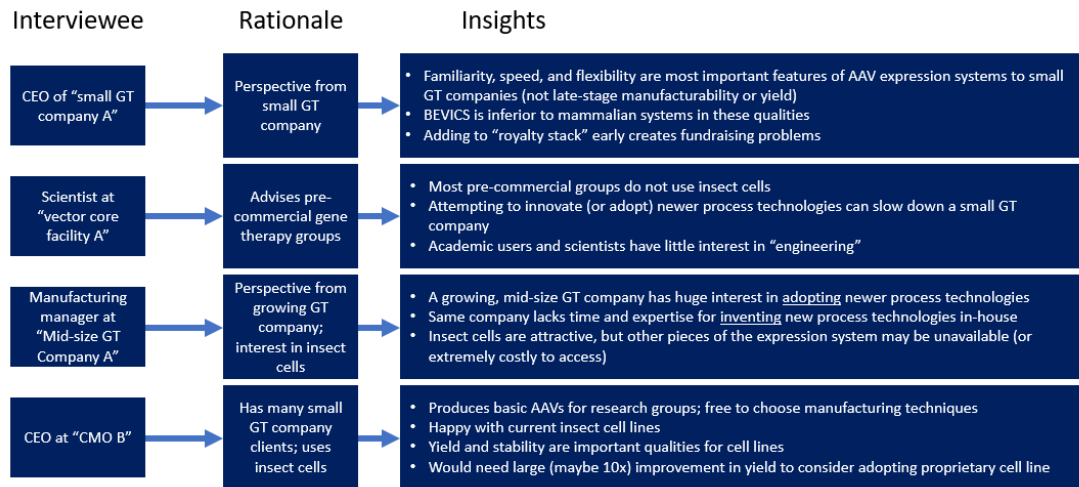


**Table 5.4: Interview Process for Concept 2b.**

Figure 5.8 illustrates how my understanding of the industry map for early-stage AAV companies evolved after I conducted interviews. First and foremost, the value propositions of the new cell lines, which were concentrated around benefits enjoyed by companies producing large quantities of AAV for clinical trials and sale, did not align with the urgent needs of gene therapy startups – these companies perceived qualities such as speed, familiarity, and flexibility to be more important to their survival than yield or stability. Resource-constrained startups were also clear that they would likely avoid using any cell lines that carried a requirement to pay usage fees, threatening the ability for the licensing company to collect short-term revenues; they also explained that adopting any technology that carries a commitment to pay royalties on sales would be unattractive to potential investors, threatening the company’s ability to raise funds. Mid-size companies appreciated the benefits that new IC lines could provide to their clinical-grade manufacturing processes and were open to the idea of paying usage and milestone fees, but had

doubts as to whether they could assemble the other pieces of the baculovirus expression vector system necessary to produce AAV; in particular, IC-compatible plasmids for each AAV serotype are needed, and mid-size companies were not confident they could develop or license these plasmids.

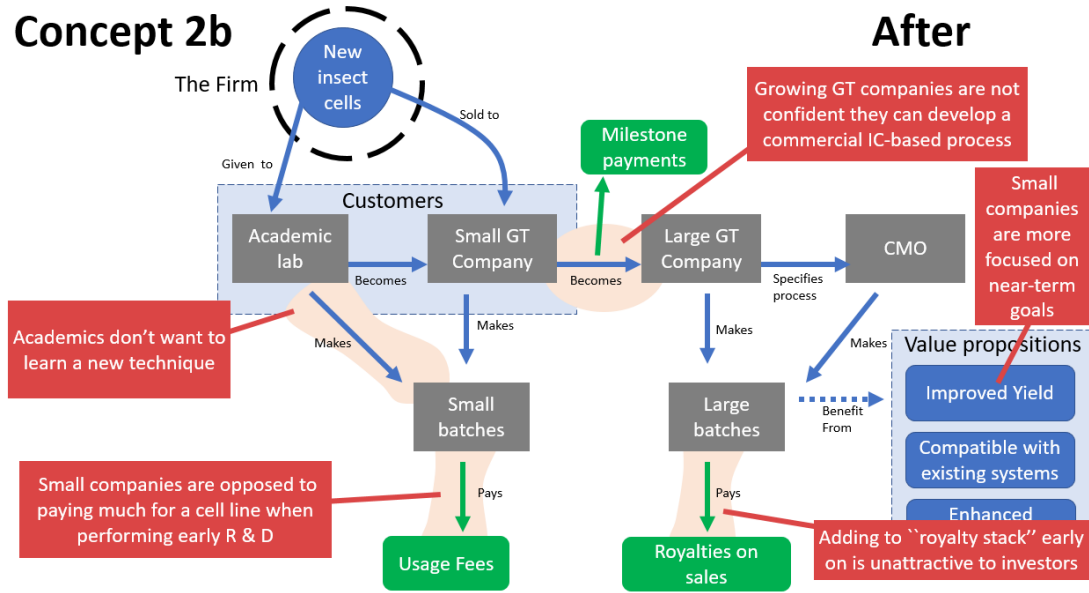


Figure 5.8: Concept 2b, After.

The hypothetical industry map for this variation of the direct licensing concept was closer to being correct than in the previous example, but contained some subtle misconceptions about how the priorities of early-stage gene therapy companies and confidence that growing gene therapies had in adopting new process technologies without outside help. At this stage in the project, I concluded that it was possible to attract new licensees to the insect cell lines as long as a process technology developer was present to ensure clients has access to a complete IC-based expression system and could provide assistance during scale-up.

## Concept 1: License insect cells to process technology developer

My investigation of the direct licensing concept had revealed that assistance from a process technology developer was necessary for most growing gene therapy companies to implement an IC-based process. I created an industry map (Figure 5.9) that hypothesized a close collaboration between the cell rights-holder and a process technology developer which could potentially allay the concerns of mid-size AAV companies considering insect cells. When the process technology is considered as customer, a primary value proposition aimed at them would be the concept of “pedigree” when it comes to cell lines: dozens of insect cell lines, even of the species *T. ni*, have been isolated, but very few have received regulatory approval in manufacture of pharmaceuticals, or have been used in any sort of industrial application. The cell lines isolated by BTI were directly descended from Hi-5, which was approved in the manufacture of a vaccine and is the second most commonly used insect cell line for recombinant protein production. Another aspect of “pedigree” is documentation: the FDA requests a complete history of ever physical manipulation ever made to a cell line, such as steps taken to isolated the cells or any times they were passaged or frozen; few cell lines have this kind of documentation attached to them, but BTI’s cell lines do. I hypothesized that process technology developers would consider the cell lines’ good pedigree (and lack of adventitious viral infections) to reduce some of the risks associated with tailoring their process technology to the cells; the last thing they would want is a surprise that makes the cells a liability. I hypothesized that clients of the process technology developer would benefit from improved yield over other insect cell lines.

I attempted to investigate this hypothesis by speaking with process technology developers who work with insect cells and might distribute them in the manner

## Concept 1

## Before

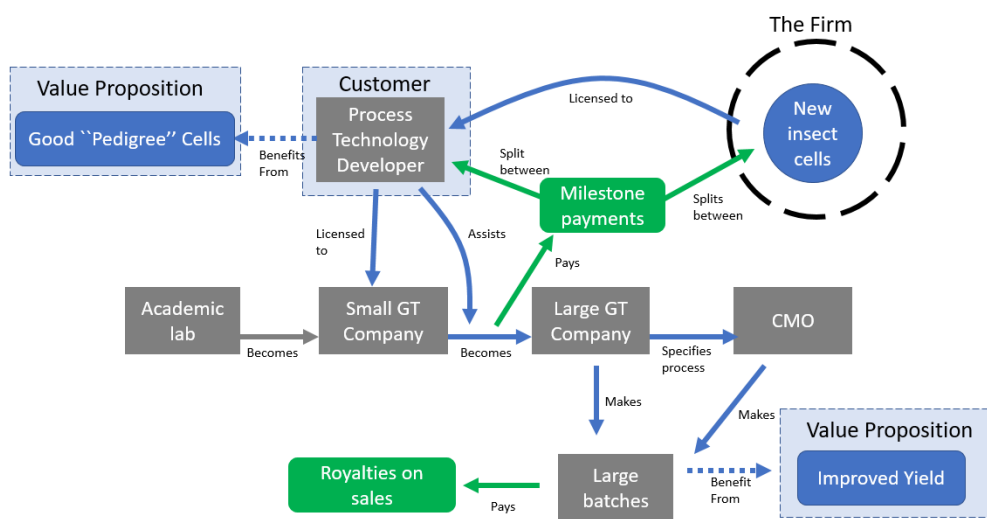


**Figure 5.9: Concept 1, Before.**

illustrated in Figure 5.9. However, as summarized in Table 5.5, no companies perfectly matched the process technology hypothesized in Figure 5.9. I spoke with some firms and experts that embodied aspects of the developer. One large company provided enabling process technologies (in the form of plasmids for natural AAV serotypes) to a variety of companies, but did not work with insect cells or have the expertise to develop new processes around insect cells. Another company made AAV in insect cells, and reported to have process technologies available for licensed, but did not have a record of successfully licensing those technologies to help smaller companies scale up IC-based AAV processes. An expert within an university vector core facility assisted companies with scaling up their AAV processes, and helped device new process technologies, but was uninterested in developing expression systems (including those based around insect cells). My conversations with the manufacturing manager at the mid-size gene therapy company revealed a lack of process technology developers for IC-based AAV production which made their

technologies available for license; certain therapy companies had the right process technology and were skilled at process development, but they did not share those assets with other firms.

Interviewee	Rationale	Insights
Team at "large GT company A"	Owns and out-licenses patents to AAV (product) designs	<ul style="list-style-type: none"> <li>This company owns patents to natural AAV serotypes – a form of process technology – and licenses them to large and small gene therapy companies</li> <li>Does not own rights to insect cell-compatible plasmids – little incentive to offer ICs to clients</li> <li>Limited process development expertise to integrate new technologies</li> </ul>
CEO at "CMO B"	Owns and out-licenses patents to IC-based AAV expression system	<ul style="list-style-type: none"> <li>Owns rights to an IC-based AAV expression system, and is open to the idea of integrating a new cell line into portfolio, but has had limited success in out-licensing to gene therapy companies</li> <li>(Later interviews also revealed that CMO B is perceived as low-quality; not suitable for medical-grade use)</li> </ul>
Scientist at "Vector Core Facility A"	Performs contract process development for GT clients	<ul style="list-style-type: none"> <li>Advises GT clients on process technologies to license, and develops some process technologies in-house for out-license</li> <li>Not interested in developing IC-based expression systems: sees separation processes as larger opportunity than new expression systems</li> </ul>
Manufacturing manager at "Mid-size GT Company A"	Potential customer for process technology developers	<ul style="list-style-type: none"> <li>This mid-size GT company wants to license an IC-based expression system, including rights to adventitious virus-free cell lines</li> <li>However, the companies which create high-quality process technologies for IC-based AAV expression (incl. improved IC lines) are not making them available for license, or insist on contractual terms that are not feasible for early- and mid-stage GT companies</li> </ul>

**Table 5.5: Interview Process for Concept 1.**

My understanding of how a process technology could help growing gene therapy companies access and improve IC-based processes for AAV manufacture, captured in Figure 5.9, was falsified in an unexpected way: the hypothesized firm did not exist. As depicted in Figure 5.10, no firm performs the three key activities – out-licensing IC-based process technology, providing dependable assistance to growing therapy companies, and readily integrating new components of an IC-based expression system – necessary for the partnership to succeed.

While I did reject this concept for further consideration, it was not because it reflected a poor understanding of what gene therapy companies need to adopt IC-based AAV processes; on the contrary, many gene therapy companies I spoke to wished such a firm would exist. Rather, this concept failed because of a lack of infrastructure – the technologies for license, experts for hire, and manufacturing facilities for lease which would together encourage growing gene therapy compa-

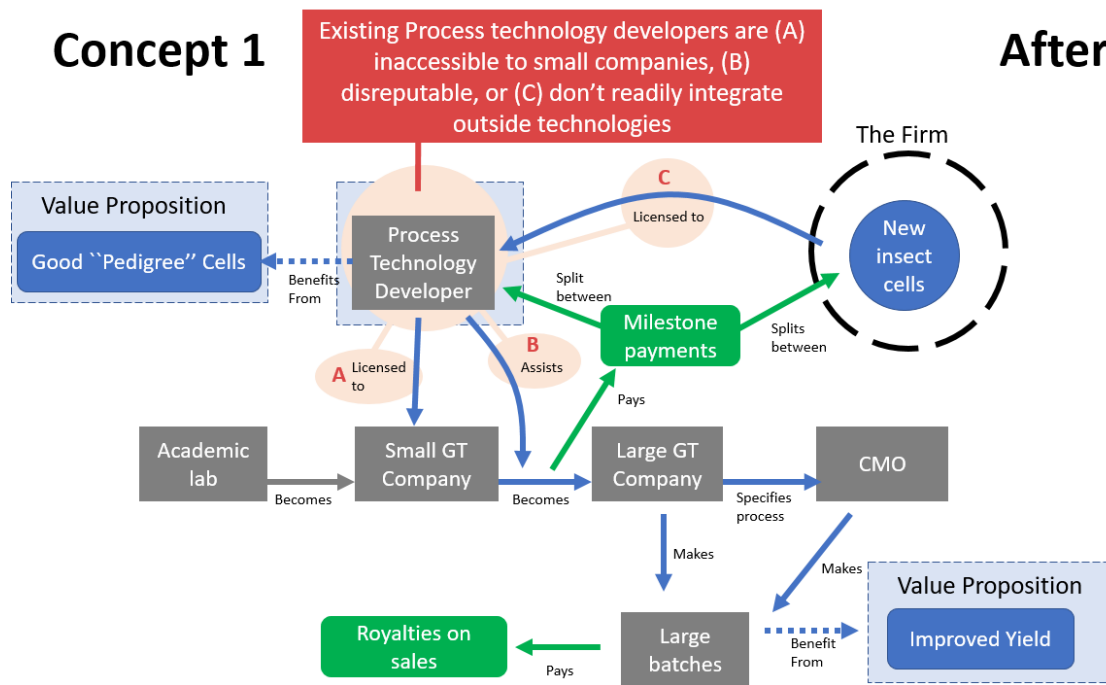


**Figure 5.10: Concept 1, After.**

nies to adopt IC-based process. This development casted doubt on the near-term prospects of licensing BTI’s cell lines in the gene therapy industry, but bolstered the prospects of the remaining business concepts, each of would add to the infrastructure available to gene therapy companies who elect to use insect cells.

#### **Concept 4: Contract process developer**

The first rounds of interviews I conducted revealed that building and accessing expertise in bioprocess development *in general* is a challenge; finding people who can perform process development on IC-based AAV production is a rarity. Following these interviews, I suspected that an firm which pools process development expertise might be more valuable than I had originally estimated. Figure 5.11 depicts a map of how this firm would typically operate: growing gene therapy companies

could consult with experts in the firm during to help make decisions during process scale up, and could directly license process designs and enabling technologies. Short-term revenue would come from consulting fees, and long-term revenue would come from royalties on licensed technologies and process designs. I hypothesized the value propositions to be that resource-constrained therapy companies could hire process development experts on short-term basis, gain access to industry best practices without years of experiential learning, and adopt new process technologies with reduced risk (knowing that expert troubleshooting would be available in the future).

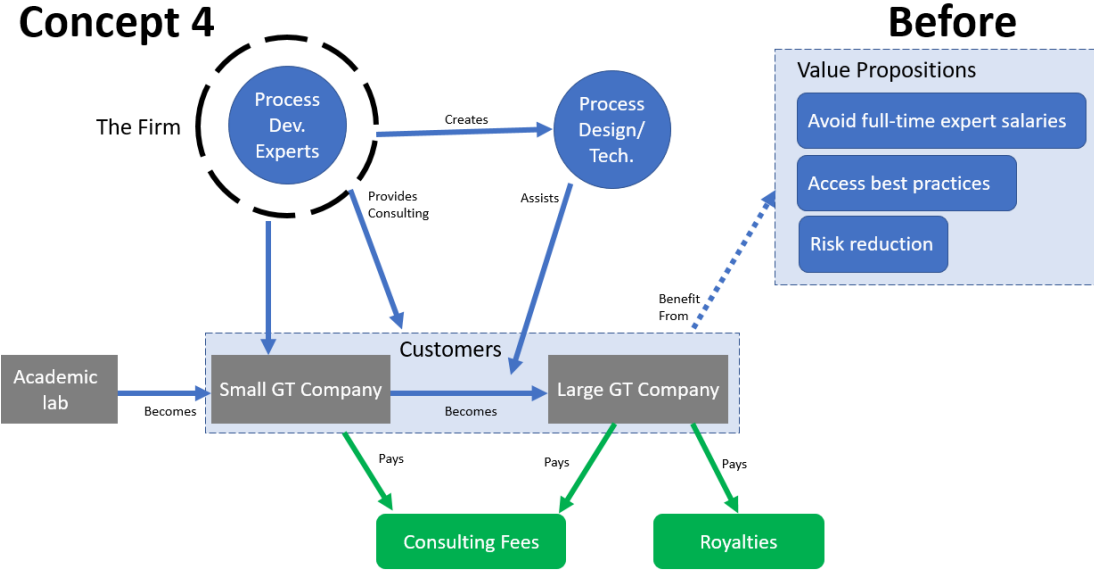


**Figure 5.11: Concept 4, Before.**

To investigate this concept, I interviewed potential clients of the hypothetical firm, as well as experts who represent potential employees the firm would need to hire – summarized in Table 5.6. I also spoke to an industry analyst who had a broad understanding of the challenges that therapy companies face when trying to hire bioprocess development experts. My conversation with the analyst confirmed that bioprocess developers were in short supply: he predicted a 30% shortfall

in bioprocess developers across all sectors of biopharmaceuticals. This posed a challenge when trying to find representatives of potential hires for the hypothetical firm; however, I found that certain people in university settings – scientists at vector core facilities and researchers of industrial biotechnology – had bioprocess development skills which were highly relevant to the AAV-BEVICS process and had not fully engaged with commercial partners (still mostly performing academic research).

Interviewee	Rationale	Insights
Manufacturing manager at "Mid-size GT Company A"	Actively searching for new process designs	<ul style="list-style-type: none"> <li>This company wants to improve its process performance, but does not have the time or personnel to innovate new process technologies in-house</li> <li>Would license process technologies – and designs for a whole new AAV process – if available</li> <li>This manager worries that pharma companies shift people around so much that process developers don't get to master a subject or form an innovative community</li> </ul>
Team at "large GT company A"	Actively searching for new process designs	<ul style="list-style-type: none"> <li>This company has limited experience with process development because they have outsourced most of their manufacturing to CMOs</li> <li>This company wants to start manufacturing in-house, and would hire a contract process developer if it could not find full-time employees with the right skills</li> </ul>
Biopharma industry analyst	Understands the labor market for hiring bioprocess developers	<ul style="list-style-type: none"> <li>This analyst has interviewed executives across all sectors of biopharma industry</li> <li>There is intense competition to hire qualified bioprocess developers (30% shortfall predicted)</li> <li>First, it takes many years of industrial practice to become a bioprocess developer</li> <li>Second, many bioprocess developers are occupied with the rapid growth of "biosimilars"</li> </ul>
Scientist at "Vector Core Facility A"	A contract process developer for AAV	<ul style="list-style-type: none"> <li>This scientist performs contract process development and must turn down some clients because he is too busy</li> <li>However, he is resistant to the idea of working with newer (better scaling) expression systems</li> <li>He would rather not leave his academic post</li> </ul>
Team at biotechnology research center	Experts in process development for insect cells	<ul style="list-style-type: none"> <li>This team performs research and contract development of commercial-scale IC-based processes</li> <li>However, this team has limited experience with AAV manufacturing</li> <li>The members of this team also have academic posts they would rather not leave</li> </ul>

**Table 5.6: Interview Process for Concept 4.**

The insights I gathered from the interviews largely confirmed my original hypotheses about the role and value proposition of the contract process developer, so minimal changes to my industry map were necessary. However, the practical challenges of even finding bioprocess developers to interview gave me a newfound respect for the challenges that would accompany trying to assemble a group of such people into a single firm. As shown in Figure 5.12, the larger business model behind a contract process developer must plan for how the necessary experts are

going to be assembled. For example, talented biomolecular scientists and engineers could be found by scouting for talent in academic research groups, but they would need to build experience in clinical-grade bioprocessing for the specific application before they could solve problems faced by client therapy companies; building this expertise, even mastery, of clinical-grade bioprocessing was reported by interviewees to be challenging in most commercial settings. Alternatively, the firm could hire bioprocess developers from existing gene therapy companies, but this might not be a profitable source of new hires because the salary requirements might be extremely high for someone with these skills already developed.

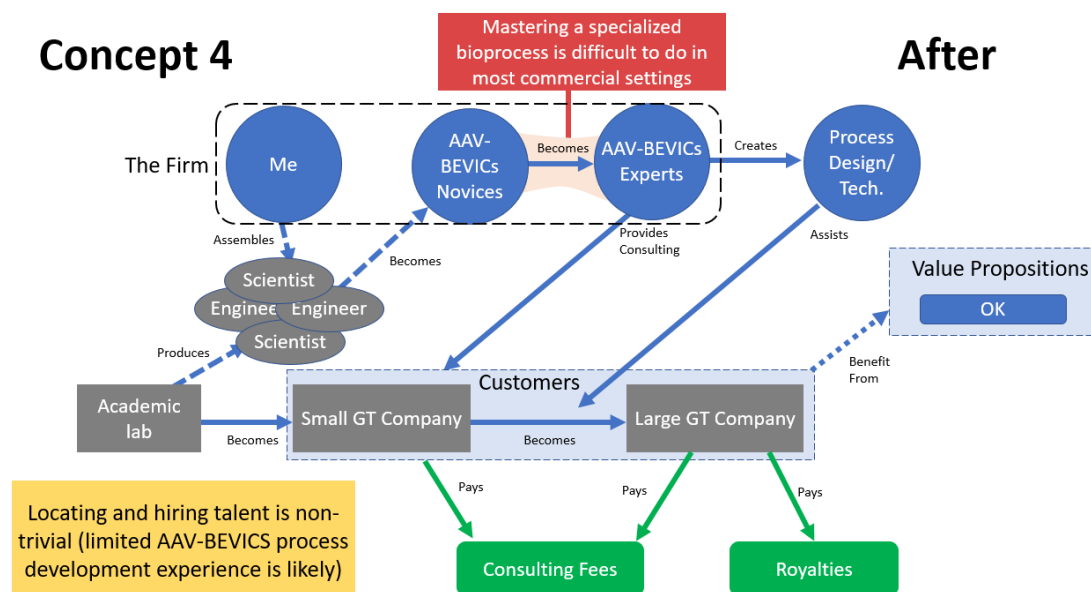


Figure 5.12: Concept 4, After.

Overall, I concluded that having a firm of process development experts-for-hire would likely be highly profitable because it would solve significant problems for gene therapy companies and would be difficult for other firms to replicate, although building the firm might hinge on finding a way to efficiently train employees in clinical-grade AAV bioprocessing.

### **Concept 3: Custom AAV-BEVICS plasmids**

My review of the literature on AAV production using the baculovirus expression vector-insect cell system (BEVICS) revealed decades of research went into developing the baculovirus plasmids that enabled insect cells to produce high quality AAV. Patents for these IC-compatible AAV plasmids are owned by entities such as the NIH and large gene therapy companies; early rounds of interviews with people knowledgeable in this topic revealed that while the NIH will license these plasmids to gene therapy start-ups, private companies which hold the patents only share them under terms that virtually all partners would reject. I hypothesized that developing and readily out-licensing new IC-compatible plasmids for AAV production would unlock value for firms across the AAV industry: this might include gene therapy companies who want to benefit from the enhanced yield of IC-based processes, technology firms who rely on potential licensees to have access to these plasmids (e.g., a firm attempting to out-license insect cell lines), and owners of AAV serotypes who want their licensees to succeed in commercializing therapies.

Figure 5.13 depicts my hypothetical industry map around the latter suggestion: a company which owns the rights to a serotype without existing IC-compatible plasmids. I predicted that partnering with the owner of a serotype would be wise because their patents would entirely cover any patents for adapting the serotype to use in insect cells; without cooperation from the serotype owner, a firm developing a modified plasmid for the serotype could have their freedom to operate revoked. I predicted that the short-term revenues for the firm developing the IC-compatible plasmid might come from consulting fees for the work of developing the plasmids; long term revenues could potentially be secured by negotiating royalties or milestone payments from the serotype owner and its licensees.



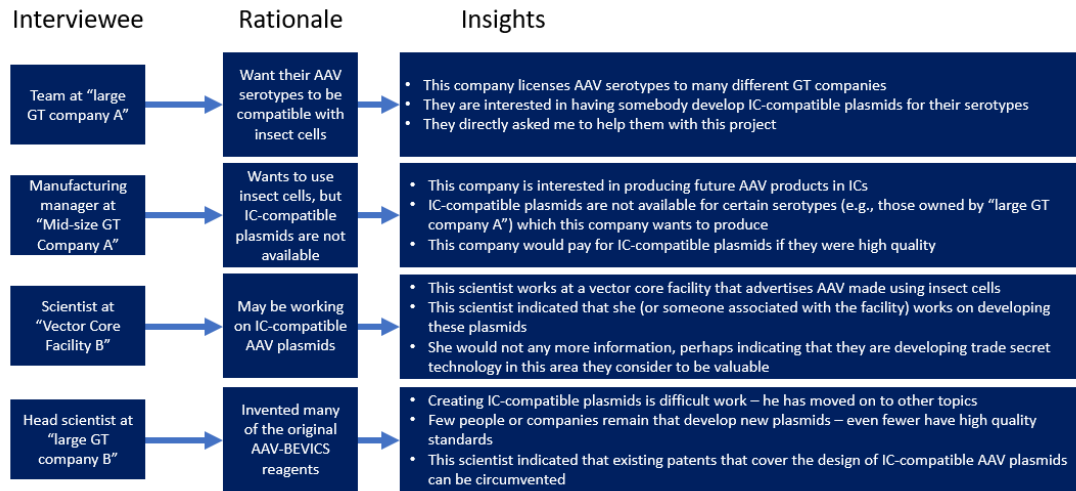


**Table 5.7: Interview Process for Concept 3.**

industry map were necessary. As in the concept of operating a contract process development business (Figure 5.12), finding the right experts to execute the project may pose a challenge. Some scientists I spoke to seemed to be already engaged in this work (and could not divulge much about it), but others were open to starting such a project, especially because it could be completed in an academic setting.

The hypothesis of organizing a project around the design of IC-compatible plasmids for AAV production emerged from a round of interviews mostly unscathed, and the concept was in a good position to start the next phase of business model design, validation (discussed below).

### **Concept 5: Contract manufacturing of AAV using insect cells**

The final concept I investigated, the creation of a contract manufacturing organization (CMO) which focused on IC-based AAV production, ranked poorly in my initial scoring matrix because I predicted that it would not receive royalties on

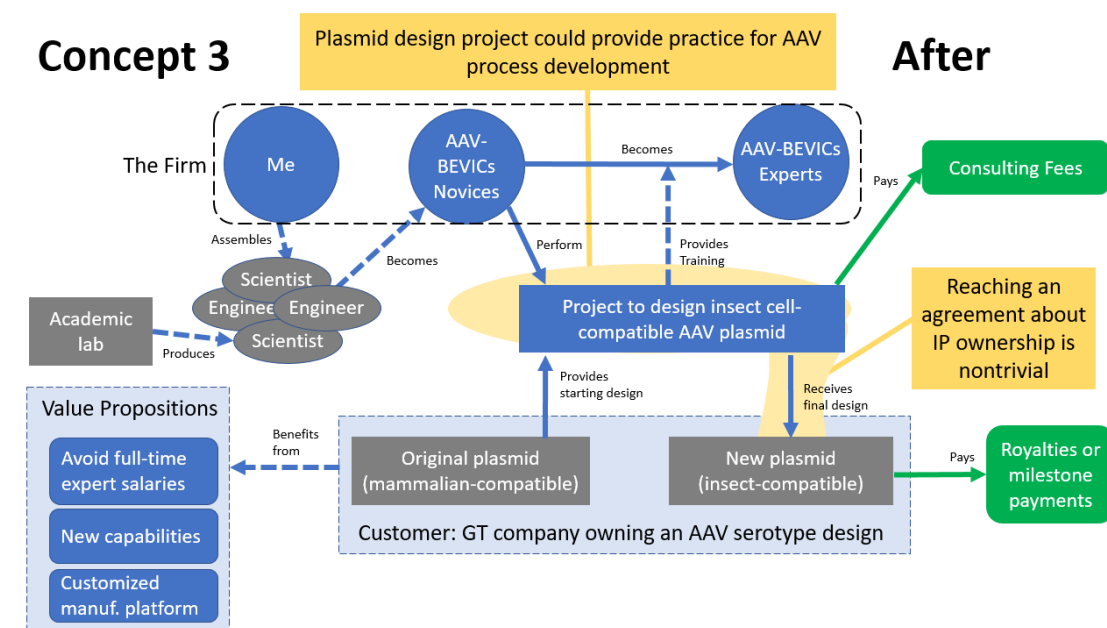


Figure 5.14: Concept 3, After.

the sales of drugs, limiting its long-term profitability versus the other concepts. However, in the process of testing the previous concepts, I discovered that firms which provide services to AAV companies as they grow are both necessary for the maturation of gene therapy and can potentially profit sooner and more reliably than concepts which rely on clients to make it to the market (which has yet to happen in the USA).

In Figure 5.15, I provide the industry map which I hypothesized to capture the customers, revenues, and value propositions of an AAV-focused CMO. I hypothesized that CMOs would be segmented by size: customers would need small (for academic researchers or startups) or large (for mature gene therapy companies) batch sizes, and would value different qualities of the CMO accordingly. I predicted that a small CMO catering to small clients would be most valuable if it was fast, cheap, and of acceptable quality; I predicted that a large CMO catering to large clients would be most valuable if it could provide the raw manufacturing

capacity necessary to complete a clinical trial and could produce clinical-grade material. In both cases, revenues be payments negotiated during the signing of the manufacturing contract and fully received upon completion.

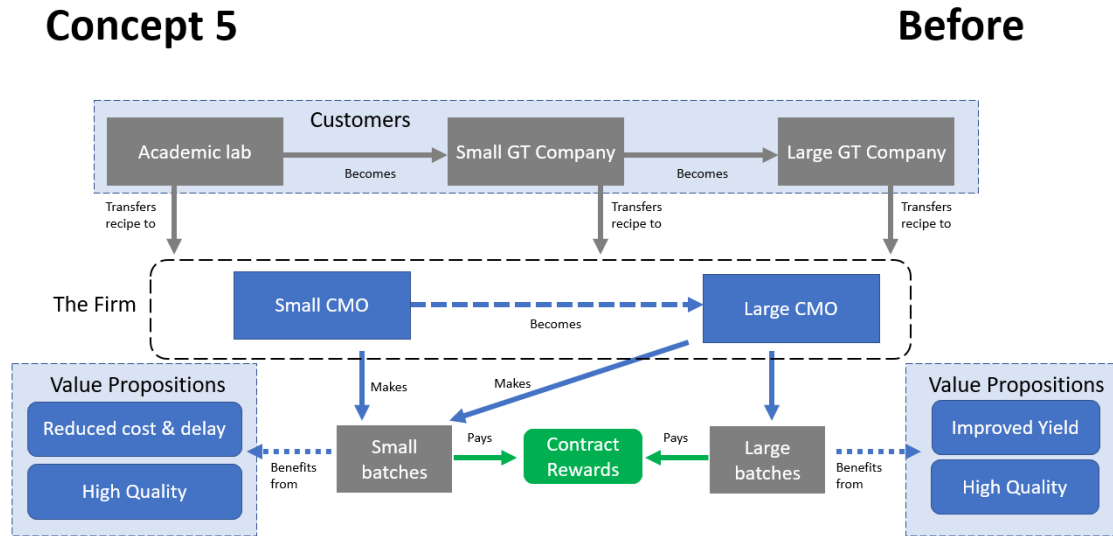


Figure 5.15: Concept 5, Before.

To test this hypothetical map, I spoke with senior employees of small, mid-size, and large AAV therapy companies, as well as representatives from CMOs which produce AAV, as summarized in Table 5.8. Every therapy company I spoke with had used, or were planning to use, a CMO for clinical-grade AAV. Interestingly, employees from larger companies generally held more unfavorable views of CMOs than employees at smaller companies, perhaps indicating that existing CMOs had a record of disappointing their clients in timely completion of contracts and in producing high-quality AAV. Of the CMOs I spoke with, few used IC-based processes, and all assured me they produced very high-quality AAV.

The interview process for this concept had mixed effects on my hypothesis for the industry map around contract manufacturing of AAV, as shown in Figure 5.16.

Interviewee	Rationale	Insights
CEO of "small GT company A"	Will use contract manufacturing to provide materials for preclinical research	<ul style="list-style-type: none"> <li>This CEO currently produces AAV in-house because existing CMOs are too expensive</li> <li>If he needed assistance in the near future, he would likely contact a university vector core facility</li> <li>This CEO anticipates that he will eventually spend \$1 million on contract manufacturing in advance of his first clinical trial</li> </ul>
Manufacturing manager at "Mid-size GT Company A"	Uses contract manufacturing to provide materials for clinical trials	<ul style="list-style-type: none"> <li>This manager felt that some CMOs were competent in non-IC-based processes, but almost none were competent with IC-based processes</li> <li>This company would rely on CMOs more if they could produce high-quality materials</li> <li>This manager estimated that it would cost \$10 to \$15 million in the first year to operate a CMO which could produce high quality AAV for clinical trials</li> </ul>
Engineer at "Mid-size GT Company B"	Uses contract manufacturing to provide materials for clinical trials	<ul style="list-style-type: none"> <li>This company has a capable in-house manufacturing team, but still use CMOs to create materials for clinical trials</li> <li>This company experienced a year-long delay because their previous CMO had limited expertise in using insect cells, leading to substandard quality in the AAV product</li> </ul>
Head scientist at "large GT company B"	Uses contract manufacturing to provide materials for clinical trials	<ul style="list-style-type: none"> <li>The scientist I spoke with believed that most CMOs which advertise the ability to make AAV provide very low quality materials, unsuitable for even basic research</li> <li>The scientist had a high opinion of only one CMO, which is actually a CDMO</li> </ul>
Manufacturing manager at "CMO C"	Offers clinical-grade manufacturing for GT companies	<ul style="list-style-type: none"> <li>This company produces clinical-grade AAV (using non-IC-based processes)</li> <li>This company quoted a year-long waitlist to begin the process of transferring a process into a CMO (and perhaps another year until the manufacturing contract is complete)</li> </ul>

**Table 5.8: Interview Process for Concept 5.**

The largest charge to the map related to how CMOs were segmented: instead of specializing in large or small batch sizes, CMOs, in the eyes of their clients, are distinguished by the quality of AAV they produce. A CMO with limited experience in AAV or substandard process designs will produce AAV which is suitable only for basic research (or may be effectively useless), while CMOs with extensive experience and GMP-level quality control can be trusted with producing materials for use in human patients. Advancing from having a basic, low-quality AAV bioprocess to having a clinical-grade, GMP-ready manufacturing facility requires significant capital expenses and the hiring of experts; one industry veteran estimated that it would cost \$10 - \$15 million in the first year to assemble and operate a clinical-grade CMO. Advancing from a small-scale, but clinical grade CMO to a CMO capable of producing the projected volume of AAV needed for market launch of a gene therapy may require an order-of-magnitude more investment, and has not been accomplished to date.

## Concept 5

## After

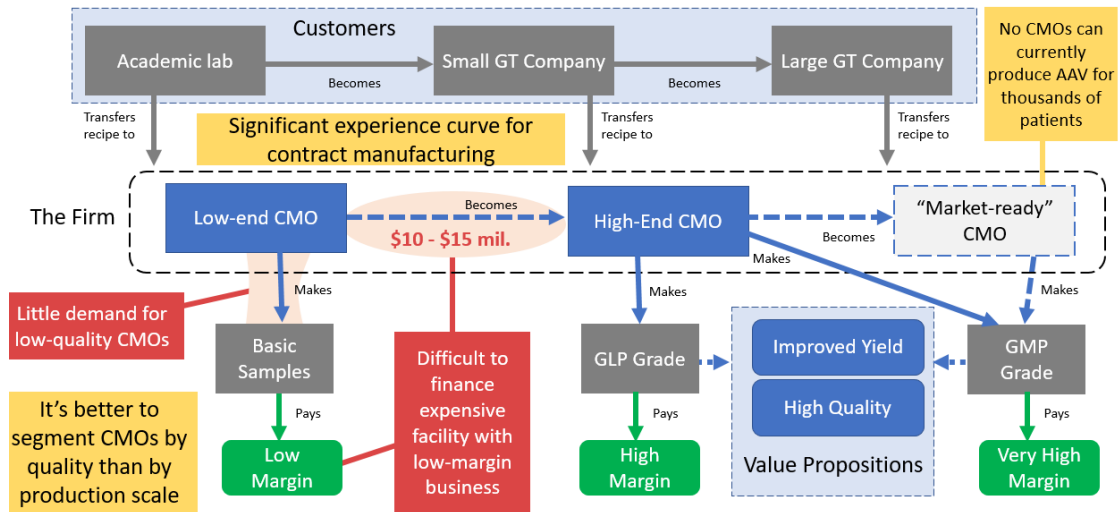


Figure 5.16: Concept 5, After.

The experts I spoke with felt that most existing CMOs produced poor-quality AAV, likely due to a lack of experience, and therefore offered limited value to the therapy companies; I expect that the perceived lack of value for an inexperienced CMO hurts the prices that such CMOs can negotiate and reduces the profitability of manufacturing AAV, perhaps leading the CMOs to limit their investment in improving their AAV production capabilities. Without a large up-front investment, it is likely difficult for a CMO to finance the construction of a clinical-grade AAV facility and the training or hiring of experts to operate it; I considered this up-front cost to be the primary challenge to the CMO concept, as a successful startup would have to establish why it should be the target of investments for new clinical-grade AAV capacity and not existing CMOs. However, I did learn that some therapy companies have successfully outsourced the manufacturing of AAV for clinical trials; in many cases, these companies contracted with either university vector core facilities or specialized contract development and manufac-

turing organizations (CDMOs), each of which are diversified entities that perform both manufacturing and R&D, suggesting a potential path towards operating a profitable CMO of clinical-grade AAV.

Overall, I found the concept of manufacturing AAV on a contract basis for a multiple gene therapy companies to be valid in terms of its value proposition to its customers, but challenged by the startup and operating costs of a clinical-grade manufacturing facility. There is an urgent need for high-quality manufacturing capacity of AAV, and supplying it may be a matter of integrating a CMO with another business concept to provide a sustainable competitive advantage that can attract up-front investment on the order of tens of millions of dollars.

#### **5.3.4 Business concept integration**

I started out with five concepts for new businesses that could exist around the theme of using insect cells to produce recombinant AAV for human gene therapy. During the process of customer discovery, I learned that while almost all of these concepts had certain value propositions that appealed to different customer segments, in most cases, the current industry landscape presented barriers to the customers enjoying the full benefits of the proposed business, or presented barriers to implementing the idea as a standalone business. For example, small gene therapy companies would be interested in using new and improved insect cell lines for upcoming drug candidates, but only if they were confident that contractors would be available to help them with process development and clinical manufacturing (Figures 5.7 & 5.8). In another example, I found that having a contract manufacturing facility for clinical-grade AAV would solve urgent needs of gene therapy customers large and small, but investors might be deterred from financing such a

facility if it could not claim a sustainable competitive advantage over other CMOs. I investigated whether I could overcome these problems by combining two or more of the original concepts into integrated business concepts.

I chose to consider Concepts 2, 3, 4, and 5 for potential integration – Concept 1 fared too poorly in the initial testing phase to be considered for integration. I used a matrix to generate all possible pairs that these four concepts could form (Table 5.9), resulting in six pairings. For each of these six pairs, I estimated three qualities to determine if integration of the concepts was recommendable: two criteria for successful business integration from Markides & Williamson<sup>155</sup> and the possibility of conflicts<sup>153</sup>. Results for each of the pairings are given in Table 5.10.

**Table 5.9:** Business concept pairing matrix

	C2	C3	C4	C5
C2	x	x	x	x
C3	C3,C2	x	x	x
C4	C4,C2	C4,C3	x	x
C5	C5,C2	C5,C3	C5,C4	x

Below, I will discuss some of the details of my rationale for the qualities and my final verdict for each pairing.

### **C2,C3: Develop and own proprietary reagents and cell lines**

This pairing describes a project to develop a whole expression system for AAV production, covering both the production substrate (proprietary insect cells) and other reagents (mainly the baculovirus plasmids which encode for specific AAV serotypes). This holistic approach to expression system development was suggested in conversations I had with experts in AAV process development; in fact,

	Description	Enables asset creation?	Best internally?	Conflicts?	Verdict
C3,C2	Develop and own proprietary reagents and cell lines	Yes – Tailoring reagents to cell lines likely synergistic	Yes – Cells and reagents could form package deal	Maybe – BTT's cells may not be ideal for all applications	<b>Yes</b>
C4,C2	Own cells and provide contract PD assistance	Maybe – Builds unique expertise w/ cells, but PD is replicable	Maybe – Providing PD assistance to BTT's licensees also viable	No – PD around the cell lines is a necessity	<b>Maybe</b>
C5,C2	Own cells and provide contract manufacturing	Maybe – Other manufacturers could imitate cell lines over time	No – Cell lines must remain tradeable	Yes – CMO should remain impartial w.r.t. cell lines, and vice-versa	<b>No</b>
C4,C3	Develop reagents and provide contract PD assistance	Yes – One-stop shop for materials and expertise	Yes – Expertise without ownership poses hold-up risk	No – GT companies want reagents with expert backing	<b>Yes</b>
C5,C3	Develop reagents and provide contract manufacturing	Maybe – More difficult (vs. cell lines) to imitate; funnels customers into CMO	Maybe – Reagents can be licensed, but it can be difficult	Maybe – Clients may bring their own reagents	<b>Maybe</b>
C5,C4	Contract process development and manufacturing	Yes – CMO activities provide PD practice, skilled PD lowers manuf. costs	Yes – Uneconomical for CMO to acquire PD assistance on a contract basis	No – These activities fit naturally	<b>Yes</b>

**Table 5.10: Evaluation of business concept pairings.** A short description of the business created by each concept pairing is given. Each pairing is evaluated using the two criteria for success in business integration given by Markides & Williamson (1994)<sup>155</sup>: does the transfer of competence between business units enhance the creation of strategic assets which are nontradeable, nonsubstitutable, and slow or costly to accumulate; and is it most efficient to transfer competence internally (rather than by trade or contract)? Any potential conflicts arising from the pairing are listed, and these three factors (the two criteria and the potential conflicts) determine whether the pairing is recommended

most process developers engage in some amount of cell line development to select clones from a larger pool, so this is pairing of activities which already exists within some firms. Integration of these concepts would create a core competency of “full-stack” design of AAV expression systems, which would be a sustainable source of value to gene therapy clients. However, a possible conflict emerged: it is far from certain that the proprietary cell lines provided by BTI, which are the cells being referred to in concepts 1 and 2, are generally the best cells to use for new AAV expression systems. For example, certain properties of Sf9, like its superior propagation rate of baculovirus and familiarity to gene therapy customers, might make it more attractive as the cell substrate to design a new expression system around. Combining ownership of a proprietary cell line and a new set of reagents under one roof would create a bias towards using the proprietary cell line, which could potentially hurt the performance of the expression system as a whole. However, the potential for this conflict was minor compared to the expected benefits (and could be mitigated by acquiring multiple different cell lines), so I ultimately recommended the integration of concepts 2 and 3.

#### **C4,C2: Own cells and provide contract process development (PD) assistance**

This pairing describes a firm which provides proprietary cell lines for license and can provide expert help in using them for commercial AAV processes. I had reservations about recommending the integration of these concepts. On one hand, a body of expertise needs to be built around a cell line before it is useful; on the other hand, but building such expertise is not as likely to be a differentiator as, say, building expertise around a whole expression system.

Insect cells are attractive because their processing requirements are relatively predictable, and a skilled process developer can learn to overcome any peculiarities of a new cell line with a few careful experiments; for example, the invention of bench-top arrays of miniature bioreactors (e.g., the BioLector<sup>®</sup> system; m2p-labs GmbH) have allowed bioprocess engineers to screen through dozens of configurations for process parameters (pH, shear rate, temperature, etc.) to find the ideal growth conditions for a new cell. Furthermore, even if specializing in a cell line as a process developer was desirable, there are few reasons that the process developer must own the cells. In general, rights holders to cell lines need to license them to make money, so it's unlikely the rights holders will hold up anyone trying to assist mutual customers with process development. However, I saw no conflicts in the pairing of cell lines and a process developer because the incentives are aligned: somebody, whether a customer the owner of the cells, will have to learn the unique processing needs of the cell lines. Overall, I gave this pairing a “maybe” – the benefits it offered were marginal but the risks were minimal.

### **C5,C2: Own cells and provide contract manufacturing**

This pairing describes a contract manufacturing organization (CMO) that owns a proprietary cell line that it attempts to steer its customers towards using it for their AAV therapies. This was the sole pairing that I saw no reason to recommend. The only benefits to this approach are that a CMO could (1) build expertise with the line (an easily imitated accomplishment) and (2) use the same sales channel to advertise the service (manufacturing) and the product (the cell line). The overlapping of sales channels is known as an “economy of scope” and while it can help a company save money, it is not a sustainable competitive advantage: if the strategy were remotely effective, other CMOs could imitate it and the competitive

edge would cease to exist. Furthermore, there's no reason to expect that combining cell rights and CMO under one roof is the most efficient way to carry out the transaction: the nature of cell lines as production substrates for multiple therapies implies that they must remain easily licensable to any company that wants to use them. Finally, integration of these concepts might pose a conflict of interest: a CMO should respect the individual needs of its customers and not attempt to steer them towards a relatively minor option in their manufacturing process just because it earns the CMO royalties.

#### **C4,C3: Develop reagents and provide contract process development assistance**

This pairing describes a firm that develops expression systems (without a cell line) for AAV production and provides process development assistance for licensees of the cell line. I recommended this pairing because a lack of licensable expression systems and expert process development assistance were two major reasons that small gene therapy companies cited in avoiding insect cells as a production substrate. The integration of these two concepts would create a sustainable competitive advantage, because expression systems and processing techniques are tailored one another: with knowledge of AAV manufacturing techniques, the combined firm could tailor reagents to suit the individual needs of its gene therapy customers to deliver the highest-possible quality AAV. Being an expert in one expression system would be a risky endeavor without owning the rights to the cell line: expression systems are tightly guarded intellectual properties, and contracts for their use may include confidentiality agreements that outside consultants (a standalone process developer) cannot experiment them without express permission. If the reagent owner maintained strict confidentiality, this could pose a “hold up” problem for

the process developer, so it is most efficient to combine process development expertise with the rights to the expression system in one firm. The conflicts of this pairing were minimal – drug development companies want help to available when using a new expression system.

### **C5,C3: Develop reagents and provide contract manufacturing**

This integrated concept is very similar to the (C5,C2) pairing in that a CMO owns the rights to an AAV expression system (sans cell line) rather than a just a cell line. As such, I also gave this pairing a “maybe”, but I had more confidence in it than the (C5,C2) pairing. I will discuss why I judge these pairings slightly differently in a dedicated subsection:

#### ***How are cell lines different than other parts of an AAV-BEVICS expression system?***

An AAV expression system generally consists of the cells (the production substrate), a transfer vector that introduces the recombinant AAV genome into the cells, and various other cell-type-specific reagents that assist the cells in transforming the AAV genome into functioning AAV particles (see Figure 5.3). An important thing to note is that most parts of the AAV expression system are specific to cell *types*, not individual (perhaps proprietary) cell *lines*. By cell type, I mean whole classes of immortalized cells used in bioprocessing; a human embryonic kidney (HEK) is an entirely different type of cell than an insect cell, but the distinction between cells descended from *Spodoptera frugiperda* and *Trichoplusia ni*, both insects of the order Lepidoptera, are less severe – some might consider them the same type of cell and the expression system might work well on both. The

distinctions between *Tnao-38* and *Hi-5*, two cell *lines* descended from the same species, are even smaller: they may have slightly different handling requirements and performance but are otherwise interchangeable.

While the choice of cell *type* can have major implications for the manufacturing prospects of an AAV therapy, the specific cell *line* a company uses within that type has less of an impact. As such, companies spend a great deal of effort, time, and money finding an expression system that suits their needs, but will often begin their development process with any standard cell line that fits the *type* stipulated by their choice expression system; these standard cell lines are often in the public domain, and do not carry royalties, though upfront fees from a cell bank may apply.

In general, whereas expression systems are highly differentiated, often highly customized, and are enabling technologies for producing new AAV products, cell lines are seen almost as commodities that should be predictable, minimally risky, and cheap. Indeed, the largest difference between *Tnao-38* and *Hi-5*, in the mind of a gene therapy producer, might be that one is free to use and the other carries a commitment to pay royalties (concerns about *Alphanodavirus* infection notwithstanding). Based on these differences, I felt that the non-cell-line parts of expression systems generally integrated better with services like contract process development and manufacturing because expertise in (and commitment to) working with these enabling technologies would create sustainable value to clients, while attempting to steer customers between less-differentiated cell lines might be seen as a mere “cash grab”.

## **C5,C4: Contract process development and manufacturing**

This pairing describes an emerging business model in the biopharmaceutical industry known as the contract development and manufacturing organization (CDMO). I was most confident about recommending this pairing because they are practically inseparable in the realm of advanced therapies. The largest hurdle for both contract manufacturing and contract process development is that it is difficult to ascend the “experience curve” in clinical grade manufacturing of experimental new therapies without continuous learning and improvement. By integrating these concepts into one firm, the regular manufacturing contracts provides the funding to hire experts in AAV process development and the opportunity to expose them to a wide variety of process design problems, while the accumulation of process development expertise helps the CMO maintain a competitive edge by cutting costs and turnaround times while improving product quality. Customers might benefit from a CDMO that produces small-to-medium-size batches of clinical-grade AAV, quickly and at a competitive cost, and feel secure knowing that the people who developed the high-performing AAV process will be available to design future commercial processes if and when the client’s manufacturing needs exceed the capacity of the CDMO.

As for whether combining these capabilities into a single firm is most efficient – process developers need to be employed by CMOs that cater to advanced new therapies (which lack mature, “industry-standard” production processes), because hiring them on a contract basis each time a new client comes in would likely be uneconomical; the real question is whether the process developers will be made available to clients as a contract development service, not whether the process developers will need to be internal to the company. The only conflict which might arise is

worry by clients that the CDMO performing contract development might transmit confidential information (even unintentionally) between clients, although the risks of information sharing can be mitigated by various policies and are balanced by clients' benefit from the sharing of best practices.

**Favorite pairings and three-unit concepts**

From the six pairings listed above, I selected three that appeared to have the highest potential for success: C2,C3; C3,C3; and C4,C5. I was also able to generate two business concepts that integrated two of these pairings, for a total of three units: C2,C3,C4 and C3,C4,C5. Figure 5.17 summarizes the integrated concepts which I recommend for further investigation.

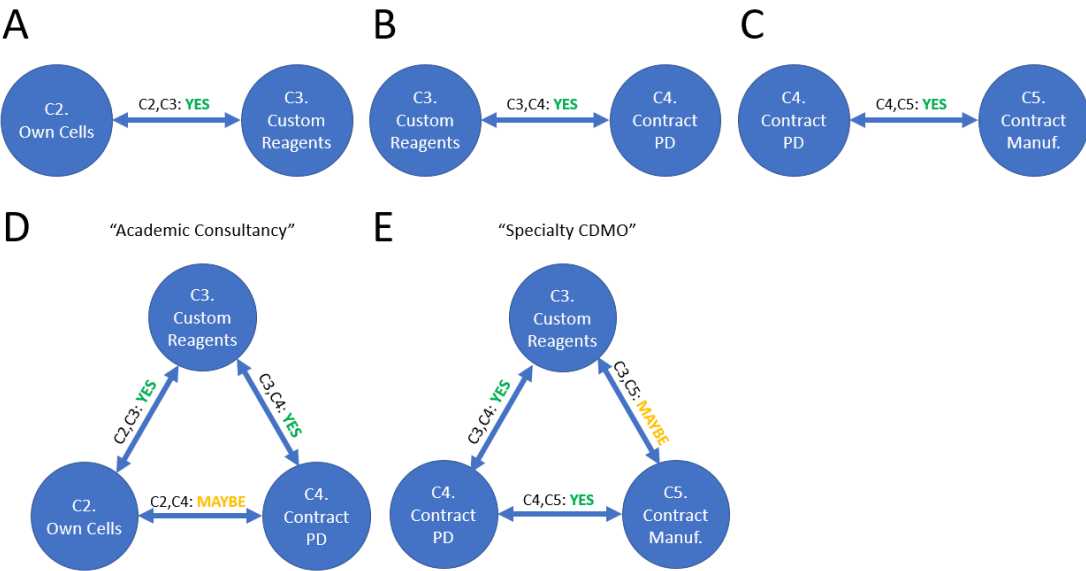


**Figure 5.17: Permutations of integrated businesses.**

The first three-unit concept (C2,C3,C4; "D" in Figure 5.17) describes a firm dedicated to inventing a AAV-BEVICS new expression system (incl. both cells and other reagents) and offering process development services to gene therapy

companies (esp. early-stage); I label this firm the “academic consultancy”. This firm could keep overhead low (perhaps operating out of a university) by keeping manufacturing capacity at a minimum, cover its operating expenses with consulting fees or research grants, and expect most of its long-term revenue to derive from royalties on licensed technologies. The second three-unit concept (C3,C4,C5; “E” in Figure 5.17) describes a firm that develops limited, but enabling, technologies in AAV expression and uses them to offer competitive contract manufacturing and process design services; I label this firm the “specialty CDMO” (contract development and manufacturing organization). This firm caters more to medium and large-scale gene therapy clients – it earns a sustainable margin from contract manufacturing, with a potential for licensing fees if clients successfully market therapies using reagents, process designs, or both. I estimated the success of the three-unit concepts by listing the three pairings that connected each of the underlying concepts. Each of these three-unit concepts had two connections that matched a recommended pairings (“Yes” in Figure 5.17), and one connection that matched a partially-recommended pairing (“Maybe” in Figure 5.17), so I estimated them to have similar potential at this level of detail.

### **5.3.5 Business concept validation & implementation**

A business model is only fully validated when it has been implemented. However, some of the business concepts I presented would require dozens of people, millions of dollars, and potentially years to implement (esp. the three-unit concepts in Figure 5.17) – it was not obvious where I should begin attempting to implement these ideas, or how to implement them.

A guiding principle was offered to me in the form of the “staircases to growth,” as summarized by an article from McKinsey & Co.<sup>159</sup> The basic premise is that companies should minimize the size each addition they make to their business model and attempt to have each increment towards the larger goal be profitable. An excellent description of the principle is offered in Beghail, et al.<sup>159</sup>, which summarizes the answers provided by managers of several growing companies when asked how they approached expanding their business model:

Their response to the question “How do I get from here to there” would typically be “not by big bold leaps but by a series of measured steps.” Each step makes money in its own right; each is a step up in that it adds new institutional skills that better prepare the company to open up – and take advantage of – opportunities; and each is a step roughly in the direction of a broader vision of where the company wishes to be.<sup>159</sup>

As such, I concluded the design process by looking for the “lowest-hanging fruit” in terms of ideas that had the highest likelihood of being implemented (and to make somebody some money), while providing as much validation potential for hypotheses about integrated concepts as possible; I would start by attempting to implement a single concept that I thought could be independently profitable, and then hypothetical work towards an integrated business if the initial idea was successful. My first consideration when selecting which concept I would begin with was understanding what barriers there were to starting the business. Next, I would consider whether the success or failure of that concept would impact the expected viability of the larger, integrated business. An example scenario: even if licensing the cell lines to outside process technology developers (Concept 1) was an easy

first step, it has minimal relevance to the integrated concepts because they would not rely on outside process technology developers.

I hypothesized that developing custom AAV-BEVICs plasmids (Concept 3) would be the most practical and informative concept to attempt to implement first. The original work of designing new insect cell-compatible AAV plasmids was highly scientific in nature, requiring people skilled in multiple aspects of recombinant AAV and BEVICS but minimal production capacity.<sup>139;143</sup> I felt that it would be easier to organize an academic research project than to assemble a team of bioprocess engineers with commercial experience, which would be necessary for several of the other concepts. Developing and building experiments with these custom plasmids would likely provide a sustainable competitive advantage in potential later activities like performing pilot studies with new insect cell lines or collaborating with an industry partners on process development.

Less preferable concepts to attempt implementing at first were out-licensing of insect cells to gene therapy clients (Concept 2) and assembling a contracting firm of process developers (Concept 4). As discussed previously, most gene therapy companies I interviewed would want to have a better developed “ecosystem” around insect-cell based AAV production before they started experimenting with insect cells. Assembling a firm of expert process developers would also be difficult for someone in my position: what would I be able to offer these highly sought-after employees that existing therapy companies or contract manufacturers could not?

Concepts which I felt were poor choices for implementing as a first step were licensing insect cells to process technology developers (Concept 1) and creating a contract manufacturing organization (Concept 5). I had trouble even finding a company that fit the description of “process technology developer for insect-

cell-based AAV manufacturing”; and I was deterred by the high startup-costs and expert hiring needed to establish a commercial AAV manufacturing facility.

I concluded that starting with a research project to create new insect cell-compatible AAV plasmids could hypothetically lead to either of the larger integrated business concepts in Figure 5.17:

- Towards “academic consultancy” (“D” in Figure 5.17): Upon establishing our basic ability to design new AAV-BEVICS reagents (validate Concept 3), my firm could explore the potential of new cells to improve performance (implement Concept 2), and then work towards designing a clinical-grade AAV process (implement Concept 4) in collaboration with growing gene therapy companies. This work could potentially all occur within an academic setting.
- Towards “specialty CDMO” (“E” in Figure 5.17): Upon establishing our basic ability to design new AAV-BEVICS reagents (validate Concept 3), my firm could immediately look for clients that want to co-develop a basic manufacturing process for a new AAV therapy (implement Concept 4), then propose those clients outsource their pre-clinical (later clinical) manufacturing needs to our company (implement Concept 5). My firm would spin out into a private company relatively early.

In the final months of this project, I helped coordinate a research proposal in conjunction with the owners of the cell line, a consortium of bioprocess developers, and a commercial gene therapy manufacturers. The proposal would have validated Concept 3 (custom AAV-BEVICS plasmids) and began to establish a center of expertise in insect cell-based AAV manufacturers central to some of the other business concepts. Ultimately, the proposal was not funded, highlighting the overall difficulty of completing efforts in this space.

## 5.4 Discussion

Gene therapy is maturing to the point where recombinant viruses which introduce foreign DNA into a patient's cells have been approved for sale in Europe, with over one hundred clinical trials underway in the United States. A great deal of work over the last decade has resolved many of the scientific and medical uncertainties associated with designing and administering gene therapies, but the technologies, infrastructure, and collective expertise around manufacturing clinical-grade live viruses poses major obstacles to gene therapy becoming economically feasible for any but the most severe and untreated hereditary diseases. The nominal purpose of this project was to determine if money could be made from using a set of newly-isolated insect cell lines to produce recombinant AAV for human gene therapy; however, my efforts here more importantly served as a case study of why the constraints – of time, of money, and of scope – inherent high-risk drug development projects demand a more holistic approach to commercializing innovations. I found that customers across the gene therapy industry, from university research staff to CEOs, placed a greater importance on the network of complimentary products and services that could associate with my technology than the value propositions of the technology itself.

### Complimentary products

I knew from the literature that insect cells worked in tandem with a specialized expression system based around baculovirus infection. However, I did not anticipate how much of a challenge it is design, or otherwise obtain, baculovirus plasmids that produce high-quality AAV. Early efforts into making AAV in insects focused

around a single serotype – AAV2 – not because it was the most common in clinical applications but because it was the only one that produced nearly-functional virus in insect cells.<sup>139</sup> Years after AAV2 was first produced in insect cells, researchers were able to produce other serotypes, but only by making hybrid serotypes that contained regions of the AAV2 genome.<sup>143</sup> As of today, baculovirus plasmids exist for many, but not all, serotypes of AAV; these plasmids are covered under broad patents that protect not only the primary sequence of the DNA, but the logic of how different alterations were made to make the plasmid produce functional virus.

Some gene therapy companies are willing to adopt AAV manufacturing processes around insect cells, but they have not been able to access plasmids for the serotypes which they use in their therapies. It can take years of research and highly specialized expertise to develop these plasmids, and some broad patents on design principles for the plasmids are owned by therapy companies who do not license them to competitors. This led me to conclude that realizing the full potential of the market for proprietary insect cell lines would likely require that plasmids for all major serotypes of AAV be made available for license on reasonable terms; furthermore, those plasmids would likely be far more valuable to clients than the improved cell lines themselves.

Because insect cell-compatible plasmids posed such an urgent need to some customers, yet would not require a large capital investment to create, I hypothesized that a project around designing these plasmids would be the best starting point for my goal of implementing and validating one of the business concepts I explored. I was successful in finding a medium-size gene therapy company who was open to the idea of funding such a project; the proposal itself was not successful, though it is unclear whether this is because the value propositions of an

insect cell-compatible AAV plasmid as a product are flawed, or if the sponsoring company was not confident that the team behind the proposal would be able to provide the necessary services to assist in implementing the plasmids.

## **Complementary services**

Businesses which provide manufacturing and design services form a critical bridge between inexperienced therapy companies and the new technology products that could help them meet deadlines and achieve manufacturing cost reductions. My realization of the need for small- and medium-size gene therapy companies to have access to contract manufacturing and consultation on process design before adopting a new technology was the primary motivator for me to understand how several of my business concepts might be integrated into a firm that both invents technology and profitably drives its adoption. In Figure 5.17, I highlight two integrated businesses that can play an active role in ensuring that AAV therapy companies are building manufacturability into their therapies as those companies advance towards regulatory approval and demand a growing amount of drug material.

One, the “academic consultancy” might be considered the lower-risk option of the two; it could be an extension of the well-established model of the university vector core facility which uses research grants as a stable source of funding to build a “center of excellence”. By remaining connected to a university, the academic consultancy solves two key problems faced by firms dedicated to innovation in bioprocessing: accessing skilled employees and allowing them to master a bioprocess – free from the turbulence of the biopharmaceutical industry that frequently requires process developers to be reassigned to new projects. I see an archetype for how this firm might be started in one group I interviewed: a small, but prestigious, vector

core facility which has mastered the traditional (transfection-based) methods of AAV production; this firm could establish the highest standards of AAV quality from the beginning, and gradually assemble expertise and intellectual property in larger-scale manufacture per client needs. I hypothesized that keeping the firm situated in a university would afford the team greater proximity to sources of process innovation emerging from academic research labs (e.g., engineered cell lines, new expression systems, etc.) to maximize the performance of the firm's process designs; this emphasis on technology licensing, rather than providing services, would orient this firm's value propositions towards increased manufacturability of AAV therapies at later stages of development and market launch.

The other integrated concept, the “specialty contract development and manufacturing organization (CDMO)”, might start out similarly to the academic consultancy (perhaps also a spin-out from a vector core facility), but would prioritize its ability to provide services to gene therapy clients – ranging from plasmid design projects to manufacturing services to comparability studies for process changes. Interviews I conducted with several gene therapy companies suggested that few existing CMOs can offer insect cell-based AAV manufacturing services of sufficient quality for clinical trials, perhaps due to a simple lack of experience. I hypothesized that starting with a project to design insect cell-compatible AAV plasmids would provide critical early learning opportunities for the firm and help build relationships with therapy companies who might award manufacturing contracts once the credibility of the firm is established. A track record of collaborations with gene therapy companies with escalating levels of responsibility and involvement with the drug development process might help attract the private investors necessary to purchase clinical-grade manufacturing capacity. By offering convenience and speed in the form of personalized manufacturing services and outsourced baculovirus plasmid

design, the specialty CDMO could solve some of the short-term concerns of small, but growing, gene therapy companies, rather than crafting nearly all of its value propositions around promises of future increases in manufacturability; I will discuss some potential challenges I see to the value proposition of “manufacturability” below.

### **Alternative view: a case against manufacturability**

The philosophy of “fail early” practiced by serial entrepreneurs and embraced by large pharmaceutical corporations, which states that a project should immediately confront the largest problem it might face over its lifetime (rather than addressing short-term concerns as they come), did not appear to be a guiding principle for the therapy startups I spoke with. In one interview I conducted, this attitude manifested as an open admission from an executive at a small gene therapy company that questions about manufacturability – which might devastate the profitability of the drug if left unanswered – were outside the scope of their business model. The executive I spoke with asserted that large pharmaceutical companies will “buy manufacturability” after acquiring the rights to the drug in later stages of the development; my suggestion that the current (and perhaps future) industry landscape (i.e., with its lack of contract process developers and technology providers) would make “buying” an improved process difficult did not seem to bother the interviewee.

One could argue that indifference about future manufacturability and profitability is evidence of mismanagement, or at least is non-optimal for the value of the drug or startup; indeed, a study which modeled how the timing of “process changes” (such as switching to a better-scaling bioreactor) impacts the value of

a drug product found that the net present value of an advanced therapy over its life-cycle are maximized when this type of process change is performed as early as possible.<sup>160</sup> This valuation was primarily based on discounted cash flows (DCF), which predict the costs and revenues over the life-time of the drug and adjust their impact on the company's value based on when they occur. However, this same study found that when probabilities of certain risks – such as changes in selling price, or failures in clinical trials – were incorporated into a Monte Carlo simulation of the business, waiting until *after* regulatory approval and full market launch to switch to a more cost-effective manufacturing process could yield a higher expected (i.e., average) present value, albeit with more variability.<sup>160</sup>

I might hypothesize that a gene therapy startup's decision to deemphasize the long-term concerns of manufacturing cost is not only understandable, but optimal, depending on how the company is valued, or what the goals and values of its managers are. One financial analyst in the pharmaceutical industry remarked that “We give anything prior to Phase II [clinical trials] a value of zero,”<sup>161</sup> indicating the extent to which the concerns between large pharmaceutical companies, who are responsible for the profitability of drug sales (and therefore manufacturability), and biotechnology start-ups, whose founders are often salaried scientist who exit upon acquisition, are disconnected. The financial analyst mentioned earlier was valuing companies using a discounted cash flow method<sup>161</sup> – same as that which recommended companies switch to cost-effective manufacturing method early.<sup>160</sup>

Valuation models which consider a wider variety of probabilistic paths to company failure (e.g., running out of cash or receiving negative results from a clinical trial) or success (e.g., negotiating an acquisition with an up-front payment for the founder regardless of future sales) than DCF, such as expanded forms of

Monte Carlo simulation<sup>160</sup> or “real options” valuation techniques,<sup>161</sup> might make a stronger case *against* a biotechnology startup investing in manufacturability than for it. Evidence in support of this hypothesis would significantly challenge the near-term prospects of the “academic consultancy” and (to a lesser extent) “specialty CDMO” business models presented here, which share a general theme of preparing gene therapies for manufacturability as they grow, not after they are approved; if companies do indeed wait until after commercial launch of the first wave of gene therapies to seek out assistance on process development, it is unclear to me what firms will be there to offer it.

## Conclusion

As viral gene therapies continue to work towards full market approval in the United States, I will be watching closely how network of businesses and academic research groups around AAV develops. A key question that stakeholders across the AAV community need to address is how to approach innovation in manufacturing: the worst case scenario would have every firm making the same gambit – to wait until post market-approval to attempt to “buy manufacturability” – only to find that no company has built such expertise and made it available for sale. This hypothetical scenario is mitigated by the fact that several gene therapy companies are investing in cost-effective manufacturing process, which they use internally, but do not out-license; should a drug emerge which shows the potential to treat a burdensome disease for a large patient population, but only if it can access those manufacturing processes, I would hope and expect that a business agreement can be met to share the process knowledge.

In contrast to this “wait-and-see” approach, I have proposed a path to building a CDMO that could profitably assist in bioprocess innovation for any company at any stage of growth. I hypothesized that the first steps towards building such the CDMO would have a group of talented scientists and bioprocessing developers, who may or may not have direct experience with AAV, simultaneously building expertise and valuable intellectual property by designing an AAV expression system of their very own – at the center of which is a new insect cell-compatible plasmid for a previously incompatible AAV serotype. My attempt at implementing the concept of designing new plasmids was not successful, but it is possible that the sponsoring company will find a CDMO (or proto-CDMO) to perform the work. A certain existing CDMO, co-founded by a former research professor who made important contributions to insect cell-based AAV manufacturing, advertises many of the same capabilities and value propositions as the firm I proposed; it would be a bittersweet validation of my efforts in this project to see this CDMO awarded a contract from the sponsoring company similar to the research proposal which I helped initiate.

In closing, this project provided me with an opportunity to build and apply a broad understanding of a biomolecular engineering problem unlike any that has come before it. This problem can be measured in dollars: a treatment of Glybera requires  $7.5 \times 10^{13}$  AAV particles (each containing 7 million Daltons worth of recombinant protein and DNA) and costs \$1 million, so the first commercial AAV product had price of roughly \$1.1 billion per gram; clinical AAV is one of the most expensive materials known to man, and manufacturing costs are expected to be the major component of this price.<sup>36</sup> This problem can be measured in lives: as of May 2016, only one patient had been treated with Glybera<sup>133</sup>; roughly 300 people in the United States have the condition which Glybera treats; but about 20,000

people in the United States are living with hemophilia, a disease for which no company has managed to commercialize a gene therapy. While the solution to the high cost and low availability of gene therapy is likely a long ways away, the work discussed in this chapter represents progress, if infinitesimal, towards defining the path that will arrive at it.

## CHAPTER 6

### CONCLUSION

I began my doctoral studies with the singular goal of bringing the future of biotechnology, as it is captured in our imaginations, closer; I quickly found that some of the greatest challenges in applying biological discoveries is in building, modeling, and executing within the systems that spring up around biology.

The preceding chapters capture my efforts in analyzing systems in applied bioscience in two distinct domains: the development of multiscale models of angiogenesis and in the manufacturing of biopharmaceuticals:

- In Chapter 2, I provided an overview of biological pattern formation starting with the pioneering efforts of Alan Turing and following through to the ongoing areas of active research; this history provides a context for my subsequent work in modeling tip cell selection.
- In Chapter 3, I analyzed the major hypotheses in tip cell selection that have received the most experimental and computational study to date, and explained the value, limitations, and opportunities of further research for these hypotheses.
- In Chapter 4, I presented two hypotheses of my own for how tip cells might increase their spacing during tip cell selection; such mechanisms might provide greater accordance with experiments showing that tip cell fractions can be very different from 50% (as predicted by lateral inhibition) in physiological and pathological contexts, and this work could assist in the development of future experiments and multiscale models of angiogenesis.
- In Chapter 5, I recount my efforts to develop and validate business concepts

around the manufacturing of adeno-associated virus for human gene therapy using the baculovirus-insect cell expression vector system with a novel insect cell line.

As captured in these chapters, I made several important contributions that span from the scientific, to the pedagogical, to the commercial:

- I used linear stability analysis and numerical simulation to provide strong evidence that mechanisms other than Delta-Notch signaling are likely responsible for the initial pattern of vascular growth from sprouting angiogenesis.
- I proposed and simulated two new hypotheses for how multiple signaling processes – such as VEGF reaction-diffusion or dual juxtacrine signaling pathways – could control the spacing of tip cells.
- As an inaugural recipient of a fellowship aimed at training doctoral students for the future of university research – which might increasingly rely on industrial collaboration in light of declining public funding – I provided a test case for students aiming to commercialize in the life sciences.
- I shaped and executed the commercialization strategy for a key university technology, with implications for how this asset will (or will not) enter the market for the manufacturing of biopharmaceuticals.

Future work around multiscale modeling of angiogenesis will likely aim to predict growth of blood vessels in tumors and wound healing or understand how artificial devices (or implants) will be vascularized. Eventually, systems bioengineers may be able to employ parametric design, as is used in architecture (see Figure 6.1), to routinely predict growth of vessels or other organs, where each cellular

## Increasing Scale

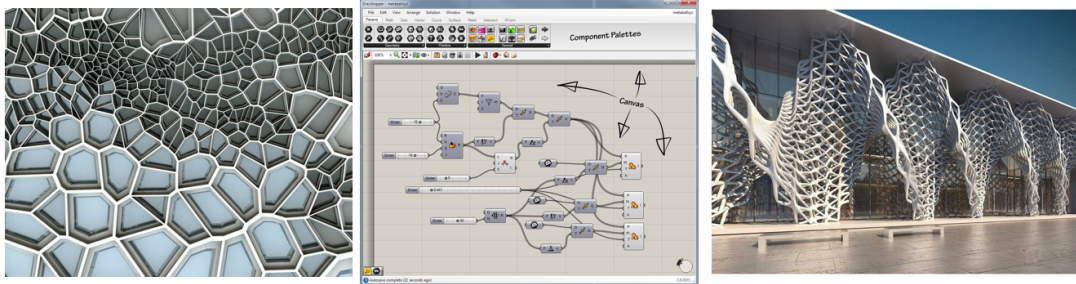


**Figure 6.1: Analogs to multiscale modeling in design of architecture.** *Left*, an example of a pattern that can be reused and included as a design module and controlled with parameters. *Middle*, a software interface for parametric design – modules, each capturing a patterning mechanism or other design features, are connected together to form a blueprint for procedural generation. *Right*, a building resulting from parametric design. Multiscale simulations of the growth of the vasculature or other physiological features (analogous to the building) could rely on connecting modules representing cellular behaviors and transport phenomena as a form of parametric design.

behavior, transport process, or pattern formation mechanism is a distinct module. The blueprint of vascularized tissue could be procedurally generated using modules based on previously studied and modeled mechanisms, and parameters could be tuned by training on live experiments. I recommend that future researchers in this field focus on collaboratively developing reusable tools alongside testing hypotheses and building models; it would be ideal if computational and mathematical models were built as inter-operable modules within a standardized simulation environment to enable a discipline of biological architecture.

The future of manufacturing of adeno-associate virus and other advanced therapies is evolving quickly. My work has led me to believe that introducing a new cell line into a manufacturing platform – even if minimally different from existing cell lines – is an uphill battle. Switches like these are typically only feasible in the early stages of development – and in the early stages, it is imperative to reduce

risk wherever possible; in the case of swapping cell lines, the risk of regulatory or other complications outweighs all but the most drastic improvements in safety or productivity. However, the emergence and sustained success of contract development and manufacturing organizations (CDMO) is a promising sign that centers of expertise that can potentially optimize therapies and their manufacturing platforms in tandem are emerging, even in the turbulent world of biopharmaceuticals, where teams are often shuffled and assets passed between companies.

In particular, it is my hope that a future researcher, whether me or another, can truly unite these two thrusts, applying an entrepreneurial mindset to the issue of integrating the exploding volume of data and proposed mechanism that exists today in angiogenesis and beyond. Mutliscale modeling will require both new technology and collaboration among human beings; the case must be made why collaboration within a common simulation environment adds incremental value to all involved, or such initiatives not achieve widespread success.

An important question raised to me throughout my studies was the extent to which my work was solving life's fundamental mysteries versus advancing a practical interest with little or no discovery involved. With industrial collaboration becoming increasingly present at research universities, these kinds of questions will become increasingly relevant. I hope this work has demonstrated that solving applied problems within complex biological systems is a science unto itself.

## APPENDIX A

### CODE SAMPLES

#### A.1 Parameter setup

```
function [Sys, params] = defineParams(Sys)

switch Sys.kinetics

case 'aCL'
% Lateral Inhibition
Sys.speclist = strsplit('R D');
Sys.nspec = length(Sys.speclist);

% Parameters using fo LR lateral inhibition
%{
params.tau = 1;
params.kappaR = 6;%10^0.8189;
params.kappaD = 0.25;%10^-0.8;
params.KV = 1;
params.VH = 1;
params.nR = 3;
params.nD = 3;
Sys.nspec = 2;
%}

% Parameters used in paper for Fig. 3

params.tau = 1;
```

```

params.kappaR = 2.5;%10^0.8189;
params.kappaD = 1/6;%10^-0.8;
params.KV = 1;
params.VH = 1;
params.nR = 2;
params.nD = 2;
Sys.nspec = 2;

case 'aDF'
% Lateral induction
Sys.speclist = strsplit('R D');
Sys.nspec = length(Sys.speclist);

params.ar = 0.325;
params.KV = 1;
params.VH = 1;

params.a = 0.2;
params.kappaD1 = 1/6;%10^-0.8;
params.nD1 = 2;
params.kappaD = 3/5;
params.nD = 2;
Sys.nspec = 2;

case 'aCLDE'
% Diffusion & Endocytosis

```

```

Sys.speclist = strsplit('V I');
Sys.nspec = length(Sys.speclist);

% -- Geometric parameters --
% length scale of cell
params.lcell = sqrt(0.4*10^-5); % cm (20 microns on each side)

% height of compartment
params.h0 = 0.001; % cm (10 microns)

% -- VEGF Fluxes --
% Degradation rate of internal VEGF
params.kdeg = 5*10^-2; % s^-1 (MacGabhann 2013)

params.BLF = 3.471*10^-18; % mol/(cm^2 s) % BaseLine Flux

% a - Basal internalization flux of VEGF
params.a = params.BLF*10; % mol/cm^2/s

% b - Increase in internalization flux of VEGF
params.b = params.BLF*20; % mol/cm^2/s

% g - Homogeneous production flux of VEGF
params.g = params.BLF*13.1*1.01; % mol/cm^2/s
%Critical point is at 13.1

```

```

% -- GRN Network elements --
% KI - 1/2 max level for positive feedback by internal VEGF Much
params.KI = 17*params.BLF/params.kdeg; % mol/cm^2

% KV - 1/2 max level for internalization of soluble VEGF
params.KV = 150*10^-15; % mol/cm^3 (150 pM)

% nI - Hill Coefficient for positive feedback
% Arbitrary.
params.nI = 4;

% -- Transport parameters --
% Diffusivity of VEGF (Rough average - VEGF164 is 1.04)
params.Dv = 1*1.04*10^-6; % cm^2 s^-1

% -- Lumped parameters --
params.alph = params.a/(params.kdeg*params.KI);% Basal consumption
params.beta = params.b/(params.kdeg*params.KI);% Bonus consumption
params.gamm = params.KI/(params.KV*params.h0); % Specific to 2.5D
params.rho = params.g/(params.kdeg*params.KI); % Production rate
params.DA = params.Dv/(params.lcell^2*params.kdeg); % Damkohler

case 'aDJ'
% Double Juxtacrine
Sys.speclist = strsplit('A B');
Sys.nspec = length(Sys.speclist);
qtarget = -0.25;

```

```

%qtargget = -1*rand(1);
params.qtargget = qtargget;
MLE = 0.1;

%Assuming tau = 1, IC at 1/2 max for all functions

params.beta = 1;

params.nP = 16;
params.nA = -params.nP/(2*params.beta*qtargget);
params.nB = 32*(MLE+1)^2*params.nA/params.nP^2; %Does not work for beta
    not = 1!!

params.KA = 1/2;
params.KP = 1/2;
params.KB = (1 + params.beta)/2;
Sys.nspec = 2;

end

```

## A.2 Kinetics

### A.2.1 Lateral inhibition

```

function [conc, spec] = kinetics_aCL(target,input,params)
%Definitions for Classical GRN kinetics
% target: identifies the species and equation (e.g. 'R_SS' or 'D_DT')

```

```

% input: struct containing the necessary input (e.g., VEGF conc)
% output: struct containing the resultant output
%     output.spec = string containing the species returns
%     output.conc = numerical answer for species conc

tau = params.tau;
kappaR = params.kappaR;
kappaD = params.kappaD;
KV = params.KV;
VH = params.VH;
nR = params.nR;
nD = params.nD;

switch target
case 'R_SS'
DN = input.DN;
R_SS = 1./(1+(kappaR*DN).^nR);

case 'D_SS'
RA = input.RA;
D_SS = f_hill_a(1,kappaD,nD,RA);

case 'RA_SS'
R = input.R;
V = input.V;
RA_SS = R.*V./(KV+V);

case 'R_DT'
R = input.R;

```

```

DN = input.DN;
R_DT = 1./(1+(kappaR*DN).^nR)-R;

case 'D_DT'
RA = input.RA;
D = input.D;
D_DT = tau*(f_hill_a(1,kappaD,nD,RA)-D);

otherwise
error('Kinetics target not found');
end

spec = target;
conc = eval(target);
end

```

## A.2.2 Lateral induction

```

function [conc, spec] = kinetics_aCL(target,input,params)
%Definitions for Classical GRN kinetics
% target: identifies the species and equation (e.g. 'R_SS' or 'D_DT')
% input: struct containing the necessary input (e.g., VEGF conc)
% output: struct containing the resultant output
%     output.spec = string containing the species returns
%     output.conc = numerical answer for species conc

ar = params.ar;
KV = params.KV;
VH = params.VH;

```

```

a = params.a;
kappaD1 = params.kappaD1;
nD1 = params.nD1;
kappaD = params.kappaD;
nD = params.nD;

switch target

case 'D_SS'
DN = input.DN;
RA = input.RA;
D_SS = a*f_hill_a(1,kappaD1,nD1,RA) + f_hill_a(1,kappaD,nD,DN);

case 'R_SS'
ar = input.ar;
R_SS = ar;

case 'RA_SS'
R = input.R;
V = input.V;
RA_SS = R.*V./(KV+V);

case 'D_DT'
RA = input.RA;
D = input.D;
DN = input.DN;
D_DT = a*f_hill_a(1,kappaD1,nD1,RA)+f_hill_a(1,kappaD,nD,DN)-D;

case 'R_DT'

```

```

R = input.R;
R_DT = ar-R;

otherwise
error('Kinetics target not found');
end

spec = target;
conc = eval(target);
end

```

### A.2.3 Double-juxtacrine

```

function [conc, spec] = kinetics_aDJ(target,input,params)
%Definitions for Classical GRN kinetics
% target: identifies the species and equation (e.g. 'R_SS' or 'D_DT')
% input: struct containing the necessary input (e.g., VEGF conc)
% output: struct containing the resultant output
%     output.spec = string containing the species returns
%     output.conc = numerical answer for species conc

beta = params.beta;
nP = params.nP;
nA = params.nA;
nB = params.nB;
KA = params.KA;
KP = params.KP;
KB = params.KB;

```

```

switch target
case 'A_SS'
BN = input.BN;
B = input.B;
A_SS = f_hill_r(1,KP,nP,B)+f_hill_r(beta,KA,nA,BN);

case 'B_SS'
AN = input.AN;
B_SS = f_hill_a(1,KB,nB,AN);

case 'A_DT'
BN = input.BN;
B = input.B;
A = input.A;
A_DT = f_hill_r(1,KP,nP,B)+f_hill_r(beta,KA,nA,BN)-A;

case 'B_DT'
AN = input.AN;
B = input.B;
B_DT = f_hill_a(1,KB,nB,AN)-B;

otherwise
error('Kinetics target not found');
end

spec = target;
conc = eval(target);
end

```

## A.2.4 Diffusion & endocytosis

```
function [conc, spec] = kinetics_aCLDE(target,input,params)
%Definitions for Classical GRN kinetics
% target: identifies the species and equation (e.g. 'R_SS' or 'D_DT')
% input: struct containing the necessary input (e.g., VEGF conc)
% output: struct containing the resultant output
%     output.spec = string containing the species returns
%     output.conc = numerical answer for species conc

% NON-DIMENSIONAL ONLY
% Parameter definitions
alph = params.alph;
beta = params.beta;
gamm = params.gamm;
rho = params.rho;
DA = params.DA;
nI = params.nI;

switch target
case 'V_f_I_g' %Find V given I for GRNs
I = input.I;
fI = alph+beta*(I).^nI./(1+(I).^nI);
V_f_I_g = I./(fI-I);

case 'V_f_I_t' %Find V given I for Transport
I = input.I;
rho_in = input.rho_in;
```

```

fI = alph+beta*(I).^nI./(1+(I).^nI);
V_f_I_t = rho./(fI-rho);

case 'V_f_I_gnb' % 'No beta' - response curve in absense of PF
I = input.I;
fI = alph+0*(I).^nI./(1+(I).^nI);
V_f_I_gnb = I./(fI-I);

case 'V_f_I_gfb' % 'Full beta' - response curve with full throughput
I = input.I;
I_MAX = 1.611;
fI = alph+beta*(I_MAX).^nI./(1+(I_MAX).^nI);
V_f_I_gfb = I./(fI-I);

case 'V_DT'
VN = input.VN;
V = input.V;
I = input.I;
rho_in = input.rho_in;
V_DT = gamm*(rho_in-(alph+f_hill_a(beta,1,nI,I)).*V./(1+V))+DA*(VN-V);

case 'I_DT'
V = input.V;
I = input.I;
I_DT = (alph+f_hill_a(beta,1,nI,I)).*V./(1+V)-I;

otherwise
error('Kinetics target not found');
end

```

```
spec = target;
conc = eval(target);
end
```

## A.3 Initial conditions

### A.3.1 Lateral inhibition

```
function inits = homogIC_aCL(Sys,params,inits)
%Classical GRN initional condition generator

tau = params.tau;
kappaR = params.kappaR;
kappaD = params.kappaD;
KV = params.KV;
VH = params.VH;
nR = params.nR;
nD = params.nD;

line_red = [237/255 27/255 35/255];
line_blue = [0 173/255 239/255];

figures = false;
stability_fig = false;

%% Analysis
```

```

% Goals:

% 1. Produce a steady-state relation (pretty!)
% 2. Calculate the uniform steady-state
% 3. Produce a stability profile (pretty!)

%1. Produce a steady-state relation (pretty!)

% The paper assumes this is with a two-cell model
V_vec = [0.1, 1, 10];
if figures
D1_1 = getD1(V_vec(1));
D1_2 = getD1(V_vec(2));
D1_3 = getD1(V_vec(3));

figure('units','inches','position',[5 5 1.675 1.675])% Half-column width
plot(D0,D1_1,'Color',line_blue,'LineWidth',1)
hold on
plot(D0,D1_2,'--','Color',line_blue,'LineWidth',1) % Blue
plot(D0,D1_3,'-.','Color',line_blue,'LineWidth',1)
plot([0 1],[0 1],'k')
legend('\it{V} = 0.1','1','10')
legend('boxoff')
set(gca,'FontSize',8)
%h1 = xlabel('\bf{\it{D}_{0}}}','FontSize',8);
%h2 = ylabel('\bf{\it{D}_{1}}}','FontSize',8);
h1 = xlabel('\bf{\it{D0 (input)}}}','FontSize',8);
h2 = ylabel('\bf{\it{D1 (output)}}}','FontSize',8);
end

```

```

function D1 = getD1(V_in)

% Two-cell model

nullcl_num = 1000;

D0 = linspace(0,1,nullcl_num);

R2 = kinetics_aCL('R_SS',struct('DN',D0),params);

RA2 = kinetics_aCL('RA_SS',struct('R',R2,'V',V_in),params);

D2 = kinetics_aCL('D_SS',struct('RA',RA2),params);

R1 = kinetics_aCL('R_SS',struct('DN',D2),params);

RA1 = kinetics_aCL('RA_SS',struct('R',R1,'V',V_in),params);

D1 = kinetics_aCL('D_SS',struct('RA',RA1),params);

end

%

-----

% 1.B Produces true nullclines of R & D

if figures

% First, calculate the D which produces steady-state R (this is
    independent
% of V)

R_points = 1000;

R_steady = linspace(0,1,R_points);

D_required = (1./R_steady-1).^ (1/nR)/kappaR;

D_points = 1000;

D_steady = linspace(0,1,D_points);

R_required_2 = (-D_steady*kappaD^nD./(D_steady-1)).^(1/nD)/(V_vec(2)/(KV
    +V_vec(2)));

```

```

figure('units','inches','position',[5 5 1.675 1.675])% Half-column width
plot(R_steady,D_required,'Color',line_red,'LineWidth',1)
hold on
plot(R_required_2,D_steady,'--','Color',line_blue,'LineWidth',1)
%plot([0 1],[0 1],'k')
%legend('\it{V} = 0.1','1','10')
%legend('boxoff')
set(gca,'FontSize',8)
%h1 = xlabel('\bf{\it{D}_{0}}','FontSize',8);
%h2 = ylabel('\bf{\it{D}_{1}}','FontSize',8);
xlim([0 1]);
ylim([0 1]);
h1 = xlabel('R','FontSize',8);
h2 = ylabel('D','FontSize',8);
end
%
```

---

```

% 1.C Produces true nullclines of R & D (attempt 2)
```

```

if figures
```

```

% First, calculate R_int_1 imposed by D_ext_1
```

```

D_ext_1_p = 1000;
```

```

D_ext_1 = linspace(0,1,D_ext_1_p);
```

```

R_int_1 = kinetics_aCL('R_SS',struct('DN',D_ext_1),params);
```

```

% Second, calculate D_ext_2 impost by a two-cell iteration of R_int_2
%
R_int_2_p = 1000;
R_int_2 = linspace(0,1,R_int_2_p);

D_ext_2_1 = getDext(V_vec(1),R_int_2);
D_ext_2_2 = getDext(V_vec(2),R_int_2);
D_ext_2_3 = getDext(V_vec(3),R_int_2);

% Plot each nullcline, with D_ext on the X axis, and R_int on Y axis

figure('units','inches','position',[5 5 1.675 1.675])% Half-column width
    (quarter page)
plot(D_ext_1,R_int_1,'Color',line_red,'LineWidth',1)
hold on
plot(D_ext_2_1,R_int_2,'Color',line_blue,'LineWidth',1)
plot(D_ext_2_2,R_int_2,'--','Color',line_blue,'LineWidth',1)
plot(D_ext_2_3,R_int_2,'-.','Color',line_blue,'LineWidth',1)

%plot([0 1],[0 1],'k')
%legend('\it{V} = 0.1','1','10')
%legend('boxoff')
set(gca,'FontSize',8)
%h1 = xlabel('\bf{\it{D}_{0}}','FontSize',8);
%h2 = ylabel('\bf{\it{D}_{1}}','FontSize',8);
xlim([0 1]);
ylim([0 1]);

```

```

h1 = xlabel('D_{ext}','FontSize',8);
h2 = ylabel('R_{int}','FontSize',8);

end

function D_ext = getDext(V_in,R_int)
RA_int = kinetics_aCL('RA_SS',struct('R',R_int,'V',V_in),params);
D_int = kinetics_aCL('D_SS',struct('RA',RA_int),params);
R_ext = kinetics_aCL('R_SS',struct('DN',D_int),params);
RA_ext = kinetics_aCL('RA_SS',struct('R',R_ext,'V',V_in),params);
D_ext = kinetics_aCL('D_SS',struct('RA',RA_ext),params);
end
%
-----

% 2. Bifurcation diagram with R as a function of V

if figures

% First, chose a vector of V concentratitons (not too large)
V_vec2_p = 1000;
V_min = 0.1;
V_max = 10;
V_vec2 = 10.^(linspace(log10(V_min),log10(V_max),V_vec2_p));

% Next, create an empty matrix for storing steady-states
ss_mat = zeros(0,5);

% Column 1 - V_index, Column 2 - V, Column 3 - R, Column 4 - RA, Column

```

```

% 5 - D

% For each element in V_vec2, calculate all possible steady-states using
    a
% two cell model.
% Will probably have to use splines and fnzero
for j = 1:V_vec2_p
ss_mat = [ss_mat;getStates(j,V_vec2(j))]; %#ok<AGROW>
end

% Split the results into 5 line segments:
%1. Homogeneous low RA activation
%2. Patterning - Tip, Homog, Stalk
%3. Homogeneous high RA activation

%1. Homogeneous low RA activation
%Start with the first index and count up until an index has >1 SS
seg_ind = 1; % segmentation index
segment1 = zeros(0,2); % [V RA]
in_seg1 = true;

while in_seg1
if sum(ss_mat(:,1) == seg_ind) == 1;
segment1 = [segment1; ss_mat(ss_mat(:,1)==seg_ind,[2 4])];
seg_ind = seg_ind + 1;
else
in_seg1 = false;

```

```

end

end

%2. Patterning
segment2 = zeros(0,4);%[V RT RH RS]
in_seg2 = true;

while in_seg2
if sum(ss_mat(:,1) == seg_ind) == 3;
ind_mat = ss_mat(ss_mat(:,1) == seg_ind,:);
segment2 = [segment2; [...
ind_mat(1,2) ... %V
max(ind_mat(:,4)) ... %RT
median(ind_mat(:,4)) ... %RH
min(ind_mat(:,4)) ... %RS
]];

clear ind_mat
seg_ind = seg_ind + 1;
else
in_seg2 = false;
end
end

%3. Homogeneous high RA activation
segment3 = zeros(0,2); % [V R]
in_seg3 = true;

while in_seg3

```

```

if sum(ss_mat(:,1) == seg_ind) == 1;
segment3 = [segment3; ss_mat(ss_mat(:,1)==seg_ind,[2 4])];
seg_ind = seg_ind + 1;
else
in_seg3 = false;
end
end

%{
% Plot each segment - RA

figure('units','inches','position',[5 5 1.675 1.675])% Half-column width
semilogx(segment1(:,1),segment1(:,2),'-', 'Color','k');

hold on
tip_line = semilogx(segment2(:,1),segment2(:,2),'-', 'Color',line_red);
semilogx(segment2(:,1),segment2(:,3),'--', 'Color','k');
stalk_line = semilogx(segment2(:,1),segment2(:,4),'-', 'Color',line_blue)
;
semilogx(segment3(:,1),segment3(:,2),'-', 'Color','k');

legend([tip_line,stalk_line], 'Tip', 'Stalk')
legend('boxoff')

set(gca, 'FontSize', 8)
ylim([0 0.5]);
h1 = xlabel('\bf{\it{V}}', 'FontSize', 8);
h2 = ylabel('\bf{\it{RA}}', 'FontSize', 8);
%}

```

```

% Plot each segment - D
%kinetics_aCL('D_SS',struct('RA',s_RA2),params);

figure('units','inches','position',[5 5 1.675 1.675])% Half-column width
semilogx(segment1(:,1),kinetics_aCL('D_SS',struct('RA',segment1(:,2)),
    params),'-', 'Color','k');
hold on
tip_line = semilogx(segment2(:,1),kinetics_aCL('D_SS',struct('RA',
    segment2(:,2)),params),'-', 'Color',line_red);
semilogx(segment2(:,1),kinetics_aCL('D_SS',struct('RA',segment2(:,3)),
    params),'--', 'Color','k');
stalk_line = semilogx(segment2(:,1),kinetics_aCL('D_SS',struct('RA',
    segment2(:,4)),params),'-', 'Color',line_blue);
semilogx(segment3(:,1),kinetics_aCL('D_SS',struct('RA',segment3(:,2)),
    params),'-', 'Color','k');

legend([tip_line,stalk_line], 'Tip', 'Stalk')
legend('boxoff')

set(gca, 'FontSize', 8)
ylim([0 1]);
h1 = xlabel('\bf{\it{V/K_V}}', 'FontSize', 8);
h2 = ylabel('\bf{\it{D/D_0}}', 'FontSize', 8);

% Non-logarithmic X axis
%{
figure('units','inches','position',[5 5 1.675 1.675])% Half-column width
plot(segment1(:,1),segment1(:,2),'-', 'Color','k');
hold on

```

```

tip_line = plot(segment2(:,1),segment2(:,2),'-', 'Color', line_red);
plot(segment2(:,1),segment2(:,3),'--', 'Color', 'k');
stalk_line = plot(segment2(:,1),segment2(:,4),'-', 'Color', line_blue);
plot(segment3(:,1),segment3(:,2),'-', 'Color', 'k');
%}

end

function ss_mat_entry = getStates(index,V_in)
% Given a V_in, calculate the steady-states of the system using a
% two-cell modell
% Start with a vector of R1
R0_p = 100;
s_R0 = linspace(0,1,R0_p);
s_RA1 = kinetics_aCL('RA_SS',struct('R',s_R0,'V',V_in),params);
s_D1 = kinetics_aCL('D_SS',struct('RA',s_RA1),params);
s_R2 = kinetics_aCL('R_SS',struct('DN',s_D1),params);
s_RA2 = kinetics_aCL('RA_SS',struct('R',s_R2,'V',V_in),params);
s_D2 = kinetics_aCL('D_SS',struct('RA',s_RA2),params);
s_R1 = kinetics_aCL('R_SS',struct('DN',s_D2),params);

% Calculate the error between s_R0 and s_R1, and its zeros
err = s_R0 - s_R1;
Errorspline = spline(s_R0,err);
Z = fnzeros(Errorspline);

% Pull out the R concentrations at each zero and enter them into a
% matrix
if isempty(Z) == 0

```

```

[~, nz] = size(Z); % nz is the number of new steady-states
ss_mat_entry(1:nz,1) = index; % Add index to first column
ss_mat_entry(1:nz,2) = V_in; % Add V conc to second column
ss_mat_entry(1:nz,3) = Z(2,:); % Add R conc to third column
% Calcute RA for each state
s_RA_f = kinetics_aCL('RA_SS',struct('R',Z(2,:), 'V',V_in),params);

ss_mat_entry(1:nz,4) = s_RA_f; % Add R conc to third column
end
% Done, return the ss_mat_entry
end

%
-----

% 3. Calculate the uniform steady states
if figures || stability_fig
% Use same VEGF concentrations, but with one-cell model

% "Fast" method based on minimization (splines are more exhaustive)
D_guess = 0.5;
Dh_1 = fminsearch( @(x) H_err(x, V_vec(1)),D_guess);
Dh_2 = fminsearch( @(x) H_err(x, V_vec(2)),D_guess);
Dh_3 = fminsearch( @(x) H_err(x, V_vec(3)),D_guess);

end
function Herr = H_err(D_g,V_in)
R2 = kinetics_aCL('R_SS',struct('DN',D_g),params);

```

```

RA2 = kinetics_aCL('RA_SS',struct('R',R2,'V',V_in),params);
D2 = kinetics_aCL('D_SS',struct('RA',RA2),params);
Herr = (D2 - D_g)^2*10^3;
end
%
-----

% 4. Perform a linear stability analysis on each steady state
if figures || stability_fig

Dseq_1 = getDseq(Dh_1,V_vec(1));
Dseq_2 = getDseq(Dh_2,V_vec(2));
Dseq_3 = getDseq(Dh_3,V_vec(3));

%{
Jmatz = zeros(2,2,length(inits.qk));
for g = 1:length(inits.qk)
Jmatz(:, :,g) = findJmat(inits.qk(g));
end
inits.Jmatz = Jmatz;
[Vseq,Dseq] = eigenshuffle(Jmatz);
inits.Jeigs = Dseq;
inits.Jvecs = Vseq;
%}

figJeigs = figure('units','inches','position',[5 5 1.675 1.675]); % Half
    -column width
% Real - Blue; Red - Imaginary

```

```

% First sequence

linewidth = 0.5;
HL1_1 = plot(inits.qk,real(Dseq_1(1,:)),'Color','k','LineWidth',linewidth);
hold all
HL2_1 = plot(inits.qk,real(Dseq_1(2,:)),'Color','k','LineWidth',linewidth);
%HL3_1 = plot(inits.qk,imag(Dseq_1(1,:)),'Color','b','LineWidth',linewidth)
    ;
%HL4_1 = plot(inits.qk,imag(Dseq_1(2,:)),'Color','b','LineWidth',linewidth)
    ;

% Second sequence
HL1_2 = plot(inits.qk,real(Dseq_2(1,:)),'--','Color','k','LineWidth',
    linewidth);
HL2_2 = plot(inits.qk,real(Dseq_2(2,:)),'--','Color','k','LineWidth',
    linewidth);
%HL3_2 = plot(inits.qk,imag(Dseq_2(1,:)),'--','Color','b','LineWidth',
    linewidth);
%HL4_2 = plot(inits.qk,imag(Dseq_2(2,:)),'--','Color','b','LineWidth',
    linewidth);

% Third sequence
HL1_3 = plot(inits.qk,real(Dseq_3(1,:)),'-.','Color','k','LineWidth',
    linewidth);
HL2_3 = plot(inits.qk,real(Dseq_3(2,:)),'-.','Color','k','LineWidth',
    linewidth);
%HL3_3 = plot(inits.qk,imag(Dseq_3(1,:)),'-.','Color','b','LineWidth',
    linewidth);
%HL4_3 = plot(inits.qk,imag(Dseq_3(2,:)),'-.','Color','b','LineWidth',

```

```

        linewidth1);

plot([-1 1],[0 0], 'r')
xlim([-1 1])

%legend([HL1_1,HL3_1], 'Real', 'Imag')
%legend([HL1_1,HL1_2,HL1_3], '\it{V/K_V} = 0.1', '1', '10', 'FontSize',8)
%legend([HL1_1,HL1_2,HL1_3], sprintf( '%s\n%s', '\it V/K_V =', '0.1' )
        , '1', '10', 'FontSize',8)
legend([HL1_1,HL1_2,HL1_3], '0.1', '1', '10', 'FontSize',8)
%legend([HL1_1,HL1_2,HL1_3], '0.1', '1', '10', 'FontSize',8)
legend('boxoff')
set(gca, 'FontSize',8)

xlabel('Structural eigenvalue, \bf{\it{q_k}}', 'FontSize',8)
ylabel('Dynamic eigenvalue, \bf{\it{\lambda}}', 'FontSize',8)

% Zoomed-in figure
figJeigsz = figure('units','inches','position',[5 5 1.675 1.675]); %
        Half-column width
% Real - Blue; Red - Imaginary

% First sequence
linewidth = 0.5;
HL1_1z = plot(inits.qk,real(Dseq_1(1,:)), 'Color','k', 'LineWidth',linewidth)
        ;
hold all
HL2_1z = plot(inits.qk,real(Dseq_1(2,:)), 'Color','k', 'LineWidth',linewidth)
        ;

```

```

% Second sequence
HL1_2z = plot(inits.qk,real(Dseq_2(1,:)), '--', 'Color', 'k', 'LineWidth',
    linewidth1);
HL2_2z = plot(inits.qk,real(Dseq_2(2,:)), '--', 'Color', 'k', 'LineWidth',
    linewidth1);

% Third sequence
HL1_3z = plot(inits.qk,real(Dseq_3(1,:)), '-.', 'Color', 'k', 'LineWidth',
    linewidth1);
HL2_3z = plot(inits.qk,real(Dseq_3(2,:)), '-.', 'Color', 'k', 'LineWidth',
    linewidth1);

plot([-1 1],[0 0], 'r')
xlim([-1 -0.75])
ylim([-0.5 0.5])

legend([HL1_1z,HL1_2z,HL1_3z], '\it V/K_V = 0.1', '1', '10')
legend('boxoff')
set(gca, 'FontSize', 8)

xlabel('Structural eigenvalue, \bf{\it{q_k}}', 'FontSize', 8)
ylabel('Dynamic eigenvalue, \bf{\it{\lambda}}', 'FontSize', 8)
end

function Dseq = getDseq(D_in,V_in)
R_in = kinetics_aCL('R_SS',struct('DN',D_in),params);
RA_in = kinetics_aCL('RA_SS',struct('R',R_in,'V',V_in),params);

```

```

GR = g_hill(1,1/kappaR,nR,D_in);
GD = g_hill(1,kappaD,nD,RA_in);
GRA = V_in/(KV+V_in);

Jmatz = zeros(2,2,length(inits.qk));
for g = 1:length(inits.qk)
Jmatz(:, :, g) = findJmat(inits.qk(g),GR,GD,GRA);
end
[Vseq,Dseq] = eigenshuffle(Jmatz);
end

```

```

function Jmat = findJmat(qk,GR,GD,GRA)
Jac = zeros(2,2);
Jac(1,1) = -1;
Jac(1,2) = -qk*GR;
Jac(2,1) = tau*GD*GRA;
Jac(2,2) = -tau;
Jmat = Jac;
end
%

```

---

```

%% Simulaiton initial conditions
% 5. Calculate the initial conditions for the simulation

```

```

% Basic, flat profile
D_guess = 0.5;
inits.DSS = fminsearch( @(x) H_err_2(x, inits.Vi),D_guess);
inits.RSS = kinetics_aCL('R_SS',struct('DN',inits.DSS),params);
inits.V = ones(Sys.M, Sys.N)*inits.Vi;

%{
% Logarithmic-sinusoidal VEGF profile
M = Sys.M;
N = Sys.N;
D_guess = 0.5;
C = zeros(M,N);
for mu = 1:M
for nu = 1:N
C(mu,nu) = 1.2*(sin(mu/M*pi)+sin(nu/N*pi)-1);
inits.V(mu,nu) = 10.^(C(mu,nu));
inits.D0(mu,nu) = fminsearch( @(x) H_err_2(x, inits.V(mu,nu)),D_guess);
inits.R0(mu,nu) = kinetics_aCL('R_SS',struct('DN',inits.D0(mu,nu)),
    params);
end
end

inits.customX0 = true;
%}

function Herr = H_err_2(D_g,V_in)
R2 = kinetics_aCL('R_SS',struct('DN',D_g),params);
RA2 = kinetics_aCL('RA_SS',struct('R',R2,'V',V_in),params);

```

```

D2 = kinetics_aCL('D_SS',struct('RA',RA2),params);
Herr = (D2 - D_g)^2*10^3;
end
%
-----

end

```

### A.3.2 Lateral induction

```

function inits = homogIC_aDF(Sys,params,inits)
%Classical GRN initional condition generator

ar = params.ar;
KV = params.KV;
VH = params.VH;
a = params.a;
kappaD1 = params.kappaD1;
nD1 = params.nD1;
kappaD = params.kappaD;
nD = params.nD;

line_red = [237/255 27/255 35/255];
line_blue = [0 173/255 239/255];

plots = true;

V_vec = [0.8, 1, 1.2];

```

```

D_max = 3/2;

%% Analysis

% Goals:
% 1. Produce a steady-state relation (pretty!)
% 2. Calculate the uniform steady-state
% 3. Produce a stability profile (pretty!)

%1. Produce a steady-state relation (pretty!)
if plots
% The paper assumes this is with a two-cell model

nullcl_num = 1000;
D0 = linspace(0,D_max,nullcl_num);

D1_1 = getD1(V_vec(1),D0);
D1_2 = getD1(V_vec(2),D0);
D1_3 = getD1(V_vec(3),D0);

figure('units','inches','position',[5 5 1.675 1.675])% Half-column width
plot(D0,D1_1,'Color',line_blue,'LineWidth',1)
hold on
plot(D0,D1_2,'--','Color',line_blue,'LineWidth',1) % Blue
plot(D0,D1_3,'-.','Color',line_blue,'LineWidth',1)
plot([0 D_max],[0 D_max],'k')
legend('\it{a} = 0','0.1','0.2')
legend('boxoff')

```

```

ylim([0 3/2]);
xlim([0 3/2]);
set(gca,'FontSize',8)
%h1 = xlabel('\bf{\it{D_{0}}}', 'FontSize',8);
%h2 = ylabel('\bf{\it{D_{1}}}', 'FontSize',8);
h1 = xlabel('\bf{\it{D0 (input)}}', 'FontSize',8);
h2 = ylabel('\bf{\it{D1 (output)}}', 'FontSize',8);

end

function D_1 = getD1(V_in,D0)
% Two-cell model
R_1 = params.ar;
RA_1 = kinetics_aDF('RA_SS',struct('R',R_1,'V',V_in),params);
D_1 = kinetics_aDF('D_SS',struct('DN',D0,'RA',RA_1),params);
end
%
-----

%{
% 1.B Produces true nullclines of R & D

% First, calculate the D which produces steady-state R (this is
independent
% of V)
R_points = 1000;
R_steady = linspace(0,1,R_points);

```

```

D_required = (1./R_steady-1).^ (1/nR)/kappaR;

D_points = 1000;
D_steady = linspace(0,1,D_points);
R_required_2 = (-D_steady*kappaD^nD./(D_steady-1)).^(1/nD)/(a_vec(2)/(KV
+a_vec(2)));

figure('units','inches','position',[5 5 1.675 1.675])% Half-column width
plot(R_steady,D_required,'Color',line_red,'LineWidth',1)
hold on
plot(R_required_2,D_steady,'--','Color',line_blue,'LineWidth',1)
%plot([0 1],[0 1],'k')
%legend('\it{V} = 0.1','1','10')
%legend('boxoff')
set(gca,'FontSize',8)
%h1 = xlabel('\bf{\it{D}_{0}}','FontSize',8);
%h2 = ylabel('\bf{\it{D}_{1}}','FontSize',8);
xlim([0 1]);
ylim([0 1]);
h1 = xlabel('R','FontSize',8);
h2 = ylabel('D','FontSize',8);
%
-----

% 1.C Produces true nullclines of R & D (attempt 2)

% First, calculate R_int_1 imposed by D_ext_1
D_ext_1_p = 1000;

```

```

D_ext_1 = linspace(0,1,D_ext_1_p);
R_int_1 = kinetics_aCL('R_SS',struct('DN',D_ext_1),params);

% Second, calculate D_ext_2 impost by a two-cell iteration of R_int_2
%
R_int_2_p = 1000;
R_int_2 = linspace(0,1,R_int_2_p);

D_ext_2_1 = getDext(a_vec(1),R_int_2);
D_ext_2_2 = getDext(a_vec(2),R_int_2);
D_ext_2_3 = getDext(a_vec(3),R_int_2);

function D_ext = getDext(V_in,R_int)
RA_int = kinetics_aCL('RA_SS',struct('R',R_int,'V',V_in),params);
D_int = kinetics_aCL('D_SS',struct('RA',RA_int),params);
R_ext = kinetics_aCL('R_SS',struct('DN',D_int),params);
RA_ext = kinetics_aCL('RA_SS',struct('R',R_ext,'V',V_in),params);
D_ext = kinetics_aCL('D_SS',struct('RA',RA_ext),params);
end

% Plot each nullcline, with D_ext on the X axis, and R_int on Y axis

figure('units','inches','position',[5 5 1.675 1.675])% Half-column width
plot(D_ext_1,R_int_1,'Color',line_red,'LineWidth',1)
hold on
plot(D_ext_2_1,R_int_2,'Color',line_blue,'LineWidth',1)
plot(D_ext_2_2,R_int_2,'--','Color',line_blue,'LineWidth',1)
plot(D_ext_2_3,R_int_2,'-.','Color',line_blue,'LineWidth',1)

```

```

%plot([0 1],[0 1],'k')
%legend('\it{V} = 0.1','1','10')
%legend('boxoff')
set(gca,'FontSize',8)
%h1 = xlabel('\bf{\it{D_{0}}}','FontSize',8);
%h2 = ylabel('\bf{\it{D_{1}}}','FontSize',8);
xlim([0 1]);
ylim([0 1]);
h1 = xlabel('D_{ext}','FontSize',8);
h2 = ylabel('R_{int}','FontSize',8);
%
-----

%}

% 2. Bifurcation diagram with D as a function of a

if plots

% First, chose a vector of a values (not too large)
V_vec2_p = 2000;
V_min = 0.1;
V_max = 10;
V_vec2 = linspace(V_min,V_max,V_vec2_p);

% Next, create an empty matrix for storing steady-states
ss_mat = zeros(0,3);
% Column 1 - a_index, Column 2 - a, Column 3 - D

```

```

% For each element in a_vec2, calculate all possible steady-states using
    a
% two cell model.
% Will probably have to use splines and fnzero
for j = 1:V_vec2_p
ss_mat = [ss_mat;getStates(j,V_vec2(j))]; %#ok<AGROW>
end

% Do a preliminary check of the data
figure
plot(ss_mat(:,2),ss_mat(:,3),'s')

% Might want to test the stability for each of those, because I don't
    have
% a clue
stable_mat_T = zeros(0,3);
stable_mat_S = zeros(0,3);
stable_mat_1 = zeros(0,3);
stable_mat_2 = zeros(0,3);
unstable_mat = zeros(0,3);
D_split = 0.3;
VU_min = 0.8627;
VU_max = 1.095;

for j = 1:length(ss_mat(:,1))
if check_stable(ss_mat(j,2),ss_mat(j,3));
if ss_mat(j,3) > D_split

```

```

if ss_mat(j,2) < VU_max
stable_mat_T = [stable_mat_T;ss_mat(j,:)];
else
stable_mat_1 = [stable_mat_1;ss_mat(j,:)];
end
else
if ss_mat(j,2) > VU_min
stable_mat_S = [stable_mat_S;ss_mat(j,:)];
else
stable_mat_2 = [stable_mat_2;ss_mat(j,:)];
end
end

else
unstable_mat = [unstable_mat;ss_mat(j,:)];
end
end

figure('units','inches','position',[5 5 1.675 1.675])% Half-column width
semilogx(stable_mat_1(:,2),stable_mat_1(:,3),'Color','k','LineWidth',1)
hold on
semilogx(stable_mat_2(:,2),stable_mat_2(:,3),'Color','k','LineWidth',1)
semilogx(stable_mat_T(:,2),stable_mat_T(:,3),'Color',line_red,'LineWidth
',1)
semilogx(stable_mat_S(:,2),stable_mat_S(:,3),'Color',line_blue,'
LineWidth',1)
semilogx(unstable_mat(:,2),unstable_mat(:,3),'k--','LineWidth',0.75)

%legend('stable','unstable')

```

```

%legend('boxoff')

set(gca,'FontSize',8)

h1 = xlabel('\bf{\it{V/K_V}}','FontSize',8);
h2 = ylabel('\bf{\it{D/D_0}}','FontSize',8);

end

function ss_mat_entry = getStates(index,V_in)
% Given a V_in, calculate the steady-states of the system using a
% two-cell modell
% Start with a vector of D1
D0_p = 100;
s_D0 = linspace(0,D_max,D0_p);
R_1 = params.ar;
RA_1 = kinetics_aDF('RA_SS',struct('R',R_1,'V',V_in),params);
s_D1 = kinetics_aDF('D_SS',struct('DN',s_D0,'RA',RA_1),params);

% Calculate the error between s_D0 and s_D1, and its zeros
err = s_D0 - s_D1;
Errorspline = spline(s_D0,err);
Z = fnzeros(Errorspline);

% Pull out the R concentrations at each zero and enter them into a
% matrix
if isempty(Z) == 0
[~, nz] = size(Z); % nz is the number of new steady-states
ss_mat_entry(1:nz,1) = index; % Add index to first column
ss_mat_entry(1:nz,2) = V_in; % Add a value to second column

```

```
ss_mat_entry(1:nz,3) = Z(2,:); % Add D conc to third column
```

```
end
```

```
% Done, return the ss_mat_entry
```

```
end
```

```
function stable_result = check_stable(V_in,D_in)
```

```
% See if the derivative is positive for qk = 1
```

```
R_1 = params.ar;
```

```
RA_1 = kinetics_aDF('RA_SS',struct('R',R_1,'V',V_in),params);
```

```
GD1 = g_hill(a,kappaD1,nD1,RA_1);
```

```
GD = g_hill(1,kappaD,nD,D_in);
```

```
GRA = V_in/(KV+V_in);
```

```
Jmat = zeros(2,2);
```

```
Jmat(1,1) = -1;
```

```
Jmat(1,2) = 0;
```

```
Jmat(2,1) = GD1*GRA;
```

```
Jmat(2,2) = GD-1;
```

```
if max(real(eig(Jmat))) > 0
```

```
stable_result = false;
```

```
else
```

```
stable_result = true;
```

```
end
```

```
end
```

```
%-----
```

```

% 3. Calculate the uniform steady states

% For this we are going to use the same set of parameters, probe each of
% the three steady-states
V_H = 1; % Chosen parameter

DH_states = getStates_2(V_H)

function D_states = getStates_2(V_in)
% Given a a_in, calculate the steady-states of the system using a
% two-cell modell
% Start with a vector of D1
D0_p = 100;
s_D0 = linspace(0,D_max,D0_p);
R_1 = params.ar;
RA_1 = kinetics_aDF('RA_SS',struct('R',R_1,'V',V_in),params);
s_D1 = kinetics_aDF('D_SS',struct('DN',s_D0,'RA',RA_1),params);

% Calculate the error between s_D0 and s_D1, and its zeros
err = s_D0 - s_D1;
Errorspline = spline(s_D0,err);
Z = fnzeros(Errorspline);

D_states = Z(2,:);

% Done, return the ss_mat_entry
end

%
-----

```

```

% 4. Perform a linear stability analysis on each steady state
if plots
Dseq_1 = getDseq(V_vec(1),getStates_3(V_vec(1)));
Dseq_2 = getDseq(V_vec(2),getStates_3(V_vec(2)));
Dseq_3 = getDseq(V_vec(3),getStates_3(V_vec(3)));

%{
Jmatz = zeros(2,2,length(inits.qk));
for g = 1:length(inits.qk)
Jmatz(:,:,g) = findJmat(inits.qk(g));
end
inits.Jmatz = Jmatz;
[Vseq,Dseq] = eigenshuffle(Jmatz);
inits.Jeigs = Dseq;
inits.Jvecs = Vseq;
%}

figJeigs = figure('units','inches','position',[5 5 1.675 1.675]); % Half
    -column width
% Real - Blue; Red - Imaginary

% First sequence
linew1 = 0.5;
HL1_1 = plot(inits.qk,real(Dseq_1(1,:)),'Color','k','LineWidth',linew1);
hold all
HL2_1 = plot(inits.qk,real(Dseq_1(2,:)),'Color','k','LineWidth',linew1);

```

```

HL3_1 = plot(inits.qk,imag(Dseq_1(1,:)),'Color','b','LineWidth',linewidth);
HL4_1 = plot(inits.qk,imag(Dseq_1(2,:)),'Color','b','LineWidth',linewidth);

% Second sequence
HL1_2 = plot(inits.qk,real(Dseq_2(1,:)),'--','Color','k','LineWidth',
    linewidth);
HL2_2 = plot(inits.qk,real(Dseq_2(2,:)),'--','Color','k','LineWidth',
    linewidth);
HL3_2 = plot(inits.qk,imag(Dseq_2(1,:)),'--','Color','b','LineWidth',
    linewidth);
HL4_2 = plot(inits.qk,imag(Dseq_2(2,:)),'--','Color','b','LineWidth',
    linewidth);

% Third sequence
HL1_3 = plot(inits.qk,real(Dseq_3(1,:)),'-.','Color','k','LineWidth',
    linewidth);
HL2_3 = plot(inits.qk,real(Dseq_3(2,:)),'-.','Color','k','LineWidth',
    linewidth);
HL3_3 = plot(inits.qk,imag(Dseq_3(1,:)),'-.','Color','b','LineWidth',
    linewidth);
HL4_3 = plot(inits.qk,imag(Dseq_3(2,:)),'-.','Color','b','LineWidth',
    linewidth);

plot([-1 1],[0 0],'r')
xlim([-1 1])

legend([HL1_1,HL1_2,HL1_3],'\it V/K_V = 0.8','1','1.2')
legend('boxoff')
set(gca,'FontSize',8)

```

```

xlabel('Structural eigenvalue, \bf{\it{q}_k}', 'FontSize', 8)
ylabel('Dynamic eigenvalue, \bf{\it{\lambda}}', 'FontSize', 8)

% Zoomed-in figure
figure('units','inches','position',[5 5 1.675 1.675]); % Half-column
width
% Real - Blue; Red - Imaginary

% First sequence
linewidth = 0.5;
HL1_1z = plot(inits.qk,real(Dseq_1(1,:)), 'Color','k','LineWidth',linewidth)
;
hold all
%HL2_1z = plot(inits.qk,real(Dseq_1(2,:)), 'Color',line_blue,'LineWidth',
linewidth);

% Second sequence
HL1_2z = plot(inits.qk,real(Dseq_2(1,:)), '--', 'Color','k','LineWidth',
linewidth);
%HL2_2z = plot(inits.qk,real(Dseq_2(2,:)), '--', 'Color',line_blue,'
LineWidth',linewidth)

% Third sequence
HL1_3z = plot(inits.qk,real(Dseq_3(1,:)), '-.', 'Color','k','LineWidth',
linewidth);
%HL2_3z = plot(inits.qk,real(Dseq_3(2,:)), '-.', 'Color',line_blue,'
LineWidth',linewidth);

```

```

%legend([HL1_1z,HL1_2z,HL1_3z],'\it{V/K_V} = 0.1','1','10')
legend([HL1_1z,HL1_2z,HL1_3z],'\it V/K_V = 0.8','1','1.2')
legend('boxoff')
set(gca,'FontSize',8)

plot([-1 1],[0 0],'r')
xlim([0 1])
ylim([-0.5 0.5])

xlabel('Structural eigenvalue, \bf{\it{q_k}}','FontSize',8)
ylabel('Dynamic eigenvalue, \bf{\it{\lambda}}','FontSize',8)
end

function D_out = getStates_3(V_in)
% Given a a_in, calculate the steady-states of the system using a
% two-cell modell
% Start with a vector of D1
D0_p = 100;
s_D0 = linspace(0,D_max,D0_p);
R_1 = params.ar;
RA_1 = kinetics_aDF('RA_SS',struct('R',R_1,'V',V_in),params);
s_D1 = kinetics_aDF('D_SS',struct('DN',s_D0,'RA',RA_1),params);

% Calculate the error between s_D0 and s_D1, and its zeros
err = s_D0 - s_D1;
Errorspline = spline(s_D0,err);
Z = fnzeros(Errorspline);

if isempty(Z) == 0
[~, nz] = size(Z); % nz is the number of new steady-states

```

```

if nz == 1
D_out = Z(2,1); % Add D conc to third column
else
D_out = Z(2,2);
end

end

% Done, return the ss_mat_entry
end

function Dseq = getDseq(V_in,D_in)

Jmatz = zeros(2,2,length(inits.qk));
for g = 1:length(inits.qk)
Jmatz(:, :, g) = findJmat(V_in,D_in,inits.qk(g));
end

[Vseq,Dseq] = eigenshuffle(Jmatz);
end

function Jmat = findJmat(V_in,D_in,qk)

% See if the derivative is positive for qk = 1
R_1 = params.ar;
RA_1 = kinetics_aDF('RA_SS',struct('R',R_1,'V',V_in),params);
GD1 = g_hill(a,kappaD1,nD1,RA_1);
GD = g_hill(1,kappaD,nD,D_in);
GRA = V_in/(KV+V_in);

Jmat = zeros(2,2);

```

```
Jmat(1,1) = -1;
Jmat(1,2) = 0;
Jmat(2,1) = GD1*GRA;
Jmat(2,2) = qk*GD-1;
```

```
end
```

```
%
```

```
-----
```

```
%% Simulaiton initial conditions
```

```
% 5. Calculate the initial conditions for the simulation
```

```
inits.X0(2) = DH_states(2);
```

```
inits.X0(1) = params.ar;
```

```
inits.customX0 = false;
```

```
%{
```

```
% Logarithmic-sinusoidal VEGF profile
```

```
M = Sys.M;
```

```
N = Sys.N;
```

```
D_guess = 0.5;
```

```
C = zeros(M,N);
```

```
for mu = 1:M
```

```
for nu = 1:N
```

```
C(mu,nu) = 1.2*(sin(mu/M*pi)+sin(nu/N*pi)-1);
```

```

inits.V(mu,nu) = 10.^(C(mu,nu));
inits.D0(mu,nu) = fminsearch( @(x) H_err_2(x, inits.V(mu,nu)),D_guess);
inits.R0(mu,nu) = params.ar;
end
end

```

```

function Herr = H_err_2(D_g,V_in)
R_1 = params.ar;
RA_1 = kinetics_aDF('RA_SS',struct('R',R_1,'V',V_in),params);
D_1 = kinetics_aDF('D_SS',struct('DN',D_g,'RA',RA_1),params);
Herr = (D_1 - D_g)^2*10^3;
end

```

```

inits.customX0 = true;
%}
%
```

---

```

end

```

### A.3.3 Double-juxtacrine

```

function inits = homogIC_aDJ(Sys,params,inits)
%Classical GRN initional condition generator

beta = params.beta;
nP = params.nP;

```

```

nA = params.nA;
nB = params.nB;
KA = params.KA;
KP = params.KP;
KB = params.KB;

line_red = [237/255 27/255 35/255];
line_blue = [0 173/255 239/255];

figures = true;
compare_qk = false;

%% Analysis
% 1. Confirm that the steady-state assumptions are working correctly
A_in = (1 + params.beta)/2;
B_in = 1/2;
A_out = kinetics_aDJ('A_SS',struct('BN',B_in,'B',B_in),params);
B_out = kinetics_aDJ('B_SS',struct('AN',A_in),params);
AisGood = A_in == A_out;
BisGood = B_in == B_out;
if ~AisGood || ~BisGood ; error('Steady-states do not match'); end

% 2. Perform a linear stability analysis on each steady state
if figures

GA = g_hill(beta,KA,nA,B_in)
GB = g_hill(1,KB,nB,A_in)
GP = g_hill(1,KP,nP,B_in)

```

```

Jmatz = zeros(2,2,length(inits.qk));
for g = 1:length(inits.qk)
Jmatz(:, :,g) = findJmat(inits.qk(g),GA,GB,GP);
end
[Vseq,Dseq] = eigenshuffle(Jmatz);

%{
Jmatz = zeros(2,2,length(inits.qk));
for g = 1:length(inits.qk)
Jmatz(:, :,g) = findJmat(inits.qk(g));
end
inits.Jmatz = Jmatz;
[Vseq,Dseq] = eigenshuffle(Jmatz);
inits.Jeigs = Dseq;
inits.Jvecs = Vseq;
%}

figJeigs = figure('units','inches','position',[5 5 1.675 1.675]); % Half
    -column width
% Real - Blue; Red - Imaginary

% First sequence
linew1 = 0.5;
HL1_1 = plot(inits.qk,real(Dseq(1,:)),'Color','k','LineWidth',linew1);
hold all
HL2_1 = plot(inits.qk,real(Dseq(2,:)),'Color','k','LineWidth',linew1);

plot([-1 1],[0 0],'r')

```

```

xlim([-1 1])

xlabel('Structural eigenvalue, \bf{\it{q_k}}','FontSize',8)
ylabel('Dynamic eigenvalue, \bf{\it{\lambda}}','FontSize',8)

end

function Jmat = findJmat(qk,GA,GB,GP)
Jac = zeros(2,2);
Jac(1,1) = -1;
Jac(1,2) = -GP-qk*GA;
Jac(2,1) = qk*GB;
Jac(2,2) = -1;
Jmat = Jac;
end
%
-----

if compare_qk
q_t = [-0.25 -0.5 -0.9];
MLE_t = [0.05 0.05 0.05];
Dseq_1 = getDseq(q_t(1),MLE_t(1));
Dseq_2 = getDseq(q_t(2),MLE_t(2));
Dseq_3 = getDseq(q_t(3),MLE_t(3));

figJeigs = figure('units','inches','position',[5 5 2.23 2.23]); % Half-
column width

```

```

% Real - Blue; Red - Imaginary

% First sequence
linewidth = 0.5;
HL1_1 = plot(inits.qk,real(Dseq_1(1,:)),'Color','k','LineWidth',linewidth);
hold all
HL2_1 = plot(inits.qk,real(Dseq_1(2,:)),'Color','k','LineWidth',linewidth);
HL1_2 = plot(inits.qk,real(Dseq_2(1,:)),'--','Color','k','LineWidth',
    linewidth);
HL2_2 = plot(inits.qk,real(Dseq_2(2,:)),'--','Color','k','LineWidth',
    linewidth);
HL1_3 = plot(inits.qk,real(Dseq_3(1,:)),'-.','Color','k','LineWidth',
    linewidth);
HL2_3 = plot(inits.qk,real(Dseq_3(2,:)),'-.','Color','k','LineWidth',
    linewidth);

plot([-1 1],[0 0],'r')
xlim([-1 1])
ylim([-0.5 0.5])

legend([HL1_1,HL1_2,HL1_3],'\it q_{max} = -0.25','-0.5','-0.9')
legend('boxoff')
set(gca,'FontSize',8)
xlabel('Structural eigenvalue, \bf{\it{q}_k}','FontSize',8)
ylabel('Dynamic eigenvalue, \bf{\it{\lambda}}','FontSize',8)

end

function Dseq_out = getDseq(q_target,MLE_target)

```

```

param_in = getParams(q_target,MLE_target);
beta_g = param_in.beta;
nP_g = param_in.nP;
nA_g = param_in.nA;
nB_g = param_in.nB;
KA_g = param_in.KA;
KP_g = param_in.KP;
KB_g = param_in.KB;

A_in_g = (1 + param_in.beta)/2;
B_in_g = 1/2;
A_out_g = kinetics_aDJ('A_SS',struct('BN',B_in_g,'B',B_in_g),param_in);
B_out_g = kinetics_aDJ('B_SS',struct('AN',A_in_g),param_in);
AisGood_g = A_in_g == A_out_g;
BisGood_g = B_in_g == B_out_g;
if ~AisGood_g || ~BisGood_g ; error('Steady-states do not match'); end

GA_g = g_hill(beta_g,KA_g,nA_g,B_in_g)
GB_g = g_hill(1,KB_g,nB_g,A_in_g)
GP_g = g_hill(1,KP_g,nP_g,B_in_g)

Jmatz_g = zeros(2,2,length(inits.qk));
for h = 1:length(inits.qk)
Jmatz_g(:, :, h) = findJmat(inits.qk(h),GA_g,GB_g,GP_g);
end
[Vseq_g,Dseq_out] = eigenshuffle(Jmatz_g);

end

```

```

function param_out = getParams(qk_in,MLE_in)

qtarget = qk_in;
MLE = MLE_in;

%Assuming tau = 1, IC at 1/2 max for all functions

param_out.beta = 1;

param_out.nP = 6;
param_out.nA = -param_out.nP/(2*param_out.beta*qtarget);
param_out.nB = 32*(MLE+1)^2*param_out.nA/param_out.nP^2; %Does not work
    for beta not = 1!!

param_out.KA = 1/2;
param_out.KP = 1/2;
param_out.KB = (1 + param_out.beta)/2;
end

inits.X0 = [1 1/2];
end

```

### A.3.4 Diffusion & endocytosis

```

function inits = homogIC_aCLDE(Sys,params,inits)

%Non dim parameters
alph = params.alph;

```

```

beta = params.beta;
gamm = params.gamm;
rho = params.rho;
DA = params.DA;
nI = params.nI;

line_red = [237/255 27/255 35/255];
line_blue = [0 173/255 239/255];
rho_vec = [0.8 1.1 1.5];

%Dimensional parameters must be called from the struct, use sparingly

nullclines = true;
%manualhss = true;
%autohss = true;
%autohssGFX = false;
jacobian = true;

if nullclines
% Limits for I
I_min = 2*10^-2;
I_max = (alph+beta);
I_num = 1000;
I_vector = linspace(I_min,I_max,I_num);

%rho_vec = [0.8 1 1.2];

% V is closed function of I

```

```

% ----- VEGF GRN Nullcline -----
% Calculate VEGF required for all possible I levels using the GRN
V_g_vector = kinetics_aCLDE('V_f_I_g',struct('I',I_vector),params);

% Split the vector into five parts
V_g_v_b = zeros(0,2); % Blue
V_g_v_u = zeros(0,2); % Dotted (unstable)
V_g_v_r = zeros(0,2); % Red
V_g_v_k1 = zeros(0,2); % black 1
V_g_v_k2 = zeros(0,2); % black 2

I_ref = 0.8;
VU_min = 5.66;
VU_max = 6.202;

for j = 1:length(V_g_vector)
if V_g_vector(j) > 0
if checkStable_split(V_g_vector(j),I_vector(j))
if I_vector(j) < I_ref
if V_g_vector(j) > VU_min
V_g_v_b = [V_g_v_b;[I_vector(j) V_g_vector(j)]];
else
V_g_v_k1 = [V_g_v_k1;[I_vector(j) V_g_vector(j)]];
end
else
if V_g_vector(j) < VU_max
V_g_v_r = [V_g_v_r;[I_vector(j) V_g_vector(j)]];
else

```

```

V_g_v_k2 = [V_g_v_k2;[I_vector(j) V_g_vector(j)]];
end
end
else
V_g_v_u = [V_g_v_u;[I_vector(j) V_g_vector(j)]];
end
end
end

% ----- VEGF GRN Nullcline (NO BETA) -----
% Hypothetical curve without positive feedback
V_gnb_vector = kinetics_aCLDE('V_f_I_gnb',struct('I',I_vector),params);

% ----- VEGF GRN Nullcline (FULL BETA) -----
% Hypothetical curve without positive feedback
V_gfb_vector = kinetics_aCLDE('V_f_I_gfb',struct('I',I_vector),params);

% Perform multiple nullclines, modify Rho parameter for each
% ----- VEGF Transport Nullclines -----
% Calculate VEGF required for all possible I levels using the Trans. eq
V_t_vector_1 = kinetics_aCLDE('V_f_I_t',struct('I',I_vector,'rho_in',rho
    *rho_vec(1)),params);
V_t_vector_2 = kinetics_aCLDE('V_f_I_t',struct('I',I_vector,'rho_in',rho
    *rho_vec(2)),params);
V_t_vector_3 = kinetics_aCLDE('V_f_I_t',struct('I',I_vector,'rho_in',rho
    *rho_vec(3)),params);

figure('units','inches','position',[5 5 1.4 1.2])

```

```

% GRN Nullclines
VEGF_SCALE = 0.7622; %Where did this number come from
%stalk1 = plot(V_g_v_b(:,1)/VEGF_SCALE,V_g_v_b(:,2),'Color',line_blue) %
    VEGF FUDGE FACTOR = 6.202
stalk1 = plot(V_g_v_b(:,1)/VEGF_SCALE,V_g_v_b(:,2),'Color','k') % VEGF
    FUDGE FACTOR = 6.202

hold on

plot(V_g_v_u(:,1)/VEGF_SCALE,V_g_v_u(:,2),'k:')
%tipl = plot(V_g_v_r(:,1)/VEGF_SCALE,V_g_v_r(:,2),'Color',line_red)
tipl = plot(V_g_v_r(:,1)/VEGF_SCALE,V_g_v_r(:,2),'Color','k')
plot(V_g_v_k1(:,1)/VEGF_SCALE,V_g_v_k1(:,2),'Color','k')
plot(V_g_v_k2(:,1)/VEGF_SCALE,V_g_v_k2(:,2),'Color','k')
%plot(I_vector(V_gnb_vector > 0)/VEGF_SCALE,V_gnb_vector(V_gnb_vector >
    0),'k--')
%plot(I_vector(V_gfb_vector > 0)/VEGF_SCALE,V_gfb_vector(V_gfb_vector >
    0),'k--')

% Transport lines
%plot(I_vector(V_t_vector_1 > 0),V_t_vector_1(V_t_vector_1 > 0),'Color
    ','g')
%hold on
%plot(I_vector(V_t_vector_2 > 0),V_t_vector_2(V_t_vector_2 > 0),'--','
    Color','g')
%plot(I_vector(V_t_vector_3 > 0),V_t_vector_3(V_t_vector_3 > 0),'-.','
    Color','g')

% Production rate points

%semilogy(I_vector,V_g_vector,'r')

```

```

%hold on
%semilogy(I_vector,V_t_vector,'b')
%semilogy(I_vector,V_gnb_vector,'r--')
ylim([0 10])
xlim([0.1/VEGF_SCALE I_max/VEGF_SCALE])

%Operating on the assumption that the steady-state internalization rate
%matches the homogeneous generation rate
I_HSS = rho;
V_HSS = kinetics_aCLDE('V_f_I_g',struct('I',I_HSS),params);
%semilogy(I_HSS,V_HSS,'ks');

%title('Nondimensional nullclines')
%xlabel('\it{I}')
%xl = xlabel('\sffamily $\dot{V}/\dot{V}_C$')
%set(xl,'interpreter','latex');
%ylabel('\it{V/V_0}')
%legend([tipl, stalkl],'Tip','Stalk')
%leg1 = legend('\sffamily $\dot{V}_C$ x 0.8', '\sffamily 1.1', '\sffamily
1.5')
%I = legend( '$\gamma$', '$\dot{\gamma}$', '$\ddot{\gamma}$');
%set(leg1,'interpreter','latex');
%legend('boxoff')
set(gca,'FontSize',8,'Fontname','Lato')
end

function stable = checkStable_split(V_in,I_in)
Jac = zeros(Sys.nspec,Sys.nspec);
fi = (alph + f_hill_a(beta,1,nI,I_in));

```

```

% V
Jac(1,1) = -gamm*fi/(1+V_in)^2+DA*(-1-1);
Jac(1,2) = -gamm*V_in/(1+V_in)*g_hill(beta,1,nI,I_in);

% I
Jac(2,1) = fi/(1+V_in)^2;
Jac(2,2) = V_in/(1+V_in)*g_hill(beta,1,nI,I_in)-1;

mle = max(real(eig(Jac)));
if mle > 0
stable = false;
else
stable = true;
end
end

%error('stop')

%Basic, flat profile
inits.customX0 = false;
I_HSS = rho;
V_HSS = kinetics_aCLDE('V_f_I_g',struct('I',I_HSS),params);

X0 = [V_HSS, I_HSS];
inits.X0 = X0;

```

```

% Logarithmic-sinusoidal VEGF profile
%{
inits.customX0 = true;
M = Sys.M;
N = Sys.N;
rho_min = 0.8;
rho_max = 1.3;
for mu = 1:M
for nu = 1:N
%Define all the rho you will encounter
inits.rho(mu,nu) = rho*(rho_min+(rho_max-rho_min)*(sin(mu/M*pi)+sin(nu/N
    *pi))/2); % Profile for altering RHO

%Set the steady-state I for each rho
inits.I0(mu,nu) = inits.rho(mu,nu);

%Set the steady-state V for each I
inits.V0(mu,nu) = kinetics_aCLDE('V_f_I_g',struct('I',inits.I0(mu,nu)),
    params);

end
end
%}

if jacobian
analyzeHSS(rho_vec);
end

```

```

function analyzeHSS(rho_v)
Dseq_1 = getDseq(rho_v(1));
Dseq_2 = getDseq(rho_v(2));
Dseq_3 = getDseq(rho_v(3));

figJeigs = figure('units','inches','position',[5 5 1.354 1.198]);

plot([-1 1],[0 0],'Color',[0.5 0.5 0.5],'Linewidth',1.5)
hold on
HL1_1 = plot(inits.qk,real(Dseq_1(1,:)),'k');
%hold all
HL2_1 = plot(inits.qk,real(Dseq_1(2,:)),'k');
HL1_2 = plot(inits.qk,real(Dseq_2(1,:)),'k--');
HL2_2 = plot(inits.qk,real(Dseq_2(2,:)),'k--');
HL1_3 = plot(inits.qk,real(Dseq_3(1,:)),'k-.');
HL2_3 = plot(inits.qk,real(Dseq_3(2,:)),'k-.');
%HL3 = plot(inits.qk,imag(Dseq(1,:)),'b');
%HL4 = plot(inits.qk,imag(Dseq(2,:)),'b');
%HL5 = plot(inits.qk,real(Dseq(3,:)),'k');
%HL6 = plot(inits.qk,imag(Dseq(3,:)),'b');
%HL7 = plot(inits.qk,real(Dseq(4,:)),'k');
%HL8 = plot(inits.qk,imag(Dseq(4,:)),'b');
%plot([min(inits.qk) 1],[0 0],'r')
ylim([-0.5 0.5])
xlim([-1 1])
%title(['Eigenvalues of the Jacobian - "CLDE"'])
xlabel('Structural eigenvalue, \bf{\it{q}_k}','FontSize',8)
ylabel('Dynamic eigenvalue, \bf{\it{\lambda}}','FontSize',8)

```

```

%legend([HL1,HL3], 'Real', 'Imag')
%legend([HL1_1,HL1_2,HL1_3], '\[{\dot V_C}\] x 0.8', '1.1', '1.5')
leg2 = legend([HL1_1,HL1_2,HL1_3], 'V = 0.8', '1.1', '1.5')
%I = legend( '$\gamma$', '$\dot{\gamma}$', '$\ddot{\gamma}$');
%set(leg2, 'interpreter', 'latex', 'Fontname', 'Lato');
set(gca, 'XTick', [-1 0 1])
legend('boxoff')
set(gca, 'FontSize', 8, 'Fontname', 'Lato')

```

```

function Dseq = getDseq(rho_in)
ISS = rho_in*params.rho;
VSS = kinetics_aCLDE('V_f_I_g', struct('I', ISS), params);
fi = (alph + f_hill_a(beta, 1, nI, ISS));

```

```

Jmatz = zeros(Sys.nspec, Sys.nspec, length(inits.qk));
for g = 1:length(inits.qk)
Jmatz(:, :, g) = findJmat(inits.qk(g));
end
[Vseq, Dseq] = eigenshuffle(Jmatz);
inits.Jeigs = Dseq;
inits.Jvecs = Vseq;
inits.J0 = findJmat(0);

```

```

function Jmat = findJmat(qk)
Jac = zeros(Sys.nspec, Sys.nspec);

% V
Jac(1,1) = -gamm*fi/(1+VSS)^2+DA*(qk-1);
Jac(1,2) = -gamm*VSS/(1+VSS)*g_hill(beta, 1, nI, ISS);

```

```

% I
Jac(2,1) = fi/(1+VSS)^2;
Jac(2,2) = VSS/(1+VSS)*g_hill(beta,1,nI,ISS)-1;

Jmat = Jac;
end
end
end
end

```

## A.4 Dynamics

### A.4.1 Lateral inhibition

```

function [T,Y] = dS_aCL(params,inits,Sys)

Tmax = Sys.Tmax;
M = Sys.M;
N = Sys.N;
Mmat = Sys.MmatS;

if isfield(inits,'customX0') && inits.customX0
V = reshape(inits.V,N*M,1);
R0 = reshape(inits.R0,N*M,1);
D0 = reshape(inits.D0,N*M,1);
Y0(1:2:2*N*M) = R0;
Y0(2:2:2*N*M) = D0;

```

```

Y0 = perturbIC(Y0,params,inits,Sys);
else
V = reshape(inits.V,N*M,1);

%Add initial perturbation
RSS = inits.RSS;
DSS = inits.DSS;
Y0 = zeros(2*N*M,1);
Y0(1:2:2*N*M) = RSS;
Y0(2:2:2*N*M) = DSS;
Y0 = perturbIC(Y0,params,inits,Sys);
end

%tvec = [0 Tmax];
tvec = linspace(0, Tmax, 300);

%dynWaitbar = waitbar(0, 'Simulating pattern formation');
[T,Y] = ode45(@patterning2DMmat,tvec,Y0);
%delete(dynWaitbar);

function dY = patterning2DMmat(t,Y)
dY = zeros(2*N*M,1);

Ymat = reshape(Y,[2,N*M]);
R = Ymat(1,:)';
D = Ymat(2,:)';
RA = kinetics_aCL('RA_SS',struct('R',R,'V',V),params);
DN = Mmat*D;
dD = kinetics_aCL('D_DT',struct('RA',RA,'D',D),params);

```

```

dR = kinetics_aCL('R_DT',struct('DN',DN,'R',R),params);

dY(1:2:2*N*M) = dR;
dY(2:2:2*N*M) = dD;

end

end

```

## A.4.2 Lateral induction

```

function [T,Y] = dS_aDF(params,inits,Sys)

Tmax = Sys.Tmax;
M = Sys.M;
N = Sys.N;
Mmat = Sys.MmatS;

if isfield(inits,'customX0') && inits.customX0
V = reshape(inits.V,N*M,1);
R0 = reshape(inits.R0,N*M,1);
D0 = reshape(inits.D0,N*M,1);
Y0(1:2:2*N*M) = R0;
Y0(2:2:2*N*M) = D0;
Y0 = perturbIC(Y0,params,inits,Sys);
else
V = reshape(inits.V,N*M,1);

%Add initial perturbation
RSS = inits.X0(1);
DSS = inits.X0(2);

```

```

Y0 = zeros(2*N*M,1);
Y0(1:2:2*N*M) = RSS;
Y0(2:2:2*N*M) = DSS;
Y0 = perturbIC(Y0,params,inits,sys);
end

%tvec = [0 Tmax];
tvec = linspace(0, Tmax, 200);

%dynWaitbar = waitbar(0, 'Simulating pattern formation');
[T,Y] = ode45(@patterning2DMmat,tvec,Y0);
%delete(dynWaitbar);

function dY = patterning2DMmat(t,Y)
dY = zeros(2*N*M,1);
Ymat = reshape(Y,[2,N*M]);

R = Ymat(1,:)';
D = Ymat(2,:)';

DN = Mmat*D;
RA = kinetics_aDF('RA_SS',struct('R',R,'V',V),params);
dD = kinetics_aDF('D_DT',struct('DN',DN,'D',D,'RA',RA),params);
dR = kinetics_aDF('R_DT',struct('R',R),params);

dY(1:2:2*N*M) = dR;
dY(2:2:2*N*M) = dD;
end
end

```

### A.4.3 Double-juxtacrine

```
function [T,Y] = dS_aDJ(params,inits,Sys)

Tmax = Sys.Tmax;
M = Sys.M;
N = Sys.N;
Mmat = Sys.MmatS;

%Add initial perturbation
ASS = inits.X0(1);
BSS = inits.X0(2);
Y0 = zeros(2*N*M,1);
Y0(1:2:2*N*M) = ASS;
Y0(2:2:2*N*M) = BSS;
Y0 = perturbIC(Y0,params,inits,Sys);

%tvec = [0 Tmax];
tvec = linspace(0, Tmax, 300);

%dynWaitbar = waitbar(0, 'Simulating pattern formation');
[T,Y] = ode45(@patterning2DMmat,tvec,Y0);
%delete(dynWaitbar);;

function dY = patterning2DMmat(t,Y)
dY = zeros(2*N*M,1);

Ymat = reshape(Y, [2,N*M]);
A = Ymat(1,:)';
```

```

B = Ymat(2,:)';
AN = Mmat*A;
BN = Mmat*B;

dA = kinetics_aDJ('A_DT',struct('A',A,'BN',BN,'B',B),params);
dB = kinetics_aDJ('B_DT',struct('AN',AN,'B',B),params);

dY(1:2:2*N*M) = dA;
dY(2:2:2*N*M) = dB;

end
end

```

#### A.4.4 Diffusion & endocytosis

```

function [T,Y] = dS_aCLDE(params,initS,Sys)
Tmax = Sys.Tmax;
M = Sys.M;
N = Sys.N;
Mmat = Sys.MmatS;

if isfield(initS,'customX0') && initS.customX0
% Spatial profile
rho_in = reshape(initS.rho,N*M,1);
V0 = reshape(initS.V0,N*M,1);
I0 = reshape(initS.I0,N*M,1);
Y0(1:2:2*N*M) = V0;
Y0(2:2:2*N*M) = I0;
Y0 = perturbIC(Y0,params,initS,Sys);
else

```

```

% Basic, flat profile
Y0 = zeros(Sys.nspec*N*M,1);
for j = 1:Sys.nspec
Y0(j:Sys.nspec:Sys.nspec*N*M) = inits.X0(j);
end

Y0 = real(perturbIC(Y0,params,inits,Sys));
%Vext = reshape(inits.V,M*N,1);
rho_in = params.rho;
end

%tvec = [0 Tmax];
tvec = linspace(0, Tmax, 200);

%dynWaitbar = waitbar(0, 'Simulating pattern formation');
[T,Y] = ode45(@patterning2DMmat,tvec,Y0);
%delete(dynWaitbar);

function DY = patterning2DMmat(t,Y)
DY = zeros(Sys.nspec*N*M,1);

Ymat = reshape(Y, [Sys.nspec,length(Y)/Sys.nspec]);
V = Ymat(1,:)';
I = Ymat(2,:)';
VN = Mmat*V;

dI = kinetics_aCLDE('I_DT',struct('I',I,'V',V),params);
dV = kinetics_aCLDE('V_DT',struct('I',I,'VN',VN,'V',V,'rho_in',rho_in),

```

```
params);

%progress = t/(Tmax);
%set(0, 'CurrentFigure', dynWaitbar);
%waitbar(progress, dynWaitbar);

DY(1:Sys.nspec:Sys.nspec*N*M) = dV;
DY(2:Sys.nspec:Sys.nspec*N*M) = dI;

end

end
```

## BIBLIOGRAPHY

- [1] Cong L, Ran FA, Cox D, Lin S, Barretto R, Habib N, et al. Multiplex Genome Engineering Using CRISPR/Cas Systems. *Science*. 2013;339(6121):819–823. doi:10.1126/science.1231143.
- [2] Thomas CE, Ehrhardt A, Kay MA. Progress and problems with the use of viral vectors for gene therapy. *Nature Reviews Genetics*. 2003;4(5):346–358. doi:10.1038/nrg1066.
- [3] Yin H, Kanasty RL, Eltoukhy AA, Vegas AJ, Dorkin JR, Anderson DG. Non-viral vectors for gene-based therapy. *Nature Reviews Genetics*. 2014;15(8):541–555. doi:10.1038/nrg3763.
- [4] Alon U. *An Introduction to Systems Biology: Design Principles of Biological Circuits*. Chapman Hall CRC; 2007.
- [5] Zheng Y, Chen J, Craven M, Choi NW, Totorica S, Diaz-Santana A, et al. In vitro microvessels for the study of angiogenesis and thrombosis. *Proceedings of the National Academy of Sciences*. 2012;109(24):9342–9347. doi:10.1073/pnas.1201240109.
- [6] Janes KA, Chandran PL, Ford RM, Lazzara MJ, Papin JA, Peirce SM, et al. An engineering design approach to systems biology. *Integr Biol*. 2017;doi:10.1039/C7IB00014F.
- [7] Folkman J. Angiogenesis. In: Jaffe EA, editor. *Biology of Endothelial Cells*. 10. Boston, MA: Springer US; 1984. p. 412–428.
- [8] Risau W. Mechanisms of angiogenesis. *Nature*. 1997;386(6626):671–674. doi:10.1038/386671a0.

- [9] Carmeliet P, Jain RK. Molecular mechanisms and clinical applications of angiogenesis. *Nature*. 2011;473(7347):298–307. doi:10.1038/nature10144.
- [10] Laschke MW, Harder Y, Amon M, Martin I, Farhadi J, Ring A, et al. Angiogenesis in Tissue Engineering: Breathing Life into Constructed Tissue Substitutes. *Tissue Engineering*. 2006;12(8):2093–2104. doi:10.1089/ten.2006.12.2093.
- [11] Lovett M, Lee K, Edwards A, Kaplan DL. Vascularization Strategies for Tissue Engineering. *Tissue Engineering Part B: Reviews*. 2009;15(3):353–370. doi:10.1089/ten.teb.2009.0085.
- [12] Carlier A, Geris L, Bentley K, Carmeliet G, Carmeliet P, van Oosterwyck H. MOSAIC: A Multiscale Model of Osteogenesis and Sprouting Angiogenesis with Lateral Inhibition of Endothelial Cells. *PLoS Computational Biology*. 2012;8(10):e1002724. doi:10.1371/journal.pcbi.1002724.
- [13] Logsdon EA, Finley SD, Popel AS, MacGabhann F. A systems biology view of blood vessel growth and remodelling. *Journal of Cellular and Molecular Medicine*. 2014;18(8):1491–1508. doi:10.1111/jcmm.12164.
- [14] Bergers G, Benjamin LE. Angiogenesis: Tumorigenesis and the angiogenic switch. *Nature Reviews Cancer*. 2003;3(6):401–410. doi:10.1038/nrc1093.
- [15] Jain RK. Normalization of Tumor Vasculature: An Emerging Concept in Antiangiogenic Therapy. *Science*. 2005;307(5706):58–62. doi:10.1126/science.1104819.
- [16] Hellström M, Phng LK, Hofmann JJ, Wallgard E, Coultas L, Lindblom P, et al. Dll4 signalling through Notch1 regulates formation of tip cells during angiogenesis. *Nature*. 2007;445(7129):776–780. doi:10.1038/nature05571.

- [17] Blanco R, Gerhardt H. VEGF and Notch in tip and stalk cell selection. *Cold Spring Harbor Perspectives in Medicine*. 2013;3(1):a006569. doi:10.1101/cshperspect.a006569.
- [18] Gerhardt H, Golding M, Fruttiger M, Ruhrberg C, Lundkvist A, Abramson A, et al. VEGF guides angiogenic sprouting utilizing endothelial tip cell filopodia. *Journal of Cell Biology*. 2003;161(6):1163–1177. doi:10.1083/jcb.200302047.
- [19] Siekmann AF, Affolter M, Belting HG. The tip cell concept 10 years after: New players tune in for a common theme. *Experimental Cell Research*. 2013;319(9):1255–1263. doi:10.1016/j.yexcr.2013.01.019.
- [20] Beets K, Huylebroeck D, Moya IM, Umans L, Zwijsen A. Robustness in angiogenesis: Notch and BMP shaping waves. *Trends in Genetics*. 2013;29(3):140–149. doi:10.1016/j.tig.2012.11.008.
- [21] Benedito R, Roca C, Sørensen I, Adams S, Gossler A, Fruttiger M, et al. The Notch Ligands Dll4 and Jagged1 Have Opposing Effects on Angiogenesis. *Cell*. 2009;137(6):1124–1135. doi:10.1016/j.cell.2009.03.025.
- [22] Bentley K, Chakravartula S. The temporal basis of angiogenesis. *Philosophical Transactions of the Royal Society B: Biological Sciences*. 2017;372(1720):20150522. doi:10.1098/rstb.2015.0522.
- [23] Travasso RDM, Corvera Poiré E, Castro M, Rodríguez-Manzaneque JC, Hernández-Machado A. Tumor Angiogenesis and Vascular Patterning: A Mathematical Model. *PLoS ONE*. 2011;6(5):e19989. doi:10.1371/journal.pone.0019989.

- [24] Liu G, Qutub Aa, Vempati P, Mac Gabhann F, Popel AS. Module-based multiscale simulation of angiogenesis in skeletal muscle. *Theoretical Biology and Medical Modelling*. 2011;8(1):6. doi:10.1186/1742-4682-8-6.
- [25] Benedito R, Hellström M. Notch as a hub for signaling in angiogenesis. *Experimental Cell Research*. 2013;319(9):1281–1288. doi:10.1016/j.yexcr.2013.01.010.
- [26] Collier JR, Monk NAM, Maini PK, Lewis JH. Pattern Formation by Lateral Inhibition with Feedback: a Mathematical Model of Delta-Notch Intercellular Signalling. *Journal of Theoretical Biology*. 1996;183(4):429–446. doi:10.1006/jtbi.1996.0233.
- [27] Okabe K, Kobayashi S, Yamada T, Kurihara T, Tai-Nagara I, Miyamoto T, et al. Neurons limit angiogenesis by titrating VEGF in retina. *Cell*. 2014;159(3):584–596. doi:10.1016/j.cell.2014.09.025.
- [28] Bentley K, Philippides A, Ravasz Regan E. Do endothelial cells dream of eclectic shape? *Developmental Cell*. 2014;29(2):146–158. doi:10.1016/j.devcel.2014.03.019.
- [29] Palm MM, Dallinga MG, Van Dijk E, Klaassen I, Schlingemann RO, Merks RMH. Computational screening of tip and stalk cell behavior proposes a role for apelin signaling in sprout progression. *PLoS ONE*. 2016;11(11):1–31. doi:10.1371/journal.pone.0159478.
- [30] Jaeger J, Sharpe J. On the concept of mechanism in development. In: *Towards a Theory of Development*. 1991. Oxford University Press; 2014. p. 56–78. Available from: <http://www.oxfordscholarship.com/view/10.1093/acprof:oso/9780199671427.001.0001/acprof-9780199671427-chapter-4>.

- [31] Turing AM. The Chemical Basis of Morphogenesis. *Philosophical Transactions of the Royal Society B: Biological Sciences*. 1952;237(641):37–72. doi:10.1098/rstb.1952.0012.
- [32] Chen SI. Economic costs of hemophilia and the impact of prophylactic treatment on patient management. *The American Journal of Managed Care*. 2016;22(5 Suppl):s126–33.
- [33] Philippidis A. Gene Therapy Briefs. *Human Gene Therapy Clinical Development*. 2016;27(2):62–65. doi:10.1089/humc.2016.29011.bfs.
- [34] Herzog RW. A Cure For Hemophilia: the Promise Becomes a Reality. *Molecular Therapy*. 2016;24(9):1503–1504. doi:10.1038/mt.2016.169.
- [35] VIROVEK. Price Listings;. Available from: <http://www.virovek.com/aav/price-listings/>.
- [36] Abou-El-Enein M, Elsanhoury A, Reinke P. Overcoming Challenges Facing Advanced Therapies in the EU Market. *Cell Stem Cell*. 2016;19(3):293–297. doi:10.1016/j.stem.2016.08.012.
- [37] Cooke P. Rational drug design, the knowledge value chain and bio-science megacentres. *Cambridge Journal of Economics*. 2005;29(3):325–341. doi:10.1093/cje/bei045.
- [38] Baker RE, Schnell S, Maini PK. A clock and wavefront mechanism for somite formation. *Developmental Biology*. 2006;293(1):116–126. doi:10.1016/j.ydbio.2006.01.018.
- [39] De Rybel B, Adibi M, Breda AS, Wendrich JR, Smit ME, Novak O, et al. Integration of growth and patterning during vascular tis-

- sue formation in Arabidopsis. *Science*. 2014;345(6197):1255215–1255215. doi:10.1126/science.1255215.
- [40] Goodman CS, Shatz CJ. Developmental mechanisms that generate precise patterns of neuronal connectivity. *Cell*. 1993;72(1001):77–98. doi:10.1016/S0092-8674(05)80030-3.
- [41] Tessier-Lavigne M, Goodman CS. The molecular biology of axon guidance. *Science*. 1996;274(5290):1123–33.
- [42] Dickson BJ. Molecular Mechanisms of Axon Guidance. *Science*. 2002;298(5600):1959–1964. doi:10.1126/science.1072165.
- [43] Othmer HG, Scriven LE. Instability and dynamic pattern in cellular networks. *Journal of Theoretical Biology*. 1971;32(3):507–537. doi:10.1016/0022-5193(71)90154-8.
- [44] Harary F. The Determinant of the Adjacency Matrix of a Graph. *Society for Industrial and Applied Mathematics*. 1962;4(3):202–210.
- [45] Sprinzak D, Lakhanpal A, LeBon L, Garcia-Ojalvo J, Elowitz MB. Mutual Inactivation of Notch Receptors and Ligands Facilitates Developmental Patterning. *PLoS Computational Biology*. 2011;7(6):e1002069. doi:10.1371/journal.pcbi.1002069.
- [46] Cohen M, Georgiou M, Stevenson NL, Miodownik M, Baum B. Dynamic Filopodia Transmit Intermittent Delta-Notch Signaling to Drive Pattern Refinement during Lateral Inhibition. *Developmental Cell*. 2010;19(1):78–89. doi:10.1016/j.devcel.2010.06.006.
- [47] Murray JD. *Mathematical Biology: II. Spatial Models*. New York: Springer; 2003.

- [48] Raspopovic J, Marcon L, Russo L, Sharpe J. Digit patterning is controlled by a Bmp-Sox9-Wnt Turing network modulated by morphogen gradients. *Science*. 2014;345(6196):566–570. doi:10.1126/science.1252960.
- [49] Metzger RJ, Klein OD, Martin GR, Krasnow Ma. The branching programme of mouse lung development. *Nature*. 2008;453(7196):745–750. doi:10.1038/nature07005.
- [50] Caolo V, van den Akker NMS, Verbruggen S, Donners MMPC, Swennen G, Schulten H, et al. Feed-forward Signaling by Membrane-bound Ligand Receptor Circuit: THE CASE OF NOTCH DELTA-LIKE 4 LIGAND IN ENDOTHELIAL CELLS. *Journal of Biological Chemistry*. 2010;285(52):40681–40689. doi:10.1074/jbc.M110.176065.
- [51] Bentley K, Gerhardt H, Bates PA. Agent-based simulation of notch-mediated tip cell selection in angiogenic sprout initialisation. *Journal of Theoretical Biology*. 2008;250(1):25–36. doi:10.1016/j.jtbi.2007.09.015.
- [52] Jakobsson L, Franco Ca, Bentley K, Collins RT, Ponsioen B, Aspalter IM, et al. Endothelial cells dynamically compete for the tip cell position during angiogenic sprouting. *Nature Cell Biology*. 2010;12(10):943–953. doi:10.1038/ncb2103.
- [53] Bentley K, Franco CA, Philippides A, Blanco R, Dierkes M, Gebala V, et al. The role of differential VE-cadherin dynamics in cell rearrangement during angiogenesis. *Nature Cell Biology*. 2014;16(4):309–321. doi:10.1038/ncb2926.
- [54] Plahte E. Pattern formation in discrete cell lattices. *Journal of Mathematical Biology*. 2001;43(5):411–445. doi:10.1007/s002850100105.

- [55] Shaya O, Sprinzak D. From Notch signaling to fine-grained patterning: Modeling meets experiments. *Current Opinion in Genetics and Development*. 2011;21(6):732–739. doi:10.1016/j.gde.2011.07.007.
- [56] Boareto M, Jolly MK, Ben-Jacob E, Onuchic JN. Jagged mediates differences in normal and tumor angiogenesis by affecting tip-stalk fate decision. *Proceedings of the National Academy of Sciences*. 2015;112(29):E3836–E3844. doi:10.1073/pnas.1511814112.
- [57] Abdulla T, Schleich JM, Summers R. Multiscale modelling of Notch-mediated lateral induction. *Proceedings - IEEE-EMBS International Conference on Biomedical and Health Informatics: Global Grand Challenge of Health Informatics, BHI 2012*. 2012;25(Bhi):257–260. doi:10.1109/BHI.2012.6211560.
- [58] Wälchli T, Mateos JM, Weinman O, Babic D, Regli L, Hoerstrup SP, et al. Quantitative assessment of angiogenesis, perfused blood vessels and endothelial tip cells in the postnatal mouse brain. *Nature Protocols*. 2014;10(1):53–74. doi:10.1038/nprot.2015.002.
- [59] Hurwitz A. Ueber die Bedingungen, unter welchen eine Gleichung nur Wurzeln mit negativen reellen Theilen besitzt. *Mathematische Annalen*. 1895;46(2):273–284. doi:10.1007/BF01446812.
- [60] Liu ZJ, Shirakawa T, Li Y, Soma A, Oka M, Dotto GP, et al. Regulation of Notch1 and Dll4 by Vascular Endothelial Growth Factor in Arterial Endothelial Cells: Implications for Modulating Arteriogenesis and Angiogenesis. *Molecular and Cellular Biology*. 2003;23(1):14–25. doi:10.1128/MCB.23.1.14-25.2003.

- [61] Nguyen DHT, Stapleton SC, Yang MT, Cha SS, Choi CK, Galie Pa, et al. Biomimetic model to reconstitute angiogenic sprouting morphogenesis in vitro. *Proceedings of the National Academy of Sciences of the United States of America*. 2013;110(17):6712–7. doi:10.1073/pnas.1221526110.
- [62] Lobov IB, Renard Ra, Papadopoulos N, Gale NW, Thurston G, Yancopoulos GD, et al. Delta-like ligand 4 (Dll4) is induced by VEGF as a negative regulator of angiogenic sprouting. *Proceedings of the National Academy of Sciences*. 2007;104(9):3219–3224. doi:10.1073/pnas.0611206104.
- [63] Suchting S, Freitas C, le Noble F, Benedito R, Breant C, Duarte A, et al. The Notch ligand Delta-like 4 negatively regulates endothelial tip cell formation and vessel branching. *Proceedings of the National Academy of Sciences*. 2007;104(9):3225–3230. doi:10.1073/pnas.0611177104.
- [64] Holderfield MT, Henderson Anderson AM, Kokubo H, Chin MT, Johnson RL, Hughes CCW. HESR1/CHF2 suppresses VEGFR2 transcription independent of binding to E-boxes. *Biochemical and Biophysical Research Communications*. 2006;346(3):637–648. doi:10.1016/j.bbrc.2006.05.177.
- [65] Williams CK. Up-regulation of the Notch ligand Delta-like 4 inhibits VEGF-induced endothelial cell function. *Blood*. 2005;107(3):931–939. doi:10.1182/blood-2005-03-1000.
- [66] Leslie JD, Ariza-McNaughton L, Bermange AL, McAdow R, Johnson SL, Lewis J. Endothelial signalling by the Notch ligand Delta-like 4 restricts angiogenesis. *Development*. 2007;134(5):839–844. doi:10.1242/dev.003244.
- [67] Joussineau CD, Soule' J, Martin M, Anguille C, Philippe Montcourrier & Daniel Alexandre. Delta-promoted filopodia mediate long-range

- lateral inhibition in *Drosophila*. *Nature*. 2003;426(December):555–559. doi:10.1038/nature02143.1.
- [68] Kornberg TB, Roy S. Cytonemes as specialized signaling filopodia. *Development*. 2014;141(4):729–736. doi:10.1242/dev.086223.
- [69] Greenwald I, Rubin GM. Making a difference: The role of cell-cell interactions in establishing separate identities for equivalent cells. *Cell*. 1992;68(2):271–281. doi:10.1016/0092-8674(92)90470-W.
- [70] Heitzler P, Simpson P. The choice of cell fate in the epidermis of *Drosophila*. *Cell*. 1991;64(6):1083–1092. doi:10.1016/0092-8674(91)90263-X.
- [71] Benedito R, Rocha SF, Woeste M, Zamykal M, Radtke F, Casanovas O, et al. Notch-dependent VEGFR3 upregulation allows angiogenesis without VEGF–VEGFR2 signalling. *Nature*. 2012;484(7392):110–114. doi:10.1038/nature10908.
- [72] Harrington LS, Sainson RCA, Williams CK, Taylor JM, Shi W, Li JL, et al. Regulation of multiple angiogenic pathways by Dll4 and Notch in human umbilical vein endothelial cells. *Microvascular Research*. 2008;75(2):144–154. doi:10.1016/j.mvr.2007.06.006.
- [73] Manderfield LJ, High FA, Engleka KA, Liu F, Li L, Rentschler S, et al. Notch activation of Jagged1 contributes to the assembly of the arterial wall. *Circulation*. 2012;125(2):314–323. doi:10.1161/CIRCULATIONAHA.111.047159.
- [74] Ubezio B, Blanco RA, Geudens I, Stanchi F, Mathivet T, Jones ML, et al. Synchronization of endothelial Dll4-Notch dynamics switch blood vessels from branching to expansion. *eLife*. 2016;5(APRIL2016):1–32. doi:10.7554/eLife.12167.

- [75] Phng LK, Stanchi F, Gerhardt H. Filopodia are dispensable for endothelial tip cell guidance. *Development*. 2013;140(19):4031–4040. doi:10.1242/dev.097352.
- [76] Toro R, Prahst C, Mathivet T, Siegfried G, Kaminker JS, Larrivee B, et al. Identification and functional analysis of endothelial tip cell enriched genes. *Blood*. 2010;116(19):4025–4033. doi:10.1182/blood-2010-02-270819.
- [77] Moya IM, Umans L, Maas E, Pereira PNG, Beets K, Francis A, et al. Stalk Cell Phenotype Depends on Integration of Notch and Smad1/5 Signaling Cascades. *Developmental Cell*. 2012;22(3):501–514. doi:10.1016/j.devcel.2012.01.007.
- [78] Okubo Y, Sugawara T, Abe-Koduka N, Kanno J, Kimura A, Saga Y. Lfng regulates the synchronized oscillation of the mouse segmentation clock via trans-repression of Notch signalling. *Nature Communications*. 2012;3:1141. doi:10.1038/ncomms2133.
- [79] Arenas A, Diaz-Guilera A, Kurths J, Moreno Y, Zhou C. Synchronization in complex networks. *Physics Reports*. 2008;469(3):93–153. doi:10.1016/j.physrep.2008.09.002.
- [80] Gutenkunst RN, Waterfall JJ, Casey FP, Brown KS, Myers CR, Sethna JP. Universally Sloppy Parameter Sensitivities in Systems Biology Models. *PLoS Computational Biology*. 2007;3(10):e189. doi:10.1371/journal.pcbi.0030189.
- [81] Babbie AC, Kirk P, Stumpf MPH. Topological sensitivity analysis for systems biology. *Proceedings of the National Academy of Sciences*. 2014;111(52):18507–18512. doi:10.1073/pnas.1414026112.

- [82] Jakobsson L, Kreuger J, Claesson-Welsh L. Building blood vessels—stem cell models in vascular biology. *The Journal of Cell Biology*. 2007;177(5):751–755. doi:10.1083/jcb.200701146.
- [83] Ruhrberg C, Gerhardt H, Golding M, Watson R, Ioannidou S, Fujisawa H, et al. Spatially restricted patterning cues provided by heparin-binding VEGF-A control blood vessel branching morphogenesis. *Genes and Development*. 2002;16(20):2684–2698. doi:10.1101/gad.242002.
- [84] Gerhardt H. VEGF and Endothelial Guidance in Angiogenic Sprouting. In: *VEGF in Development*. December. New York, NY: Springer New York; 2008. p. 68–78.
- [85] Daneman R, Agalliu D, Zhou L, Kuhnert F, Kuo CJ, Barres BA. Wnt/ $\beta$ -catenin signaling is required for CNS, but not non-CNS, angiogenesis. *Proceedings of the National Academy of Sciences*. 2009;106(2):641–646. doi:10.1073/pnas.0805165106.
- [86] Nichols JT, Miyamoto A, Olsen SL, D’Souza B, Yao C, Weinmaster G. DSL ligand endocytosis physically dissociates Notch1 heterodimers before activating proteolysis can occur. *The Journal of Cell Biology*. 2007;176(4):445–458. doi:10.1083/jcb.200609014.
- [87] Zhang J, Fukuhara S, Sako K, Takenouchi T, Kitani H, Kume T, et al. Angiopoietin-1/Tie2 signal augments basal notch signal controlling vascular quiescence by inducing delta-like 4 expression through AKT-mediated activation of  $\beta$ -catenin. *Journal of Biological Chemistry*. 2011;286(10):8055–8066. doi:10.1074/jbc.M110.192641.
- [88] Sawamiphak S, Seidel S, Essmann CL, Wilkinson Ga, Pitulescu ME, Acker T,

- et al. Ephrin-B2 regulates VEGFR2 function in developmental and tumour angiogenesis. *Nature*. 2010;465(7297):487–491. doi:10.1038/nature08995.
- [89] Adam MG, Berger C, Feldner A, Yang WJ, Wüstehube-Lausch J, Herberich SE, et al. Synaptojanin-2 binding protein stabilizes the notch ligands DLL1 and DLL4 and inhibits sprouting angiogenesis. *Circulation Research*. 2013;113(11):1206–1218. doi:10.1161/CIRCRESAHA.113.301686.
- [90] Yaron A, Sprinzak D. The cis side of juxtacrine signaling: A new role in the development of the nervous system. *Trends in Neurosciences*. 2012;35(4):230–239. doi:10.1016/j.tins.2011.12.003.
- [91] Aspalter IM, Gordon E, Dubrac A, Ragab A, Narloch J, Vizán P, et al. Alk1 and Alk5 inhibition by Nrp1 controls vascular sprouting downstream of Notch. *Nature Communications*. 2015;6:7264. doi:10.1038/ncomms8264.
- [92] Simons M, Gordon E, Claesson-Welsh L. Mechanisms and regulation of endothelial VEGF receptor signalling. *Nature Reviews Molecular Cell Biology*. 2016;17(10):611–625. doi:10.1038/nrm.2016.87.
- [93] Koch S, Van Meeteren LA, Morin E, Testini C, Weström S, Björkelund H, et al. NRP1 Presented in trans to the endothelium arrests VEGFR2 endocytosis, preventing angiogenic signaling and tumor initiation. *Developmental Cell*. 2014;28(6):633–646. doi:10.1016/j.devcel.2014.02.010.
- [94] Dejana E, Orsenigo F, Lampugnani MG. The role of adherens junctions and VE-cadherin in the control of vascular permeability. *Journal of Cell Science*. 2008;121(13):2115–2122. doi:10.1242/jcs.017897.
- [95] Gavard J, Gutkind JS. VEGF controls endothelial-cell permeability by pro-

- moting the  $\beta$ -arrestin-dependent endocytosis of VE-cadherin. *Nature Cell Biology*. 2006;8(11):1223–1234. doi:10.1038/ncb1486.
- [96] Lampugnani MG, Orsenigo F, Gagliani MC, Tacchetti C, Dejana E. Vascular endothelial cadherin controls VEGFR-2 internalization and signaling from intracellular compartments. *Journal of Cell Biology*. 2006;174(4):593–604. doi:10.1083/jcb.200602080.
- [97] Roth L, Prahst C, Ruckdeschel T, Savant S, Weström S, Fantin A, et al. Neuropilin-1 mediates vascular permeability independently of vascular endothelial growth factor receptor-2 activation. *Science Signaling*. 2016;9(425):1–11. doi:10.1126/scisignal.aad3812.
- [98] Barbieri MA, Kohn AD, Roth RA, Stahl PD. Protein kinase B/akt and Rab5 mediate Ras activation of endocytosis. *Journal of Biological Chemistry*. 1998;273(31):19367–19370. doi:10.1074/jbc.273.31.19367.
- [99] Gampel A, Moss L, Jones MC, Brunton V, Norman JC, Mellor H. VEGF regulates the mobilization of VEGFR2/KDR from an intracellular endothelial storage compartment. *Blood*. 2006;108(8):2624–2631. doi:10.1182/blood-2005-12-007484.
- [100] Jopling HM, Odell AF, Hooper NM, Zachary IC, Walker JH, Ponnambalam S. Rab GTPase regulation of VEGFR2 trafficking and signaling in endothelial cells. *Arteriosclerosis, Thrombosis, and Vascular Biology*. 2009;29(7):1119–1124. doi:10.1161/ATVBAHA.109.186239.
- [101] Wang S, Sun J, Xiao Y, Lu Y, Zhang DD, Wong PK, et al. Intercellular Tension Negatively Regulates Angiogenic Sprouting of Endothelial Tip

- Cells via Notch1-Dll4 Signaling. *Advanced Biosystems*. 2017; p. 1600019. doi:10.1002/adbi.201600019.
- [102] Fleury V. Branched fractal patterns in non-equilibrium electrochemical deposition from oscillatory nucleation and growth. *Nature*. 1997;390(6656):145–148. doi:10.1038/36522.
- [103] Bentley K, Mariggi G, Gerhardt H, Bates Pa. Tipping the Balance: Robustness of Tip Cell Selection, Migration and Fusion in Angiogenesis. *PLoS Computational Biology*. 2009;5(10):e1000549. doi:10.1371/journal.pcbi.1000549.
- [104] Domigan CK, Iruela-Arispe ML. Stealing VEGF from thy neighbor. *Cell*. 2014;159(3):473–474. doi:10.1016/j.cell.2014.10.008.
- [105] Nakayama M, Nakayama A, van Lessen M, Yamamoto H, Hoffmann S, Drexler HC, et al. Spatial regulation of VEGF receptor endocytosis in angiogenesis. *Nature Cell Biology*. 2013;15(3):249–260. doi:10.1038/ncb2679.
- [106] Gaengel K, Betsholtz C. Endocytosis regulates VEGF signalling during angiogenesis. *Nature Cell Biology*. 2013;15(3):233–235. doi:10.1038/ncb2705.
- [107] Fulton D, Gratton JP, McCabe TJ, Fontana J, Fujio Y, Walsh K, et al. Regulation of endothelium-derived nitric oxide production by the protein kinase Akt. *Nature*. 1999;399(6736):597–601. doi:10.1038/21218.
- [108] Wang G, Moniri NH, Ozawa K, Stamler JS, Daaka Y. Nitric oxide regulates endocytosis by S-nitrosylation of dynamin. *Proceedings of the National Academy of Sciences of the United States of America*. 2006;103(5):1295–300. doi:10.1073/pnas.0508354103.
- [109] Priya MK, Sahu G, Soto-Pantoja DR, Goldy N, Sundaresan AM, Jadhav V,

- et al. Tipping off endothelial tubes: nitric oxide drives tip cells. *Angiogenesis*. 2015;18(2):175–189. doi:10.1007/s10456-014-9455-0.
- [110] Mac Gabhann F, Ji JW, Popel AS. Computational Model of Vascular Endothelial Growth Factor Spatial Distribution in Muscle and Pro-Angiogenic Cell Therapy. *PLoS Computational Biology*. 2006;2(9):e127. doi:10.1371/journal.pcbi.0020127.
- [111] Simons M. An Inside View: VEGF Receptor Trafficking and Signaling. *Physiology*. 2012;27(4):213–222. doi:10.1152/physiol.00016.2012.
- [112] Tan WH, Popel AS, Mac Gabhann F. Computational Model of Gab1/2-Dependent VEGFR2 Pathway to Akt Activation. *PLoS ONE*. 2013;8(6):e67438. doi:10.1371/journal.pone.0067438.
- [113] Imoukhuede PI, Popel AS. Quantification and cell-to-cell variation of vascular endothelial growth factor receptors. *Experimental Cell Research*. 2011;317(7):955–965. doi:10.1016/j.yexcr.2010.12.014.
- [114] Mac Gabhann F, Popel AS. Dimerization of VEGF receptors and implications for signal transduction: A computational study. *Biophysical Chemistry*. 2007;128(2-3):125–139. doi:10.1016/j.bpc.2007.03.010.
- [115] Simakov DSA, Pismen LM. Discrete model of periodic pattern formation through a combined autocrine–juxtacrine cell signaling. *Physical Biology*. 2013;10(4):046001. doi:10.1088/1478-3975/10/4/046001.
- [116] Anderson A. Continuous and Discrete Mathematical Models of Tumor-induced Angiogenesis. *Bulletin of Mathematical Biology*. 1998;60(5):857–899. doi:10.1006/bulm.1998.0042.

- [117] McDougall SR, Watson MG, Devlin aH, Mitchell Ca, Chaplain MaJ. A Hybrid Discrete-Continuum Mathematical Model of Pattern Prediction in the Developing Retinal Vasculature. *Bulletin of Mathematical Biology*. 2012;74(10):2272–2314. doi:10.1007/s11538-012-9754-9.
- [118] Lee KY, Peters MC, Anderson KW, Mooney DJ. Controlled growth factor release from synthetic extracellular matrices. *Nature*. 2000;408(6815):998–1000. doi:10.1038/35050141.
- [119] Lund EL, Thorsen C, Pedersen MW, Junker N, Kristjansen PE. Relationship between vessel density and expression of vascular endothelial growth factor and basic fibroblast growth factor in small cell lung cancer in vivo and in vitro. *Clinical Cancer Research*. 2000;6(11):4287–91.
- [120] Wang Y, Nakayama M, Pitulescu ME, Schmidt TS, Bochenek ML, Sakakibara A, et al. Ephrin-B2 controls VEGF-induced angiogenesis and lymphangiogenesis. *Nature*. 2010;465(7297):483–486. doi:10.1038/nature09002.
- [121] Salvucci O, Tosato G. Essential Roles of EphB Receptors and EphrinB Ligands in Endothelial Cell Function and Angiogenesis. vol. 114. 1st ed. Elsevier Inc.; 2012. Available from: <http://dx.doi.org/10.1016/B978-0-12-386503-8.00002-8>.
- [122] Daneshjou N, Sieracki N, van Nieuw Amerongen GP, Schwartz MA, Komarova YA, Malik AB. Rac1 functions as a reversible tension modulator to stabilize VE-cadherin trans-interaction. *Journal of Cell Biology*. 2015;208(1):23–32. doi:10.1083/jcb.201409108.
- [123] Gabhann FM, Popel AS. Systems Biology of Vascular En-

- dothelial Growth Factors. *Microcirculation*. 2008;15(8):715–738. doi:10.1080/10739680802095964.
- [124] Carmeliet P, Ferreira V, Breier G, Pollefeyt S, Kieckens L, Gertsenstein M, et al. Abnormal blood vessel development and lethality in embryos lacking a single VEGF allele. *Nature*. 1996;380(6573):435–439. doi:10.1038/380435a0.
- [125] Siemerink MJ, Klaassen I, Vogels IMC, Griffioen AW, Van Noorden CJF, Schlingemann RO. CD34 marks angiogenic tip cells in human vascular endothelial cell cultures. *Angiogenesis*. 2012;15(1):151–163. doi:10.1007/s10456-011-9251-z.
- [126] Reddy CL, Yosef N, Ubogu EE. VEGF-A165 Potently Induces Human Blood–Nerve Barrier Endothelial Cell Proliferation, Angiogenesis, and Wound Healing In Vitro. *Cellular and Molecular Neurobiology*. 2013;33(6):789–801. doi:10.1007/s10571-013-9946-3.
- [127] Belair DG, Whisler JA, Valdez J, Velazquez J, James A, Vickerman V, et al. HHS Public Access. 2015;11(3):511–525. doi:10.1007/s12015-014-9549-5.Human.
- [128] De Rosa L, Finetti F, Diana D, Di Stasi R, Auriemma S, Romanelli A, et al. Miniaturizing VEGF: Peptides mimicking the discontinuous VEGF receptor-binding site modulate the angiogenic response. *Scientific Reports*. 2016;6(1):31295. doi:10.1038/srep31295.
- [129] Chen RR, Silva EA, Yuen WW, Brock AA, Fischbach C, Lin AS, et al. Integrated approach to designing growth factor delivery systems. *The FASEB Journal*. 2007;21(14):3896–3903. doi:10.1096/fj.06-7873com.

- [130] Hashambhoy YL, Chappell JC, Peirce SM, Bautch VL, Mac Gabhann F. Computational modeling of interacting VEGF and soluble VEGF receptor concentration gradients. *Frontiers in physiology*. 2011;2(October):62. doi:10.3389/fphys.2011.00062.
- [131] Bryant LM, Christopher DM, Giles AR, Hinderer C, Rodriguez JL, Smith JB, et al. Lessons Learned from the Clinical Development and Market Authorization of Glybera. *Human Gene Therapy Clinical Development*. 2013;24(2):55–64. doi:10.1089/humc.2013.087.
- [132] Mullin E. The World’s Most Expensive Medicine Is Being Pulled from the Market. *MIT Technology Review*. 2017;.
- [133] Regalado A. The World’s Most Expensive Medicine Is a Bust. *MIT Technology Review*. 2016;.
- [134] Merten OW. AAV vector production: state of the art developments and remaining challenges. *Cell and Gene Therapy Insights*. 2016;2(5):521–551. doi:10.18609/cgti.2016.067.
- [135] Brian K. Industrialization of MAb production technology. *MAbs*. 2009;(5):443–452. doi:10.4161/mabs.1.5.9448.
- [136] Zincarelli C, Soltys S, Rengo G, Rabinowitz JE. Analysis of AAV Serotypes 1–9 Mediated Gene Expression and Tropism in Mice After Systemic Injection. *Molecular Therapy*. 2008;16(6):1073–1080. doi:10.1038/mt.2008.76.
- [137] Clément N, Grieger JC. Manufacturing of recombinant adeno-associated viral vectors for clinical trials. *Molecular Therapy - Methods & Clinical Development*. 2016;3(November):16002. doi:10.1038/mtm.2016.2.

- [138] van Oers MM, Pijlman GP, Vlak JM. Thirty years of baculovirus-insect cell protein expression: from dark horse to mainstream technology. *Journal of General Virology*. 2015;96(Pt\_1):6–23. doi:10.1099/vir.0.067108-0.
- [139] Urabe M, Ding C, Kotin RM. Insect Cells as a Factory to Produce Adeno-Associated Virus Type 2 Vectors. *Human Gene Therapy*. 2002;13(16):1935–1943. doi:10.1089/10430340260355347.
- [140] Smith RH, Levy JR, Kotin RM. A Simplified Baculovirus-AAV Expression Vector System Coupled With One-step Affinity Purification Yields High-titer rAAV Stocks From Insect Cells. *Molecular Therapy*. 2009;17(11):1888–1896. doi:10.1038/mt.2009.128.
- [141] Cecchini S, Virag T, Kotin RM. Reproducible High Yields of Recombinant Adeno-Associated Virus Produced Using Invertebrate Cells in 0.02- to 200-Liter Cultures. *Human Gene Therapy*. 2011;22(8):1021–1030. doi:10.1089/hum.2010.250.
- [142] Negrete A, Kotin RM. Production of recombinant adeno-associated vectors using two bioreactor configurations at different scales. *Journal of Virological Methods*. 2007;145(2):155–161. doi:10.1016/j.jviromet.2007.05.020.
- [143] Kohlbrenner E, Aslanidi G, Nash K, ShklyaeV S, Campbell-Thompson M, Byrne BJ, et al. Successful Production of Pseudotyped rAAV Vectors Using a Modified Baculovirus Expression System. *Molecular Therapy*. 2005;12(6):1217–1225. doi:10.1016/j.ymthe.2005.08.018.
- [144] Granados RR, Guoxun L, Derksen ACG, McKenna KA. A new insect cell line from *Trichoplusia ni* (BTI-Tn-5B1-4) susceptible to *Trichoplusia ni* single

- enveloped nuclear polyhedrosis virus. *Journal of Invertebrate Pathology*. 1994;64(3):260–266. doi:10.1016/S0022-2011(94)90400-6.
- [145] Wilde M, Klausberger M, Palmberger D, Ernst W, Grabherr R. Tnao38, high five and Sf9 – evaluation of host-virus interactions in three different insect cell lines: baculovirus production and recombinant protein expression. *Biotechnology Letters*. 2014;36(4):743–749. doi:10.1007/s10529-013-1429-6.
- [146] Ma H, Galvin TA, Glasner DR, Shaheduzzaman S, Khan AS. Identification of a Novel Rhabdovirus in *Spodoptera frugiperda* Cell Lines. *Journal of Virology*. 2014;88(12):6576–6585. doi:10.1128/JVI.00780-14.
- [147] Li TC, Scotti PD, Miyamura T, Takeda N. Latent Infection of a New Alphavirus in an Insect Cell Line. *Journal of Virology*. 2007;81(20):10890–10896. doi:10.1128/JVI.00807-07.
- [148] Maghodia AB, Geisler C, Jarvis DL. Characterization of an Sf-rhabdovirus-negative *Spodoptera frugiperda* cell line as an alternative host for recombinant protein production in the baculovirus-insect cell system. *Protein Expression and Purification*. 2016;122:45–55. doi:10.1016/j.pep.2016.02.014.
- [149] Hashimoto Y, Zhang S, Blissard GW. Ao38, a new cell line from eggs of the black witch moth, *Ascalapha odorata* (Lepidoptera: Noctuidae), is permissive for AcMNPV infection and produces high levels of recombinant proteins. *BMC Biotechnology*. 2010;10(1):50. doi:10.1186/1472-6750-10-50.
- [150] Hashimoto Y, Zhang S, Zhang S, Chen YR, Blissard GW. Correction: BTI-Tnao38, a new cell line derived from *Trichoplusia ni*, is permissive for AcMNPV infection and produces high levels of recombinant proteins. *BMC Biotechnology*. 2012;12(1):12. doi:10.1186/1472-6750-12-12.

- [151] Blank S, Dorf B. *The Startup Owner's Manual: The Step-By-Step Guide for Building a Great Company*. K & S Ranch; 2012.
- [152] Osterwalder A. *The Business Model Ontology: A Proposition in a Design Science Approach*. Université de Lausanne; 2004.
- [153] Osterwalder A, Pigneur Y. *Business Model Generation*. Wiley; 2010.
- [154] Osterwalder A, Pigneur Y, Bernarda G, Smith A. *Value Proposition Design*. Wiley; 2014.
- [155] Markides CC, Williamson PJ. Related diversification, core competences and corporate performance. *Strategic Management Journal*. 1994;15:149–165. doi:10.1002/smj.4250151010.
- [156] Simon CJ, Sullivan MW. The Measurement and Determinants of Brand Equity: A Financial Approach. *Marketing Science*. 1993;12(1):28–52. doi:10.1287/mksc.12.1.28.
- [157] Prahalad CK, Hamel G. The Core Competence of the Corporation. In: *Strategische Unternehmensplanung — Strategische Unternehmensführung*. Berlin/Heidelberg: Springer Berlin Heidelberg; 2006. p. 275–292.
- [158] Besanko D, Dranove D, Shanley M, Schaefer S. *Economics of Strategy*. Wiley; 2013.
- [159] Baghai M, Coley SC, White D, Conn C, McLean RJ. Staircases to growth. *McKinsey Quarterly*. 1996;(4):38–61.
- [160] Hassan S, Huang H, Warren K, Mahdavi B, Smith D, Jong S, et al. Process change evaluation framework for allogeneic cell therapies: impact on drug

development and commercialization. *Regenerative Medicine*. 2016;11(3):287–305. doi:10.2217/rme-2015-0034.

[161] Mayer Brown. *Drug Development: Valuing the Pipeline*; 2009.